MODELLING OF WAVE GENERATION IN SEWER SYSTEMS BY INTERMITTENT DISCHARGE DEVICES USING THE SAINT-VENANT AND BOUSSINESQ EQUATIONS

A thesis submitted for the degree of Doctor of Philosophy

by

Wolney Alves

Department of Building Engineering and Surveying

Heriot-Watt University

November 1996

Modelling of wave generation in sewer systems by intermittent discharge devices using the Saint-Venant and Boussinesq equations

Abstract

Although the International Drinking Water Supply and Sanitation Decade (1981-1990) has brought important acquirements in terms of covered population increasing and in terms of conceptual and technical development, the present deficit points to the necessity to continue and improve the Decade achievements. Innovative, appropriate and low-cost technologies played a major role on this struggle.

Unsteady flow equations applied to sewer networks are a precious instrument on the description of actual phenomena on sewers leading to more rational and economic design, construction and operation.

The use of intermittent discharge devices as a means of reducing pipe slopes in separated sewer networks, leading to a reduction in construction costs, mainly in flat areas, is explored.

A unidimensional model directed to simulate the flow generated on sewers through intermittent discharge devices is presented. Two mathematical equations are used to the generated wave modelling: the Saint-Venant and the Boussinesq equations.

Numerical integration, through finite-difference methods, is used to solve mathematical systems. Three numerical models are applied: the method of characteristics, McCormack scheme and the two-four scheme.

A computer program was developed providing hydraulic variables simulation. Three alternatives are embraced: the Saint-Venant equations using the method of characteristics and the McCormack scheme and the Boussinesq equations using the "2-4" scheme. Linear and Everett and Newton-Gregory interpolation are provided on the method of characteristics. Lister (1960) and Standing (1986) iterative process are also provided. An analysis method to determine the flow regime on the method of characteristics is incorporated in the program. Special schemes for friction and vertical acceleration adjustment are also available.

Comparison with laboratory data showed that in general the "2-4" scheme produced better results in terms of wave velocity. The wave generated through the developed experimental discharge device had better simulated results in terms of water depth profiles and wave velocity using the Boussinesq equations, solved through the "2-4" method. The model showed clear response differences depending on friction and vertical acceleration values. Strictly under Boussinesq's hypothesis however, vertical acceleration has shown not to be relevant.

The oscillation of the wave peak water depth along the pipeline was an interesting finding of laboratory works. A major problem on the processing was the formation of a pulse on the wave front.

Research continuation and field application are planned.

Acknowledgements

The work here presented is one of the activities included in the Link Plan agreed by Heriot-Watt University and Instituto de Pesquisas Tecnológicas do Estado de São Paulo S.A. - IPT ("Institute for Technological Research of the State of São Paulo", Brazil). It was supported by The British Council, Fundação de Amparo a Pesquisa do Estado de São Paulo - FAPESP ("Foundation for Research Support of the State of São Paulo") and CNPq - Conselho Nacional de Desenvolvimento Científico e Tecnológico ("Scientific and Technological Development National Council"). The participation and contribution of all institutions are gratefully acknowledge.

I would like to thank Prof. John Swaffield of the Department of Building Engineering and Surveying for his support and encouragement.

I would also like to thank to several colleagues, old and new friends that have in some way helped me to conclude this work.

Finally my profound gratitude and love to Arlete, Wolney Martini and mamãe.

TABLE OF CONTENTS

List of Figures

List of Tables

NOTATION

A	cross-sectional area of flow (m^2)
c	wave celerity (m/s)
C+	positive characteristic
C-	negative characteristic
C	Chézy coefficient (m/s^2)
C_n	Courant number
d	uniform flow or still water depth (m)
D	pipe diameter (m)
f	Darcy resistance coefficient
f_j^k	variable computed at node position j and instant k
FD	friction force horizontal component added to Euler's equation (m/s^2)
F_f	water/pipe bed friction force (N)
F_R	Froude number
g	acceleration due to gravity (m/s^2)
h	flow water depth (m)
h_c	critical flow water depth (m)
j	generic position referred to the vertical axis of coordinate system, defined as $j = y - y_f$, (m)
k	roughness coefficient on Colebrook-White formula (m)
K	friction multiplicative factor
L	wave length (m)
p	water pressure (Pa)
Q	flow rate (m^3/s)
Q_w	water flow rate per unity width (m^2/s)

Q_b	uniform base flow rate (m^3/s)
R	hydraulic radius (m)
R_e	Reynolds number
S_f	flow energy grade line slope
S_o	canal bed slope
S_c	critical flow bed slope
t	time (s)
T	water free surface width (m)
U	Ursell number
u	horizontal component of flow velocity (x axis direction) (m/s)
v	vertical component of flow velocity (y axis direction) (m/s)
v_s	water free surface vertical velocity (m/s)
V_t	tipping tank discharged volume (L)
x	generic position referred to the horizontal axis of coordinate system (m)
y	generic position referred to the vertical axis of coordinate system (m)
y_f	pipe bed vertical coordinate (m)
z	generic position referred to the horizontal axis of coordinate system (perpendicular to x,y plane) (m)
α	water surface vertical acceleration (m/s^2)
σ'	damp factor in Lax-Wendroff expression
ß	channel bottom local slope or bottom vertical acceleration in erodible beds (equation 2.54) (m/s^2)
γ	liquid specific weight (N/m^3)
ζ	flow water surface vertical coordinate (m)

η	water surface fluctuation level above the still or uniform flow water surface level (m)
ξ	elevation of a bed point (m)
σ	ratio d/L
τ	shear stress (N/m^2)
υ	kinematic viscosity (m^2/s)
ε	ratio η_{max}/d
ϱ	water density (kg/m^3)
Δt	computation time-step (s)
Δx	distance between adjacent grid nodes (m)
λ	$\Delta t/\Delta x$ ratio (s/m)

Subscripts

t, x and y partial differentiation in t, x and y respectively

J	rectangular grid node spatial order number

Superscripts

k	rectangular grid node time step order number
*	predictor time level
**	corrector time level

Abbreviations

HOT	higher order terms
LHS	left hand side (of a equation)
RHS	right hand side (of a equation)

CHAPTER 1

AN APPRAISAL OF THE STATE OF THE ART ON THE SANITATION FIELD AND THESIS PRESENTATION

1.1 Urbanization and Sanitary Conditions in Developing Countries on the XXI Century Threshold

By the end of this century, approximately 2.25 billion people will be living in cities of developing countries, corresponding to 45% of their population (Imparato et Abiko, 1994), while the same figure was 28.7% in 1980 and 33.4% in 1990. According to the Global Report on Human Settlements of March 1996 prepared for the United Nations Conference on Human Settlements, HABITAT II, held in Istanbul, from 3 to 14 of June, 1996, "about 500 million urban dwellers are homeless or live in inadequate housing". HABITAT II Bulletin recognizes that urban problems "is getting worse because housing cannot keep up with an exploding urban population, which will double from 2.4 billion in 1995 to 5 billion in 2025". The same Bulletin remarks that "substandard housing, unsafe water and poor sanitation in densely populated cities are responsible for 10 million deaths worldwide every year, and are a major factor in preventable environmental hazards, which are responsible for 25 per cent of all premature deaths worldwide. Water-borne

diseases alone kill 4 million infants and children annually.", (United Nations, 1996). Accordingly, water supply, sanitation and waste were specially focused on HABITAT II Conference through seven meetings.

1.1.1 The International Drinking Water Supply and Sanitation Decade

A central issue of the 1976 United Nations Conference on the Human Settlements (HABITAT I), held in Vancouver, was the deficit of clean water for drinking and absence of proper sanitation. The Conference called for a global approach to achieving full water supply and sanitation coverage in all countries by 1990.

The theme had strong influence on the United Nations Water Conference, held in Mar del Plata, in 1977. The Conference commonly agreed that "all peoples, whatever their stage of development and their social and economic conditions, have the right to have access to drinking water in quantities and of a quality equal to their basic needs" (United Nations, 1992). The Mar del Plata Conference made also more specific the Vancouver Conference approach by designating the period 1981-1990 as the International Drinking Water Supply and Sanitation Decade.

In December 1977, the General Assembly of the United Nations adopted the Mar del Plata Water Conference Report and, finally, on 10 November 1980, proclaimed the period 1981-1990

as the International Drinking Water Supply and Sanitation Decade. The primary goal of the Decade was to achieve full access to water supply and to sanitation for all inhabitants in developing countries by 1990. The majority of countries participating on the General Assembly however, stated that "service for all" was not feasible, and adopted instead other, more realistic, objectives, as the Mar del Plata Water Conference recommended (Kalbermatten, 1991). The Brazilian Government, for example, established as the goal for the Decade to supply 90% of the urban population with potable water and to collect sewage of 65% of the same population through sewage networks. For rural areas no figures were fixed (ABES/OPS, 1990).

According to Warner D.B. et Laugeri L. (1991) "the origins of the Decade lie in the growing international concern for global approaches to development problems that characterized the 1960s and 1970s. This concern was expressed in broad development strategies, such as the UNDP First and Second Development Decades, which began in 1960 and 1970, and in the Charter of Punta del Este, which set out a development strategy for the Americas in 1961". However, general development programmes could not meet the acute needs of water and sanitation. In the early 1970s, it was estimated that only one out of three persons in the developing countries had adequate access to potable water supplies and sanitary excreta disposal (67% unserved). In rural areas the situation was still worst: it was not uncommon to find less than ten per cent

of the population served with acceptable water and sanitation facilities (Warner et Laugeri, 1991).

1.1.2 The Decade Evaluation

Figure 1.1 shows the Decade performance on water supply and sanitation coverage according to the World Health Organization (Christmas et Rooy, 1991).

Coverage global numbers, referring to 1980 and 1990,

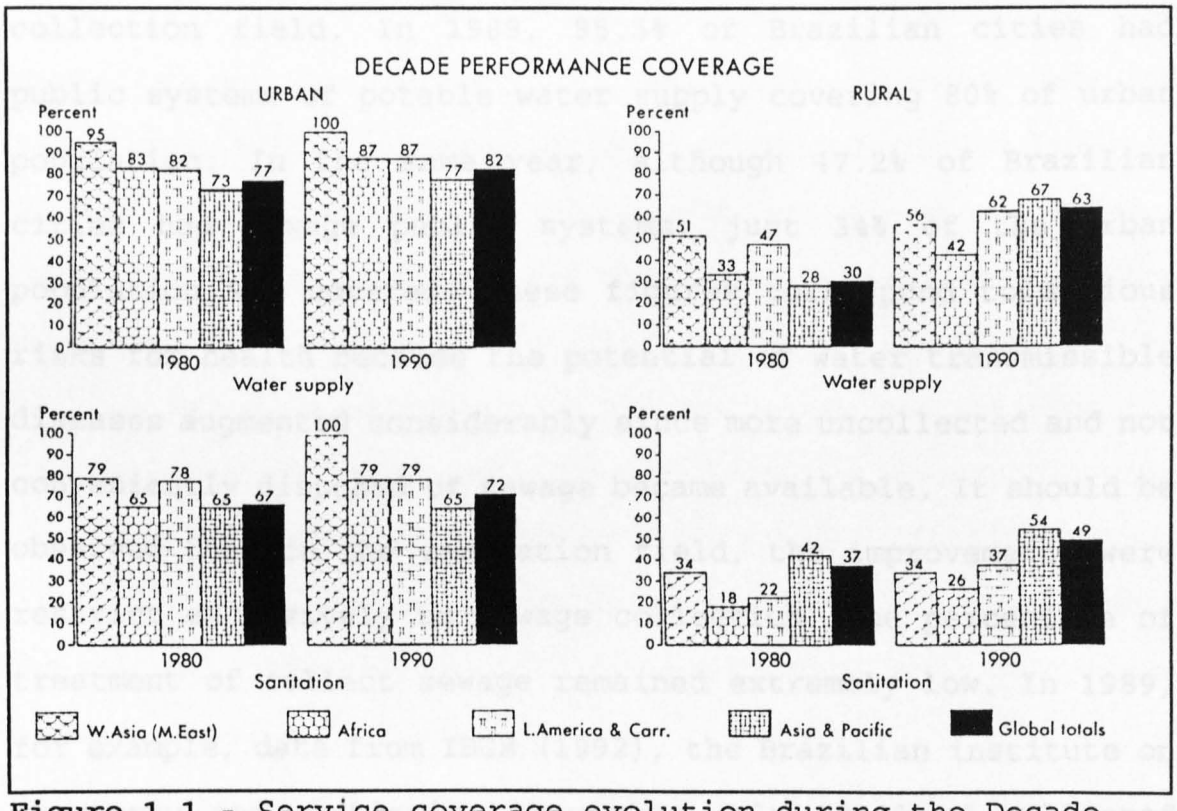

Figure 1.1 - Service coverage evolution during the Decade

are presented at Table 1.1.

Referring to Brazil, during the Decade its urban population enjoyed a significant growth of potable water supply

Table 1.1 - Global totals on water supply and sanitation (population in millions)

Global Totals	1980				1990			
	Population	Per cent coverage	Number served	Number unserved	Population	Per cent coverage	Number served	Number unserved
Urban Water	933.47	77	720.77	212.70	1332.22	82	1088.52	243.70
Rural Water	2302.99	30	690.25	1612.74	2658.51	63	1669.79	988.72
Urban Sanitation	933.47	69	641.39	292.08	1332.22	72	955.22	377.00
Rural Sanitation	2302.99	37	860.64	1442.35	2658.51	49	1294.72	1363.79

but, no corresponding evolution was observed in the sewage collection field. In 1989, 95.5% of Brazilian cities had public systems of potable water supply covering 80% of urban population. In the same year, although 47.2% of Brazilian cities had sewage public systems, just 34% of the urban population was covered. These figures correspond to serious risks for health because the potential of water transmissible diseases augmented considerably since more uncollected and not conveniently disposed of sewage became available. It should be observed that in the sanitation field, the improvements were restrict exclusively to sewage collection. The percentage of treatment of collect sewage remained extremely low. In 1989, for example, data from IBGE (1992), the Brazilian institute on geography and statistic, show that only 19.9% of collected sewage passed through treatment. For rural areas no reliable figures were available.

In a broad evaluation of the Decade Christmas J. et Rooy C. (1991) say that "though the Decade has not achieved its

numerical objective of universal access to water and sanitation, it has been quite successful in creating awareness about the sector and in developing workable strategies and models which enhance sector sustainability." For the same authors, since the primary goal of the Decade has not been achieved by the target year of 1990, "consequently, both the developing countries themselves, and the External Support Agencies have reached a broad consensus to continue the existing thrust" of the Decade, " beyond 1990, to coincide with the goal of "Health for All by the Year 2000".

An important evaluation of the Decade was the Global Consultation on Safe Water and Sanitation convened by the United Nation Development Programme and the Government of India. From 10 to 14 September 1990, about 600 experts from 115 countries met together in this event and produced the "New Delhi Statement", emphasizing the "some for all rather than more for some" approach.

Recognizing the merits of the Decade and pointing for the necessity to continue and improve its achievements aiming to reach full coverage on water supply and sanitation, since 33% of population remained unserved in 1990, the Global Consultation established four guiding principles to be applied on the 1990s:

1) Protection of the environment and safeguarding of health through the integrated management of water resources and liquid and solid wastes;

2) Institutional reforms promoting an integrated approach and including changes in procedures, attitudes and behaviour, and

the full participation of women at all levels in sector institutions;

3) Community management of services, backed by measures to strengthen local institutions in implementing and sustaining water and sanitation programmes;

4) Sound financial practices, achieved through better management of existing assets, and widespread use of appropriate technologies.

Referring to guiding principle 4, the Global Consultation showed that the need on investment in the developing world would be approximately US$ 50 billion per year. During the Decade, however, the actual amount invested on the sector was US$ 10 billion. Thus, "increased efficiency in the use of available funds" together with "mobilization of additional funds from existing and new sources" were recommended. Referring to research and development in developing countries, the New Delhi Statement urged for the maintenance and development in the next 10 years of the momentum established during the 1980s. Pointed also that "among the priority needs for the 1990s are improved household technologies for protecting water quality from source to mouth and low-cost waste-water disposal systems for low-income urban areas."

A few months after the New Delhi Global Consultation, the General Assembly of the United Nations passed the Resolution A/RES/45/181 to record sector accomplishments in the 1981-1990 Decade and to exhort the world to achieve even greater results in the future. In the same Resolution it is

emphasized "the importance of intensifying the co-ordination of national activities undertaken with the assistance of different agencies in the field of water supply and sanitation through the Steering Committee for Cooperative Action for the International Drinking Water Supply and Sanitation Decade and the Water and Sanitation Collaborative Council". The Water Supply and Sanitation Collaborative Council (WSSCC) had been created in 1988 by the Decade participant members, in Haia. In 1990, immediately prior to the global consultation the WSSCC was enlarged with the participation of developing countries members.

1.1.3 World Financial Needs on Water Supply and Sanitation

Aiming to have a financial panorama for universal coverage by the year 2000, Christmas et Rooy (1991) developed a costing model with respect to capital investment. This model was based on 3 technologies categories: high-cost, intermediate and low-cost technologies, applied to water supply and sanitation in urban, peri-urban and rural areas, respectively.

According to that study the 10-year capital investment cost in developing countries would be US$ 357 billion, being US$147 billion for water supply and US$ 210 for sanitation. These estimates imply in an investment of about US$36 billion per year over a 10 year period (1991-2000). Considering that the annual average during the Decade was US$ 10 billion and the world economic climate, Christmas et Rooy (1991) recognized

that a sector funding of US$ 36 billion annually would not likely to be forthcoming. Looking for a more feasible goal, or maybe a possible one, the same authors performed an analysis focused on population classe on the figures constituting the deficit of coverage. Considering the "provision of services of the needy (poor), herein categorized as the total rural population plus 50 per cent of the urban population (essentially peri-urban), it is clear that with only 30 per cent(US$ 110 billion) of the total investment (US$ 357 billion), over 2 billion needy people could be reached with sanitation and 1.6 billion with water supply". It has to be remarked that this exercise was performed basically through the use of essentially low-cost technologies and a few intermediate ones. It should be noticed that in the more viable criteria the model lead to a condition where the majority of unserved population in developing countries would be served. In fact, "30% of the total cost can service 80% of the unserved, if the low-cost option is emphasized" (Christmas et Rooy, 1991).

1.1.4 The Water Supply and Sanitation for All Struggle Pursuing

The Earth Summit Agenda 21, held in Rio de Janeiro, in June 1992, in its programme of action chapter 18 ("Protection of the quality and supply of freshwater resources: Application of integrated approaches to the development, management and use of water resources") established that "the general objective

is to make certain that adequate supplies of water of good quality are maintained for the entire population of this planet, while preserving hydrological, biological and chemical functions of ecosystems, adapting human activities within the capacity limits of nature and combating vectors of water-related diseases. Innovative technologies, including the improvement of indigenous technologies, are needed to fully utilize limited water resources and to safeguard those resources against pollution." Specifically to drinking-water and sanitation actions, Agenda 21 again reemphasized that "one realistic strategy to meet present and future needs, ..., is to develop lower-cost but adequate services that can be implemented and sustained at the community level" (United Nations, 1992).

New theories and integrated approaches, special broad cooperative schemes, expansion of multi-institutional partnership, community participation, new international mutual support agreements, scientific and technological development, etc., are all necessary because the world urbanization process, exhibits such impressive growth figures, bounded with its correspondent numbers related to poverty, human suffering, environmental degradation and threatens to national economies, that put the humankind in face of a risk condition never seem before on the planet's existence.

Although the increases of urban population in developing countries far exceed those in the more developed regions, grave urban problems are increasingly threatening people quality of life in megacities on developed countries,

as also revealed HABITAT II.

Referring to water supply and sanitation services the Brazilian Government plans presented to the HABITAT II Conference established an annual investment of R$ 2.2 billion (approximately the same as US$ 2.2 billion) per year to be applied up to year 2010, aiming to reach full coverage. This plan foresaw that by 1999, 80% of the population should be covered by sewage collection and that 40% of produced sewage would be treated. Unfortunately, that investment figure is far from the actually provided values to the sector by the Brazilian central government in the last years.

In Brazil, the present generally accepted estimate on water supply and sanitation service coverage through networks in urban centres account for 85% and 35% of covered population, respectively. A rough assessment, to give a magnitude order, shows that on sanitation would be necessary the construction of 200000 Km of sewage networks to obtain full coverage (Alves, 1993) on urban centres. But, the necessity exceeds network construction: IBGE data referring to 1991 shows that an average of 24,61% of population does not have toilets at home, including urban and rural areas. This need is more pronounced at north and northwest but, even other industrialized and urbanized areas present significative figures.

In a very recent survey, covering the period from 1993 to 1995, the Brazilian institute on geography and statistic reveals the proportion of houses covered with services both for urban and rural areas. The number of houses served with water from networks services increased from 75.4% in 1993 to 76.2%.

The number of houses without any sanitation decreased from 12.4% in 1993 to 11.4% in 1995. Referring to sanitation, three kinds of solution were considered in the survey: sewer networks that covered 39.1% of houses in 1993 and 39.5% in 1995; houses served with septic tanks, that were 19.9% in 1993 and 20.4% in 1995 and other kind of solution, 28.5% in 1993 and 28.7% in 1995 (IBGE, 1996).

The same institute points that urban growth will continue mainly through migration from field to medium and large cities. In very large cities and metropolitan areas the rate of growth shows declination.

The situation pictured shows that there is much to be done. Begun during the International Drinking Water Supply and Sanitation Decade period, the work presented here, aligns with many other initiatives pursuing solutions for sewer services, developing low-cost appropriate technologies.

1.2 Historical Tradition on Sewerage Systems

Refuse, or any of its enormous amount of synonyms and correlated meanings, seems to refer, in several era or human civilizations, to a concept included in the field of the things regarded as useless, non-essential, to be discarded, inopportune, non-productive, etc. Therefore, a nuisance, something absolutely undesirable. Something one would like to see very distant, or more probably, would like not to see. Waste water is a kind of these undesirable things.

These observations, obviously, generalize too much. The intention is to remark that a broad overview on human behaviour, at least since from Roman period hitherto, confirms that on urban centres of Europe and other countries formed through the influence of european culture, waste water is undoubtedly considered an undesirable thing.

This generalization on human behaviour related to refuse and, in particular, to waste water, is invoked by the necessity to understand another sort of historical observation: the technological development on sewer systems or, at least, the comparative development of these systems with technology development of other areas is very small. Particularly, sewer networks around the world remains essentially in the same stage they were about 100 to 150 years ago. Codes or technical papers about sewer networks of the end of last century and actual codes are not significatively different.

1.2.1 The Present Water Supply and Sanitation State of the Art

A historical review on sanitary services would pass through Indians, Egyptians, Mesopotamians, Greeks, Romans, the sanitary chaos of medieval era, up to the industrial revolution period, when cities implemented their infrastructure in a very similar form they are today.

Earliest community sanitary systems are reported to be found in India. José M. de Azevedo Netto, an eminent Brazilian

sanitarist, in an article published probably in the 50's, on the chronology of sanitation services, shows that in 3750 BC a sewer network was constructed in Nippur, India. Kalbermatten (1991) also mentions archaeologists report showing that as long as 5000 to 6000 years ago the cities of the Indus Valley had central water supply and waste water disposal systems.

It would be a very large historical period of different cultures to be analyzed. This is not the purpose of this work. It would suffice here to remark on the development of sanitary services since modern cities formation period. In the words of Kalbermatten, "the present state of the art was developed incrementally over a period of some 150 years. Of necessity, it is based as much on economics (use of already made investments and self-interest) as on scientific knowledge. Evidence suggests that, in the absence of 'sunk investment', the present state of the art is not the optimal solution to sustainable water supply and sanitation, indeed environmental services in general. Simply because something was right and appropriate in the past does not mean that it must necessarily be so under today's changed conditions" (Kalbermatten, 1991). Kalbermatten's appraisal intended to serve as an orientation to developing countries in a situation of service deficiency similar to those prevailing in industrialized countries a hundred years ago.

1.2.2 The Brazilian Water Supply and Sanitation Experience

Referring to Brazil, in particular, it should be noted that its pattern of urban development was basically influenced by European countries. Silva (1990) shows the intimate relation between economic and political dependence on European countries and the Brazilian sanitary sector development. An emblematic example of dependence quoted by Silva are the Roman type Arches of Rio de Janeiro, built around the end of eighteenth century, during the colonial period, to supply water to the city. This magnificent masterpiece, today a historical monument called "Arcos da Lapa", was constructed with stones brought from Portugal. Colonial government argued that there were not suitable stones in Brazil... Other example of dependence is given by the public fountains carved on in Portugal, Italy and France, to be installed all around Brazilian cities. But, these kind of problems were not only directly related to Portugal. Due to Portugal's heavy economic dependence on English manufactured products and the accumulated financial debts of the former to the latter, many English interests were transferred to Brazil, an important primary products producer that become also an important consumer market at the end of last century. This was true during the colony period (up to 1822) and was gradually intensifying up to the end of the century and first two decades of this century. Thus, many conventional water supply and sanitation systems would be constructed with pipes and other components and equipment produced in England. Many of these services were also

implemented and operated by English companies. But, from the last decades of last century onwards the Brazilian industry of components and equipments developed. Besides this growth, an important improvement on human technical resources was observed.

Is from the last decade of nineteenth century up to the first two decade of this century the remarkable work of the most important Brazilian sanitarist, Saturnino de Brito, that promoted a deep development on the Brazilian sanitary sector. He designed, invented and developed many components and equipments for building and public installation. His four models of flush tanks, the Santos and Recife sanitation programs and other cities network designs became famous technical references. Many water supply and sanitation networks designed and constructed by Saturnino de Brito, in several Brazilian cities, still are the basis of present networks (Saturnino de Brito, 1943).

As mentioned in Azevedo Netto sanitation service chronology, sanitary system implementation in Brazil were contemporary with those of European and north American countries. Thus, to conclude this assessment on Brazilian sanitary history, it can be said that the present state of the art in Brazil is the same as that of Kalbermatten evaluation referred to industrialized countries, except for some types of sewage treatment processes that are not broadly known.

A natural question on the reasons for the present Brazilian deficit on water supply and sanitation coverage would arise: if Brazilian systems are as old as in industrialized

countries and the technological patterns are the same as those practised in these countries, why did they not follow and reach the same level of coverage? The answer would require a lot of space but, it seems to be possible to condensate it. The Brazilian process of industrialization grew enormously from the 1940's to the 1980's. During this period the population rose from 41,2 million to 119 million inhabitants. In 1994 the country had 159 million. But, another phenomenon is more important: urban population growth was absolutely chaotic. The vegetative growth and the migration from rural areas and from poor cities and regions to industrialised areas was very intense. In 1994 77.6% (123.4 million) of the population lived in urban areas. Up to the 1940's the proportion between rural and urban population was approximately the inverse. On the other hand, the investments during this period were not enough to face the urban explosive growth and, in many cases, the adopted technology was not compatible.

1.2.3 The Sanitation Sector Evolution

Returning to the main characteristics of modern water supply and sanitation services, as they develop from medium nineteenth century hitherto, two main acquirement on the sector could be pointed: first was the creation of central municipal governmental bodies to implement and operate water and sanitation services, although it could be argued that this was not exactly a novelty because in the Roman empire, water and

sanitation were also governed by governmental bodies.

Another important moment was the strategic discussion on combined or separated sewerage systems. Many new systems constructed since them have opted for the separation of sewage and storm water, breaking with the old Roman tradition of a unique network.

Referring to technical aspects, significative conceptual changes on sewer network design and operation are exceptions considering the period from the end of last century to the present. The main question refers to the actual phenomenon occurring into the pipe interior. It was already known at that time that sewage contributions to sewer networks originated a flow regime type that could only be considered steady uniform in a rough approximation. The difficulty on assessing these contributions as well as to describe the unsteady flow had led to very rough simplifications. It should be remarked that was not a theoretical deficiency. Unsteady flow formula had already been developed and applied in 1848 by de Saint-Venant, for example.

Famous technical literature from the end of last century invariably treated collector pipe dimensioning in terms of rules of thumb. Normally minimum slopes or velocities were adopted based on a process of trial and error of certain early constructed networks being then used in other cities.

Saturnino de Brito, in 1900, established his own rules of minimum slopes, velocities and water depth in sewer collectors through the analogous values preconized by Americans and British authors from the two last decade of nineteenth

century (Baldwin Lathan, Waring(1889), Staley & Pierson and Moore(1898)). Among theses authors, the most advanced theoretical consideration was done by Saturnino de Brito in an attempt to compute the reach of a flush tank. In this case he used the propagation velocity formula for long waves of small amplitude to calculate the flow velocity of a flush tank discharge onto a collector pipe. But, the subsumed hypothesis on the existent base flow were completely unreal.

The main criteria on sewer design always was the self-cleansing property. Minimum slope or minimum velocity combined with minimum water depth, have been generally used as a guaranty for that property. Hydraulic variables are computed normally for a certain "design" flow rate, using steady uniform flow formula. These criteria are still in use, being required in several technical standards and codes.

To have an idea of these values in the past and now some authors may be cited . Referring to a 6" diameter pipes, Waring (1889) recommended a minimum slope of 0.0032 m/m, Baldwin Lathan and Staley & Pierson, quoted by Saturnino de Brito (1943), recommended 0.00704 m/m and 0.0050 m/m respectively. The British Water Authorities Association, in 1989, established the minimum slope of 0.0067 m/m for separated systems (Water Authorities Association, 1989). The computation through the Brazilian Standard would yield a slope of 0.0045 m/m. It should remarked that each value of these values is normally associated to other conditions as, for example, a minimum water depth. Additionally it should be remembered that in the past flush tanks were normally used at the head of

sewers.

Another technical aspect of importance refers to the use of flush tanks at the head of sewage collector pipes. Thousands of these devices were applied all around the world since the beginning of first sewer network construction. Several models and patents were registered. Between the second and the fourth decade of this century however, flush tank use was abandoned in most of cities. In São Paulo and Rio de Janeiro, for instance, they were abandoned during the 1940's and no problem with the network functioning was identified. It should be noted that in the abandonment period the situation had changed considerably. Generally the sewage contribution had augmented significatively due to natural higher occupation density on the area served by the network. It could be also remarked that new alimentary and other domestic habits have changed sewage characteristics.

As concluded by Alves (1990), flush tank abandonment brings a suggestive clue: minimum values for water velocity and for water depth providing self cleansing have always been mentioned for pipe collector design but, no reference was found for the same parameters when referring to flush tank flow behaviour. The ultimate conclusion is that these devices were applied in conditions of overdimensioning and that the ignorance in force in the past, did not permit the exploration of several possibilities of pipe line laying in drastically reduced slopes when using flush tanks. Technical mentioned reasons for the abandonment were the potential risk of cross connection between sewer and water supply networks and the use

of potable water in its use.

Referring to new approaches on on site sanitation certainly there is a lot to be explored. In the Brazilian case, for example, probably most of the houses without toilets at home are located in areas were conventional sewage network systems were not immediately feasible. In these cases, local systems serving one or a group of houses should be adopted.

However, in crowded cities, with high rate of land occupation and already endowed of sewer network, s e w a g e collection and transport to a distant point seems to be the natural solution. However, due to the very large, complex and costly sewer networks and treatment plants in metropolitan areas, a question has been posed: how large and sophisticated shall a sewer network and correspondent treatment plant be? Which would be the more rational, economic and environmental suitable size and type of a system? The absence of proper answers to these questions and inflexible technical traditional concepts have caused environmental catastrophes. In São Paulo city, for example, the pressure for sewage treatment in very large and costly plants and the explosive population growth has postponed any solution for sewage treatment for decades. The consequence is tragic: every river crossing the city has been transformed in open channel sewage conducts.

1.3 Innovative Techniques on Sanitation Systems

A significative number of studies, experiments and applications of new techniques and approaches on water supply and sanitation have been developed mainly since the beginning of the International Drinking Water Supply and Sanitation Decade.

Referring to sanitation systems much research and applications have been developed to attend a massive population living in circumstances in which conventional urban sewer systems are not suitable. These circumstances refer to rural areas of underdeveloped and developing countries as well as to millions of people living in the periphery of urban areas or even inside urban areas excluded from the necessary infrastructure of these kind of occupation. On site sanitation alternatives have gained special importance for these cases.

Pit latrines were the particular on site alternative that has been subject to major development. Ventilated pit latrines and pour-flush latrines have been studied, tested and developed under several surroundings of distinct countries in Africa (Botswana, Ghana, Kenya, Lesotho, Tanzania and Zimbabwe), in Brazil and India (Mara, 1984 and 1985).

Focusing more directly the sewer systems, i.e., that part of sanitary structures whose function is to conduct the sewage from its origin to treatment and final disposal, it will be shown in the sequence some new techniques also developed under the momentum of the Decade. In some new approaches, however, the traditional functions of sewage transport followed

by treatment are partially reversed as, for example, in the case of small bore system explained below.

1.3.1 Tractive Stress Concept Applied to Sediment Transport on Sewers

Departing from the concept of drag or tractive force of flow and data on experiments with sediment hydraulic transport, the Brazilian engineers Tsutiya et Machado Neto (1983) proposed the introduction of a more rational method for sewers design. In this method the self-cleansing requirement is accomplished through a minimum tractive force or tractive stress acting on discrete solid particles present on the sewage.

When liquid flows in a pipe it gives origin to a force on the canal bed in the direction of the flow. This force is called tractive, shear or drag force. Figure 1.2 illustrates the applicable scheme in the uniform flow case in a pipe.

In the uniform flow case this force corresponds to the flow weight component of a certain reach acting on the flow direction. Dividing this component by the area of the bed pipe where it acts it is obtained the tractive stress mathematically expressed as

$$\tau = \frac{W_L \sin \theta}{P L} \qquad (1.1)$$

In this equation W_L is the weight of the liquid in the reach of length L, θ is the angle between the pipe and

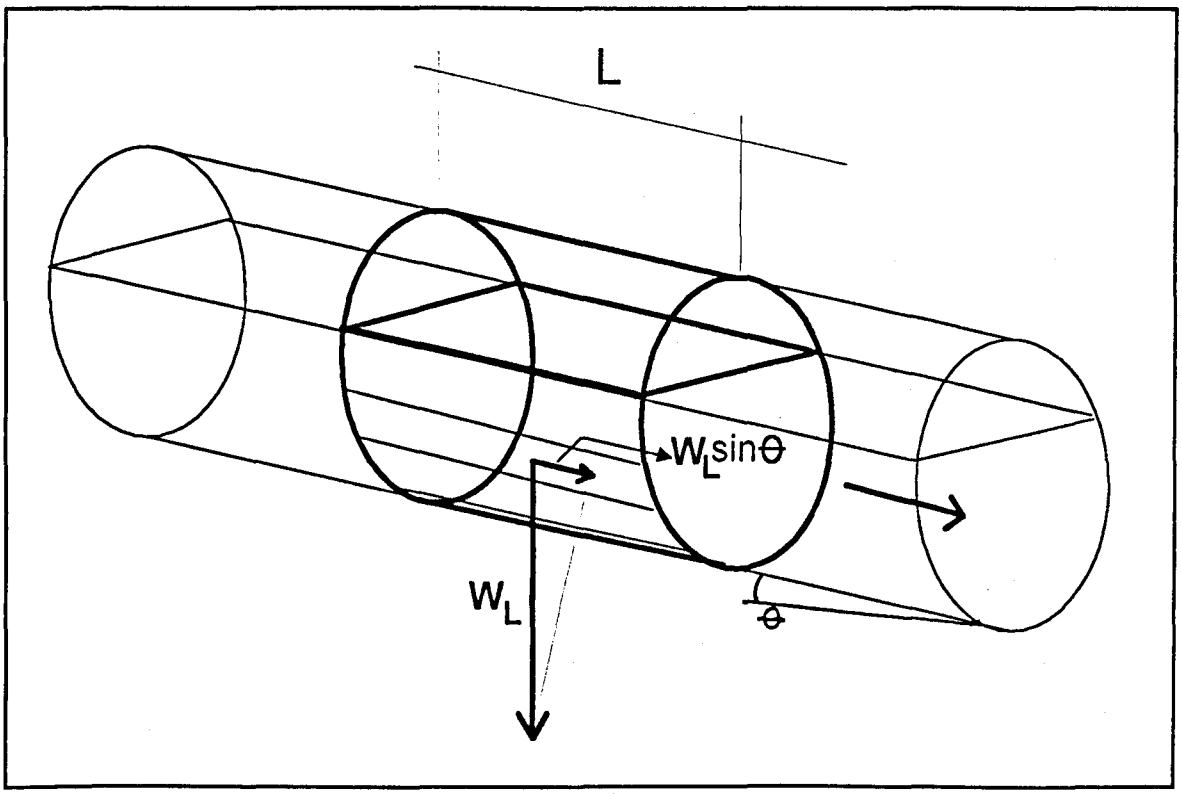

Figure 1.2 - Uniform flow tractive force scheme

the horizontal and P is the wet perimeter. Equation (1.1) can be simplified as follows

$$\tau = \frac{\rho g A L \sin\theta}{P L} = \gamma R S_o \qquad (1.2)$$

where ρ is the liquid density, g is the gravity acceleration, A is the wet cross sectional area, γ is the liquid specific weight and R is the hydraulic radius and S_o = tang θ is the pipe slope considering that for small θ, $\sin\theta = \tan\theta$.

Taking into account laboratory and field values of γ for sediment hydraulic transport, Tsutiya et Machado Neto (1983) proposed a minimum value for the mean tractive stress. This value, equal to 1 Pa, corresponds to a stress that promotes the beginning of movement of previously deposited

particles. On this criteria it would be sufficient that at least once a day the mean tractive stress reached the minimum value in a certain pipe section for the self-cleansing criteria to be attended.

The Brazilian standard for sewage collection networks (ABNT, 1986) adopted the tractive stress concept as a criteria for the self-cleansing requirement in separated systems. The minimum value of the mean shear stress in this standard is also equal to 1 Pa.

It should be remarked that the Brazilian standard establishes that hydraulic variables have to be computed through steady uniform flow formula. Thus, although the tractive stress concept brings more rationality to the design, still remains an enormous distance between the project and the reality since it is well known that flow in sewer pipes is essentially unsteady.

Another aspect of importance on deposit particle starting of movement can be observed in laboratory. Turbulence, in wave front for example, has a major role on particle movement initiation. In a simplified manner turbulence could be understood as a composition of water movement in the direction of flow and in the perpendicular direction. Thus, the tractive stress value could be not enough to describe the beginning of movement. This assertion is confirmed in rivers where, in the lose boundary layer, there is an intense particle movement that have been related to a certain level of turbulence associated with the flow velocity (Souza, 1994).

1.3.2 Sewer Design Based on a Rationally Computed Sewage Contribution

In 1962 the Brazilian sanitarist Eugenio Silveira de Macedo presented a new method for sewer design (Macedo, 1962) based in measurements of sewage hydrographs in areas already endowed of sewers and in the characteristics of the constructions pertaining to that area. Therefore, the method relates the hydrograph of a certain basin with its occupational parameters like: number of houses, constructed area, number of people, available sanitary appliances, etc. The development of this relationship permitted to establish patterns of sewage contribution of an area according to its characteristics. Using this method, the design of a sewer network, in terms of sewage contribution, depends on the present and expected occupational characteristics of the area to be covered.

On Macedo's method the sewer is dimensioned for the maximum sewage flow rate generated by the covered area. The maximum flow rate was computed through probabilistic analysis of sanitary appliances use as it was developed by Roy B. Hunter for domestic sewage installations. Analysing the several parameters of a certain area, Macedo (1962) observed that there was a minor variation between the constructed area and the contribution units mean rates. Considering peak attenuation, Macedo adopted new units and proceeded the computation as in Hunter development. The result was an excellent relationship between the maximum flow rate and the constructed area, proved through comparison with measured flow rates on the collector

pipes (Leme, 1977).

This method represents a significative advance compared with the widely used contribution assessment through mean sewage contribution based on generalized daily water per-capita consumption, present in many codes and standards. However, as in the case commented in 1.3.1, Macedo's method also consider the sewage flow in collector pipes in terms of steady uniform flow.

1.3.3 Unsteady Flow Analysis Applied to Sewage Pipe Flow

Together with a sensible assessment method of sewage contribution, the unsteady pipe flow analysis seems to be a major acquisition in the knowledge for a consistent development on sewer design and operation.

As early as 1848 de Saint-Venant derived the long wave unsteady flow equations. However, up to the advent of the digital computer and further development of numerical methods the application of these equations have been limited to isolated flow problems because its use implied hard and lengthy manual numerical solution in conjunction with graphical methods. Thus, since the middle of the 50's computers have been in use for calculating non-stationary channel and river flow expressed by the Saint-Venant equations (Priessmann, 1976).

In open channels the Saint-Venant equations are theoretical applicable to flow with mild surface variation or, on other words, with mild streamline curvatures. As will be

analyzed in detail in Chapter 2, this requirement corresponds to the hypothesis of hydrostatic pressure distribution on the water depth. For large streamline curvatures nonhydrostatic pressure distributions can be produced. This is the case of a steeped wave front, for example. The equations incorporating large streamline curvatures effects were developed by Boussinesq and presented in 1872 (Boussinesq, 1872).

The development of an unsteady flow model for building drainage systems have been developed by Swaffield since 1980 (Swaffield, 1980; Swaffield et Galowin, 1989). Although the models have been produced for the analysis and design of a building drainage networks, its structure and embodied theories and procedures can be adapted and developed to be used in public sewers.

Several models using unsteady flow analysis are presently available for design and operation of sewer networks. However, probably all of them, have been developed for combined systems or only for urban storm systems. Separated sewage systems have specific structural and functioning characteristics quite different from combined systems thus, requiring specific models.

A sewage separated system model should incorporate building sewage contributions, constituted by hydrographs, similar to those used in Swaffield's building drainage system model. These contributions could be standardized according to particular patterns of covered area occupation using, for instance, the methodology developed by Macedo (1962). In this case, instead of using a maximum flow rate value, it would be

determined typical contribution hydrographs according to present and expected occupational patterns. The flow on pipes and singularities would be described through the unsteady flow equations.

The development of a sewage separated model would be a major contribution to the design and operation of sewers. Field and laboratory work would be necessary to feed such model. Sediment hydraulic transport on unsteady flow conditions and frequency and type of sewage contribution, seems to be the main aspects to be studied.

1.3.4 Reduced Slope Sewers Using Intermittent Discharge Devices

The opportunity of intermittent discharges application through flush devices in building installations was renewed on the context of low volume sanitary appliances use in water conservation programmes. In 1981 in the "Instituto de Física da Universidade do Rio de Janeiro" (Institute of Physics of the University of Rio de Janeiro), work for the development of a tipping tank to be installed in building drains was carried out. Inspired on the Brazilian initiative, researchers at Brunel University, London, carried on works to develop a tipping tank able to work in a building drainage installation (Wakelin et alii, 1982). Two types of tipping tanks fed by nonfecal waste waters were successfully tested in building installations.

Also under the water conservation objectives an intermittent tank based on siphonic action was developed and successfully tested in building installations in Sweden.

The main question on water conservation programme actions based on low volume sanitary appliance use was on the possibility of solid deposition due to the lower amount of water transporting sewage solids. Discharges of low volume WC caused particular concern. Further field tests have shown, however, that the use of reduced discharge volume W.C. did not require the aid of additional discharges through these devices.

The use of flush tanks is associated with the development of modern building and public sewage installations. Murray (1982) quoting Wright (1980) shows the earliest reference of flush tanks use describing a tipping tank used to flush a water closet in 1718 in England. Several types of these devices were developed and largely used in building and mainly in public sewers (Alves, 1990).

As mentioned in section 1.2.3 flush tanks were applied in public sewers in a condition of ignorance over its real behaviour in terms of the actual role of the generated flow.

The idea of flush tank use in public sewer networks was retaken in 1986 in the Instituto de Pesquisas Tecnológicas do Estado de São Paulo - IPT, ("Institute for Technological Research of the State of São Paulo"), Brazil. However, now, the objective was to explore the wave generation action in collector pipes as a means of drastic diminishing of pipe slopes mainly in flat areas leading to sewer construction cost reduction.

The implantation of sewer networks in flat areas is particularly problematic. Maintaining the minimum slope that assure the self cleansing of sewage collector pipes implies increasing depth of pipes that leads to high construction costs. In flat areas with an elevated water table, and with soft organic soils, for example, the cost will be much higher. The exemplified conditions of soil and water table will not rarely be found in a great number of flat coastal cities. Additionally the incidence of pump stations has to be considered.

The magnitude of excavation costs can be appreciated with some figures extracted from a technical paper presented to the Brazilian Congress of Sanitary and Environmental Engineering where the authors presented the cost of implantation of two networks (Accioli and Fernandez, 1981). The rate of earth works costs to the total cost in the first network was 91.5% and 68.5% in the second. The high cost incidence of timbering in the first case is responsible for the pronounced difference. Although these are isolated examples, in general earth works costs are normally very significative. Obviously, all the possibilities looking forward the reduction of this item are very important.

Under these conceptions, a research program exploring intermittent discharge use on sewer networks was undertaken at Heriot-Watt University, Department of Building and Engineering Surveying. The program aimed to develop a tipping tank apt to operate in sewer systems being fed by fecal and nonfecal sewage and to develop a mathematical model for the generated wave

modelling.

A tipping tank was designed, constructed and tested in laboratory and in the field. The experimental device showed good performance on its capability of discharging regularly all its contents and on its property of generating a steeped front wave (Alves, 1990).

The referred field test was carried on at the University campus aiming to show the tank performance on discharging fecal and nonfecal waste waters. A new field test is presently being prepared. Now a specially designed tipping tank will be installed in a more typical condition, i.e., in a reach of a urban sewer network laid in a very low slope.

The experimental tank developed during the research was designed to generate a discharge with good properties of solid particle transportation. This objective was plentifully reached since the device discharge produced a steeped front wave showing the ability of initializing and transporting solid particles previously deposited at the pipe invert.

The photography in Figure 1.3 is a demonstration of the wave front steepness. This photo was taken in the glass pipeline of the laboratory rig. The wave front "foot" in this case is in a position distant about 2.8 m from the pipeline entrance. The wave was originated from the experimental tank discharge.

Figures 1.4 to 1.8 illustrate the experimental tipping tank generated flow evolution through fixed segments of the pipe on the laboratory rig. In all cases the tipping tank discharged 39.5 L, being the pipe slope equal to 0.0005 m/m.

Figure 1.4 refers to the wave passing sections between 2 m and 3.5 m of distance of the pipe entrance. The previously steady uniform flow rate (base flow) on the pipeline was zero. Figure 1.4 shows the wave passing the same positions but, now with a base flow rate equal to 0.1 L/s.

On Figure 1.6 the central metallic clamp on the pipeline is on a section distant approximately 9 m from the pipeline entrance. In this case the base flow rate is 0.1 L/s.

Figure 1.7 illustrates the wave reaching the pipeline end, distant approximately 14 m from its entry. The base flow rate is 0.1 L/s.

Finally, Figure 1.8 shows the very high level of turbulence of the wave entering the pipeline.

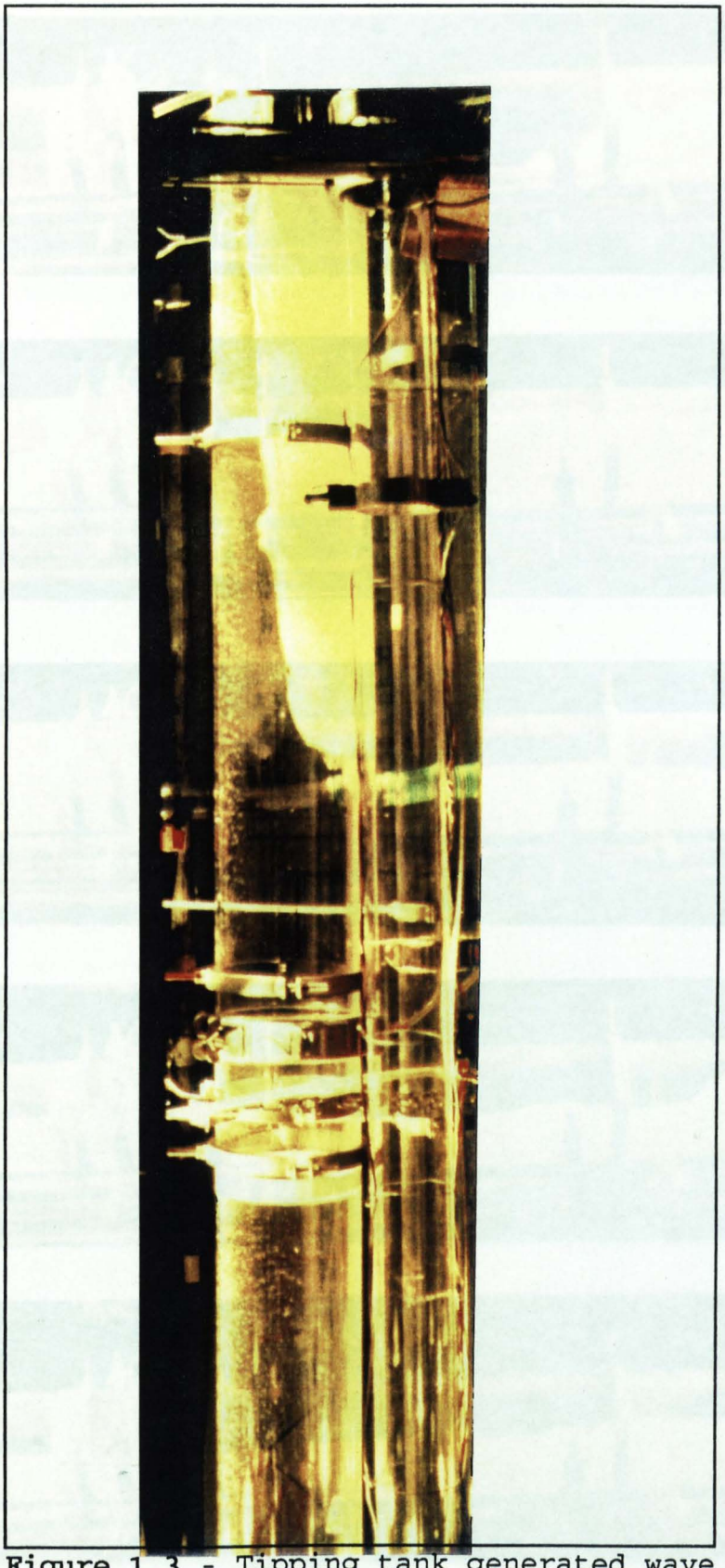

Figure 1.3 - Tipping tank generated wave in the laboratory rig

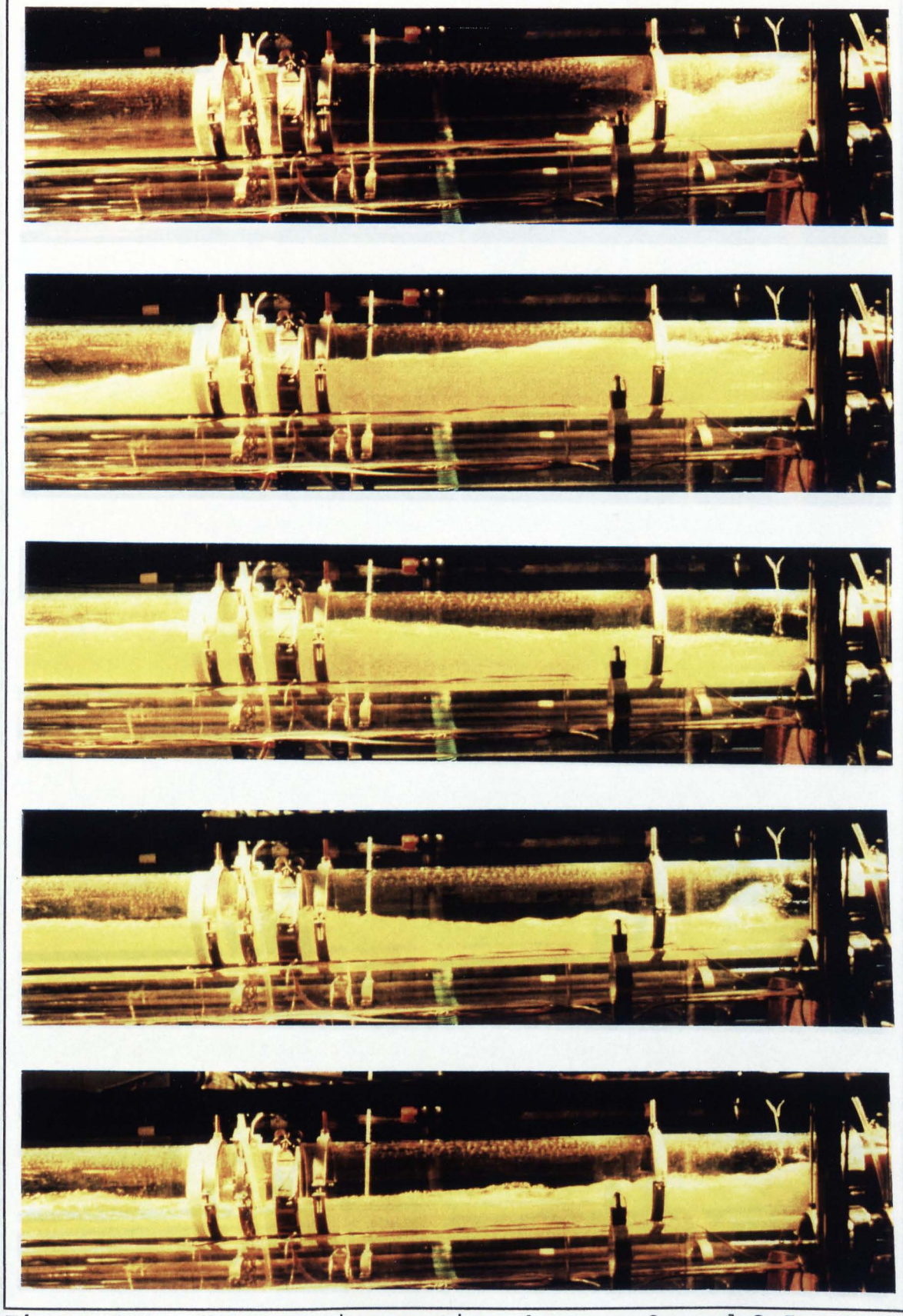

Figure 1.4 - Wave passing sections between 2m and 3.5m; Q_b=0

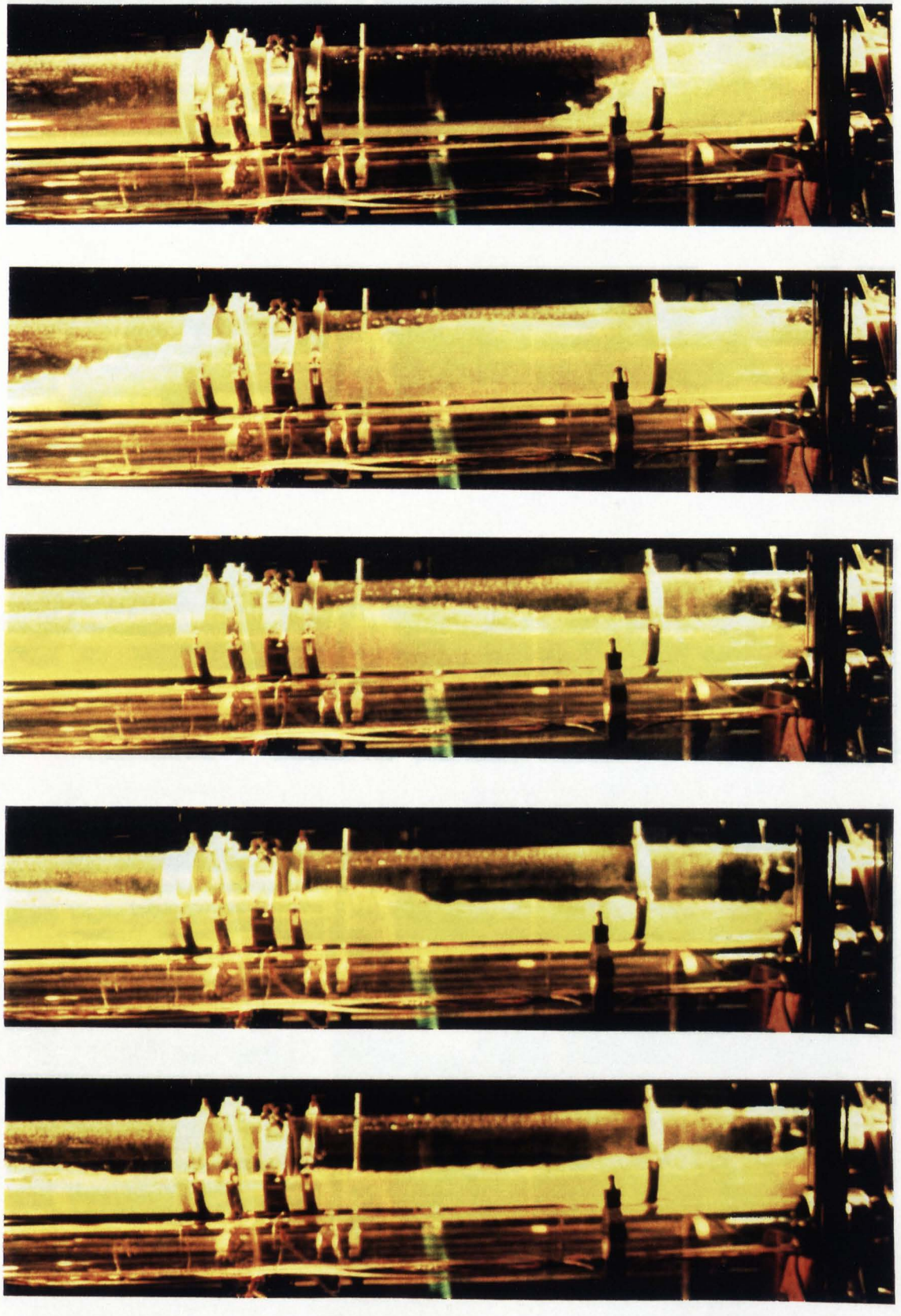

Figure 1.5 - Wave passing sections between 2m and 3.5m; Q_b=0.1 L/s

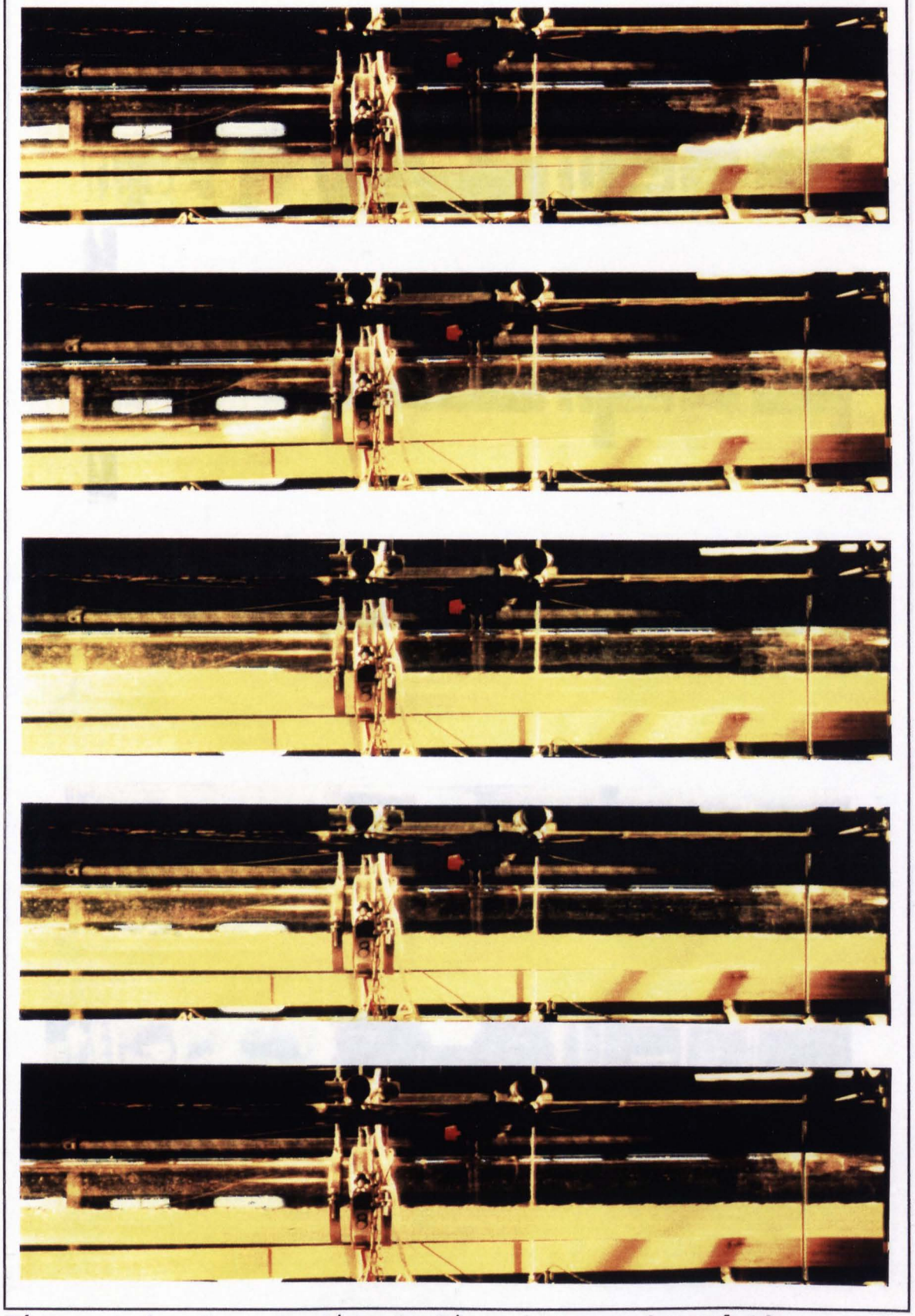

Figure 1.6 - Wave passing sections between 8m and 10m - Q_b=0.1 L/s

Figure 1.7 - Wave in the pipeline end (14 m) - Q_b=0.1 L/s

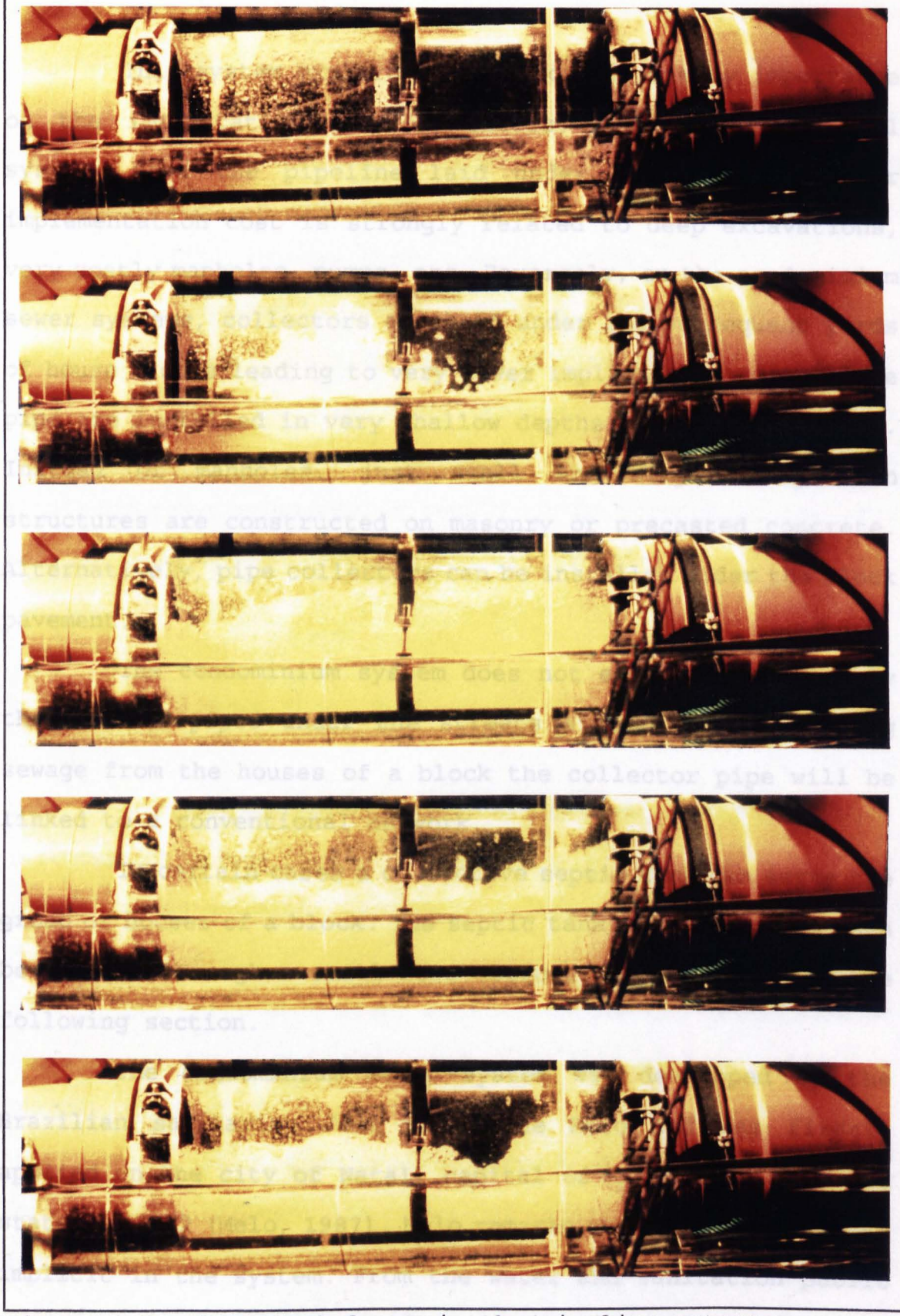

Figure 1.8 - Wave turbulence in the pipeline entrance

1.3.5 Condominium Sewer Systems

This system explores one aspect of primary importance on the implantation cost of sewers. Because conventional systems have the pipeline laid under the streets, their implementation cost is strongly related to deep excavations, very costly manholes, pumps, etc. Reversely, on the condominium sewer systems, collectors are laid under the subsequent yards of house blocks leading to very lower implantation costs since pipe are installed in very shallow depths (0.30 m to 0.50 m). Instead of manholes, just small and simple inspection structures are constructed on masonry or precasted concrete. Alternatively, pipe collectors can be installed under the block pavement.

The condominium system does not eliminate completely the need of pipes under the streets since after collecting sewage from the houses of a block the collector pipe will be linked to a conventional network.

In certain cases a collective septic tank can serve the group of houses of a block. The septic tank effluent would then be conduct through a small bore network, as described in the following section.

The condominium sewer system was developed by the Brazilian sanitarist José Carlos de Melo and was firstly applied on the city of Natal, capital of Rio Grande do Norte state, in 1982 (Melo, 1987). Melo remarks two important aspects implicit in the system. From the water and sanitation public company point of view, the block of houses is considered as a

unique point to be covered, i.e., the block is taken as an actual vertical condominium. Thus, the company will have only one connection of the condominium collector to the public network under its responsibility. On the other hand, the block dwellers have to establish a mutual acceptance on the system since the construction and maintenance of the condominium collector will be under their responsibility.

The condominium sewer system started to be applied in districts of very irregular pattern of land occupation in Natal city but, now, it has been implemented in very regular districts of Brasilia, for example. The system has shown to be very effective on several types of urban occupation patterns and has been widely applied in Brazilian cities.

1.3.6 Small Bore Sewer Systems

Conventional sewer pipelines are dimensioned to conduct non-treated sewage. Although solid is a very small part of sewage (0.08% to 0.1%), solid deposition in pipes always was the main concern.

The small bore sewer system explore the advantages of conducting primary treated sewage. In this system, sewage is firstly treated in interceptor tanks, usually designed as septic tanks, being then conduct through small bore pipelines. Septic tank effluent is free of settleable solids and, depending on the treatment efficiency, also part of dissolved solids will be removed.

According to Otis et Mara (1985) this system has four principal advantages: a) reduced water requirements because there will be no solids to be hydraulic transported through the network; b) reduction excavation costs since sewers do not need to be designed to maintain a minimum flow velocity for self-cleansing. The pipeline can be laid following the natural topography more closely than the conventional system; c) reduced material costs because peak flows are much lower than those experienced with conventional systems requiring pipes and pumping equipment reduced in size. Additionally, manholes can be replaced with much less costly cleanouts or flushing points; d) reduced treatment requirements since the septic tank performs treatment processes thus, eliminating the necessity of anaerobic ponds or other equivalent treatment structure.

The critical points for a good performance of the small bore sewer system are the need for periodic evacuation and disposal of solids from each interceptor tank and the guaranty that sewage containing solids will not be introduced in the network (through illegal connections, for example). These conditions lead to the necessity of a well established organism for the system operation and control.

The small bore sewer system can be used to upgrade existing sanitation facilities. That would be the case of certain areas where septic tanks is a tradition but, proper destination for its effluent is not available. The system also would be indicated in areas where the water low volume availability would impede conventional sewers.

Small bore sewer systems applications have been related

in Zambia, Australia, Nigeria, United States and Brazil (Otis et Mara, 1985; Cynamon, S.E., 1986).

The Brazilian sanitarist Szachna Eliasz Cynamon developed a very interesting alternative for the septic tank sludge removal. Normally the sludge is removed pumping it to a truck-mounted tank, being transported to drying beds. In many cases trucks are not available and in other cases the septic-tanks are located in non-accessible places. Considering these difficulties Cynamon developed a sludge drying system incorporated to the septic-tank. This innovation permits that the sludge dries out beside the septic-tank being easily removed with manual tools. Another innovation on the small bore systems implemented by Cynamon was the use of siphonic action discharges on the pipeline regions where the velocity was lower than 0.1 m/s (CEPAM, 1988).

1.3.7 Simplified Sewer Networks

The simplified sewer network has been developed incorporating a series of new approaches and techniques aiming to obtain a rational procedure for the design of low-cost and appropriate solutions. The design criteria have been organized in a Technical Manual published by the Brazilian federal government (Guimarães, 1987).

Basically the simplified sewer network system adopts the following concepts and techniques:

a) the sewer hydraulic design uses the same method as in conventional systems. Hydraulic variables are computed assuming steady uniform flow;

b) the sewer is designed considering the particular position of each connection to the house building drainage installation;

c) pipes are designed to be laid on the minimum possible depth;

d) the network is designed considering the more economic possibilities of geometric disposition. Thus, it is admitted that pipe collectors can be laid under private properties, crossing blocks, etc., requiring owners concordance;

e) the condominium sewer system is adopted as an alternative;

f) the small bore sewer system is also adopted as an alternative;

g) systems are delimited through the concept of small basins of sanitation according to the natural topography avoiding the complicated transposition of sewage through several basins.

Networks using these concepts have been designed and implanted in some cities of Rio de Janeiro.

1.4 Thesis Presentation

The work here presented is part of a research program aiming to develop technological alternatives for the implementation of more economic and appropriate sewer networks.

One particular technological alternative pursued is the intermittent discharge devices use as a means of drastic

reduction of collector pipe slopes. This thesis is more directly related to this alternative.

A central directive on the research is the development of a better knowledge on sewer system functioning as a means of substituting the old empiric criteria for more rational and modern concepts. One important part of this development is the description of flow behaviour in sewers and for that it is very clear that the unsteady flow approach must be applied. Pipe conduction hydraulic capacity, sediment hydraulic transport, needs for ventilation, etc. can be better described through the unsteady flow approach.

Intermittent discharge device generated flow, as well as building sewage contributions flowing through sewers, are governed by the hydrodynamic equations where hydraulic variables vary continuously in time and distance. Therefore, the development and application of these equations to flow in sewers is of the foremost importance.

1.4.1 Objective

The thesis objective is to present the development of a model directed to simulate the flow generated in sewers through intermittent discharge device operation. The development includes mathematical and numerical model derivation and improvement and a computer program to process numerical solutions.

The basic hypothesis is that the flow modelling will

provide a more economic and appropriate tool for the design, construction an operation of sewers.

1.4.2 Field of Application

The model is suitable to be applied in all kinds of unsteady partially filled pipe flow.

Application can be extended to flow on other types of open channel of fixed bed, i.e., without loosed sediment at the bottom.

1.4.3 Research Methodology and Development

In the first phase of the research an intermittent discharge device based on the tipping action was developed (Alves, 1990).

A literature survey and discussion, together with flow behaviour characteristics observed in the laboratory, oriented the mathematical and the numerical model development. These models are presented in Chapter 2 and 3 respectively.

Departing from the mathematical and numerical model a first version of a computer program was produced to process numeric calculations. The computer program characteristics are presented in Chapter 4.

A model validation process was carried on. In this process simulated results obtained through the computer program

were compared with the corresponding laboratory measured values, as presented in Chapter 5.

An adjustment iterative process to calibrate the model was performed, aiming to validate it. Chapter 6 presents the results of the calibration process. In the iterative procedure new developed versions of the computer program were required.

CHAPTER TWO

FREE-SURFACE UNSTEADY FLOW GOVERNING EQUATIONS

2.1 Introduction

The analysis of flow characteristics from direct visual observation of a tipping tank discharge on the horizontal laboratory rig, together with consideration of the main patterns of open channel flow, has been shown to be a very useful approach for governing equation development.

Figure 2.1 illustrates the tipping tank generated wave profile in the laboratory pipeline. The wave front, F-H, is passing through the pipe segment I-II distanced respectively about 1.0 m to 3.0 m from the pipe entrance. The pipeline end (A) is a free overfall of the 14 m length rig. The wave is generated by the tipping tank discharging onto a previously established steady-uniform pipe base flow.

In fact Figure 2.1 exhibits the interaction of the most characteristic types of open channel flow. From point C to D the water surface profile is parallel to the pipe bed. In any section located in this segment the velocity is constant with time. Every section exhibits the same velocity profile that is usually represented by the depth averaged velocity. The

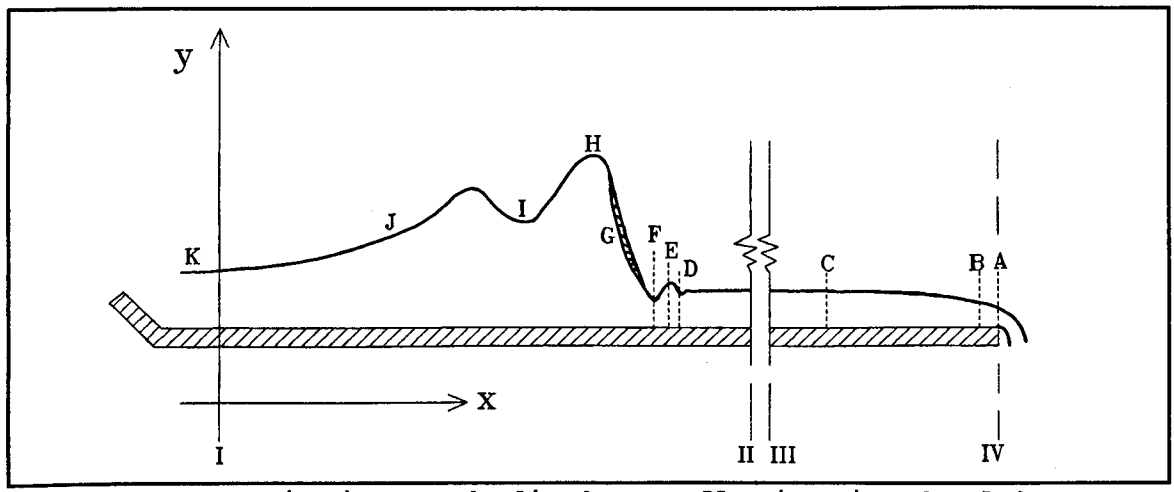

Figure 2.1 - Tipping tank discharge flowing in the laboratory horizontal pipeline

vertical water particle acceleration components can be neglected and the pressure distribution through a vertical line in each section is hydrostatic. The flow is classified as steady-uniform in this segment, as long as it is not reached by the moving wave, in which case both the water depth and velocity will vary with time and space.

Segments B to C and J to K correspond to profiles where the flow is said to be gradually-varied. In this case the curvature of the water profile is mild with a gradual change in the water depth along the length of each respective segment. The pressure distribution can still be considered hydrostatic along any vertical line because the water particles do not present strong vertical accelerations components relatively to the total acceleration. In any section the velocity is considered to be constant with depth and is usually computed as the depth averaged velocity.

Upstream of point B up to point D the flow has Froude numbers less than unity, being, therefore, subcritical. From

point B, where the flow is at critical depth, the profile decreases up to a minimum depth at the free overfall (section IV). In each flow section at A-B segment the pressure distribution can not be considered hydrostatic because the presence of significant vertical water particle acceleration which can be assessed from the pronounced water profile curvature in this area. However, A-B length is very small and thus in practical computation usually the critical depth is assumed to be at the free overfall (Ranga Raju, 1981).

The segment J-K, as water depth and velocity vary with time during the flow development, is classified as unsteady flow. The velocity can be assumed constant with depth, but has to be computed for each particular moment. On the other hand the water surface profile and the velocity at B-C segment remain unaltered with time as long as the wave does not reach it. In this segment the flow is classified as steady gradually-varied flow. Between points A and B water profile and velocities are also in steady state but the flow is classified as rapidly varied since water depth changes are pronounced.

Segment F to H illustrates an area where the water surface presents an inclination that strongly departs from those before discussed above. This is clearly a rapidly-varied flow zone. As the velocity and the water depth vary with time the flow is classified as unsteady rapidly-varied. The wave front profile remains steep during its passage along the entire pipeline length.

In the reach comprised between sections I and II, mainly on its initial part, the wave front, F-H, presents

some turbulence similar to that observed in hydraulic jumps.

The pronounced profile curvatures around points F and H indicate that significant vertical water particle acceleration are present and therefore the pressure distribution along any vertical in this zone can no longer be considered hydrostatic. Details on the pressure distribution will be evident from the subsequent mathematical analysis.

The velocity distribution in the wave front can not be considered uniform (Terzidis et Strelkoff, 1970) although the horizontal water velocity component is assumed to be constant with water depth and is usually represented by the depth average for each particular moment. However, now there is a vertical velocity profile to be considered. Thus the flow is no longer one-dimensional, as assumed in all former cases, although it will be possible to reduce it to an one-dimensional case in the equation development.

The water profile between H and J is of a transition type. The presence of a second hump upstream of the wave front can be observed in Figure 2.1. In certain tipping tank discharges, mainly in the beginning of the pipeline, the inclination of the water profile of this second peak was as abrupt as the wave front, although it suffered a mild attenuation as it travelled downstream along the pipeline. Thus, the H-J segment has the same properties as the wave front, i.e., unsteady rapidly-varied flow, in the beginning of the pipe, tending to the unsteady gradually-varied flow at the end.

An overview of the entire phenomenon shows that there

is a short zone of rapidly-varied flow propagating in a steady-uniform or steady gradually-varied field that can be thought of as a segment bounded by two cross sections of essentially hydrostatic pressure distribution and nearly uniform velocity distribution. Describing a similar phenomenon Terzidis et Strelkoff (1970) state that "the flow pattern on the low-depth side is totally unaffected by the bore until the latter actually arrives; on the high-side, the zone of rapidly-varied flow gradually merges with the long wave behind".

The friction between the liquid and the pipe plays different roles according to the flow type. For the steady uniform and the unsteady gradually-varied flow areas the friction has a significant effect and will be taken into account; in the region of the wave front many authors consider that it can be neglected, although some others recommend more research on this aspect (Basco, 1983). In fact, the friction between liquid and pipe seems to be an open subject, however some specific application can be found in the literature. Standing (1986), for example, assuming unsteady gradually-varied flow for a wave similar to that presented here, defined a practical form for friction effect reduction at the wave front.

Concerning the effect of water inter-particle friction and collision occurring in the flow as a whole and in particular in the wave front, where it is more important, the difficulties are even greater comprising another field of research.

2.2 Free Surface Unsteady Flow Literature Review

The literature review, mainly focused on rapidly-varied, free surface unsteady flow, was aimed at the identification of mathematical formulations and hydraulic related parameters applicable to the description of the tipping tank generated wave and its simulation. It was found that rapidly-varied flow could more advantageously studied as its formulation reduced to the gradually-varied case as well as to other simpler flow cases.

Basco (1983) considered that, in large surface gradient free surface flows, the assumption of hydrostatic pressure is no longer valid. Spiked river hydrographs in steep gorges, canyons and channels, rapid reservoir releases, dam breaks, etc, are mentioned by Basco as examples of rapidly-varied flow. Also in hydraulic structures such as spillways, control and measurement devices (weirs, flumes, gates), energy dissipators, and near sudden slope changes rapidly-varied flow can be created. In these situations the presence of large streamline curvatures can introduce a significant departure from hydrostatic pressure profiles that in turn may have an important additional effect in the momentum balance (Basco, 1989). McCowan (1985) also included in the same field undular hydraulic jumps and bores, and short waves in shallow water, in both one and two horizontal dimensions.

The case being studied here is also an example of a flow where the inclusion of large streamline curvatures effects may be proved to be pertinent.

2.2.1 Boussinesq Equation

In unsteady rapidly-varied flow zones the water particle movement shall be decomposed into at least two components, i.e., in the main direction of flow, normally horizontal, and in the vertical direction. However, this two-dimensional flow can be reduced, in mathematical terms, to a one-dimensional form if vertical accelerations effects on the pressure distribution are incorporated to the horizontal motion. This procedure was first presented by Boussinesq in 1872 and has been developed leading to the several forms of the Boussinesq equations, presented at section 2.2.3.

According to Boussinesq's basic assumption, in each section the water particle horizontal velocity can be taken as constant with depth and the magnitude of the vertical velocity may be assumed to increase linearly from zero at the bed to a maximum at the free surface. In general, any momentum equation that accounts for the effect of superposition of forces induced by the vertical acceleration upon the hydrostatic pressure forces, in this simplest way, is called the Boussinesq equation (Abbott, 1979).

According to Basco (1983), the basic Boussinesq equations in one dimension for an uniform cross-section, with a horizontal bottom, neglecting bed and surface stresses are

$$h_t + d\,u_x + u\,h_x = 0 \qquad (2.1)$$

and

$$u_t + u\,u_x + g\,h_x = \frac{1}{3}d^2\,u_{xxt} \qquad (2.2)$$

corresponding respectively for mass and momentum conservation. In the above equations, $h = \eta + d$ is the total water depth, η the instantaneous water surface fluctuation about the still or uniform flow water surface level and d the uniform flow or still water depth. The instantaneous depth-averaged flow velocity is given by u and g is the gravitational acceleration. Subscripts indicate partial differentiation in respect to the independent variables x and t, respectively, space and time.

Equation (2.2) is identical to the non-linear long wave or nearly horizontal flow Saint Venant momentum conservation equation except for the third order derivative term at the right hand-side, (RHS), called the Boussinesq or dispersive term. The third order derivative term accounts for streamline curvature effects that alter both the vertical pressure distribution and the vertical velocity distribution, giving rise to an additional horizontal momentum (Basco, 1989). The Boussinesq term can be derived directly from the non hydrostatic pressure distribution resulting from the water vertical velocity variation assumption as will be demonstrated in section 2.2.3.

The difference between the second term of left hand side (LHS) of equation (2.1) ($d.u_x$) and the corresponding $h.u_x$ of Saint Venant's equation will be commented in the next section.

2.2.2 Boussinesq Equation Position in Water Wave Theories

Assuming that the depth of water is sufficiently small compared with other significant lengths, such as, for example, the radius of curvature of the water surface, Stoker (1957) derived shallow water theory. According to Stoker the water is considered to be shallow when the square of the ratio of a typical flow depth to a typical flow length is a small quantity. The basic assumption of shallow water theory is that the vertical component of the water particle acceleration has a negligible effect on the pressure. This is the same as considering that the pressure profile is hydrostatic with water depth.

In this theory it is not necessary to assume that the water surface displacement and slope are small as is usually done for waves of small amplitude. Accordingly the theory is also called finite-amplitude shallow water theory.

Starting from exact hydrodynamical equations, Stoker (1957) obtained the basic finite amplitude shallow water theory equations as the approximation of lowest order in a perturbation procedure where all quantities were developed in terms of the ratio of the original water depth to a characteristic length associated with the horizontal direction. In this derivation process the hydrostatic pressure distribution is a logical consequence.

The shallow water theory is a theory commonly referred to in hydrodynamics texts as the theory of long waves since this latter theory embraces waves whose ratio (still water

depth)/(wavelength) are much smaller than one. Its equations can be linear in its lowest accuracy form, or non-linear to a higher level of accuracy.

The shallow water theory, in its lowest approximation, as derived by Stoker, is the theory most used by engineers in dealing with flows in open channels and, according to Peregrine(1966), is an adequate approximation for most shallow-water flows if an empirical friction term is added (Abbott et Rodenhuis, 1972).

Studying short waves in shallow water, Abbott et al. (1978) showed that what are called "short" waves in engineering practice are in fact subsumed under long wave theory in classical hydrodynamics since their length is still large compared with the depth of water in which they propagate.

The finite-amplitude shallow water equations in one dimension for rectangular uniform cross-section, on a horizontal bottom neglecting bed and surface stresses are

$$h_t + h\,u_x + u\,h_x = 0 \qquad (2.3)$$

$$u_t + u\,u_x + g\,h_x = 0 \qquad (2.4)$$

Equation (2.4) does not have the Boussinesq term appearing in (2.2) and equation (2.3) differs from (2.1) only in the second term of LHS. The reason for this second difference is the order of magnitude of the water surface variation (η) that is considered to be very small in (2.1) thus h≈d.

Starting from Euler's equations and suitable boundary conditions, and performing a power series expansion procedure, the mass equation (2.3) and the motion equation (2.4) result in the lowest order approximation, i.e., all terms in these equations are zero order terms. Following the expansion process the Boussinesq equations can be derived in the next order approximation level. Therefore, the Boussinesq equations can be regarded as the second order approximation equations of shallow water theory arising from the basic Euler's formulation.

Stoker (1957) showed that Keller, in developing a similar scheme, found that Friedrichs' shallow water theory, when carried out to second order approximation, yields both the solitary wave and cnoidal waves of the type found by Korteweg and de Vries (1895). These wave types are special cases simulated through Boussinesq equations.

Ursell (1953) mentions that Boussinesq derived his equations from potential theory in the earliest mathematical description of the solitary wave, firstly observed by J. Scott Russel in 1843 (Boussinesq, 1871), and extended his theory to unsteady flow. The engineer Scott Russel observed solitary wave formation and travelling when stopping the animals used to pulled the boats in the canal joining Edinburgh to Glascow in that time.

Abbott et al. (1978) regards the Boussinesq theory as the most uniformly valid basis for finite amplitude water wave models so long as the ratio (water depth)/(wavelength) remains small and wave breaking does not occur.

In the formal analysis of long wave theory two scaling parameters have importance. One is the ratio of amplitude to depth

$$\varepsilon = \frac{\eta_{max}}{d} \tag{2.5}$$

that is a measure of the degree of non-linearity of the flow and the second is the ratio of depth to wavelength (L)

$$\sigma = \frac{d}{L} \tag{2.6}$$

whose square is a measure of the dispersive effects caused by streamline curvature (McCowan, 1985).

Using appropriate scales Peregrine (1967) put the equations in dimensionless form and assumed that all expanded variables and their derivatives were of order O(1) so that when the expansions were made, the order of magnitude of each term in the equations appeared explicitly.

Referring to Peregrine's work McCowan (1985,1987) and Basco (1983) showed that non-dimensionalization and expansion processes for the Boussinesq equations, using ε and σ as scale parameters, provided an assessment of the relative order of magnitude of each term in the equations (2.1) and (2.2), depicted by the characters in brackets below each respective term, as follows

$$h_t + d\,u_x + u\,h_x = 0 \qquad (2.1)$$
$$[1] \quad [1] \quad [\varepsilon]$$

$$u_t + u\,u_x + g\,h_x = \frac{1}{3}d^2\,u_{xxt} \qquad (2.2)$$
$$[1] \quad [\varepsilon] \quad [1] \quad [\sigma^2]$$

Therefore the Boussinesq equations contain terms of order (ε, σ^2), being higher order terms neglected in this approximation. It is apparent in the above equations that the convective acceleration term and the Boussinesq term have equal importance when $\varepsilon \approx \sigma^2$.

Reduced equations referring to different types of waves can be obtained if certain terms in equations (2.1) and (2.2) are neglected.

If the term of σ^2 order is eliminated, then the non-linear long wave equations or the Saint Venant equations for horizontal bed frictionless flow appear. Therefore, $\sigma^2 << \varepsilon$ is a criterion for Saint Venant equations applicability. In this case Basco (1989) points out that each part of the solution travels at a local speed dx/dt = u ± (gh)½ (the Lagrange celerity) so that the higher surface elevations tend to overtake the low sections with time. Thus, the wave travels with variable form, continually steepens and eventually wave break can occur. This tendency is called amplitude dispersion or non-linear dispersion and is dependent on the non-linear character of the equations associated with the scaling parameter ε. Basco shows that the applicability of the Boussinesq equations up to the breaking limit on beaches is an active research area.

In the wave model classification adopted by Ponce et Simons (1977), the Saint Venant equations (including bed slope and friction effects), would correspond to the dynamic wave while, without friction and bed slope effects, it would be called gravity wave.

If the terms of order ε and σ^2 are small they can be neglected, resulting in the lowest order accuracy linearized equations. These are the linear long-wave equation set of classical wave mechanics. In this case the wave has a permanent form and moves with celerity c = (gd)½ .

$$h_t + d\,u_x = 0 \qquad (2.9)$$

$$u_t + g\,h_x = 0 \qquad (2.10)$$

Another possibility arises from eliminating only terms of ε order from (2.1) and (2.2). This results in a linearized version of the Boussinesq equation where vertical accelerations, resulting from streamline curvature, produce a celerity, on a horizontal bed, equal to

$$c = \frac{(g\,d)^{1/2}}{[1 + \frac{4\pi^2 d^2}{3L^2}]^{1/2}} \qquad (2.11)$$

where L is the wavelength of any wave component in the solution. Each Fourier wave component of a long wave disturbance now travels at its own speed depending on its wave length. This tendency is termed frequency (or wave-length) dispersion (Basco, 1987).

The full Boussinesq equations, applied to a horizontal-bed flow, maintain a balance between amplitude and frequency dispersion, i.e. $\varepsilon \approx \sigma^2$. In this case it simulates a progressive wave of permanent form in shallow water called the cnoidal wave by Korteweg and de Vries (1895). The limiting case of cnoidal waves occurs when the wavelength tends to infinity and that is the case of a solitary wave that consists in a single hump wave of constant shape and constant velocity.

Ursell (1953) developed a criterion for applying the Boussinesq equation and special cases with terms omitted on the basis of the scaling parameters. Ursell defined the following relation, later called the Ursell number:

$$U = \frac{(\textit{wave amplitude/water depth})^3}{(\textit{wave steepness})^2} = \frac{\left(\frac{\eta_{max}}{d}\right)^3}{\left(\frac{\eta_{max}}{L}\right)^2} = \frac{\eta_{max} L^2}{d^3} \qquad (2.12)$$

It can be shown that the Ursell number relates to the above defined parameters ε and σ through

$$U = \frac{\varepsilon}{\sigma^2} \qquad (2.13)$$

becoming apparent that the Ursell number makes comparison between amplitude dispersion (ε) and frequency dispersion (σ^2).

Basco (1983,1989) defines a field for equation application, through relations (2.14), as follows:

$U > 1$ *Nonlinear, long-wave de Saint-Venant equations*

$U = O(1)$ *Nonlinear, quasi-long wave Boussinesq equation*

$U < 1$ *Linearized Boussinesq equation*

In these relations O(1) means the value is on the order of unity. According to Basco these relations have to be considered as a rough guide for engineering use. Basco (1983), quoting Peregrine (1967), mentions that the region where U is comparable to unity is applicable to cnoidal wave theory, already verified against experimental data. The expression "quasi-long wave" is not explicitly defined by Basco, but it seems that its origin is the fact that the Boussinesq equation is applicable to a condition where the long wave parameter σ is not small. A possible explanation is to consider the actual phenomenon where a certain wave can initially be described by the long wave equations, thus having $\sigma << 1$, but the progressive overtaking of water layers leads to a steeper wave front, a condition where the Boussinesq equation is applicable. However the wavelength is now not so long as before, i.e., σ becomes greater. The same consideration led Peregrine to consider that the finite-amplitude long wave equations are not uniformly valid (Peregrine, 1967, 1968).

The applicability of criteria involving the σ parameter to the tipping tank generated discharge can not be directly performed mainly because the difficulty of defining the wavelength (L) in the actual wave.

The equation of motion is rather more complicated for

sloping beds and will be analyzed in the next sections.

Finally, to conclude, the Boussinesq theory, in a condensed form "can be considered applicable for finite-amplitude quasi-long waves propagating in shallow water where the interplay between nonlinearity (convective acceleration term), dispersiveness (Boussinesq term) and bottom curvature or slope (additional terms) are critically intertwined", Basco (1983).

2.2.3 Different Forms of Boussinesq Equations

Discussing, in 1974, the mathematical formulation presented by Abbott et Rodenhuis in 1972, Peregrine presented several different approaches to the derivation of Boussinesq equation (Abbott et Rodenhuis, 1974). McCowan (1985) and Basco (1987) also give accounts of these different approaches.

This multiplicity is mainly due to the accuracy of the terms retained, different simplifying assumption and methods of derivation, different adopted dependent variables, algebraic manipulations and transformations of terms using the linear nearly horizontal flow equations (Abbott et Rodenhuis, 1972; McCowan, 1985; Basco, 1987).

2.2.3.1 Abbott's Engineering Derivation

Following Boussinesq (1872), Abbott developed a so

called "engineering derivation" to obtain the equations. This method is the simplest way to demonstrate how the effects of vertical acceleration can be introduced.

Firstly consider Euler's equations for a two-dimensional flow.

$$u_t + u\,u_x + v\,u_y = -\frac{1}{\rho}\,p_x \qquad (2.15)$$

$$v_t + u\,v_x + v\,v_y = -\frac{1}{\rho}\,p_y - g \qquad (2.16)$$

Then, as stated in 2.2.1, Abbott assumed that the vertical velocity, **v**, increased linearly from zero at the bed to a maximum $\mathbf{v}_s$ at the surface. Thus the vertical velocity is given by

$$v_s = \frac{dh}{dt} = h_t + u\,h_x \qquad (2.17)$$

If the convective term (uh_x) is neglected, the vertical velocity along the water depth can be written as

$$v = v(y) = h_t\,\frac{y}{h} \qquad (2.18)$$

Taking the vertical component of Euler equation without its convective terms and introducing into it equation (2.18) provides

$$\frac{y}{h}\,h_{tt} - \frac{y}{h^2}\,(h_t)^2 = -\frac{1}{\rho}\,p_y - g \qquad (2.19)$$

Following Boussinesq's (1872) methodology, Abbott (1979) neglected the powers of derivatives as compared with

derivatives themselves. Thus equation (2.19) reduces to

$$\frac{y}{h} h_{tt} = -\frac{1}{\rho} p_y - g \qquad (2.20)$$

that, when integrated from the free surface, y = h, where p = 0, to an generic elevation y in the liquid, provides

$$p(y) = \rho g (h - y) + \frac{\rho}{2h} h_{tt} (h^2 - y^2) \qquad (2.21)$$

that express the pressure variation with depth.

It can now be seen that the pressure profile is given by the hydrostatic component plus an extra term corresponding to the vertical velocity. The second order time derivative introduces the effect of the vertical acceleration on the pressure.

The pressure expression (2.21), can then be introduced in the horizontal Euler equation giving (2.22) as follows

$$\frac{du}{dt}|_y = -g (h - y)_x - \frac{1}{2h} h_{ttx}(h^2 - y^2) - \frac{1}{2h} h_{tt} (h^2 - y^2)_x$$

that again can be reduced, neglecting the product of derivatives, to

$$\frac{du}{dt}|_y = -g (h - y)_x - \frac{1}{2h} h_{ttx} (h^2 - y^2) \qquad (2.23)$$

If the horizontal velocity is assumed constant with depth and defined through the depth average, i.e.

$$\overline{u} = \frac{1}{h} \int_0^h u \, dy \qquad (2.24)$$

then, deriving (2.24) and using (2.23), it can be written that

$$\frac{d\overline{u}}{dt} = \frac{1}{h}\int_0^h \{-g\,(h-y)_x - \frac{1}{2h}\,h_{ttx}\,(h^2-y^2)\}\,dy \qquad (2.25)$$

$$\frac{d\overline{u}}{dt} = -g\,h_x - \frac{h}{3}\,h_{ttx} \qquad (2.26)$$

Finally taking (2.15) in terms of average velocities, substituting it in (2.26) and suppressing the bar over u, yields Abbott's form for the Boussinesq equation.

$$u_t + u\,u_x + g\,h_x + \frac{h}{3}\,h_{ttx} = 0 \qquad (2.27)$$

2.2.3.2 Different Simplifying Assumptions

Depending on the simplifying assumptions adopted on the engineering derivation, different forms of the Boussinesq equations can be obtained.

McCowan (1985) shows that if the convective term were retained in equation (2.17) it would result in a new form for the momentum equation,

$$u_t + u\,u_x + g\,h_x + \frac{h}{3}\,(h_{ttx} + u\,h_{txx}) = 0 \qquad (2.28)$$

and if the horizontal convective term of Euler's vertical equation, (2.16), were also retained, it would have result in equation (2.29) as follows

$$u_t + u\,u_x + g\,h_x + \frac{h}{3}\,(h_{ttx} + 2\,u\,h_{txx} + u^2\,h_{xxx}) = 0$$

Further, if bed slope effects are included and the product of derivatives and third order space derivative terms

are not neglected, it would have result in a more complete momentum equation

$$u_t + u\,u_x + g\,h_x = -\frac{1}{h}\left[\left(\frac{B}{2} + \frac{A}{3}\right) h^2\right]_x - \left(B + \frac{A}{2}\right) d_x \quad (2.30)$$

where $A = D^2(h)$, $B = D^2(d)$, being D a derivative operator defined through $D(\theta) = (\theta)_t + u.(\theta)_x$, $\theta = f(x,t)$.

According to McCowan (1985) equation (2.30) is a Boussinesq momentum equation of the type first derived by Serre in 1953, and is consistent with the equations used by Hauguel (1981). Expanding its right hand side would result in the same third derivatives as given in (2.17) along with another 23 third order product and/or bed slope terms.

Seabra Santos (1986) and Carmo (1990) show that Serre's equations were originally derived for a horizontal bottom and differ from equations (2.1) and (2.2) also because Serre's equations are applicable to finite-amplitude while Boussinesq's original equations are restricted to small amplitude waves in shallow water.

The analysis of the order of magnitude of Boussinesq equations through the non-dimensionalization process shows that equations (2.27), (2.28), (2.29) and (2.30) are all equivalent to Boussinesq original equation (2.2) down to order (ε, σ^2) although they do include an increasing number of terms in higher orders of ε and σ^2 (McCowan,1985).

2.2.3.3 Transformations Using Linear Long Wave Equations

Alternative forms of Boussinesq equations can be

obtained transforming third order derivatives using the linear long wave equations. This procedure was extensively used by Boussinesq in the 19th century.

According to the arguments presented in section 2.2.2 the Boussinesq equations can be considered to be a second order approximation to the long wave equations. Peregrine (Abbott et Rodenhuis, 1972) states that this means that terms such as uu_x and u_{xxt} may be rewritten by using equations (2.9) and (2.10). Basco (1983), quoting Long (1964), shows that this is possible because third order derivatives can be rewritten by means of first order relations and still maintain third order accuracy.

For example, if equation (2.9) is derived in x and t it would result

$$h_{xtt} = - d\, u_{xxt} \qquad (2.31)$$

Thus the Boussinesq term can be rewritten as

$$\frac{1}{3} d^2\, u_{xxt} = - \frac{1}{3} d\, h_{xtt} \qquad (2.32)$$

Through this new form, it is clear that when the free surface varies most rapidly, the Boussinesq term will have the most influence on the solution.

If other forms of long wave equations are used in these transformations care must be taken to ensure that the required order of approximation is maintained (McCowan,1985).

The transformation procedure can be an useful tool in the numerical computation process depending on available data.

2.2.3.4 Different Derivational Procedures and Order-of-Magnitude of Terms

More modern, rigorous methods of derivation have been developed. Basco (1983) makes a detailed analysis of the three main groups of such methods. Based on Basco's work, the results of each of these methods will be presented, mainly focusing on the more valuable formulations concerning the specific application to tipping tank generated flows.

The presented equations in all methods reviewed here were developed for one-dimensional flow in wide, rectangular channels where the local water depth and hydraulics radius are identical. For the governing equations, developed in section 2.3, suitable adaptations will be considered.

A key aspect of the Basco analysis is the relative order-of-magnitude of equation terms in each method. As will be shown, different methods and respective scaling parameters do not lead conclusively to a unique set of comprehensive equations.

The first procedure was the asymptotic expansion method. Peregrine (1966,1967) and Mei et LéMéhauté (1966) were the first to employ expansion procedures to derive the Boussinesq equations for water of variable depth. In Peregrine's derivation both ε and σ^2 are relatively small, i.e. much less than unity.

Peregrine (1967) introduced the two above mentioned scaling parameters, ε and σ, and expands all the dependent variables, η, p, and u in terms of the nonlinearity parameter

ε in the form

$$f = f_o + \varepsilon f_1 + \varepsilon^2 f_2 + \ldots \qquad (2.33)$$

where f is a dummy variable standing for η, p or u. The vertical velocity, v was expanded in terms of the frequency dispersion parameter σ and also ε as

$$v = \sigma(v_o + \varepsilon v_1 + \varepsilon^2 v_2 + \ldots) \qquad (2.34)$$

First considering a horizontal bottom, Peregrine's derivation put Euler's inviscid fluid equations (continuity and motion) with correspondent boundary conditions and irrotational motion condition onto a dimensioless form. The still water depth (d) is used as reference length and $(gd)^{1/2}$ is used as the reference velocity. As also commented in section 2.2.2, all expanded variables and their derivatives are assumed to be of order O(1) so that when expansions are made, the order of magnitude of each term in the equations appears explicitly.

Power series developments of each variable. i.e., expanded variables, are then inserted into Euler's equation to obtain, by equating coefficients of like powers of ε and σ, equations for the successive coefficients in the series. The zero-order solution gave the equation of statics, the first-order approximation are the linearized, long wave equations and the second order approximation leads to Boussinesq type equations (Peregrine, 1967).

Referring to flows with variable water depth Basco (1983) quoting Peregrine, shows that the same procedure may be followed but new length scales should be considered. For one-dimensional frictionless flow on uniform sloping beds,

Peregrine's expansion procedure gives, respectively for mass and motion equations:

$$\eta_t + (d + \eta)\, u_x + u\, h_x = 0 \qquad (2.35)$$

$$u_t + u\, u_x + g\, h_x - g\, d_x = \frac{1}{3}\, d^2\, u_{xxt} + d\, u_{xt}\, d_x \qquad (2.36)$$

In equation (2.36), $d_x = S_o$ is the constant bottom slope. For a condition $\varepsilon << 1$, η is very small compared with d and the mass equation (2.35) reduces to equation (2.1). By comparison with equation (2.2), water depth variation introduces two new terms in the motion equation. In the case of a horizontal bottom, i.e. $S_o = 0$, (2.36) reduces to equation (2.2).

As signalled by Basco (1983), the fundamental aspect of the expansion derivation by Peregrine is the consistency in the order-of-magnitude of terms retained. In equations (2.35) and (2.36) all terms of higher order ($\varepsilon.\sigma^2$, ε^2, σ^4, etc.) are omitted under the conditions that $\varepsilon \approx \sigma^2 < 1$ and $\sigma \geq ß$ where ß is the local bed slope. The last restriction limits the applicability of Boussinesq equation derived by expansion methods to small bed slopes.

Basco (1983) quoted that Mass and Vastano developed another set of Boussinesq equation employing variational methods. Working with the formulation developed by Mass and Vastano, Basco (1983) presents a reduced form for the equations considering finite amplitude waves in water of variable depth. In this derivation all products of derivatives and third spaces derivatives are neglected except those involving bottom gradients and bottom curvature terms. Conservation of mass equation is identical to (2.3) and the resulting motion

equation abandoning bottom curvature terms is

$$u_t + u u_x + g h_x + g \xi_x = -\frac{1}{3} h h_{xtt} - \frac{2}{3} u h h_{xxt} - (\frac{1}{2} h u_{xt} + u h u_{xx}) \xi_x + H.O.T. \quad (2.37)$$

where $\xi_x = -S_o$ is the uniform bottom slope and H.O.T. stands for "higher order terms". Except for the bottom gradient terms equation (2.37) equates with the momentum equation derived by Whalin for finite amplitude flow on horizontal bottom also using variational methods (Basco, 1983).

Comparing Peregrine's derivation and the last method the main differences between the small amplitude and finite amplitude assumptions in the derivation process may be seen. Firstly, in the mass equation (2.3) the full water depth h appears in contrast with equation (2.1) or the reduced form of (2.35). Referring to the motion equation it can be seen that the variational method produces a primary Boussinesq term [(-1/3) h h_{xtt}] and a second Boussinesq term [-(2/3) u h h_{xxt}].

Through equation (2.35) it is possible to show that

$$-\frac{1}{3} h h_{xtt} - \frac{2}{3} u h h_{xxt} = \frac{1}{3} h^2 u_{xxt} - \frac{1}{3} u h h_{xxt} \quad (2.38)$$

so that the primary Boussinesq term of equation (2.37) differs from the Boussinesq term of equation (2.36) in the coefficient of u_{xxt}, that in the finite amplitude case is the square of the full water depth h.

Concerning the bed slope terms, equation (2.37) contains an additional term (uhu_{xx}) compared with Peregrine's small amplitude equation (2.36). Basco (1983) shows that this

term is of higher order ($O(\varepsilon.\sigma^2)$) and thus could be consistently abandoned if the maximum order of equation retained terms is (ε,σ^2), as in the case of the Peregrine derivation. The remaining term ($1/2hu_{xt}$) was found to be significant by Peregrine, except he did not get the (1/2) multiplier in the bed slope term. The reasons for the discrepancy are not available in the literature.

Another important characteristic when comparing derivation through variational methods and Peregrine's expansion method is that in the latter it is assumed that the motion is irrotational while in the former the flow is rotational (Peregrine, 1967; Basco, 1983).

A third rigorous approach for the derivation is called the conservation method or method of direct fluid sheets. The method begins with the differential equations of continuity and energy. It is assumed that the velocity field is uniform with depth in the horizontal direction and that the vertical velocity varies linearly with depth, as in all the previous methods presented. Thus the flow is rotational in the horizontal plane as normally occurs in shallow water with large wave amplitudes relative to water depth (Basco,1983).

Basco(1983) presents two derivations using the conservation method. Naghdi produced a motion equation with both the Boussinesq terms of equation (2.37) plus 16 additional terms consisting of products of derivatives and third order space derivatives. For a rectangular channel of horizontal bed, the Venezian derivation lead to the usual mass equation (2.35) and, for motion, to the equation (2.39) in the Eulerian form

as follows:

$$u_t + u\,u_x + g\,h_x + h\,h_x(u_x^2 - u_{xt} - u\,u_{xx}) + \frac{1}{3}\,h^2\,(u_x\,u_{xx} - u_{xxt} - u\,u_{xxx}) = 0 \qquad (2.39)$$

If product of derivatives and third space derivatives are neglected in equation (2.39) the resulting Boussinesq term is the same as in equation (2.37) when equation (2.38) is substituted in its RHS. However the Boussinesq secondary term [(2/3) u h h_{xxt}] does not appear.

Equation (2.39) is also consistent with Serre's equation type what can be obtained developing, for example, equation (2.30).

Basco (1983) put the equations derived by Venezian in dimensionless form in order to study the relative order-of-magnitude of the individual terms. In this analysis Basco used a set of scaling parameters also utilized by Mass and Vastano, obtaining for mass conservation the dimensionless equation

$$h_t + (\epsilon)\,h\,u_x + (\epsilon)\,u\,h_x = 0 \qquad (2.40)$$

and for the momentum, equation (2.41)

$$u_t + (\epsilon)\,u\,u_x + (\frac{\sigma}{\epsilon})\,g\,h_x = \frac{1}{3}\,(\sigma^2)\,h^2\,u_{xxt} + (\sigma^2)\,h\,h_x\,u_{xt} + O(\epsilon.\sigma^2)$$

In these dimensionless equations the nondimensional variables (u,h,x,t) have magnitudes of the order unity and the coefficients of each term give a scale to each term.

The differences in the order-of-magnitude of equations (2.1), (2.2) respectively to (2.40) and (2.41) are apparent. By comparison with equation (2.2) it can be seen that the

convective term and the Boussinesq term still have lower magnitude in equation (2.41) but now the pressure term can also be lower than the local acceleration term. As in equation (2.2) the convective term and the Boussinesq term are equally important when $\varepsilon \approx \sigma^2$. However a result of paramount importance refers to the second term at RHS. It results from a product of derivatives being other terms, except the Boussinesq term, of $O(\varepsilon.\sigma^2)$ and smaller. The key conclusion is that not all derivative products are of minor significance. The non dimensional Venezian momentum equation shows that a certain product of derivatives can be as important as the Boussinesq term itself for finite-amplitude waves. The same dimensionless analysis applied to the sixteen additional terms of the Whalin equations revealed that seven terms are of $O(\sigma^2)$, two of $O(\sigma^2/\varepsilon)$ and the remaining seven of higher order $O(\varepsilon.\sigma^2)$ (Basco, 1983).

The same scaling parameters applied to equation (2.37) with the RHS substituted by equation (2.38), adopting the bed slope term as derived by Peregrine and abandoning the bottom curvature term gives the dimensionless equation (2.42) as follows

$$u_t + (\epsilon)\, u\, u_x + (\frac{\sigma}{\epsilon})\, g\, h_x + (\beta) g = + (\sigma^2)\, \frac{1}{3}\, h^2\, u_{xxt} - (\sigma^2)\, \frac{1}{3}\, u\, h\, h_{xxt} - (\sigma.\beta)\, h\, u_{xt} + (\sigma^2)\,(\textit{additional terms}) + O(\epsilon.\sigma^2,\ \epsilon^2,\ \sigma^4,\ \textit{etc.}) \qquad (2.42)$$

Again terms of the same order-of-magnitude of the

Boussinesq primary term may be observed. The additional (σ^2) order terms correspond to the product of derivatives. Third space derivatives are of higher order (Basco, 1983).

In order to explore further the importance of each term in these equations, Basco (1983) performed a perturbation analysis following the same procedure as adopted by Ponce et Simons (1977) to study the long wave equations and his own previous study in 1981. The analysis was conducted over a set of chosen pairs of equations, taking into account the previously obtained results in terms of order-of-magnitude. In the perturbation analysis the significance of the non-linear, primary and secondary Boussinesq term, bed-slope and other terms was verified.

Chosen equations are mainly based on equations (2.37) including the friction effect and the bed slope term as found by Peregrine.

The following pair of Boussinesq-type equations was developed assuming constant bottom slope and real fluid flow, for uniform rectangular channels:

$$h_t + h\,u_x + u\,h_x = 0 \qquad (2.43)$$

$$u_t + u\,u_x + g\,h_x - g\,S_o + g\,S_f = + \frac{1}{3}\,h^2\,u_{xxt} - \frac{1}{3}\,u\,h\,h_{xxt} + S_o\,h\,u_{xt} \qquad (2.44)$$

In Equation (2.44) S_f is the slope of energy grade line and is computed through uniform steady flow resistance formula.

It is important to observe that equation (2.44) does not include the product of derivatives, such as the term

($h.h_x.u_{xt}$) that appears in the Venezian derivation (see equation 2.41) or those found in Whalin's derivation. Basco states that its inclusion would result in the method too becoming mathematically intractable, besides the fact that the perturbed form of the product of derivatives would contain products of perturbed variables that are generally neglected in the method on the assumption of their lower order of magnitude. A non-dimensionalization process was also conducted on the perturbed equations.

Some other specific conclusions from Basco's work will be mentioned since they are meaningful to the type of governing equations established for the flow generated through the tipping tank discharge.

The most important conclusions refer to the Boussinesq term effects. It was found that the wave celerity is strongly influenced by the Boussinesq term. For very long waves the wave celerity tended to the Lagrange celerity, i.e., the long wave equation celerity, $u \pm (gh)^{1/2}$, as expected. However, for shorter wave lengths the Boussinesq wave celerity gradually decreases. If the Boussinesq term is neglected in a rapidly-varied flow the short waves components can have 100% error in the wave celerity. On the other hand, the use of the full Boussinesq equations automatically leads to the correct long wave celerity values for the long wave components for all Froude numbers.

Decreasing celerity for short waves was generally verified for all slopes and for Froude numbers $F_R < 1$. For $F_R \approx 1$ and higher values, the celerity approaches the uniform

base flow velocity, as expected, for any wave length. Therefore, the Boussinesq equation is more important for short waves in flat beds with low Froude numbers.

Referring to the friction effect Basco concludes that very long wave components are damped when considering the friction action. On steeper slopes, as F_R increases, shorter wave length components are also damped but the very shorter wave length components never are damped. According to the author these wave components never "feel" the bottom. It is also pointed out that the Chezy or Mannings empirical resistance formula certainly are inadequate for Boussinesq type flows, nevertheless these formulae have to be extensively used because of the nonexistence of suitable formulations mainly for flows in channels.

The inclusion of the bed slope term ($S_o hu_{xt}$) in the motion equation produced very minor changes in all conducted tests and could be neglected.

Referring to the secondary Boussinesq term, Basco's analysis demonstrates that its isolated inclusion in equation (2.44) is incorrect since celerity values obtained with this term included do not reduce to the Lagrange celerity. In all tests the inclusion of the secondary Boussinesq term leads to a wave celerity higher than that obtained with only the primary Boussinesq term irrespectively of the wave length. This effect was more apparent for short wave components and large Froude numbers. Basco also shows that for a consistent analysis the secondary term would require additional higher order terms to be included.

Analysing different forms of Boussinesq equations McCowan (1985,1987) concludes that to order of magnitude (ε, σ^2) all become equivalent to the Boussinesq system of equations 2.1 and 2.2. Performing a series of algebraic manipulations and retaining terms of order $(\varepsilon, \sigma^2$ and $\varepsilon.\sigma^2)$, McCowan was able to isolate 4 levels of Boussinesq type dispersive terms:

$$1st \qquad -\frac{(d+\eta)}{3} \cdot \eta_{xtt} \qquad (Abbott, 1979) \qquad (2.45)$$

$$2nd \qquad -\frac{d}{3} \cdot \eta_{xtt} \qquad (Boussinesq, 1877) \qquad (2.46)$$

$$3rd \qquad -\frac{d^2}{3(d+\eta)} \cdot \eta_{xtt} \qquad (Hauguel, 1980) \qquad (2.47)$$

$$4th \qquad -\frac{d^3}{3(d+\eta)^2} \cdot \eta_{xtt} \qquad (Peregrine, 1966) \qquad (2.48)$$

These four dispersive levels were tested in order to identify the range of application of the Boussinesq equations. They were evaluated by comparing their ability to propagate waves with the correct celerity, surface profile and crest elevation. Numerical results for wave propagation were compared with analytical solutions for solitary waves (McCowan, 1985) and with the analytical solutions provided by the reformulated stream function theory of Chaplin (McCowan, 1987). Compared to the solitary wave, McCowan (1985) concluded that the fourth level is more suitable for waves at its limiting wave height. Referring to the stream function, McCowan (1987) found that for finite amplitude waves the 3rd level, i.e., Hauguel formulation, had the best performance in shallow water.

Deriving Euler equations Seabra Santos (1986) obtained a more complete set of equations that can also be reduced to the Serre's type. The momentum equation is given by (2.49) as follows.

$$h(u_t + uu_x) + [h^2 (\frac{g}{2} + \frac{\phi}{2} + \frac{\Gamma}{3})]_x = - h \xi_x(g + \phi + \Gamma/2)$$

where

$$\phi = \xi_x (u_t + uu_x) + u^2 \xi_{xx} \qquad (2.50)$$

and

$$\Gamma = h (u_x^2 - uu_{xx} - u_{xt}) \qquad (2.51)$$

In these equations ξ_x and ξ_{xx} are the local bed slope and local bed curvature respectively. Without these two terms equation (2.49) reduces to Serre's equation type. Seabra Santos' equations do not include friction effects.

Carmo (1990), studying the development and propagation of waves in dam reservoirs, generalized Serre's equations for a two horizontal dimension flow on a bed of variable depth. Considering one dimension flow the momentum equation according to Carmo's derivation would be:

$$(Q_w)_t + (uQ_w)_x + [(\frac{g + \beta}{2} + \frac{\alpha}{3}) h^2]_x = - (g + \beta + \frac{\alpha}{2}) h \xi_x - \tau_{(x)} + R\ lap\ Q_w \qquad (2.52)$$

where

$$\alpha = \frac{d^2h}{dt^2} \qquad (2.53)$$

$$\beta = \frac{d^2\xi}{dt^2} \qquad (2.54)$$

In these equations $Q_w = uh$, ξ is the bed elevation, $\tau_{(x)}$ corresponds to the bed friction stress in x direction, lap Q_w stands for the Laplacian of Q_w and R corresponds to the summation of the dispersion coefficients and kinematic viscosity. Maciel (1993) derived a similar expression for rectangular cross sections. However Maciel's derivation has more generality being applicable to an arbitrary cross section.

Carmo's formulation is presented in the conservation form differentiating it from the Eulerian non-conservation form in which all previous equations were presented.

Following Anderson (1984) conservation form equations could be defined as a system of equations that could be expressed through

$$U_t + F_x = S \qquad (2.55)$$

where U, F and S are interpreted as column vectors normally representing flux variables, like Q_w in equation (2.52), for example.

Equations written in the conservation form generally present better performance on numerical computation of shock capturing methods because of stability or small variation of conservation form flux variables, like Q_w when equation (2.52) is simulating a hydraulic jump, for example. According to Anderson (1992) "for the shock-capturing method, experience has shown that the conservation form of the governing equations should be used."

2.2.4 Physical Description of Streamline Curvature Effects

Chow (1959) presents the general relationship between water surface curvature or streamline curvature and pressure distribution. Hydrostatic pressure distribution corresponds to flows where the streamlines are straight and parallel. i.e, where streamlines have neither substantial curvature nor divergence. In this conditions the flow filaments have no acceleration components in the plane of the flow cross section. The presence of such components would disturb the hydrostatic pressure distribution. If the flow has substantial streamline curvature, appreciable acceleration components, or centrifugal forces normal to direction of flow, will appear. Convex streamlines will attenuate the hydrostatic profile, i.e., for each depth the pressure will be smaller than the hydrostatic pressure corresponding to the depth. Concave streamlines will enlarge the pressure profile, i.e., for each depth the pressure will be higher than the corresponding hydrostatic pressure.

Peregrine (1966) analysing the development of undular bores gives an interesting physical description based on the relationship between surface curvature and type of pressure profile. Peregrine's description will be based on the points represented on Figure 2.1, that are analogous to those presented in the author referred article, nevertheless Peregrine's derivation always refers to small amplitude. However, the actual mechanism seems to be also valid for finite-amplitude waves.

The actual situation is that of a stream of water

flowing towards an area of still water in a rectangular, horizontal channel. The wave front initially shows a small change in level related to the still water, increasingly steepens up to a configuration similar to that depicted in Figure 2.1. Then, in the wave front region, the water surface between the two uniform levels is sufficiently abrupt for the vertical acceleration of the water to affect the pressure significantly.

Between points E and G of Figure 2.1, the vertical acceleration of water is upward. In this zone the pressure gradient downward must be greater than hydrostatic for this acceleration to occur. Similarly between G and I the water has a downward acceleration which corresponds to a downward pressure gradient lesser than hydrostatic. Peregrine considers that the greatest changes from hydrostatic pressure will occur at F and H, points of maximum vertical acceleration and of maximum surface curvature.

Considering the horizontal pressure gradients, Peregrine shows that between F and H there is an extra horizontal pressure gradient from F to H as beneath F the pressure is greater than hydrostatic and beneath H it is less. In a similar form there is an slight extra horizontal pressure gradient from F to E and from I to H. These pressure gradients cause an extra elevation at H, a corresponding depression at F, a slight depression at I and a slight elevation at E. Then the author concludes that this process continues and a sequence of waves is formed, which grow in amplitude until their tendency to steepen is just balanced by the horizontal pressure

gradients due to the vertical acceleration of the water.

Another interesting description is given by Peregrine (1967) when analysing the development of a simulated solitary wave reaching a beach. In deeper water the solitary wave keeps its characteristic profile and the balance between the two small parameters ε and σ. As the wave approaches the shore its profile changes continually. The wave amplitude increases and a wave front grows, becoming steeper and at a certain height the wave front will break. In this situation the two parameters no long can be considered small, as was assumed during the derivation through expansion methods, and when the wave starts breaking the equations are no longer mathematically valid. Peregrine (1967) carried out simulations up to a maximum value of the ratio of amplitude to the initial depth of water, at the position of the crest, equal to 0.6. The author quotes experiments performed by Ippen & Kulin where this ratio reached 2 before the waves broke.

Abbott (1979), commenting on the simple wave deformation due to differences in celerity, shows that the continuous overtaking of deeper sections over shallow sections leads to a situation where the vertical accelerations influence the solution. This process may have the tendency, in nature, to prevent further deformation locally, so that the system runs further as a simple wave composed of waves with significant vertical accelerations. This would be the case of a train of waves.

2.2.5 Conclusion of the Literature Review

Initially it seems to be transparent that equations limited to small amplitude waves are not suitable for the tipping tank generated wave, at least in the conditions observed in the laboratory, since the discharges promote a relatively high water surface elevation over the existing base flow. This first conclusion denotes that an expansion in series of powers in terms of the parameters ε and σ would not be feasible since the method requires that these parameters must be small. In particular, ε, is never small in the conditions observed in laboratory. Thus, for the development of series expansion, would be necessary the adoption of new suitable expansion parameters.

The literature review shows that the Boussinesq type equations have been consistently developed in the field of general theory of unsteady open channel flow and water waves. But, this theoretical coherence does not have a parallel in terms of a conclusive set of appropriate equations. Referring to the order-of-magnitude analysis, a certain degree of indeterminacy is apparent and requires more study. These indefiniteness indicate that the equations should be tested in research of an exploratory nature as suggested by Basco (1983). However, a few articles, mainly referring to open channel flow, have been found in the available literature. Specifically referring to open channel flow two articles could be mentioned. The work of Basco (1989) comparing the Boussinesq and Saint Venant equations in the description of a dam-break problem and

the numerical simulation of hydraulic jumps performed by Guarangik and Chaudhry (1991).

A positive facet revealed through the literature review is the general convergence of all presented equations in their reduction to the simpler Saint-Venant equations. This is an important aspect since the Saint-Venant equations has been shown sufficient in several cases of wave propagation even involving steep front waves. These equations will be necessary in all the situations where vertical accelerations may be neglected and probably this will be the majority of practical cases.

The diversity of methods and respective equations, and the problems mentioned, recommend that it would be prudent to adopt the more generic formulation, avoiding as much as possible neglecting the products of derivatives and other higher order derivative. Obviously this guideline should be considered together with the availability of suitable numeric methods of solution.

In the work developed by Carmo (1990) and by Maciel (1993) these guidelines seems to have been observed. A set of comprehensive equations were developed, a minimum of simplifications were adopted and a suitable numeric method was chosen. These directives will also command the development of the governing equations that follows. The general lines of Maciel's derivation procedure will be followed at section 2.3.2.

2.3 Governing Equations

2.3.1 Mass Conservation Equation

The continuity of the flow may be expressed by the mass conservation law which states that mass can neither be created or destroyed.

The infinitesimal space between two channel sections illustrated in Figure 2.2 is a control volume over which the equation of continuity will be developed. The continuity of flow can be enunciated in the following terms: the variation of water mass between sections 1 and 2 during a certain interval dt is equal the inflow water mass through section 1 minus the outflow mass through section 2 in the same interval dt. As the liquid mass density is constant. i.e., it is incompressible, the above enunciation could use volume instead of mass of water. Alternatively the volumetric flow rate (Q) could be used leading to the following equation:

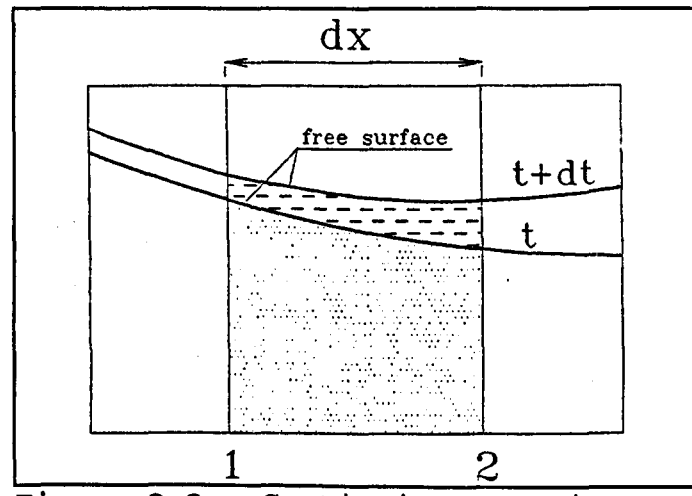

Figure 2.2 - Continuity equation sketch

$$Q\,dt - (Q + Q_x\,dx)\,dt = A_t\,dx\,dt \qquad (2.56)$$

where A is the cross sectional area of flow.

Taking Q = u.A where u is the depth averaged velocity and working out equation (2.56) it is obtained the more compact form of equation of mass conservation as follows:

$$A_t + Q_x = 0 \qquad (2.57)$$

2.3.2 Conservation of Momentum Equation

In the following derivation it will be assumed that (1) the flow horizontal velocity is uniform over the flow depth; (2) the flow velocity in the lateral direction is zero; and (3) the Boussinesq assumption is valid, i.e., the flow velocity in the vertical direction varies linearly from zero at the bottom to a maximum value at the flow surface. Terms appearing on the equations are based on the sketch illustrated at Figure 2.3 representing the flow profile in the pipe longitudinal section.

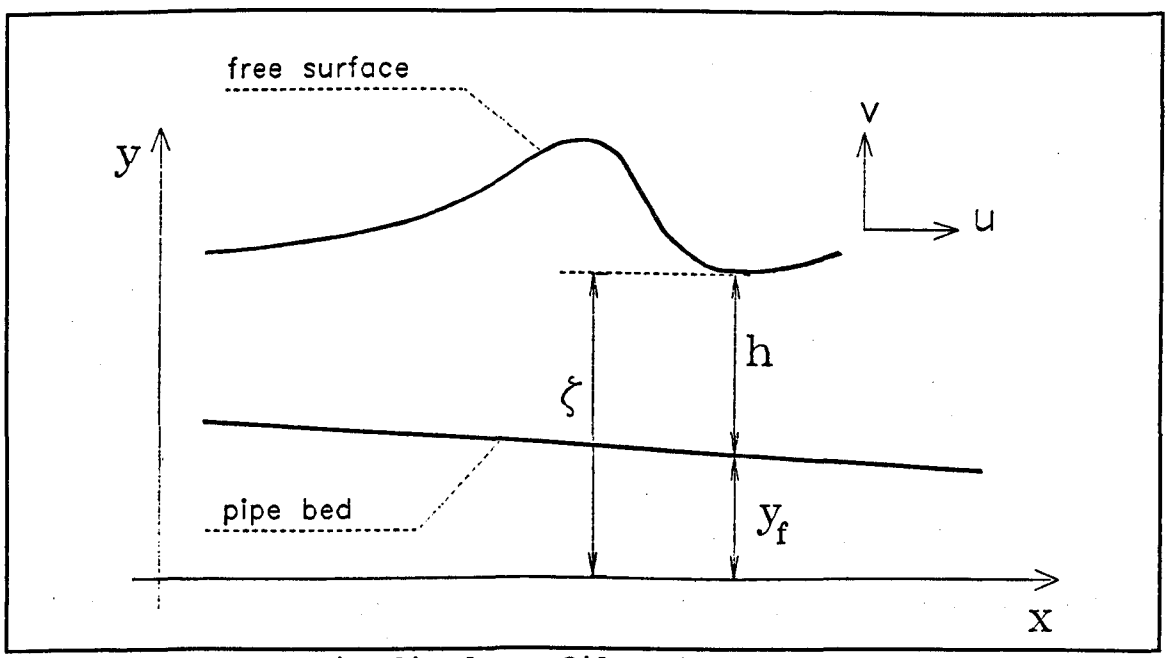

Figure 2.3 - Longitudinal profile of the flow

2.3.2.1 Pressure and Vertical Velocity Equations

The rate at which the vertical velocity varies through the vertical can be expressed as

$$v_y = \frac{1}{h}\frac{dh}{dt} \tag{2.58}$$

where the y subscript indicate partial differentiation in respect to the independent variable y.

The vertical velocity expression according to Boussinesq's assumption is

$$v(y) = \frac{(y - y_f)}{h}\frac{dh}{dt} \tag{2.59}$$

Euler's vertical equation (2.16) is integrated from a generic position y to the water surface (ζ) to give the pressure expression. The water free surface is at air pressure, i.e., $p(\zeta) = 0$.

$$\frac{p(y)}{\rho} = \int_y^{\zeta} (v_t + u\,v_x + v\,v_y + g)\,dy \tag{2.60}$$

Using equation (2.59) and integrating equation (2.60) it will result in equation (2.61) as follows:

$$\begin{aligned}\frac{p(y)}{\rho} &= (\zeta - y)\,g \\ &- (\zeta - y)\left[\,y_f\left(\frac{1}{h}\frac{dh}{dt}\right)_t + u\,y_f\left(\frac{1}{h}\frac{dh}{dt}\right)_x + \frac{y_f}{h^2}\left(\frac{dh}{dt}\right)^2\right] \\ &+ \frac{(\zeta^2 - y^2)}{2}\left[\left(\frac{1}{h}\frac{dh}{dt}\right)_t + u\left(\frac{1}{h}\frac{dh}{dt}\right)_x + \frac{1}{h^2}\left(\frac{dh}{dt}\right)^2\right]\end{aligned}$$

Considering that for a generic function f(x,t) it is valid to write the relation (2.62), it is possible to manipulate equation equation (2.61) leading to (2.63),

$$\frac{1}{h}\frac{d(fh)}{dt} = f_t + u f_x + f\frac{1}{h}\frac{dh}{dt} \qquad (2.62)$$

$$\frac{p(y)}{\rho} = \frac{(\zeta - y)}{h}\,[g h - y_f \alpha] + \frac{(\zeta^2 - y^2)}{2 h}\,\alpha \qquad (2.63)$$

where α has already been defined through equation (2.53). It should be observed that equation (2.63) is much more complete than equation (2.21) because of the simplifications adopted in Abbott's engineering derivation. Equation (2.63) can be further manipulated resulting

$$\frac{p(y)}{\rho} = (\zeta - y)\,[g + \frac{\alpha}{2}] + (\zeta - y)(y - y_f)\frac{\alpha}{2h} \qquad (2.64)$$

If water particle vertical movement effects are neglected, i.e., if $\alpha = 0$, equation (2.64) reduces to the hydrostatic pressure equation.

2.3.2.2 Momentum Equation

Friction effects can be accounted for by adding to Euler's horizontal equation (2.15) the corresponding term FD, as follows

$$u_t + u u_x + v u_y = -\frac{1}{\rho} p_x + FD \qquad (2.65)$$

where FD represents the friction effect in terms of Euler's equations units (force per unit mass).

Equation (2.65) can be equated to zero, multiplied by the free surface width T (see Figure 2.4) and integrated from y_f to ζ. According to previously established hypotheses $u_y = 0$.

From Figure 2.4 it is clear that dA = T.dy so that

$$A = \int_{y_t}^{\zeta} T\, dy \qquad (2.67)$$

The several terms of equation (2.66) will be integrated separately.

$$\int_{y_t}^{\zeta} (u_t + uu_x)\, T\, dy = A\, u_t + A\, uu_x$$

$$= (A\, u)_t + (A\, u^2)_x \qquad (2.68)$$

The net pressure force component in the horizontal direction acting on a control volume is represented by the integral of the pressure variation in x direction on the flow area. The third term of (2.66) to be integrated refers to this force. To obtain the respective equation the pressure equation (2.64) shall be firstly derived in x. Following the simplification adopted by Maciel (1993), in this derivation the variation of α with x is neglected. The y^2 are also neglected, appearing both on the pressure expression and on its derivative.

Deriving (2.64) with these assumptions leads to

$$\frac{1}{\rho} p_x = \zeta_x \left(g + \frac{\alpha}{2}\right) \qquad (2.69)$$

that can be integrated to give (2.70).

The fourth term of equation (2.66) to be integrated refers to the friction of the liquid against the flow bed. As mentioned before there is a lack of knowledge of frictional

effects in rapidly-varied flow. The nonexistence of friction specific formulae has led to the use of uniform steady state flow resistance formulae that can be used as a first approximation to assess the frictional effect. These expressions can also be used

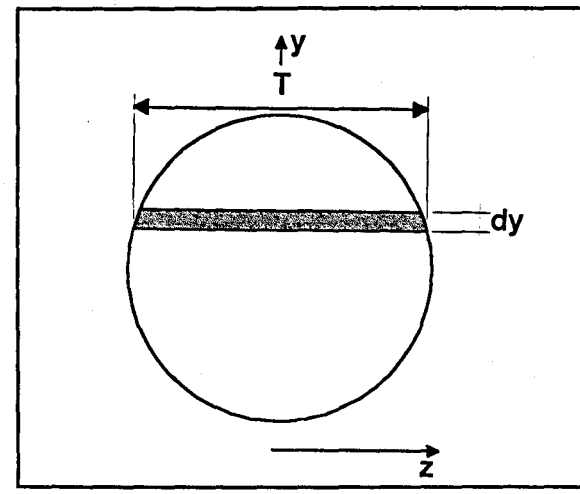

Figure 2.4 - Flow cross section

$$\int_{y_f}^{\zeta} \frac{1}{\rho} p_x T \, dy = \zeta_x \left[g + \frac{\alpha}{2} \right] A \qquad (2.70)$$

$$= h_x \left(g + \frac{\alpha}{2} \right) A + (y_f)_x \left(g + \frac{\alpha}{2} \right) A$$

as a factor of adjustment in mathematical model calibration processes.

For a certain control volume located between two cross sections of a free surface pipe flow the friction force F_f acting on it is given by

$$F_f = \rho \, g \, A_m \, dx \, S_f \qquad (2.71)$$

where A_m is the flow area in the middle section of the control volume, dx is the elementary distance between the two cross sections and S_f is the flow energy grade line slope. Euler's equations are expressed in terms of force per unity mass. Thus, the Eulerian form of equation (2.71) is

$$F_{fe} = g \, S_f \qquad (2.72)$$

and the integral of the fourth term of equation (2.66) can be written as

$$\int_{y_t}^{\zeta} FD\ T\ dy = \int_{y_t}^{\zeta} g\ S_f\ T\ dy = g\ S_f\ A \qquad (2.73)$$

Standing (1986) refers to Swaffield and Bridge (1983) work on the applicability of steady state friction factors to unsteady pipeflow. It is shown that the Colebrook-White equation is substantially better than the Manning equation in predicting wave attenuation in both glass and cast-iron pipes in the case of small bore partially filled pipeflow. Laboratory experiments showed that, for small bore pipes, the Colebrook-White equation has a better performance than Manning's in predicting wave velocity and is also slightly better at predicting the maximum depth of flow along the pipe.

Thus, to assess the friction slope S_f Colebrook-White equation will be used

$$\frac{1}{\sqrt{f}} = -2 \log_{10}\left(\frac{k}{14.83\ R} + \frac{2.52}{R_e \sqrt{f}} \right) \qquad (2.74)$$

where f = Darcy resistance coefficient

k = roughness coefficient (m)

R_e = Reynolds number

Bridge (1982) used Chézy and Darcy coefficients relationship, $C = (8g/f)^{0.5}$, the Chézy equation, $Q = AC(RS_o)^{0.5}$, and the Reynolds number $R_e = (4QR)/(A\upsilon)$ to express Colebrook-White equation as

$$Q = \sqrt{32\ g\ R\ S_o}\ A \log_{10}\left(\frac{k}{14.83\ R} + \frac{2.52\ \nu}{R \sqrt{128\ g\ R\ S_o}} \right) \qquad (2.75)$$

The addition of all integrated terms leads to the

momentum equation (2.76) as follows

$$(A\,u)_t + (A\,u^2)_x + h_x\,(g + \frac{\alpha}{2})\,A = -(y_f)_x\,(g + \frac{\alpha}{2})\,A - g\,S_f\,A$$

Referring to the needs of a future numerical solution, it would be desirable to have equation (2.76) in the conservation form. Hence the third term of the left hand side of equation (2.76) should be transformed into a partial derivative form. The development presented by Maciel (1993) will also be followed here.

Equation (2.64) is transformed into a direct function of the depth referred to the bed. This is possible through the variable change $j = y - y_f$. In terms of j, equation (2.64) becomes

$$\frac{p(j)}{\rho} = (h - j)\,(g + \frac{\alpha}{2} + \frac{\alpha}{2}\,\frac{j}{h}) \qquad \textbf{(2.77)}$$

The Leibnitz rule to derive an integral function, presented in equation (2.78) as follows, reads that

$$\frac{d}{dx}\int_{\phi_1(x)}^{\phi_2(x)} F(j,x)\,dj = \int_{\phi_1(x)}^{\phi_2(x)} [F(j,x)]_x\,dj + F(\phi_2,x)\,\frac{d\phi_2}{dx} - F(\phi_1,x)\,\frac{d\phi_1}{dx}$$

Defining a function P(x) as

$$P(x) = \int_0^h p'(j)\,T(x,j)\,dj \qquad \textbf{(2.79)}$$

where $p'(j) = (1/\rho)p(j)$ and applying Leibnitz rule gives equation (2.80). Considering that $T(x,0)=0$ and that $p'(h)=0$ equation (2.80) leads to (2.81).

Deriving $p'(j)$ and solving the first term of the right

$$[P(x)]_x = \int_0^h [p'(j)\ T(x,j)]_x\, dj + p'(h)\ T(x,h)\ \frac{dh}{dx} - p'(0)\ T(x,0)\ \frac{d0}{dx} \quad (2.80)$$

$$[P(x)]_x = \int_0^h [p'(j)]_x\, T(x,j)\ dj + \int_0^h p'(j)\ [T(x,j)]_x\, dj \quad (2.81)$$

hand side of equation (2.81) gives

$$h_x\ (g + \frac{\alpha}{2})\ A = [P(x)]_x - B(x) \quad (2.82)$$

where

$$B(x) = \int_0^h p'(j)\ [T(x,j)]_x\, dj \quad (2.83)$$

Finally, using (2.82), equation (2.76) can be rewritten as (2.84) as follows

$$(A\ u)_t + [A\ u^2 + P(x)]_x = (g + \frac{\alpha}{2})\ S_o\ A - g\ S_f\ A + B(x) \quad (2.84)$$

where $S_o = -\ [y_f]_x$.

2.3.2.3 Boussinesq Hypothesis Applied to Pipe Flow

The derivation up to this point has been developed aiming to preserve the generality to a maximum. However, an analysis has to be performed to study the particular applicability of Boussinesq basic hypothesis to pipe flow.

The discussion will be based on the elements depicted on Figure 2.5. The first point refers to the variation of water particle vertical velocity. It is apparent that equation (2.59)

is not valid for the pipe flow simply because in the circular cross section $h = (\zeta - y_t)$ is not constant in z. An alternative velocity equation considering the variation, i.e., for $y_t(z)$ would be

$$v(y,z) = \frac{[y - y_f(z)]}{[\zeta - y_f(z)]} \frac{d\zeta}{dt} \qquad (2.85)$$

This equation is valid inside the region delimited by the two segments PP' and QQ' of Figure 2.5 but in the flow area outside of this region the equation is physically questionable.

Aside boundary questions on the water particle contact with the pipe surface it is not reasonable to accept that vertical velocities in these confined regions have the same profile as in the free surface band. Certainly the proximity to the pipe surface would affect the profile displacing the maximum vertical velocity to a lower position. Obviously adopting these considerations would make the problem very complicated because of having two different hypotheses for the inside and outside regions.

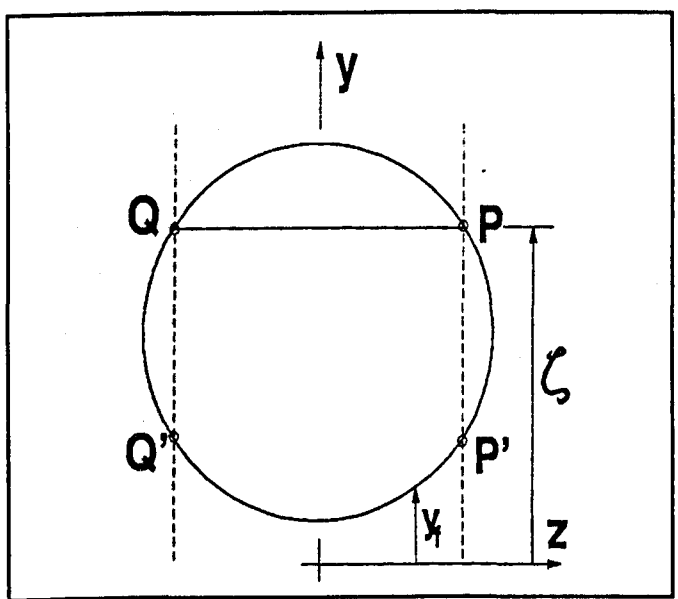

Figure 2.5 - Flow cross section

However, even without these questions there is another kind of problem that has shown not to have a solution.

It is mathematically intractable to integrate the pressure expression p(y,z) on the flow area. Some attempts have shown the difficulty of this task.

It was found that a practical solution is to consider the flow dynamics effects as if the flow cross section were amenable to study. In other words it is possible to use the momentum equation for the situation where the Boussinesq assumption is wholly applicable, i.e., a rectangular section of a wide canal, using data from a different geometric condition. The flow area to be used is numerically equal to the actual flow pipe area. The same is applied to the wet perimeter and the hydraulic radius. This procedure corresponds to considering an elemental control volume with a dz width whose dynamic properties could be extended to the whole section.

Considering a rectangular section equation (2.84) becomes (2.86) as follows

$$(A\,u)_t + [A\,u^2 + (h\frac{g}{2} + h\frac{\alpha}{3})A]_x = (g + \frac{\alpha}{2})\,S_o\,A - g\,S_f\,A \qquad (2.86)$$

There is a common constant factor T implicit in the value of A that can be removed, resulting finally

$$(h\,u)_t + [h\,u^2 + (\frac{g}{2} + \frac{\alpha}{3})h^2]_x = (g + \frac{\alpha}{2})\,S_o\,h - g\,S_f\,h \qquad (2.87)$$

If $\alpha = 0$ the equation reduces to the conservation form of Saint-Venant equation. Further developing the group derivatives will result in the Eulerian form of the same equation. Equation (2.87) compares with those derived

by Carmo (1990) and Maciel (1993) for fixed flow bed (ß=0) and if viscosity effects are neglected. Equation (2.87) also reduces to Serre's equation for horizontal bed flow neglecting friction effect.

The mass conservation equation (2.57) will introduce the actual area value into the equation system. Mathematical manipulation of equation (2.57) provides an expression relating α with the flow area A. From equation (2.57) it can be shown that

$$\frac{dh}{dt} = - \frac{A}{T} u_x \qquad (2.88)$$

Deriving equation (2.88) and grouping terms will result in the relation of α with A

$$\alpha = \frac{A}{T} [(u_x)^2 - u_{xt} - u\, u_{xx}] + \frac{A}{T^2} [T_t\, u_x + u\, T_x\, u_x] \qquad (2.89)$$

If the first term in the right hand side is designated - E1 and the second term is named E2, equation (2.87) can be expressed through equation (2.90) as follows

$$(h\,u)_t + [h\,u^2 + h^2 \frac{g}{2} - \frac{h^2}{3} E1 + \frac{h^2}{3} E2]_x = \qquad (2.90)$$

$$h\,g\,(S_o - S_f) + \frac{h}{2} S_o\,(E2 - E1)$$

Equations (2.90), (2.57), (2.75) plus geometric formula referred to area, perimeter and flow width together with hydraulic formula for hydraulic radius, Froude number and other common parameters comprise the mathematical model proposed to simulate the flow generated through the tipping tank discharges.

CHAPTER THREE

NUMERICAL METHODS APPLIED TO THE MATHEMATICAL MODEL

3.1 Introduction

Continuity equation (2.57), momentum equation (2.90) complemented with accessory equations for friction slope S_f, geometric and hydraulic parameters, comprise a system of equations which, when solved, predict water depth (h) and velocity (u) as a function of time. Suppressing the vertical acceleration components E1 and E2 from (2.90) the system is known as the Saint-Venant equations. Including these terms the system can be considered a particular form of the Boussinesq equations.

No analytical general solution is known for this set of governing equations (either for the Saint-Venant or for the Boussinesq equations). Thus, numerical integration, using finite-differences approximation, is used to solve the system.

Three numerical methods are applied: first-order accurate finite-differences applied to the method of characteristics; the McCormack explicit scheme and the two-four explicit scheme. These three methods, applied to the governing

equations, will be compared in order to determine the most suitable scheme for the tipping tank generated flow simulation.

The literature shows that explicit schemes are used mainly because they provide relatively simple computer programs. They also are used because explicit higher-order schemes are available. The main disadvantage of explicit methods are the small time steps necessary to satisfy stability conditions, nevertheless Fennema et al. (1986) obtained smaller overall computation time when comparing the explicit McCormack method to Preissmann's implicit method, applied to a unsteady flow in open channel.

The governing equation terms can be written as column vectors terms U, F and S of equation (2.52) ($U_t + F_x = S$). Time derivative terms are embraced under the U matrix, F comprises space derivatives and S contains terms that can not be included in the partial derivatives of the left hand side. These system is expressed through equations (3.1) to (3.3), as follows.

$$U = \begin{bmatrix} A \\ hu \end{bmatrix} \tag{3.1}$$

$$F = \begin{bmatrix} uA \\ hu^2 + h^2\frac{g}{2} - \frac{h^2}{3}E1 + \frac{h^2}{3}E2 \end{bmatrix} \tag{3.2}$$

$$S = \begin{bmatrix} 0 \\ hg(S_o - S_f) + \frac{h}{2}S_o(E2 - E1) \end{bmatrix} \tag{3.3}$$

3.2 The Method of Characteristics Applied to the Saint-Venant Equations

Characteristic curves of the Saint-Venant equations will be derived from its Eulerian form as follows.

Conservation of mass:

$$A_t + u_x A + uA_x = 0 \tag{3.4}$$

Conservation of momentum:

$$u_t + uu_x + gh_x = g(S_o - S_f) \tag{3.5}$$

The system comprised by equations (3.4) and (3.5) can be written in the matrix form of equation (3.6).

$$\begin{bmatrix} 0 & A & T & uT \\ 1 & u & 0 & g \\ dt & dx & 0 & 0 \\ 0 & 0 & dt & dx \end{bmatrix} \begin{bmatrix} u_t \\ u_x \\ h_t \\ h_x \end{bmatrix} = \begin{bmatrix} 0 \\ g(S_o - S_f) \\ du \\ dh \end{bmatrix} \tag{3.6}$$

Equation (3.6) includes the general derivative relations (3.7) and (3.8) as follows.

$$\frac{du}{dx} = u_x + u_t \frac{dt}{dx} \tag{3.7}$$

$$\frac{dh}{dx} = h_x + h_t \frac{dt}{dx} \tag{3.8}$$

In equation (3.6) the left hand side of equation (3.4) appears on its equivalent form expressed through

$$A_t + uA_x = T\,h_t + u\,T\,h_x \tag{3.9}$$

The characteristic curve directions can be found making the determinant of coefficient matrix equal to zero (Sanchez,

1978), resulting

$$T\,(dx - u\,dt)^2 = g\,A\,dt^2 \qquad (3.10)$$

from which the inclinations of characteristic curves in the (x,t) plane are

$$\frac{dx}{dt} = u \pm \sqrt{\frac{g\,A}{T}} = u \pm c \qquad (3.11)$$

The term c is the local wave speed and the expression (u ± c) is known as the wave celerity. (u + c) corresponds to forward characteristic curves, i.e., curves of increasing values of x with time, while (u - c) corresponds to backward characteristic curves in subcritical flows and forward curves in supercritical flows.

The expression (u ± c) is also the solution of a quadratic equation in dx/dt. This equation would appear in its usual form developing (3.10). The discriminant of this quadratic equation ($\Delta = 4gTA$) is always positive leading, therefore, to the classification of equations (3.4) and (3.5) as a system of quasi-linear partial differential equations of the hyperbolic type (Sanchez, 1978).

Substituting the second column of the coefficient matrix of equation (3.6) by the right hand side column results in the matrix designated by (3.12) as follows.

$$\begin{bmatrix} 0 & 0 & T & uT \\ 1 & g(S_o - S_f) & 0 & g \\ dt & du & 0 & 0 \\ 0 & dh & dt & dx \end{bmatrix} \qquad (3.12)$$

This matrix also has to be of rank 3 to meet the indeterminacy condition of the method of characteristics, i.e.,

its determinant must be equal to zero. Applying this condition leads to

$$(\frac{dx}{dt} - u)\ [Tdu - g(S_o - S_f)\,Tdt] + gTdh=0 \qquad (3.13)$$

Through equation (3.11) the first term of (3.13) can be replaced resulting

$$du \pm \frac{g}{C}dh = g(S_o - S_f)\,dt \qquad (3.14)$$

Equations (3.11) and (3.14) is a system comprised by two pair of differential equations that can be integrated between two time values t^k and t^{k+1}, providing the system solution, i.e., h and u values, at the instant t^{k+1}.

Integrating equation (3.14) leads to

$$(u + \int_{h^k}^{h^{k+1}} \frac{g}{C}dh)_{t^k}^{t^{k+1}} = g\int_{t^k}^{t^{k+1}} (S_o - S_f)\,dt \qquad (3.15)$$

along the c+ characteristic and

$$(u - \int_{h^k}^{h^{k+1}} \frac{g}{C}dh)_{t^k}^{t^{k+1}} = g\int_{t^k}^{t^{k+1}} (S_o - S_f)\,dt \qquad (3.16)$$

along the c- characteristic.

The difference (S_o-S_f) is generally of small magnitude. Thus, the left hand side of equations (3.15) and (3.16) have also a small variation. For this reason the left hand side of these equations are called "quasi invariants".

Integrating equation (3.11) it is acquired

$$(x)_{t^k}^{t^{k+1}} = \int_{t^k}^{t^{k+1}} (u + c)\,dt \qquad (3.17)$$

and

$$(x)_{t^k}^{t^{k+1}} = \int_{t^k}^{t^{k+1}} (u - c)\,dt \qquad (3.18)$$

Integrals on equations (3.15), (3.16), (3.17) and (3.18) will be computed using first-order finite difference approximations. Variables will be assessed in equally distanced points of the space in a marching forward process. A fixed rectangular grid in the space-time plane (x,t) is adopted as illustrated in Figure 3.1.

In Figure 3.1 the projection of the characteristic curves in the (x,t) plane is approximated by straight lines (C+ and C-) with slopes respectively equal to 1/(u+c) and 1/(u-c). The dashed line corresponds to the C- characteristic if the flow is supercritical.

Figure 3.1 indicates that variable values are known at the t^k time level in all sections (in particular, at points A, B and C) and in the sections upstream of the position x_j (point P) at time level t^{k+1}.

At time level t^{k+1} variable values at point P are computed through the finite difference form of equations (3.15), (3.16), (3.17) and (3.18) according to each characteristic direction. At points R, S or S' water velocity and water depth can be assessed by interpolation of variable values on points A, B and C. In the subcritical flow, variables at R are computed interpolating between A and C and between C and B to compute variables at S. For supercritical flow, variables at R and S' are assessed interpolating between A and C.

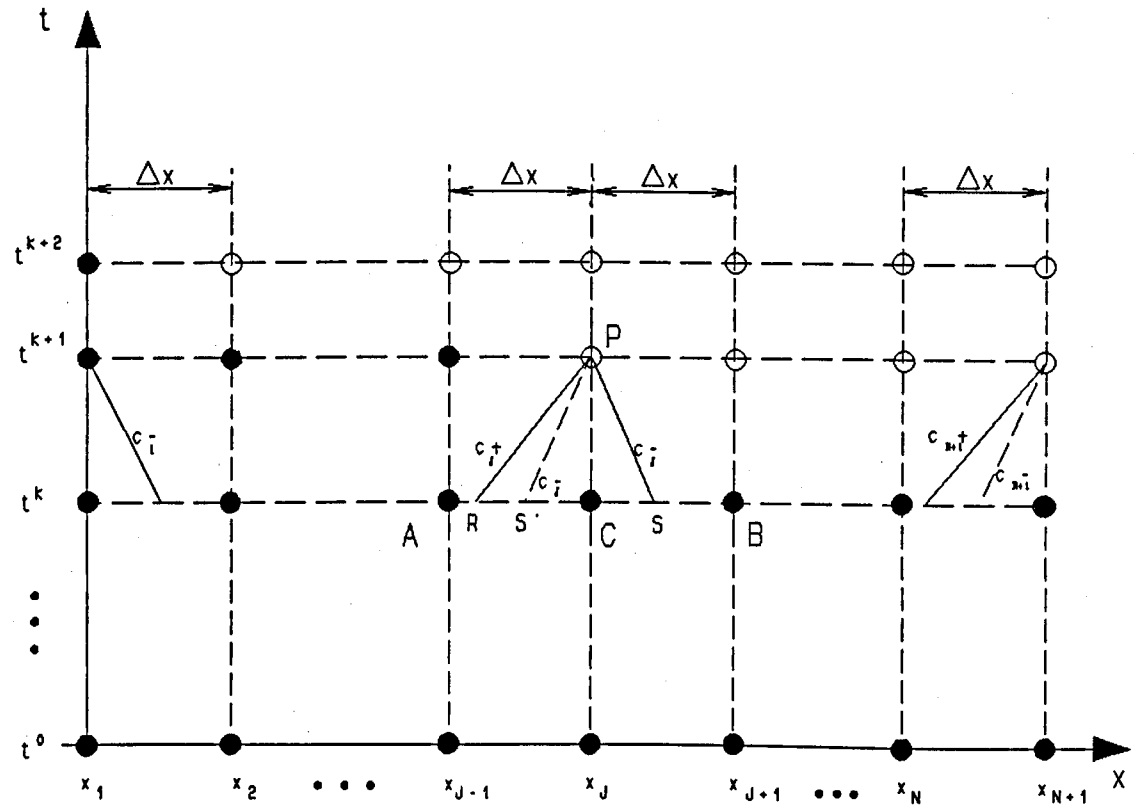

Figure 3.1 - Rectangular fixed grid scheme

The flow regime, i.e., sub or supercritical, in a certain section x_J, is identified by comparing u and c in this section and in adjacent sections at time level t^k. A special scheme for the flow regime identification is presented on section 4.4.3. The flow is subcritical if u<c and supercritical if u>c.

From equations (3.15) to (3.18) and referring to the points indicated at Figure 3.1, for the positive characteristic C+ it can be written

$$x_P - x_R = (u_R + c_R)(t^{k+1} - t^k) \qquad (3.19)$$

$$u_P - u_R + \frac{g}{c_R}(h_P - h_R) = g(S_o - S_{f_R})(t^{k+1} - t^k) \qquad (3.20)$$

For the negative characteristics C- results

$$x_P - x_S = (u_S - c_S)(t^{k+1} - t^k) \qquad (3.21)$$

and

$$u_P - u_S - \frac{g}{c_S}(h_P - h_S) = g(S_o - S_{f_S})(t^{k+1} - t^k) \qquad (3.22)$$

In the supercritical flow the subscript S in equations (3.21) and (3.22) shall be substituted by S'.

The approximation on the integrals involving the local wave speed c will be commented in section 3.2.3.

Since x_P, t^k and t^{k+1} are known values and all variables are known on points A, B and C at time level t^k, it is possible to compute x_R, x_S, h_R, h_S, u_R and u_S by interpolation and from these values to calculate h_P and u_P using the two pairs of equations: (3.19), (3.20) and (3.21), (3.22).

3.2.1 Interpolation Formula

Linear interpolation between A, B and C was initially attempted by Bridge (1984) and Standing (1986), studying waves flowing in partially filled pipes. Three main problems were observed with this type of interpolation: backwater profile collapse, numerical dispersion at wave front and wave front steepness damping. Preliminary computation on the present work using the method of characteristics with linear interpolation have shown a progressive damping and eventual collapse in the gradually varied flow profile at the pipe end region before the arrival of the wave front.

The procedures developed by Standing (1986) and created by Lister (1960), will be adopted here.

An iterative process is carried on to find the position of x_R and x_s. It shall be observed, initially, that the characteristic line through P in Figure 3.1 has an unknown slope. The process can be explained as follows.

a) firstly, it can be assumed that the slope of the characteristic line at P is the same as that at C, i.e., the slope corresponding to the moment t^k at point x_J. From this assumption $[x_R]_i$ and $[x_s]_i$ are determined (i indicates the order of the iteration);
b) through a non-linear interpolation using surrounding grid points, $[h_R]_i$, $[u_R]_i$, $[h_s]_i$ and $[u_s]_i$ are computed;
c) with $[h_R]_i$ and $[h_s]_i$, $[c+]_i$ and $[c-]_i$ are calculated;
d) a new value $[x_R]_{(i+1)}$ is computed now assuming that the characteristic lines through P have slope corresponding to the previous values of x_R. This condition is expressed by

$$x_P - [x_R]_{(i+1)} = [u_R + c_R]_i \, dt \qquad (3.23)$$

and

$$x_P - [x_S]_{(i+1)} = [u_S - c_S]_i \, dt \qquad (3.24)$$

e) the process is repeated from b) until the difference between successive iterations of x_R and x_s are less than 0.001 m. The process is also valid for S'.

This process simplifies the iteration developed by Lister (1960) where after each new x_R and x_s the variable values at P were computed and the resulting characteristic line

slope through P was compared with the previous slope at R and S. The procedure was repeated until the difference between successive iterations of u_p and h_p were small. Obviously, the Lister method takes more computer processing time.

Once the iteration to determine the position of R, S or S' is completed, the values of u and h at these points can be computed through an interpolation process.

A difference method, involving central differences, is chosen. For the internal nodes Everett method was applied and near the ends of the pipe, where central differences could not be applicable, the Newton-Gregory forward and backward difference formulae are used.

Everett formula is expressed through equation (3.25) as follows.

Equation (3.25):

$$f(x_R) = E_o f_o + E_2 \delta^2 f_o + E_4 \delta^4 f_o + \ldots + F_o f_1 + F_2 \delta^2 f_1 + F_4 \delta^4 f_1$$

where:

$$E_o = 1 - p \qquad (3.26)$$

$$E_2 = \frac{-p\,(1 - p)\,(2 - p)}{3\,!} \qquad (3.27)$$

$$E_4 = \frac{-(-1 - p)\,p\,(1 - p)\,(2 - p)\,(3 - p)}{5\,!} \qquad (3.28)$$

$$F_o = p \qquad (3.29)$$

$$F_2 = \frac{p\,(p^2 - 1)}{3\,!} \qquad (3.30)$$

$$F_4 = \frac{p\,(p^2 - 1)\,(p^2 - 4)}{5\,!} \tag{3.31}$$

$$p = \frac{x_R - x_{J-1}}{x_J - x_{J-1}} \tag{3.32}$$

$$f_o = f\,(x_{J-1}) \tag{3.33}$$

$$f_1 = f\,(x_J) \tag{3.34}$$

and δ^2, δ^4, etc, are the even progressive cumulative differences between adjacent points. $f(x_R)$ stands for h_R or u_R. Analogue formula are used for variable at points S or S'.

Newton-Gregory forward difference formula is

$$f\,(x_R) = f_o + p\,\delta\,f_o + \frac{p\,(p-1)}{2\,!}\,\delta^2 f_o + \frac{p\,(p-1)\,(p-2)}{3\,!}\,\delta^3 f_o \ldots + \frac{p\,(p-1)\ldots(u-n+1)}{n\,!}\,\delta^n \tag{3.35}$$

Newton-Gregory backward difference formula is

$$f\,(x_R) = f_o + p\,\Delta\,f_o + \frac{p\,(p+1)}{2\,!}\,\Delta^2 f_o + \frac{p\,(p+1)\,(p+2)}{3\,!}\,\Delta^3 f_o \ldots + \frac{p\,(p+1)\ldots(u+n+1)}{n\,!}\,\Delta^n \tag{3.36}$$

where Δ, Δ^2, Δ^3, etc are regressive cumulative differences between adjacent points.

3.2.2 Energy Line Slope

Energy line slope S_f is computed through equation (2.75) replacing S_o by S_f.

At the wave front there is a deficiency of knowledge on the role of friction as already discussed in Chapter 2. The friction effect is generally used as a calibration factor in large hydraulic structure simulation.

Standing (1986) developed a special formulation for the wave front friction effect. According to Standing less than the whole wet area of cross section flow would have a significant effect in terms of friction. As illustrated in Figure 3.2, from the whole wet area should be removed the part corresponding to the existing base flow over which the wave "slips" without friction. In other words, only the contact surface (water-pipe) corresponding to arcs AA' and BB' depicted at Figure 3.2 are significant. Some computer simulation tests carried on by the author have revealed that Standing's procedure has just a slight effect of reduction of the steady state energy line slope S_f.

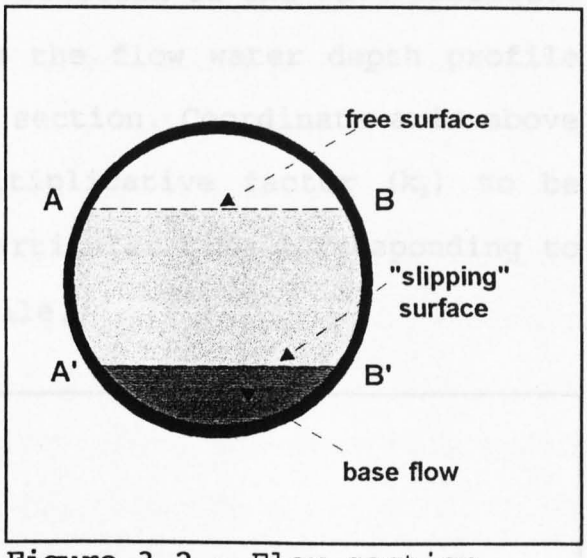

Figure 3.2 - Flow section

Others authors simply neglect the friction effect at the front wave arguing that energy dissipation due to turbulence in the front zone would be much more significant than water-pipe wall friction (Souza, 1994). In this case the corresponding changes in the momentum equation should be comprised by other terms. However, this approach is much too complicated and intractable because it involves turbulence that

still can not be practically handled.

In the present work a special scheme of friction effect evaluation, mainly in the wave front, is used. Multiplicative factors are applied to the steady state flow energy line slope S_f according to each particular position of the wave profile.

Figure 3.3 illustrates the flow water depth profile varying with time in a certain section. Coordinate axis above the profile indicates the multiplicative factor (k_f) to be applied to S_f according to a particular time corresponding to a certain position of the profile.

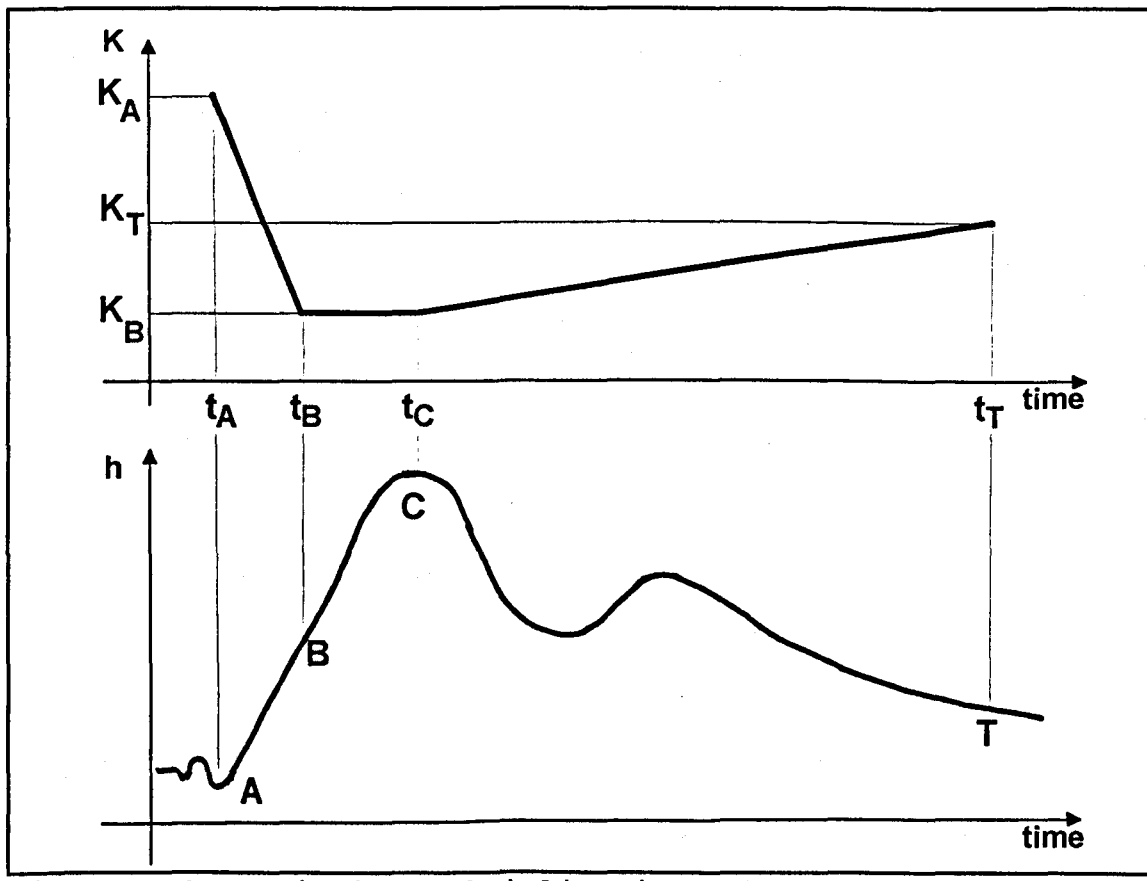

Figure 3.3 - Friction multiplicative scheme

In the case exemplified at Figure 3.3 the steady state energy line slope (S_f) corresponding to the wave front base point A would be multiplied by k_A. From this point the

multiplicative factor would decrease linearly up to a minimum at point B, remaining in this situation up to point C. Thus, sections within B and C would have friction equal to a certain minimum value. Upstream of the wave peak the multiplicative factor would increase up to a value k_r that probably would be equal to 1, i.e., the friction effect would be well assessed through S_f.

In the wave front region (from points A to B, see Figure 3.3) a exponential variation of multiplicative factors was also attempted. This type of variation seemed to be closer to the physical situation since a strong multiplicative factor could be applied to the wave front base and from this point decrease very quickly to the wave peak. Thus, it would have preserved laboratory observations that had shown the pronounced shock effect of the wave front against the existing base flow. However, the use of a exponential variation in computational processing has shown to be complicated because the difficulty of manipulation within a practical adjustment procedure.

In every computation at an internal node the linear friction multiplicative scheme can be applied since a device to capture the wave front arriving is triggered. This was obtained by controlling the relative water depth variation respectively to the computation time step. Relative water depth variation is expressed by the relation

$$(\Delta h_{rel})_J^{k+1} = \frac{h_J^{k+1} - h_J^k}{t^{k+1} - t^k} \qquad (3.37)$$

The water depth appearing in equation (3.37) was initially computed through the ordinary process using S_f. If

the variation exceeded a certain value (preliminary verified), the whole calculation process is repeated now using ($k_t.S_t$) as the new energy line slope for that particular section.

Taking into account the wave attenuation, the scheme provides decreasing of the multiplicative factors with distance along the pipe. Final values, corresponding to a wave front not so steep, tend to approximate the friction effect to the steady state flow normal S_t, i.e., K tends to 1.

3.2.3 Local Wave Speed in Partially Filled Pipe Flow

In equations (3.15) and (3.16) integrals involving the local wave speed ($c = (g.A/T)^{0.5}$) were approximated as follows:

$$\int_{h^k}^{h^{k+1}} \frac{g}{c}\, dh = \int_{h^k}^{h^{k+1}} \sqrt{\frac{gT}{A}}\, dh = \frac{g}{c}\,(h^{k+1} - h^k) \qquad (3.38)$$

It is apparent that this solution is not mathematically correct since c is a function of h.

To overcome the difficulty of integration, Henderson (1966), quoting Escoffier's work, presented a solution introducing a "stage variable" ω that replaces h as a measure of the water depth. This variable is defined as

$$\omega = \int_0^A c\, \frac{dA}{A} = \int_0^h \sqrt{\frac{gA}{T}}\, \frac{T dh}{A} = \int_0^h \sqrt{\frac{gT}{A}}\, dh \qquad (3.39)$$

From equation (3.39) it can be written

$$d\omega = \sqrt{\frac{gT}{A}}\, dh = \frac{g}{c}\, dh \qquad (3.40)$$

that can be substituted in equations (3.15) and (3.16) giving

$$(u \pm \omega)\Big|_{t^k}^{t^{k+1}} = g \int_{t^k}^{t^{k+1}} (S_o - S_f)\, dt \qquad (3.41)$$

As developed previously, equation (3.41) could be solved using finite differences, based on a graphical or tabular form of ω(h) previously prepared.

Studying the relationship between ω, pipe diameter and water depth Swaffield (1986) found a general expression relating the three terms as follows

$$\ln\left(\frac{\omega}{c}\right) = K_1 + K_2 \ln\left(1 - \frac{h}{D}\right) + K_3 \left[\ln\left(1 - \frac{h}{D}\right)\right]^2 \qquad (3.42)$$

where K_1, K_2 and K_3 are numerical coefficients obtained applying a least squares fit polynomial technique. In this study a full range of pipe diameters from 50 mm to 225 mm was utilized.

Bridge (1984) and Standing (1986), however, found that the utilization of equation (3.42) merely speeded up computer processing when compared with the processing of approximated equations (3.19) to (3.22), without improving accuracy of results. Thus, it can be concluded that the assumed approximation on the integrals involving c in equations (3.15) and (3.16) are acceptable.

3.2.4 Stability Condition and Oscillation Control

The stability condition for hyperbolic equations is

defined through the Courant number or the Courant-Friedrichs-Lewy criterion (CFL). This criterion says that a stable explicit finite difference method has a numerical zone of dependence which must include the region defined by the characteristic curves. The criterion is mathematically expressed through the Courant number which reads

$$C_n = \frac{\Delta t}{\Delta x} [\max(|u| + c)] \qquad (3.43)$$

Numerical solution stability is obtained for $C_n \leq 1$. This condition rules the maximum computation time-step Δt since a C_n value have been established. The criterion is verified in every grid point before starting a new computation step and the most unfavourable time-step. i.e., the smallest, is applied to all computation nodes.

Preliminary computation using the Saint-Venant equations solved through the method of characteristics to simulate the tipping tank discharge has shown water depth instabilities at the wave front. In some cases the artificial peaks propagated and evolved in height breaking up the computation process.

Abbott (1989) considers that not only the numerical process is responsible for these instabilities. The mathematical model itself, as is the case of the Saint-Venant equations, does not embrace all the physical phenomena occurring mainly at wave fronts. Turbulence in the wave front is the main aspect not considered in the mathematical formulation. Thus, the numerical solution needs some mechanism

to dissipate energy at the wave front, comparable to a natural, internal turbulence dissipator.

Among the several ways to promote dissipation Abbott (1989) quotes the "automatic" numerical-dissipation of schemes running with $C_n < 1$ that provide wave damping avoiding oscillations. However, damping effects are also noticeable in gradually varied areas of the flow where damping would not be necessary. Thus, as recommended by Abbott, it is better to run the scheme at the best accuracy (e.g. $C_n \approx 1$) and to eliminate oscillations problems by use of a dissipative interface that can be adjusted to intervene only as discontinuities occur. This method is classified as a filtering method because the oscillations are controlled by numerical filters.

Quoting Richtmyer's version of Lax-Wendroff two-step scheme, Abbott (1979, 1989) presents the simplest form of numerical dissipative interface based on the following expression

$$(f_j^k)^d = \sigma' f_{j+1}^k + (1 - 2\sigma') f_j^k + \sigma' f_{j-1}^k \qquad 0<\sigma'<0.5 \qquad (3.44)$$

to be applied on internal nodes. For the ultimate left-hand boundary node the expression is

$$(f_j^k)^d = \sigma' f_{j+1}^k + (1-\sigma') f_j^k \qquad 0 < \sigma' < 1 \qquad (3.45)$$

and for the ultimate right-hand boundary node the expression is

$$(f_j^k)^d = (1-\sigma') f_j^k + \sigma' f_{j-1}^k \qquad 0 < \sigma' < 1 \qquad (3.46)$$

In equations (3.44) to (3.46) the left-hand side term

is the damped variable, computed after all nodes have been calculated at a certain time-level k.

Dampening is applied just to the region of wave where some instabilities have manifested. For that the same scheme of wave front capture, developed for the friction multiplicative scheme is applied. In this way, only a select part of the wave in a certain pipe length is subjected to the process after each computed time-step.

The numerical filter can be applied in one of the variables or in both.

3.2.5 Initial Conditions

As described in detail in Chapter 5, the upstream boundary in the laboratory pipeline is a section distant approximately 1 m from the pipe entry. In this section the tipping tank discharge has known characteristics. The hydrographs describing the variation of flow rate and water depth on time were measured at this section.

The downstream boundary, at the pipeline end, is a free overfall.

The initial condition is a steady state flow along the entire pipeline. As described in Chapter 2, the water surface profile varies gradually in the pipe end region if the flow is subcritical. In all other sections the flow is parallel to the pipe bed. In the supercritical flow case the water profile would be parallel in all sections including the free overfall.

In the actual laboratory measurements, however, invariably, the initial conditions were of subcritical flow since the pipeline slope and the initial steady state flow rates were very low.

In the numerical computation the initial condition is described through the water depth and flow velocity values in all nodes. The Colebrook-White formula, equation (2.75), was used to compute normal water depth.

In the gradually varied region of subcritical flow, water depth and velocity were computed through a step method for uniform channels. Deriving the specific energy equation in h and assuming that the specific energy decay can be assessed through friction (water vs pipe bed) losses, its possible to demonstrate that the following expression is valid

$$d x' = d h \frac{(1 - F_R^2)}{(S_o - S_f)} \qquad (3.47)$$

where $F_R=(u/c)$ is the Froude number and dh is the water depth variation in the segment dx'. The symbol (') is used just to differentiate this coordinate from that previously defined that has opposite direction. Equation (3.47) can be numerically handled in finite difference form to compute the gradually varied profile. The energy line slope was calculated with the Colebrook-White formula as referred before.

In the gradually varied profile computation dh was taken as a fixed increment of water depth dividing the difference of the normal depth to the free overfall depth in 50 parts. Starting with the water depth at the free overfall and adding the fixed variation it was possible to know the water depth in all these particular 51 sections. Then, the

distance between these sections was computed using equation (3.47). Taking mean values of F_R and S_f between the downstream and upstream sections of each computation step it was determined the corresponding segment length. Finally, the profile was calculated for each node of the computation grid using linear interpolation over the values obtained in the step method.

The free overfall water depth in the subcritical case is theoretically equal to the flow critical depth. However, the actual phenomenon shows that the water streamline curvatures near the pipe end are great enough to introduce water vertical acceleration. For this reason the actual brink water depth is smaller than the theoretical. According to Chow (1959) the critical depth in fact occurs at a distance approximately 4 to 5 times h_c, the critical water depth, upstream of the brink. Empirical measurements and correlations presented by Ranga Raju (1981) for circular canals verify this. It was found for this particular application that the commented discrepancy would not be relevant and the critical depth was assumed to occur at the pipe end.

Still referring to the critical depth, the difference of computation through the energy equation derivation and the Straub semiempirical formula quoted by French (1986) was analyzed. Straub's formula for circular canal reads

$$h_c = \frac{1.01}{D^{0.26}} \left(\alpha\, Q^2/g\right)^{0.25} \qquad (3.48)$$

$$0.02 \leq \frac{h_c}{D} \leq 0.85$$

where D is the pipe diameter, α is the kinetic energy

correction factor which is used to correct the non-uniformity of the velocity profile, assumed equal to 1. Using Straub's formula critical water depth was approximately 5% higher than the depth computed through the energy equation for the flow rate range of values normally used in the laboratory measurements. Nevertheless the relative small difference, Straub's formula was adopted for critical water depth computation.

If the base flow is supercritical the initial condition is given by the normal water depth and corresponding velocity in all sections.

3.2.6 Unsteady Flow Boundary Conditions

The entry boundary conditions are giving by the tipping tank discharge hydrographs at the initial section of the pipeline. If the inflow on the upstream boundary section is a supercritical flow there is no influence from downstream sections on the initial section. This is the actual situation for most of the tipping tank discharge. However at the hydrograph "tail" there is an asymptotic convergence of the discharge to the existing base flow. Thus, subcritical flow can be expected. In this case there is an influence from downstream sections on the entry section. This influence is mathematically described by the C_1- characteristic depicted in Figure 3.1. However in the present work both flow rate and associated water depth profile were measured at the entry section. Thus, the

downstream influence is already incorporated on entry data.

The exit boundary condition for the subcritical flow case is governed by the energy equation and the $C_{N+1}+$ characteristic (see Figure 3.1) equation. At the free overfall the flow specific energy reaches its minimum value. This condition can be expressed deriving specific energy equation and equating it to zero, resulting

$$1 - \frac{[u_{N+1}]^2}{[c_{N+1}]^2} = 0 \qquad (3.49)$$

In this case the point P corresponds to the position (N+1). Working out equation (3.20), it is possible to express the point P velocity as a function of h_p. Substituting u_p velocity in equation (3.49) results in equation (3.50).

Equation (3.50):

$$1 - \frac{\left[u_R + \frac{g}{c_R}(h_P - h_R) + g(S_o - S_{f_R})(t^{k+1} - t^k)\right]^2}{c_P^2} = 0$$

Assuming values of h_p equation (3.50) can be verified using the bisection method.

In the supercritical flow exit boundary conditions are described through ($C_{N+1}+$) and ($C_{N+1}-$) characteristics, passing respectively by points R and S' in Figure 3.1.

3.3 The McCormack Scheme Applied to the Saint-Venant Equations

The McCormack scheme is widely used in computational fluid dynamics being suitable for shock capturing problems. This is a explicit scheme of simple implementation being second-order accurate in both space and time.

The McCormack scheme is a variation of a class of difference methods developed by Lax and Wendroff generally known as two-steps schemes (Fennema, 1986). These methods are based on second-order Taylor series expansion in time.

The method is developed according to a two level predictor corrector scheme. Following Gharangik et Chaudhry (1991) application of the scheme, the spatial derivatives are developed through forward finite-difference approximations in the predictor part and through backward finite-difference approximations in the corrector part.

In the predictor step, indicated with the superscript asterisk (*), variables are evaluated by the expression

$$U_j^* = U_j^k - \lambda (F_{j+1}^k - F_j^k) + \Delta t\, S_j^k \qquad (3.51)$$

and in the corrector step, indicated with the superscript double asterisk (**), variables are computed through

$$U_j^{**} = U_j^* - \lambda (F_j^* - F_{j-1}^*) + \Delta t\, S_j^* \qquad (3.52)$$

In these equations the subscript j refers to the computation node in the x direction of the computation grid and k superscript refers to the time level. λ is the ratio of the time step by the inter node distance, i.e., $\lambda = \Delta t/\Delta x$, where

$\Delta x = L/N$, L the simulated length and (N + 1) the number of nodes points of the simulated length. From equations (3.51) and (3.52) it is apparent that variables are computed in the interior nodes, i.e., from j = 2 to j = N. Variables with the k superscript are known. Unknown variables values at the time level (k + 1) are computed through

$$U_j^{k+1} = \frac{1}{2} (U_j^k + U_j^{**}) \tag{3.53}$$

Applying the McCormack scheme to the Saint-Venant equations leads to the following formulation to be used in the flow simulation.

PREDICTOR LEVEL:

$$A_j^* = A_j^k - \lambda [(uA)_{j+1}^k - (uA)_j^k] \tag{3.54}$$

$$(uh)_j^* = (uh)_j^k - \lambda [(u^2h + \frac{g}{2}h^2)_{j+1}^k - (u^2h + \frac{g}{2}h^2)_j^k] + g \Delta t [h(S_o - S_f)]_j^k \tag{3.55}$$

CORRECTOR LEVEL:

$$A_j^{**} = A_j^* - \lambda [(uA)_j^* - (uA)_{j-1}^*] \tag{3.56}$$

$$(uh)_j^{**} = (uh)_j^* - \lambda [(u^2h + \frac{g}{2}h^2)_j^* - (u^2h + \frac{g}{2}h^2)_{j-1}^*] + g \Delta t [h(S_o - S_f)]_j^* \tag{3.57}$$

VARIABLE VALUES AT TIME LEVEL (k + 1):

$$f_j^{k+1} = \frac{1}{2}(f_j^k + f_j^{**}) \qquad (3.58)$$

In equation (3.58) f corresponds either to area (A) or to the product (uh).

3.3.1 Stability Condition and Oscillation Control

The numerical stability condition is the same as defined by equation (3.43) applicable to the solution through the method of characteristics.

Higher-order explicit finite difference schemes usually produce numerical oscillations near the steep wave front. In this case it become necessary to numerically damp these oscillations. This is obtained by adding what is called an artificial viscosity to smooth the oscillations. In fact this procedure is of the same nature as that applied through equations (3.44), (3.45) and (3.46).

Among several possibilities reported in the literature Fennema and Chaudhry (1986), used that developed by Jameson et al. (1981). Jameson's procedure is advantageous because its selective high-frequency capability, i.e., the procedure smoothen the high-frequency oscillations near the steep gradients areas of the solution while having mild effect on smooth areas.

The application of Jameson's procedure has shown good results in computer simulations validated through comparison

against laboratory measurements (Fennemma et Chaudhry, 1986; Gharangik et Chaudhry, 1991 and Bhallamudi et Chaudhry, 1991).

In Jameson's procedure a parameter ϵ_i is computed from the computed flow depths or from velocities. Here the parameters was computed from the flow depths as follows:

$$\varepsilon_j = \frac{|h_{j+1} - 2h_j + h_{j-1}|}{|h_{j+1}| + 2|h_j| + |h_{j-1}|} \qquad (3.59)$$

In the middle position (j + ½) ϵ is computed as

$$\varepsilon_{j+\frac{1}{2}} = K \frac{\Delta x}{\Delta t} \max(\varepsilon_{j+1}, \varepsilon_j) \qquad (3.60)$$

where K is used to adjust the dissipation. Simulating hydraulic jumps Gharangik et Chaudhry (1991), used K values ranging from 0.01 to 0.05.

After each time step variables can then be damped through the expression (3.61) as follows.

$$f_j^{k+1} = f_j^{k+1} + \varepsilon_{j+\frac{1}{2}} (f_{j+1}^{k+1} - f_j^{k+1}) - \varepsilon_{j-\frac{1}{2}} (f_j^{k+1} - f_{j-1}^{k+1}) \qquad (3.61)$$

Expression (3.61) is not a mathematical sentence but a Fortran statement where f corresponds to the variables to be updated.

3.3.2 Boundary and Initial Conditions

Initial conditions are the same as those already described for use in the method of characteristics.

Considering that computation through the McCormack scheme is applicable to the interior nodes (j=2,3,..(N-1),N)

it is necessary to complement the computation in the upstream boundary (j=1) and in the downstream boundary (j=N+1). In these sections variables are computed using the same equations and procedures of the method of characteristics.

According to Fennema et Chaudhry (1986) the overall accuracy of the scheme is not impaired if the order of accuracy of the boundary conditions is one less than that of the interior nodes.

3.4 The Two-Four Scheme Applied to the Saint-Venant and Boussinesq Equations

Gottlieb et Turkel (1976) extended the McCormack scheme developing the dissipative two-four scheme being, therefore, also a generalization of the Lax-Wendroff method. The two-four scheme is fourth-order accurate in space and second-order accurate in time. The scheme has intrinsic dissipative properties being able to handle shocks without the necessity of adding artificial viscosity.

The method is also developed according to a two level predictor corrector scheme. Forward finite differences are applied in the predictor level and backward differences are applied in the corrector level. A variant of this application is obtained with backward differences in the predictor level and forward differences in the corrector level. According to Gottlieb et Turkel (1976) a two-four accuracy scheme is obtained even for a system of variable coefficients if these

two variants are alternated at successive time levels.

Similar alternating procedures have also been used by Garcia et Kahawita (1986) and by Carmo (1990) when applying the McCormack method.

The alternate procedure can be expressed through the following application to compute a generic variable f

$$f_j^{k+2} = L_2(\Delta t)\ L_1(\Delta t)\ f_j^k \qquad (3.62)$$

where L_1 and L_2 are finite-difference operators defined in the two-four scheme. The L_1 operator applies forward differences in the predictor level and backward differences in the corrector level. Inversely, the L_2 operator applies backward differences in the predictor level and forward differences in the corrector level.

The predictor step of L_1 operator, indicated with the superscript $^{(1*)}$, is computed by equation (3.63).

$$U_j^{1*} = U_j^k + \frac{\lambda}{6}(F_{j+2}^k - 8F_{j+1}^k + 7F_j^k) + \Delta t S_j^k \qquad (3.63)$$

Referring to L_2 operator the predictor step is indicated with superscript $^{(2*)}$ and is calculated using equation (3.64) as follows.

$$U_j^{2*} = U_j^{k+1} + \frac{\lambda}{6}(F_{j-2}^{k+1} - 8F_{j-1}^{k+1} + 7F_j^{k+1}) + \Delta t S_j^{k+1} \qquad (3.64)$$

The corrector step of L_1 operator, indicated with superscript $^{(1**)}$, is computed by equation (3.65).

$$U_j^{1**} = U_j^{1*} + \frac{\lambda}{6}(-7F_j^{1*} + 8F_{j-1}^{1*} - F_{j-2}^{1*}) + \Delta t\, S_j^{1*} \qquad (3.65)$$

The corresponding L_2 corrector step is calculated by equation (3.66).

$$U_j^{2**} = U_j^{2*} + \frac{\lambda}{6}(-7F_{j+2}^{2*} + 8F_{j+1}^{2*} - F_j^{2*}) + \Delta t\, S_j^{2*} \qquad (3.66)$$

Variable values are computed at the end of each operator using equation (3.58).

Applying the two-four scheme to the Boussinesq governing equations (2.57) and (2.90) leads to the following formulation to be used in the computation of the L_1 operator.

PREDICTOR LEVEL

$$A_j^{1*} = A_j^k + \frac{\lambda}{6}\left[(uA)_{j+2}^k - 8(uA)_{j+1}^k + 7(uA)_j^k\right] \qquad (3.67)$$

$$\begin{aligned}(uh)_j^{1*} = (uh)_j^k + \frac{\lambda}{6}\Big[&\left(u^2h + \frac{g}{2}h^2 - \frac{1}{3}h^2E1 + \frac{1}{3}h^2E2\right)_{j+2}^k \\ &- 8\left(u^2h + \frac{g}{2}h^2 - \frac{1}{3}h^2E1 + \frac{1}{3}h^2E2\right)_{j+1}^k \\ &+ 7\left(u^2h + \frac{g}{2}h^2 - \frac{1}{3}h^2E1 + \frac{1}{3}h^2E2\right)_j^k\Big] \\ &+ g\,\Delta t\, h_j^k S_o - g\,\Delta t\, h_j^k S_f \\ &+ S_o\frac{\Delta t}{2} h_j^k E2_j^k - S_o\frac{\Delta t}{2} h_j^k E1_j^k\end{aligned} \qquad (3.68)$$

CORRECTOR LEVEL

$$A_j^{1**} = A_j^{1*} + \frac{\lambda}{6}\left[-7(uA)_j^{1*} + 8(uA)_{j-1}^{1*} - (uA)_{j-2}^{1*}\right] \qquad (3.69)$$

$$
\begin{aligned}
(uh)_j^{1**} = {} & (uh)_j^{1*} \\
& + \frac{\lambda}{6}\Big[-7\left(u^2h + \frac{g}{2}h^2 - \frac{1}{3}h^2E1 + \frac{1}{3}h^2E2\right)_j^{1*} \\
& + 8\left(u^2h + \frac{g}{2}h^2 - \frac{1}{3}h^2E1 + \frac{1}{3}h^2E2\right)_{j-1}^{1*} \\
& - \left(u^2h + \frac{g}{2}h^2 - \frac{1}{3}h^2E1 + \frac{1}{3}h^2E2\right)_{j-2}^{1*}\Big] \\
& + g\,\Delta t\, h_j^{1*}\, S_o - g\,\Delta t\, h_j^{1*}\, S_{f_j}^{1*} \\
& + S_o \frac{\Delta t}{2}\, h_j^{1*}\, E2_j^{1*} - S_o \frac{\Delta t}{2}\, h_j^{1*}\, E1_j^{1*}
\end{aligned}
\qquad (3.70)
$$

Space derivatives terms appearing in E1 and E2 are approximated using three-point central finite-difference and time derivatives are approximated using backward finite-differences both in the predictor and corrector parts.

In equation (3.68) E1 is expressed through equations (3.71) to (3.73) and E2 through equations (3.74) to (3.76), as follows.

$$
E1_j^k = \left(\frac{A}{T}\right)_j^k \left[\left(\frac{u_{j+1}^k - u_{j-1}^k - u_{j+1}^{k-1} + u_{j-1}^{k-1}}{2\,\Delta t\,\Delta x}\right) + u_j^k\left(\frac{u_{j+1}^k - 2u_j^k + u_{j-1}^k}{\Delta x^2}\right) - \left(\frac{u_{j+1}^k - u_{j-1}^k}{2\,\Delta x}\right)^2\right] \qquad (3.71)
$$

$$
E1_{j+1}^k = \left(\frac{A}{T}\right)_{j+1}^k \left[\left(\frac{u_{j+2}^k - u_j^k - u_{j+2}^{k-1} + u_j^{k-1}}{2\,\Delta t\,\Delta x}\right) + u_{j+1}^k\left(\frac{u_{j+2}^k - 2u_{j+1}^k + u_j^k}{\Delta x^2}\right) - \left(\frac{u_{j+2}^k - u_j^k}{2\,\Delta x}\right)^2\right] \qquad (3.72)
$$

$$E1_{j+2}^{k} = \left(\frac{A}{T}\right)_{j+2}^{k} \left[\left(\frac{u_{j+3}^{k} - u_{j+1}^{k} - u_{j+3}^{k-1} + u_{j+1}^{k-1}}{2\,\Delta t\,\Delta x}\right) + u_{j+2}^{k}\left(\frac{u_{j+3}^{k} - 2u_{j+2}^{k} + u_{j+1}^{k}}{\Delta x^{2}}\right) - \left(\frac{u_{j+3}^{k} - u_{j+1}^{k}}{2\,\Delta x}\right)^{2}\right] \qquad (3.73)$$

$$E2_{j}^{k} = \left[\frac{A}{T^{2}}\right]_{j}^{k}\left(\frac{u_{j+1}^{k} - u_{j-1}^{k}}{2\Delta x}\right)\left[\left(\frac{T_{j}^{k} - T_{j}^{k-1}}{\Delta t}\right) + u_{j}^{k}\left(\frac{T_{j+1}^{k} - T_{j-1}^{k}}{2\Delta x}\right)\right] \qquad (3.74)$$

$$E2_{j+1}^{k} = \left[\frac{A}{T^{2}}\right]_{j+1}^{k}\left(\frac{u_{j+2}^{k} - u_{j}^{k}}{2\Delta x}\right)\left[\left(\frac{T_{j+1}^{k} - T_{j+1}^{k-1}}{\Delta t}\right) + u_{j+1}^{k}\left(\frac{T_{j+2}^{k} - T_{j}^{k}}{2\Delta x}\right)\right] \qquad (3.75)$$

$$E2_{j+2}^{k} = \left[\frac{A}{T^{2}}\right]_{j+2}^{k}\left(\frac{u_{j+3}^{k} - u_{j+1}^{k}}{2\Delta x}\right)\left[\left(\frac{T_{j+2}^{k} - T_{j+2}^{k-1}}{\Delta t}\right) + u_{j+2}^{k}\left(\frac{T_{j+3}^{k} - T_{j+1}^{k}}{2\Delta x}\right)\right] \qquad (3.76)$$

In equation (3.70) E1 is expressed through equations (3.77) to (3.79) and E2 through equations (3.80) to (3.82), as follows.

$$E1_{j}^{*} = \left(\frac{A}{T}\right)_{j}^{*}\left[\left(\frac{u_{j+1}^{*} - u_{j-1}^{*} - (u_{j+1}^{*})^{k-1} + (u_{j-1}^{*})^{k-1}}{2\,\Delta t\,\Delta x}\right) + u_{j}^{*}\left(\frac{u_{j+1}^{*} - 2u_{j}^{*} + u_{j-1}^{*}}{\Delta x^{2}}\right) - \left(\frac{u_{j+1}^{*} - u_{j-1}^{*}}{2\,\Delta x}\right)^{2}\right] \qquad (3.77)$$

$$E1^{*}_{j-1} = \left(\frac{A}{T}\right)^{*}_{j-1} \left[\left(\frac{u^{*}_{j} - u^{*}_{j-2} - (u^{*}_{j})^{k-1} + (u^{*}_{j-2})^{k-1}}{2\,\Delta t\,\Delta x}\right) + u^{*}_{j-1}\left(\frac{u^{*}_{j} - 2u^{*}_{j-1} + u^{*}_{j-2}}{\Delta x^{2}}\right) - \left(\frac{u^{*}_{j} - u^{*}_{j-2}}{2\,\Delta x}\right)^{2}\right] \tag{3.78}$$

$$E1^{*}_{j-2} = \left(\frac{A}{T}\right)^{*}_{j-2} \left[\left(\frac{u^{*}_{j-1} - u^{*}_{j-3} - (u^{*}_{j-1})^{k-1} + (u^{*}_{j-3})^{k-1}}{2\,\Delta t\,\Delta x}\right) + u^{*}_{j-2}\left(\frac{u^{*}_{j-1} - 2u^{*}_{j-2} + u^{*}_{j-3}}{\Delta x^{2}}\right) - \left(\frac{u^{*}_{j-1} - u^{*}_{j-3}}{2\,\Delta x}\right)^{2}\right] \tag{3.79}$$

$$E2^{*}_{j} = \left[\frac{A}{T^{2}}\right]^{*}_{j} \left(\frac{u^{*}_{j+1} - u^{*}_{j-1}}{2\Delta x}\right)\left[\left(\frac{(T^{*}_{j})^{k} - (T^{*}_{j})^{k-1}}{\Delta t}\right) + u^{*}_{j}\left(\frac{T^{*}_{j+1} - T^{*}_{j-1}}{2\Delta x}\right)\right] \tag{3.80}$$

$$E2^{*}_{j-1} = \left[\frac{A}{T^{2}}\right]^{*}_{j-1} \left(\frac{u^{*}_{j} - u^{*}_{j-2}}{2\Delta x}\right)\left[\left(\frac{(T^{*}_{j-1})^{k} - (T^{*}_{j-1})^{k-1}}{\Delta t}\right) + u^{*}_{j-1}\left(\frac{T^{*}_{j} - T^{*}_{j-2}}{2\Delta x}\right)\right] \tag{3.81}$$

$$E2^{*}_{j-2} = \left[\frac{A}{T^{2}}\right]^{*}_{j-2} \left(\frac{u^{*}_{j-1} - u^{*}_{j-3}}{2\Delta x}\right)\left[\left(\frac{(T^{*}_{j-2})^{k} - (T^{*}_{j-2})^{k-1}}{\Delta t}\right) + u^{*}_{j-2}\left(\frac{T^{*}_{j-1} - T^{*}_{j-3}}{2\Delta x}\right)\right] \tag{3.82}$$

For the L_2 operator formula are analogous.

Two-four scheme can also be applied to the Saint-Venant equations. For that, it suffices to make E1 = E2 = 0.

3.4.1 Stability Condition and Oscillation Control

According to Gottlieb et Turkel (1976) the two-four scheme must have the Courant number less than to 2/3 to be stable.

3.4.2 Boundary and Initial Conditions

Initial conditions are the same as already described for use in the method of characteristics.

In the two-four scheme, variables are computed in interior nodes varying from j=4 to j=N-2. The scheme is complemented with the McCormack method for nodes j=2, j=3, j=N and j=N-1 and with the method of characteristics for node j=N+1. Again, the overall accuracy level is maintained despite the smaller accuracy level in the extremities (Guarangik et Chaudhry, 1991).

3.4.3 Vertical Acceleration Variation

According to Boussinesq's assumption, in each flow section the water particle horizontal velocity can be taken as constant with depth and the magnitude of the vertical velocity may be assumed to increase linearly from zero at the bed to a maximum at the free surface.

Boussinesq's basic assumption can be taken as a first

approximation to the vertical water particle acceleration. Thus, it could be adjusted in a calibration process of a given real condition of flow. This hypothesis was adopted here and an adjustment process analogous to that applied to friction was developed.

In Chapter 2 from vertical acceleration developed equation, (2.89), it can written

$$\alpha = E2 - E1 \tag{3.83}$$

To adjust vertical acceleration a multiplicative factor acting on it was adopted. Thus, its expression become

$$\alpha' = Z(x,t)\,(E2 - E1)$$

In this assumption Z factor varies linearly in space and time. Similarly to the friction multiplicative scheme, in the numerical development process, the vertical acceleration factor was applied just to the wave front. This was possible using the computer program wave front capture scheme. The scheme can be illustrated through Figure 3.3 where K factors shall replaced by Z.

Reasons for this procedure arise not only from theoretical consideration, but also because the numerical process has been shown not to be sufficiently accurate to express the small magnitude of vertical acceleration relatively to the other derivative terms of equation (2.90). Therefore, the process can be understood as a means to manage with a lack of knowledge both from mathematical and numerical development.

CHAPTER FOUR

MATHEMATICAL MODEL NUMERICAL DEVELOPMENT

4.1 Introduction

A computer program was written to process the numerical methods applied to the mathematical models. This version embraces three alternative combinations of mathematical model and numerical method in order to compare simulation results for a given set of entry data.

The three numerical methods presented in Chapter 3 applied to the mathematical models derived in Chapter 2 comprise the set of three alternative process that are developed. Alternative process response can be adjusted through a calibration procedure where not well known parameters can be varied in order to find the best process response relatively to real data.

The entry data comprises several possibilities of tipping tank discharges according to a given geometric configuration used in laboratory measurements, as described in detail in Chapter 5.

The computer program is in a "research" stage, i.e., its applicability is mainly limited to the development

improved models, procedures and adjustment factors for flow simulation. Nevertheless, program improvements are planned, aimed at obtaining a useful tool for sewer network design and operation. It is important to observe that although the program has been developed to simulate a particular type of flow, its capabilities include the description of most typical discharges and flows occurring in sewer pipelines.

4.2 Computer Program Structure

The alternative mathematical and numerical models to be used in the computation are indicated on Table 4.1. As the Boussinesq equations comprise higher-order derivatives, the two-four higher order numerical scheme are used for these equations. Saint-Venant equations are computed through two accuracy level numerical schemes, namely, method of characteristics with first-order finite differences and the McCormack second order scheme.

Table 4.1 - Computer program processing alternatives

math. models / num.models	Saint-Venant equations	Boussinesq equations
method of characteristics	E	-
McCormack scheme	B	-
two-four scheme	-	D

The general program structure can be easily understood through the flowchart depicted at Figure 4.1.

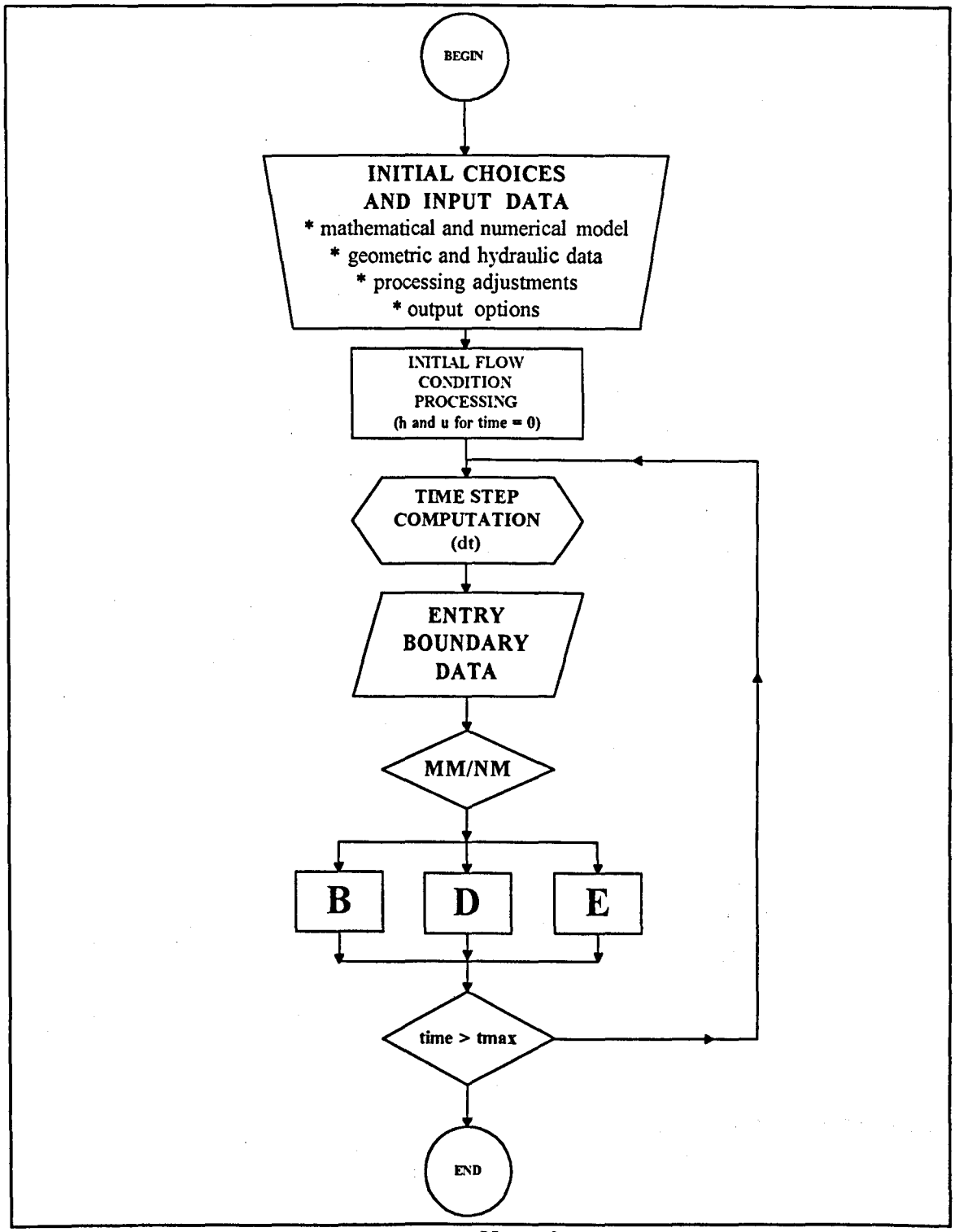

Figure 4.1 - Computer program flowchart

The first block corresponds to the interactive part of the program. In this part the user can choose the alternative methods to be used in the computation as well as indicating the internode distance, adjustment factors, geometric and hydraulic input data and output options.

Geometric data refer to the pipeline characteristics, namely, bed slope, diameter and length.

Hydraulic data refer to pipe surface roughness coefficient, k, in the Colebrook-White equation (2.75) and data concerning initial and boundary conditions. For the particular case of the glass pipe used in laboratory measurements, k = 0. The initial flow condition is given by the base flow rate. Data corresponding to the entry boundary condition, i.e., computer file names containing the tipping-tank hydrographs at the computation initial section, are also indicated. These files, and the process for the acquisition of the data are described in Chapter 5. Entry data on the present version of the program is limited to this particular format of computer files.

Adjustment factors are, in fact, a set of calibration coefficients providing the tools to approximate the "raw" results of strict mathematical and numerical methods to the actual variable values measured in the laboratory. This iterative process is described below.

Adjustment factors comprise the following: the Courant number C_n (see section 3.2.4); the friction multiplicative scheme (see section 3.2.2); the vertical acceleration multiplicative scheme (see section 3.4.3); the oscillation control factors α or K (equations (3.44) to (3.46) and (3.59)

to (3.61), respectively); and finally the space step, i.e., the fixed distance between computation nodes (Δx).

The desired time of simulated flow is also indicated in this phase.

Output options comprise the choice of computer files containing the simulated flow time, water depth and flow velocity to be registered. ASCII characters are used in these files. Registered files refer to flow sections corresponding to computed nodes, to particular chosen sections or to space profiles. The following options of flow variable saving are available at the program: space periodic node sections in a frequency previously defined by the user; control sections of laboratory measurements; particular chosen sections of verification defined by the user; time periodic space profiles in a frequency defined by the user and space profiles in particular instants defined by the user. Also provided is an alternative of a heading file with the main characteristics of a particular set of processed data; this file is used mainly to register entry data referring to a certain process.

Following this interactive process the program runs automatically, performing loops of time-step calculations until the maximum simulated flow time is reached.

Other blocks appearing in Figure 4.1 refer to phases already explained in other Chapters.

The decision block with letters MN/NM depicted, refers to chosen alternative of mathematical and numerical model (B, D or E).

4.3 Computer Program Characteristics

The program was written to operate on personal computers, using Fortran, as defined in the Microsoft Fortran 5.1, 1991.

The Fortran 5.1 runs under Microsoft DOS (version 3.0 or later) and OS/2 (version 1.1 or later) operating systems. It requires 512 Kbytes of RAM memory. Programs written in this Fortran version can run on machines with or without a mathematical coprocessor.

Due to the enormous quantity of operations of any chosen processing alternative, it is advisable to run the program on computers using very fast processors. Computers with processors of 33 MHz (386-DX Intel processors) and 66 MHz and 100 MHz (486-DX Intel processors) have been used. An assessment of computer time is given in section 4.3.1.

Output files can occupy a rather big space on the computer hard disk or in a virtual RAM-drive, depending on the user choices. This will depend on the processing alternative, on the number of files chosen and on the simulated flow time. Registration on files located in floppy disks were not provide due to slow saving process in this case.

4.3.1 Preliminary Computer Program Tests

The computer program was submitted to preliminary tests using simplified entry data, aimed at the verification of its

logic structure and consistency. Two types of entry data were used: uniform steady state subcritical flow and uniform steady state supercritical flow.

The main aspects verified were the program's capability to maintain steady flow condition in both the uniform region (parallel to the pipe bed) and the steady gradually varied region (the pipe end extremity, in subcritical flow). Additionally, the total time processing and the mean time step of each alternative was registered for comparison.

The steady entry data used to test subcritical and supercritical flow cases corresponded to a flow rate of 0.0024575 m^3/s . In the subcritical flow test it was adopted a pipe slope of 0.0005 m/m (the same as used in laboratory measurements, see Chapter 5) and in the supercritical flow test the adopted pipe slope was 0.004 m/m.

The simulated pipe length was 49.5 m with a fixed distance between computation nodes of 0.15 m in all cases, resulting a total of 331 grid nodes. Entry data referring to pipe diameter and roughness also corresponds to values actually existing in the laboratory, i.e., D = 0.156 m and k = 0 m (glass surface), respectively.

A total simulated flow time of 100 s was required in each test. Files containing the simulated time, water depth and flow velocity in sections distanced 3 m were registered. Additionally sections distanced 0.15 m, 49.35 m and 49.5 m from pipe entry were also registered. Files were saved on the computer hard disk.

Following Guarangik and Chaudhry (1991) and Bhallamudi

and Chaudhry (1991) a Courant number C_n=0.8 was used in the processing alternative B, C_n=0.667 in alternative D and C_n=1 at E alternative.

Table 4.2 summarizes obtained time processing and mean time-step for each alternative. A 66 MHz processor computer was used.

Table 4.2 - Preliminary processing results

processing alternative	flow regime	total processing time	number of time-steps	mean time-step
E	subcritic	57 min.	801	0.125 s
	supercritic	65 min.	767	0.130 s
B	subcritic	99 min.	999	0.100 s
	supercritic	87 min.	958	0.104 s
D	subcritic	124 min.	1198	0.083 s
	supercritic	120 min.	1149	0.087 s

Figures 4.2 and 4.3 illustrates the spatial profile of each processing alternative at three instants: time = 0, i.e., initial condition, time = 50 s and 100 s.

Figure 4.2 shows the superposed spatial profiles of the three processing alternatives on the supercritical flow case. The complete coincidence of profiles is observed and the

stability of the water depth profile for the complete simulation time confirmed.

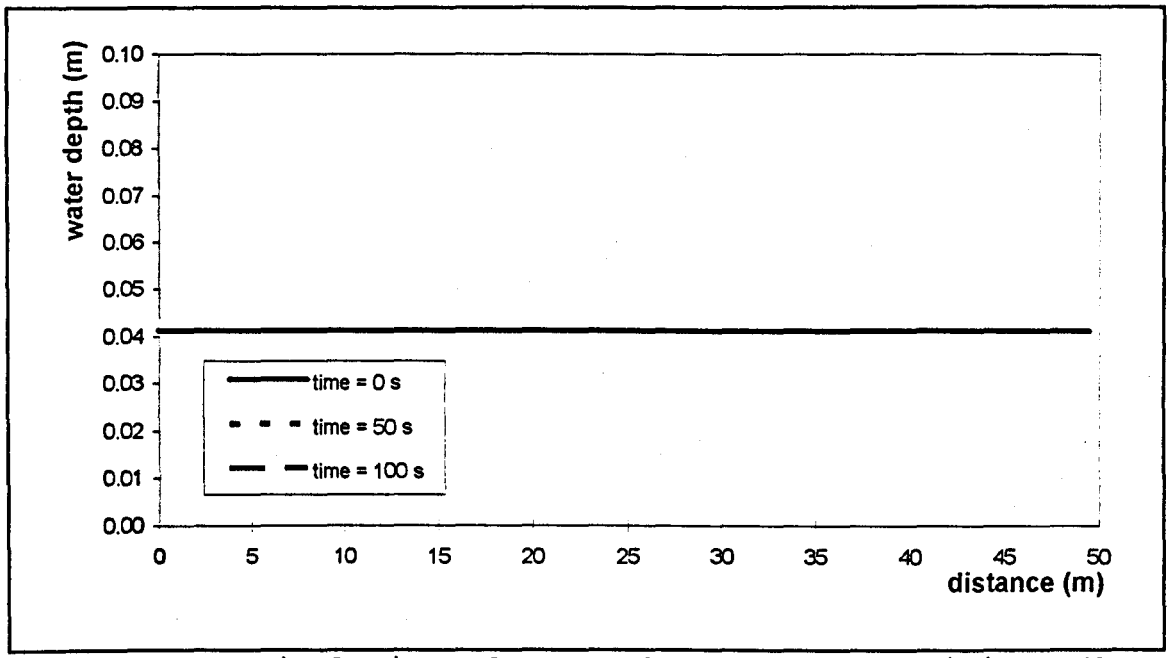

Figure 4.2 - Simulation of a steady state supercritical flow

Figure 4.3 illustrates the spatial profile on the subcritical flow case. Figure 4.3 a) refers to the processing alternative E, i.e., the Saint-Venant equations computed through the method of characteristics using Everett and Newton-Gregory interpolation. Figure 4.3 b) corresponds to the same equations computed through the McCormack scheme (processing alternative B) and Figure 4.3 c) shows profiles referring to alternative D, i.e., the Boussinesq equations computed through the two-four method.

It can be observed that the method of characteristics is stable on water depth profile maintenance while the other two methods present a slight deviation on the final computing sections. This deviation appeared in the early moments of computation and soon stabilized resulting in the coincident

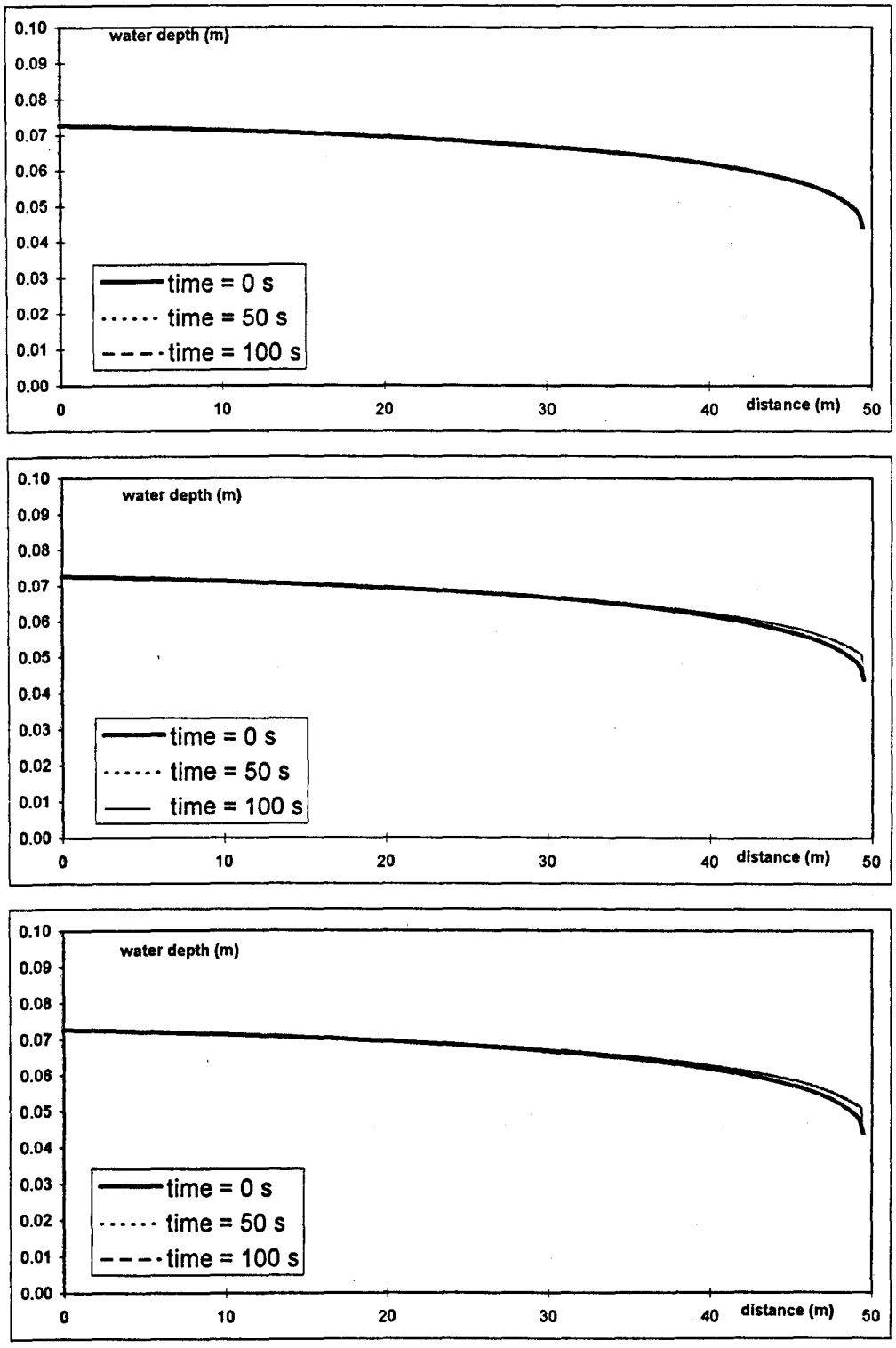

Figure 4.3 - Simulation of steady state subcritical flow

profiles corresponding to time 50 s and 100 s.

It was observed on the processing that the deviation is associated with the water depth difference between two grid nodes. The deviation increased with this difference and is particularly pronounced at section j = N where the proportional water depth difference to the last section (j=N+1) is highest. Is also apparent that neither the higher accuracy level of numerical methods nor additional terms of Boussinesq equations had contributed to any relevant difference between alternatives B and D. It will be observed, however, that the probable influence of Boussinesq additional terms in the last sections (N-1, N and N+1) could not be appreciated since the two-four method is applied from the grid nodes j=4 to j=N-2 (see 3.4.2).

Swaffield et Standing (1986) had observed the same problem on the backwater profile of subcritical flow. They have analyzed the problem in detail and found that the linear interpolation on the method of characteristics caused the referred differences. The problem was eliminated through the use of a more accurate interpolation method (see section 3.2.1).

Unfortunately, on the present stage of the computer program the more developed method of interpolation is not available on alternatives B and D in the last computed sections.

Computer simulation tests have shown that this deviation decreases with increasing Froude numbers and eventually disappears for a critical flow condition. Other

tests, decreasing the Courant number or decreasing the distance step have shown no influence on the deviation.

The influence of this deviation on the simulation subsequent analysis was taking into account, however, the magnitude of the phenomenon (maximum of 7% of water depth elevation at section j = N) is small.

4.4 Model Validation Process

Model validation is a process that establishes the degree, conditions and limits in which the continuum mathematical formulation and the correspondent discrete numerical solution simulate real phenomena. In large channel study practice this process is normally divided in two parts, namely, calibration and verification.

In more general terms the mathematical model can be considered validated if the predictions are verified to an acceptable degree of agreement.

In the calibration process certain free adjustment factors are manipulated to optimize the model while in the verification process the optimization itself is judged through the comparison of model and actual data.

French (1986) comments that a high level of calibration and verification make the model more likely to be applicable to a range of situations beyond the limits of the data used in the calibration and verification processes.

Results of model calibration and verification of simulated results against laboratory measured data is presented in Chapter 6.

4.4.1 Model Calibration Parameters

In Chapters 2 and 3 it was shown that in the governing equations, among other parameters, the value of the resistance of the bed against the flow is not exactly known in unsteady flows. Energy dissipation due to inter-water particle shocks is unknown as well. Adopting values from the uniform flow resistance equation is acceptable and usually applied just as a first approximation, nevertheless good results have been quoted by several authors simulating unsteady flows under this assumption.

Another adjustment possibility foreseen in the computational program and shown in Chapter 3 refers to the vertical acceleration particle acceleration. As was described, Boussinesq's hypothesis of linear variation of vertical velocity on water depth can be increased or decreased performing together with the friction adjustment an important tool to fit simulated data to laboratory measured data.

In conclusion, the calibration of the one-dimensional free surface unsteady flow model is a process where the value of the friction slope term (S_f) and the vertical acceleration (α) associated with other numerical variables are optimized, i.e, the friction and the vertical acceleration term values and

other free adjustment terms (distance-step, time-step, dampening factors, etc) are progressively refined to produce a best fit.

A widely used method to accomplish this goal is to solve repeatedly the governing equations for different values of S_f and α in a trial-and-error process up to a point where model and prototype data are within a certain degree of agreement (French, 1986). The model can then be said to be calibrated and the verification process for a wide range of flow conditions can be initialized.

In the present case the prototype is represented by the laboratory pipeline and the data for the purpose of calibration is presented in Chapter 5.

The whole consideration of calibration factors has made the calibration process quite complex, being a strongly time consuming activity. Another characteristic of this process was its subjective basis for decision taking, exemplifying the artistic character, quoting Cunge (1987) and Abbott (1987), inherent of modelling processes.

4.4.2 Calibrated variable

The surge flowing through the pipe can be described in terms of the main hydraulic variables (h=h(x,t) and u=u(x,t)) correlated through governing equations.

Both variables would have to be verified in comparison with real data to rigorously validate the model, but in the

validation process carried on here, it was assumed that verification of one of the variables would ensure that the other would be indirectly verified, due to the mathematical inter-dependence of equations. Although the literature shows that this procedure is commonly applied in similar validation processes, a complete verification of all variables would be desirable mainly because the gap of knowledge that exists between the derivative equations and theirs numerically developed forms, and also because some physical aspects (friction, energy dissipation, etc) could not be properly incorporated into the mathematical model.

The calibration and the verification processes are carried on by comparing the water depth simulation program prediction with the water depth measured in the laboratory for a well defined set of conditions.

As an extension of this process the velocity and celerity predictions will be implicitly accepted. From these variables a set of important complementary values can be assessed, e.g., the flow volume and energy and the peak trajectories.

4.4.3 Distance Between Grid Nodes

The distance between nodes in the rectangular fixed grid is a free factor of adjustment and, therefore, is not subject to an unequivocal decision, i.e., to find a suitable or perhaps an optimal distance between nodes is also a matter

for choice in a trial-and-error process.

In consequence the time step is indirectly subjected to the same process since it is determined in the model under the Courant criterion for stability that depends on that distance.

In this calibration process the distance between computing nodes was initially fixed in 0.30 m following the experience on similar computation developed by Swaffield and Standing. However, due to the quite rapid variation of profile with time and distance, preliminary program operation showed that a smaller distance would avoid excessive profile dampening on flow rapidly varied regions. Some further experimental program operation have shown that a distance of 0.10 m yielded better results.

4.4.4 Flow Regime Identification (Method of Characteristics)

The identification of flow regime at the computing node is crucial when running with the method of characteristics alternative. It was seen in Chapter 2 that the flow originated by the tipping tank discharge represents a number of different regimes. In fact the flow, as a whole, is a sequence of subcritical and supercritical zones continuously changing in relative position. More generally the flow can be depicted as a wave that advances onto a subcritical steady flow. This wave has a front in the supercritical regime while its tail is in subcritical flow but, this scheme evolves with time. In all

these cases the flow regime is judged according to the relation between u and c at the section (node) where the variables are to be determined at a certain time. However, variable values are unknown at point P (section j, time t^{k+1} ,i.e., the node where the variables are to be calculated according to Figure 3.1) and the flow regime can not be readily identified at this point. In fact the flow regime only can be definitely identified after the computation at this point.

A specific scheme for flow regime assessment at a certain node was developed. This scheme utilizes the concepts of the domain of dependence and region of influence of a certain computation node in the method of characteristics. In this analysis it is necessary to understand how the characteristic lines and zones evolve with time. This evolution brings information on the probable flow regime at the computation node.

Figure 4.4 illustrates the two flow regimes focusing at computation grid point C, where variables are already known,

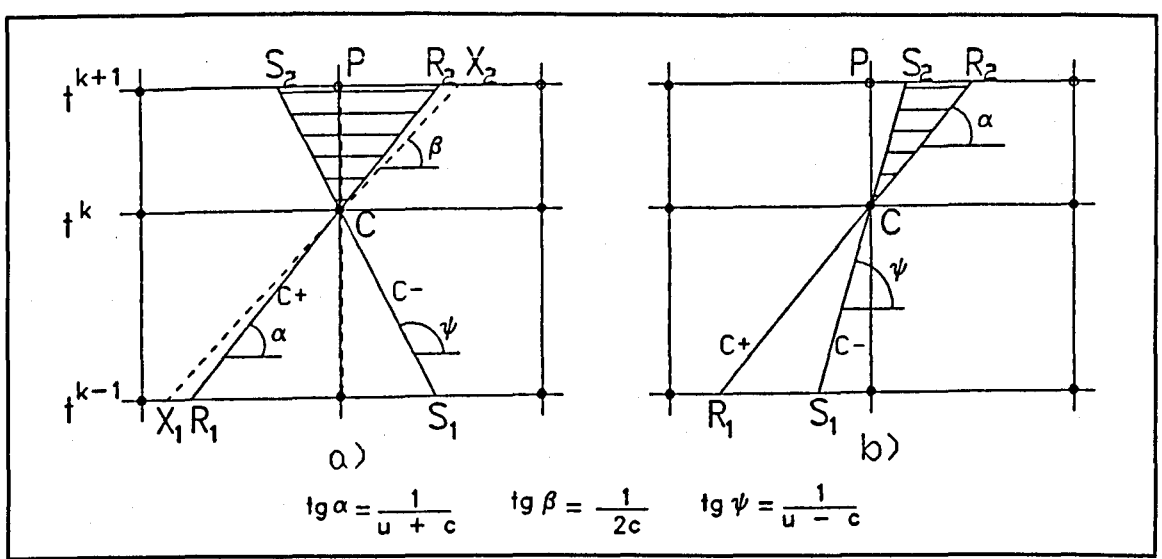

Figure 4.4 - Dependence domain and influence zone in the method of characteristics

and point P where they are not known. Figure 4.4 a) shows the characteristic lines of a subcritical flow in the section at time level t^k. The domain of dependence of point C is the segment R_1-S_1 and its zone of influence is the area bounded by C-S_2-R_2. It should be observed that the characteristic lines and their region of influence could be understood as flow property propagation paths. As remarks Abbott (1966), however, the region of influence of C can effectively influence the flow behaviour in S_2-R_2 but, not to determine it.

It could be imagined that the flow regime is one of the properties or attributes that is being propagated. Thus, since point C corresponds to a section at subcritical flow it could be assumed that the same section at time level t^{k+1} (point P) would be at subcritical flow, for this point is within the C region of influence. However, a closer observation of flow properties inside the C zone of influence should be undertaken to see how the relation between u and c behaves.

Equation (3.11), giving the characteristic direction will aid in the analysis. The limiting case between subcritical and supercritical flow is the critical flow which corresponds to u=c. For this limiting case the two characteristic directions would be dx/dt = 0 or dx/dt = 2c. In Figure 4.4 a), dashed lines show the characteristic corresponding to a hypothetical critical flow in C. It can be seen that there is an area of superposition with point C zone of influence. It should be remarked that the hypothesis of flow regime as an attribute propagating from C is now slightly disfigured since inside a subcritical flow zone of influence is comprehended a

critical one. The triangle at right of point P (C-P-R_2) (Figure 4.4 a)) is an area where $u \geq c$ and the triangle at left (C-P-S_2) corresponds to $u \leq c$. If the S_1-S_2 segment rotated around C in the clock wise direction, the critical flow limiting case would be overpassed and the flow would become supercritical as illustrated by Figure 4.4 b). In this case the attribute propagation hypothesis is completely unsuitable for point P since the influence zone of C now only reaches sections downstream of this point.

In conclusion it seems clear that the flow regime at point C does not provide a good indication for the same property at point P. The flow regime at point P would be exactly identified if a unique pair of characteristics cross at it. That is the case of characteristic lines passing through adjacent points R and S (or S') at level t^k as follows.

Figure 4.5 depicts four situations combining subcritical and supercritical flow through points adjacent to the nodes at level t^k. Below each particular drawing is presented a probable graphic of u and c evolution in the flow sections in the segment limited by nodes A and B.

It is apparent on Figure 4.5 that the flow regime in P will be determined by two characteristic lines limiting the zone of influence of two different points of the previous time level and that these points are exactly on the characteristics passing through P. It is also clear that point P is always at the right side of R zone of influence and at left side of S (or S') zone of influence. Point R is determined by iteration

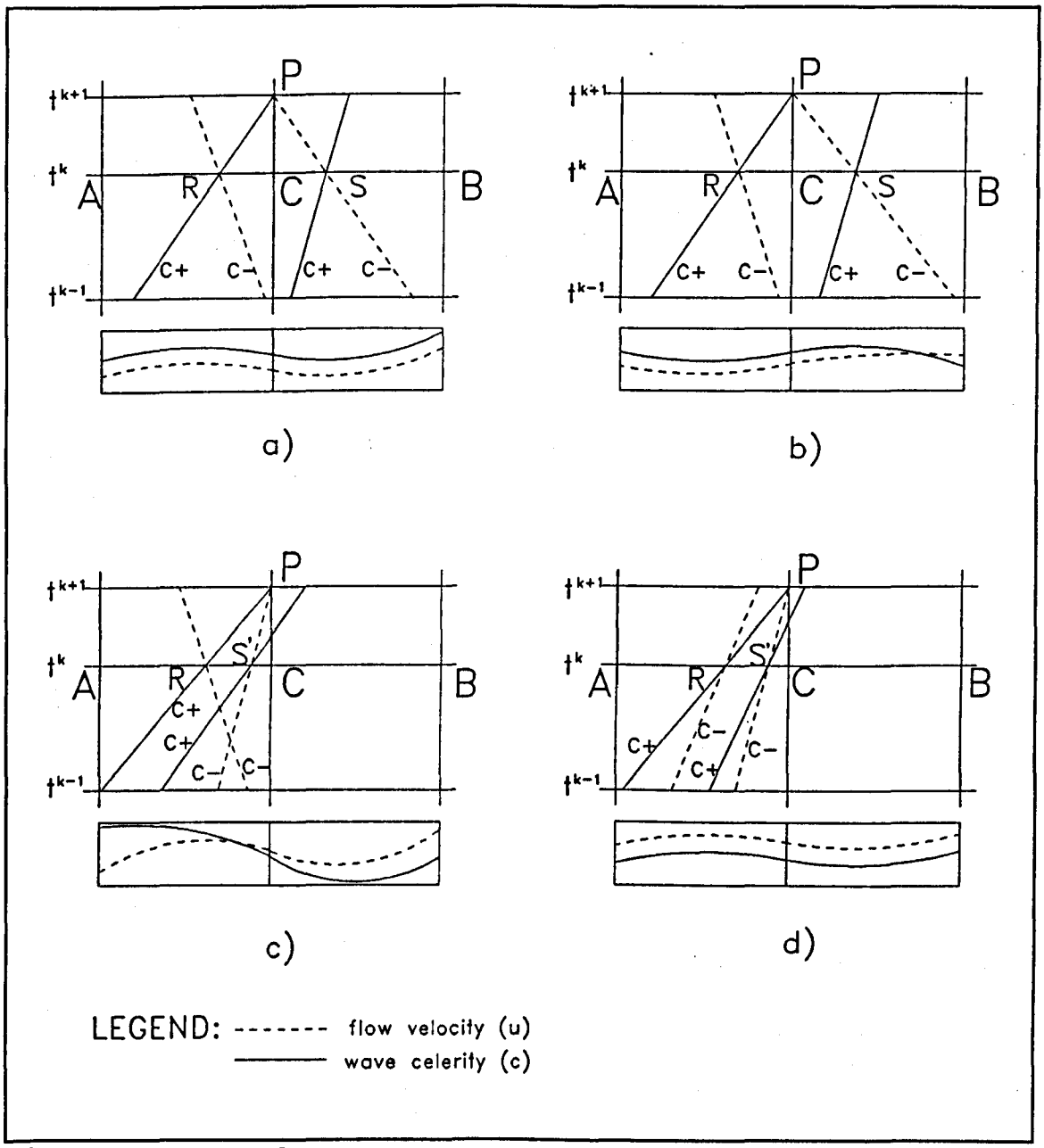

Figure 4.5 - Influence zones on P

and interpolation between nodes A and C as explained on section 3.2.1. The mathematical condition to be respected in this case is

$$u_R + c_R = u_P + c_P \qquad (4.1)$$

The C- characteristic also is computed through the same iteration and interpolation process that will converge to a point where the following mathematical condition must be observed

$$u_S - c_S = u_P - c_P \qquad (4.2)$$

These processes are readily applicable when the relative evolution of u and c are "well behaved", as in the cases presented in Figure 4.5. Analysis of this Figure shows that the relative position of u and c values leads to a unique possibility in terms of influence on point P. For example at Figure 4.5 c): firstly in the segment CB the flow is supercritical since u>c and, thus no influence on P can be expected from this region. In the segment AC however, the flow presents a zone of subcritical flow and a zone of supercritical flow. Thus, it can be concluded that the influence of a subcritical zone and of a supercritical zone will be present on P. Figures 4.5 c) illustrates this fact showing that exactly the limits of these two flow regimes could define point P flow regime through the C+ characteristic line passing through R and the C- characteristic line passing through S'. The same reasoning applied to cases a), b) and d) of Figure 4.5 shows that a unique solution is obtainable. It is implicit in this scheme a simplification on the variation of u and c. As can see on Figure 4.5 it is admitted that u and c does not change relative position on a distance step more than once.

Another set of conditions, however shows a situation where the solution is not immediate. It is assumed again that

u and c will not change their relative position more than one time in the distance comprehended between two grid nodes. In other words, the graphics of u and c will have only one cross along the Δx length, as illustrates Figure 4.6.

Applying the same reasoning developed for the cases depicted on Figure 4.5 it can be seen that the cases illustrated in Figure 4.6 does not lead to a unique solution

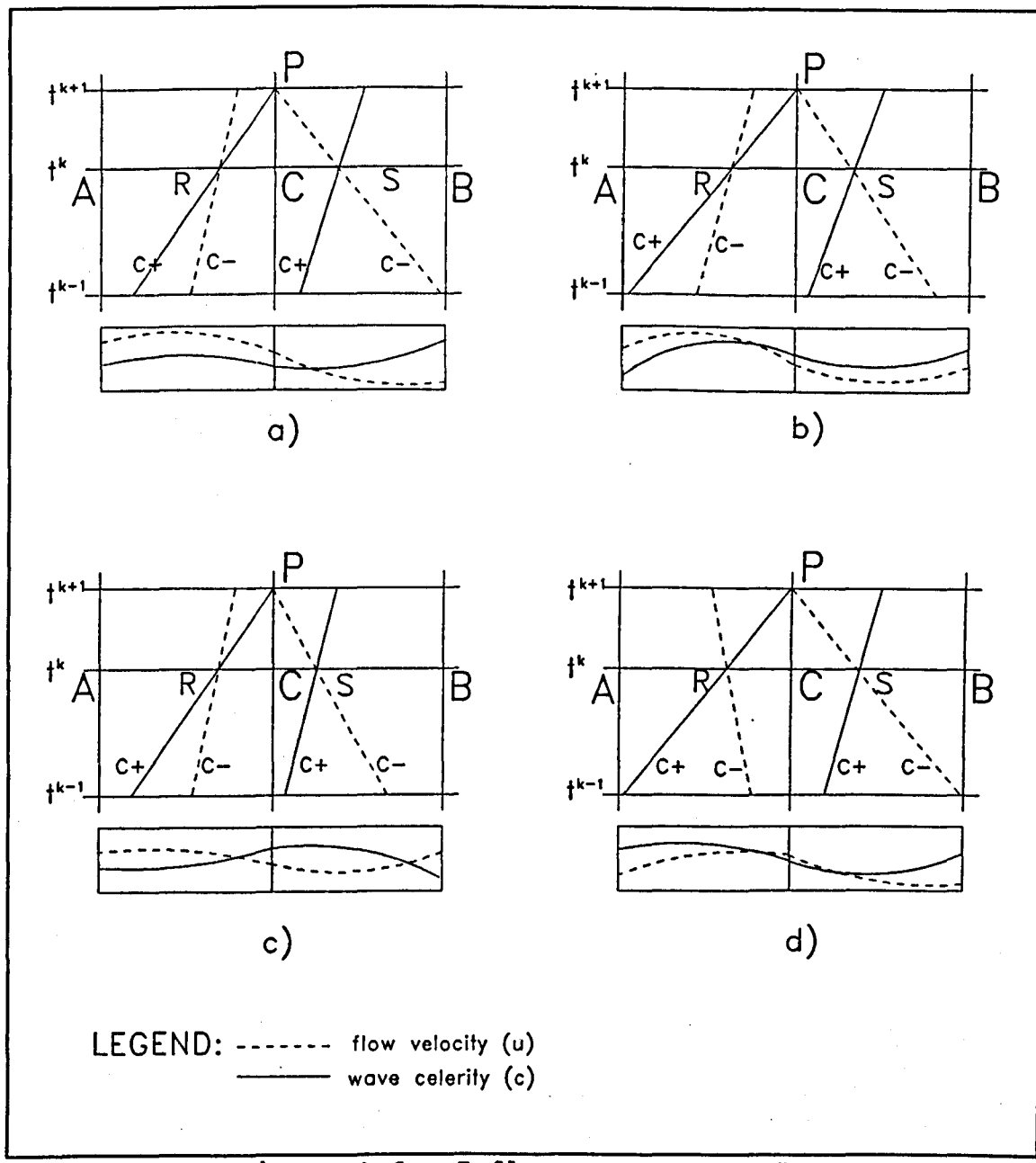

Figure 4.6 - Influence zones on P

of point P flow regime. In other words, in the four cases illustrated at Figure 4.6 the identification of point P flow regime is not immediate since the evolution of u and c graphics show that a C- characteristic both on backward and forward direction are possible depending basically on u and c values along the length of the segment.

In these cases a special procedure was introduced in the computation program aiming to identify point P flow regime. Initially the point R related characteristic (C+) is determined by the iteration and interpolation process. It is important to remark that point R C+ characteristic can refer to a subcritical or supercritical flow regime at point R on t^k time level.

For points S or S' the sequence of verifications below presented is carried on. In this sequence, referring to the iteration process, non convergence corresponds to a situation where a pair of values of u and c tends to be obtained outside of adjacent grid nodes, i.e., the iteration and interpolation lead to a position of S at right of node (j+1) or at left of node (j). Respectively, point S' would be at left of node (j-1) or at right of node (j).

a) if the iteration between nodes A and C leads to a pair of values u and c for that $(u_{s'} - c_{s'}) = (u_P - c_P)$, i.e, if there is convergence for S', and if there is no convergence for S between nodes C and B, then point P flow regime is supercritical;

b) if iterations lead to convergence for S and non convergence for S', then point P flow regime is subcritical;

c) if iterations lead to convergence of both S and S', then the point with greater propagation velocity will prevail. This condition can be mathematically formulated as follows. If the propagation velocity through characteristic passing by S is $|u_s - c_s| = a$ and the same parameter in S' is $|u_{s'} - c_{s'}| = b$, then, if a>b point P flow regime is subcritical and if a<b point P flow regime is supercritical;

d) if no convergence is obtained at all, neither for S nor for S', then the tendency observed in the iteration process is used to decide. These tendencies can be combined to identify the most probable flow regime at point P. Table 4.3 encloses possible cases.

In Table 4.3 the letter R corresponds to a non convergence tending to the right position either for S or S'. Letter L corresponds to a tendency to the left position. In three cases it is possible to identify a probable final tendency and in these cases it is assumed that points S or S' position coincides with the grid node according to the direction to which the point tends. When non convergence of S

Table 4.3 - Probable flow regime at point P in non convergence cases

		S	
		R	L
S'	R	subcritic HS = H(J+1) US = U(J+1)	supercritic HS = H(J) US = U(J)
	L	higher propagation velocity	supercritic HS = H(J-1) US = U(J-1)

and S' tends to symmetrical opposite directions it is assumed that the higher propagation velocity of the adjacent grid nodes will prevail as adopted in item c) above.

4.4.5 Friction Effect Adjustment

In many cases of large hydraulic structure calibration, friction adjustment is the core of the process. Many examples of large structure studies refer to the behaviour of flow in certain fixed sections over which the calibration process is applied. In the present case, however the adjustment refers to a wave passing along the pipe. Thus, the calibration process aims to find general formulations that can be generically applied to a flow continuously changing its characteristics in space and time. This peculiarity obviously make the process much more complicated.

Additionally it should be considered that it is improbable to have a unique adjustment scheme independent of the processing alternative. Thus, the friction multiplicative scheme presented at section 3.2.2 will probably yield different results when applied to processing alternatives B, D or E.

It should also be remarked that the friction effect can hardly be viewed separately from other factors. The adjustment process practice has shown the difficulty in isolating a particular factor from others. Thus, only a comparative evaluation is possible over a broad final result

of each processing alternative, with its particular set of adjustment parameters.

Chapter 5 describes in detail the flow behaviour as observed in the laboratory. The crucial aspect in terms of friction has been shown to be related to the wave front "foot". The base of the wave front shocks against the previous base flow (of small water depth) in the pipe or, if there is no base flow, the wave front "foot" generates a strong turbulence due to the friction with the pipe bed. It is clear from visual observation in the laboratory that in this region friction has a strong action against the water mass movement. However, this fact can not be generalized. Standing (1986), for example, concluded in the opposite direction because in that case the wave "slipped" over the existing base flow without shocking against it. Standing introduced this fact into the formulation, reducing the area of friction between water and pipe bed (see section 3.2.2).

This section presents a general overview of the friction multiplicative scheme application to the tipping tank flow simulation. Results referring to each specific entry data are presented and discussed in Chapter 6.

The friction multiplicative scheme presented in 3.2.2, and depicted again in Figure 4.7, was used.

Trial-and-error simulation running with entry data corresponding to tipping tank discharge volume of 39.5 L over a nominally zero base flow rate (Q_b=0.001 L/s) and over a Q_b=0.1 L/s base flow rate, were performed.

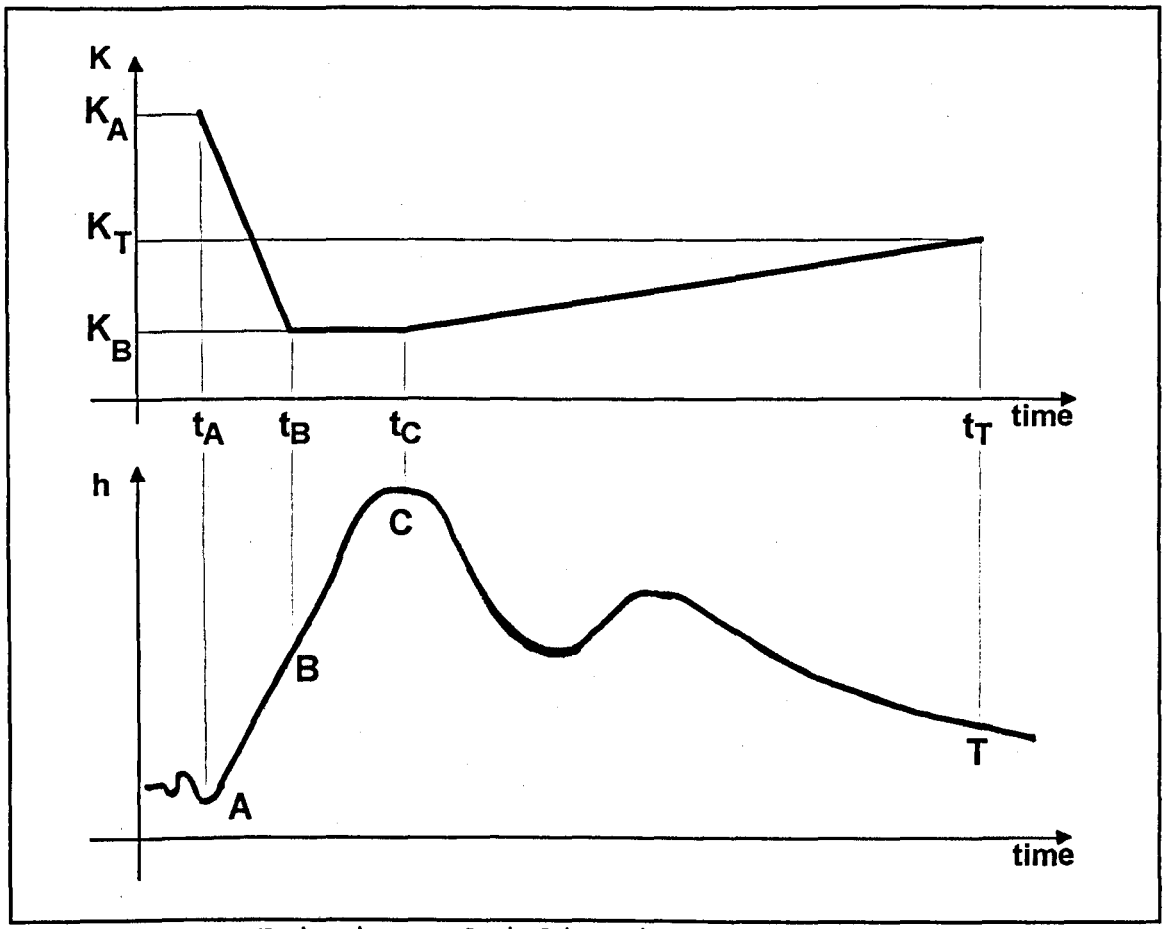

Figure 4.7 - Friction multiplicative scheme

Preliminary running had tried to isolate adjustment factors in an attempt to study each factor effect separately. In the case of the friction effect, for example, when running with the B and E process alternatives this was not possible because wave front presented strong instabilities requiring the use of numerical filters. In the D alternative, wave front instabilities were milder. In this case the observation of water depth and velocity variation with friction was possible within a certain degree. Water depth and wave front velocity revealed to be very susceptible to friction variation. Very high K multiplicative factors applied to the wave front region lead to the wave front main peak quick rising. Sometimes the

wave "exploded", i.e., the water depth reached values much beyond the pipe diameter. In these cases only a combination of friction, vertical acceleration and dampening factors has shown to be effective to control the process.

In conclusion, it is practically impossible to establish a generally valid set of unique friction multiplicative values since in the simulation process these values are combined with a number of others adjustment factors that can also have a similar effect on the simulated flow behaviour. In fact, in any of the program alternatives, a better fit is obtained only if a set of the friction multiplicative factor K and the dampening factor α (equations 3.44 to 3.46) is used. In addition, in the D alternative, the vertical acceleration factor Z has also to be used.

The conclusion above did not impede some observation on the effect of friction multiplicative factor K variation. Since some wave front stabilization was obtained it was possible to vary K within a certain range of values. K values bigger than 1 promote the water surface to rise and horizontal velocity to decrease. This is coherent with the dynamic analysis of the flow. When applied to the main wave peak region K values had to be carefully adjusted because a permanent trend of water depth "explosion" in this region was observed leading to absurd results or to subsequent processing breaking down. K value smaller than 1 showed opposite effect, i.e., water surface dampening and horizontal velocity increasing. These variations had also, consequently, promoted a change of the wave position in time. K values bigger than 1 lead to a wave

slowing down while K values smaller than 1 lead to faster movement.

Figure 4.8 shows K values according to position on the wave profile (see Figure 4.7) and according variation along the first 3 m of pipeflow simulation, for the case of null base flow rate. For 0.1 L/s base flow rate, K would be slightly bigger. These values will be considered restricted to the tipping tank generated wave and serve just as an initial reference. Again, it has to be remembered that K variations on Figure 4.8 are combined with α dampening factor and Z vertical acceleration factor variations.

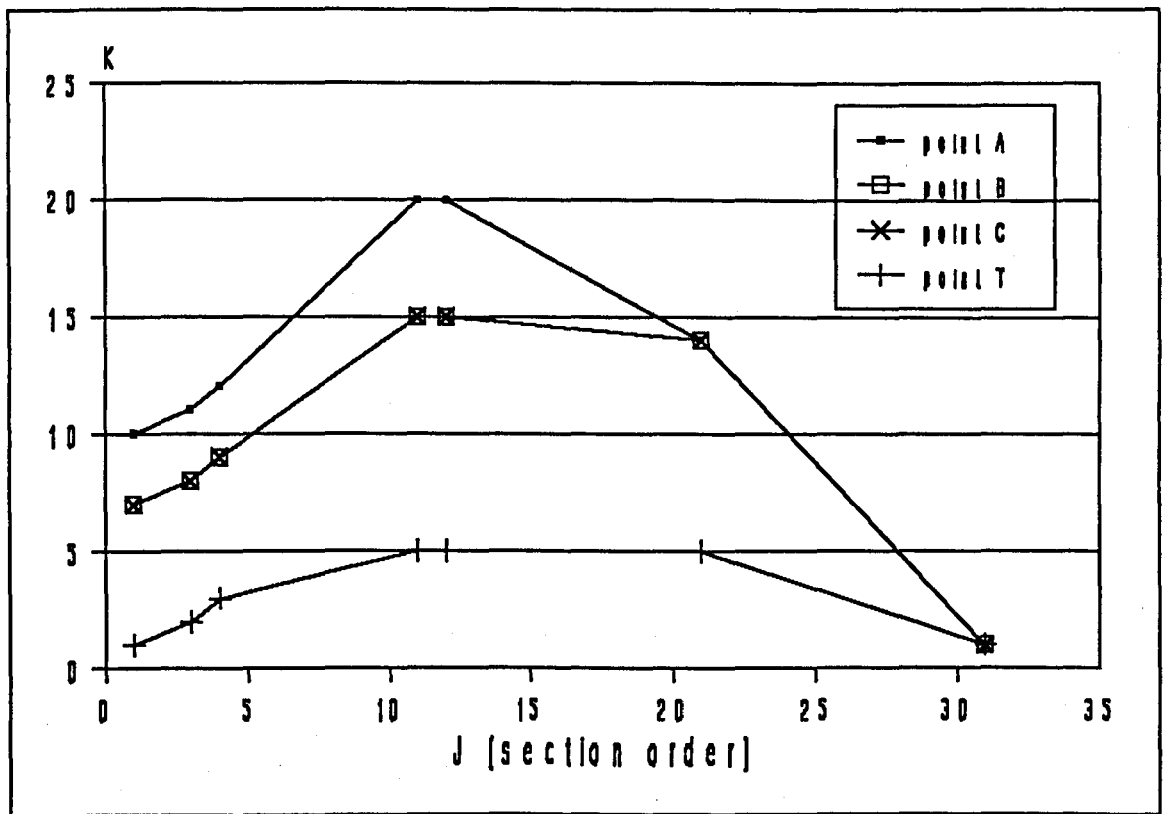

Figure 4.8 - K variation in the first 3 m of flowpipe simulation

Finally, it seems that all these considerations lead to a problem of a very difficult nature: in which circumstance would be possible to analyze separately the friction behaviour in a wave containing vertical acceleration components of significant magnitudes? The trial and error procedure here adopted here could only manage to arrange a way to combine the effects in order to find a best fit, but could not find a methodology to isolate them.

4.4.6 Instability Control

According to the analysis developed in Chapter 3 some sort of oscillations could be expected in the simulation of the tipping tank generated wave since its front has the distinctive characteristic of shock fronts. In addition, explicit numerical methods exhibits intrinsic oscillation properties.

During the calibration process the phenomenon was observed at the wave front. When not properly controlled the oscillation can propagate leading to false results.

Simulations using the processing alternative E used the numerical dissipative interface described through relations (3.44), (3.45) and (3.46). The minimum value of α that provided a good oscillation control was 0.2. For processing alternative B relations (3.59), (3.60) and (3.61) were used. Following Gharangik et Chaudhry (1991) the coefficient K was adopted equal to 0.03 leading to good oscillation control.

4.4.7 Vertical Acceleration Adjustment

Vertical acceleration adjustment process was analogous to the friction adjustment, i.e., it uses also a multiplicative scheme based on linear variation of Z and it could not be performed in isolation. However, it was also possible in this case to observe the particular effect of vertical acceleration variation within a certain interval.

Vertical acceleration manipulation can be justified in two ways. Firstly, the Boussinesq assumption of linear vertical velocity variation is just a first approximation to the real phenomena. Secondly, the degree in which numerical methods reproduce the mathematical model included phenomena is not known.

In a first approximation, Z values bigger than 1 lead to the water surface dampening and horizontal velocity increases, while Z values less than zero lead to water surface rising and horizontal velocity decreases. The consequent variation on horizontal velocity is similar to the friction case, but of smaller intensity. More precisely, it has to be remembered that vertical acceleration is referred to the water depth profile curvature ($\alpha = d^2h/dt^2$). Thus, Z could be depicted in terms of its effect on water depth curvature in time. For example, the water depth profile variation with time (see Figure 4.7) shows a sequence of opposite curvatures. It can be observed in these profiles that the wave is coarsely composed of two peaks with a profile of opposite direction between them, the trough. Applying Z bigger than 1 to this

region flattens both the peaks and the trough. Contrarily, Z smaller than zero promotes curvature increase, i.e., rising of peaks and lowering of trough.

Following Peregrine's reasoning in his physical description of streamline curvature effects (see section 2.2.4), it is possible to conclude that Z values smaller than zero, in fact, accentuate vertical acceleration effects since zones with more pronounced profile curvature have correspondence with bigger values of vertical acceleration. According to that reasoning, peak areas have downward pressure gradients lesser than the hydrostatic while the trough area has a downward pressure gradient greater than the hydrostatic. These areas have, respectively, downward and upward water vertical acceleration.

It should be remarked that vertical acceleration magnitudes are very small. Thus, to be significant, Z had to reach relatively high values as Figure 4.9 depicts.

According to the exposed relationship between K, Z and the water surface position, it could be expected, from observation of Figures 4.8 and 4.9, that the wave had a oscillation on its water depth along the pipe length. In fact, this occurs as will be shown in Chapter 5 and 6. Here, it is important to remark that wave peaks and trough fluctuation along the pipe orientated the calibration process. Thus, departing from the "natural" numerical model response, i.e., with K and Z equal to 1 and no numerical filter applied, the water profile was gradually fitted applying appropriate K, Z values, accompanied by numerical filter control.

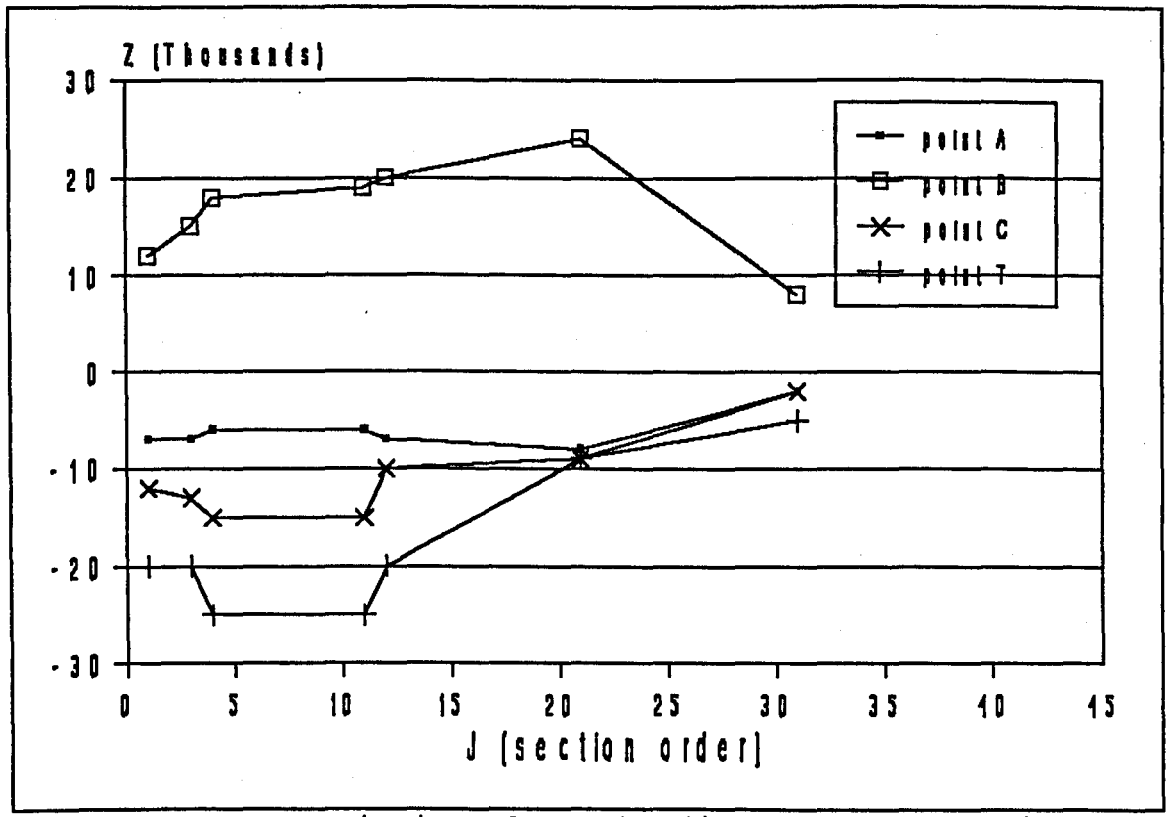

Figure 4.9 - Z variation along the first 3 m of flowpipe simulation

4.4.8 Pulse Control on the Wave Front

Computer simulation has shown a very interesting response on the wave front. Simulated water depth profiles developed a pulse on the wave front for certain entry data range values. Depending on u and h values in the entry section, a more or less pronounced protuberance developed on the first sections. This pulse evolved on downstream sections overpassing the wave main peak. This response pattern has manifested on the three program alternatives, although in different intensity for each one. Figures 4.10, 4.11 and 4.12 illustrate the phenomenon

on five initial sections of computer simulations using entry data originated from laboratory measurements described in Chapter 5. Figures 4.10, 4.11 and 4.12 correspond to simulation using program alternative E, B and D respectively.

Figures 4.10 to 4.12 show clearly that the water depth pulse evolves more rapidly than the main peak, overpassing it.

Simulation tests using rectangular channel have also shown the same phenomenon. The real meaning of this response could not be promptly understood and it should be observed that this unexpected behaviour causes enormous problem in program processing. Depending on the magnitude of h, in the simulated water depth pulse, special procedures had to be implemented in the computer program to avoid process collapse.

The phenomenon was initially considered to be of a stability nature, i.e., a problem linked to numerical solution. However two aspects made this consideration inconsistent. First, the E program alternative uses the method of characteristics that is not subject to instabilities and in second, simulation tests using entry data with smaller values of u did not show the same response. A proof of this behaviour was obtained using data presented by Standing (1986). Entry data composed by the (hxt) profile measured by Standing (1986) and by an augmented profile of horizontal velocity was used in simulation tests showing also pulse formation. Original data from Standing, i.e., with smaller u values, did not led to pulse formation, as will be shown in Chapter 6.

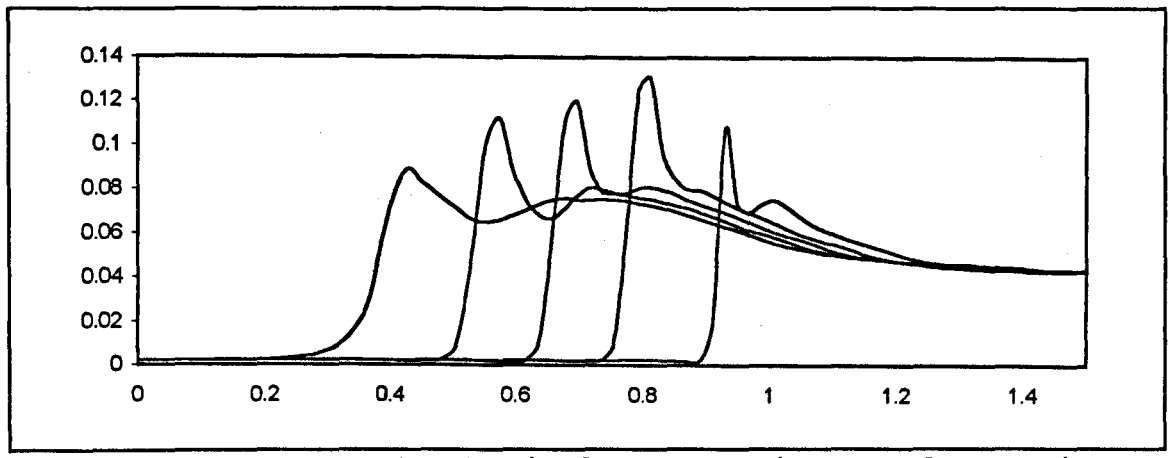

Figure 4.10 - Water depth simulated sections - alternative E
Water depth (y axis, m) on time (x axis, s)

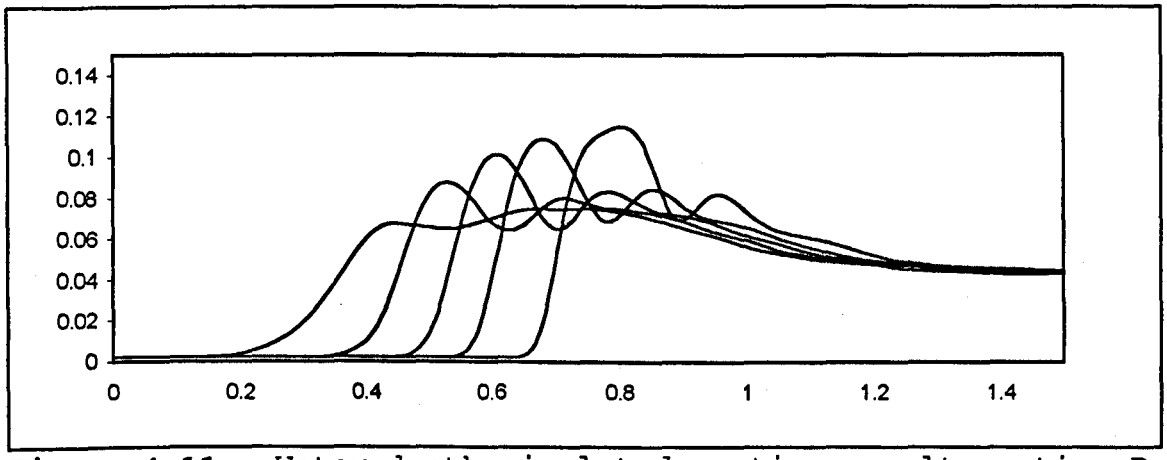

Figure 4.11 - Water depth simulated sections - alternative B
Water depth (y axis, m) on time (x axis, s)

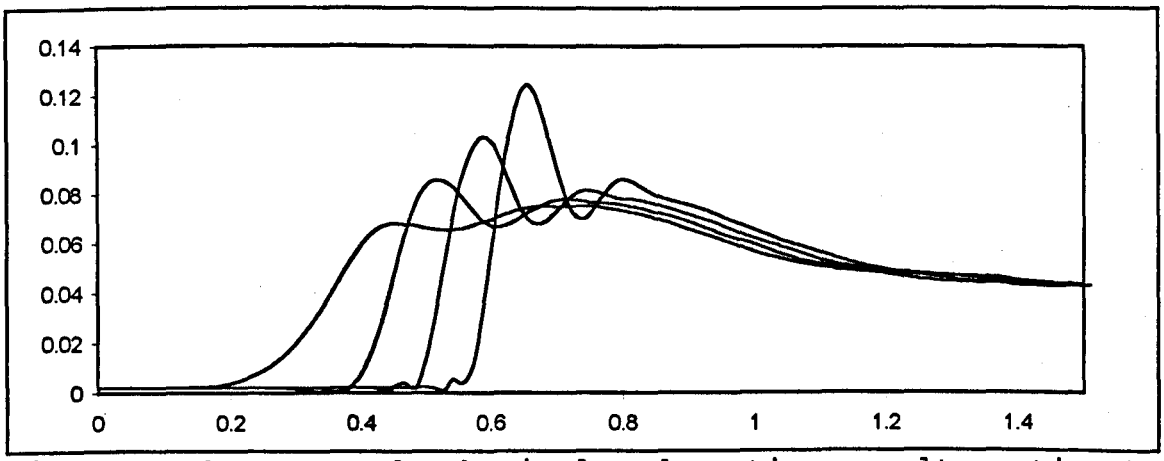

Figure 4.12 - Water depth simulated sections - alternative D
Water depth (y axis, m) on time (x axis, s)

Swaffield et Standing (1986) also have observed a pulse of this type on a wave front simulated through the method of characteristics using linear interpolation. According to the illustration of the author's referred technical article, the problem start developing approximately on the fifth or sixth computation node evolving from there. Using a more developed interpolation, Everett and Newton-Gregory method, the pulse problem disappeared.

On the present case the pulse starts forming from the first computation node (J=2) being very strong. Some attempts have been made to control it using also Everett and Newton-Gregory interpolation method and the complete Lister(1960) iteration but, no control was obtained. The interpolation was also combined with Courant number lesser than one but it has shown to be useless on the pulse control.

Instability control, as described in 4.4.6, was applied leading to pulse dampening. However, pulse control through numerical filter, at least as an isolated operation, has shown to be unsuitable since that to constrain the pulse an unacceptable deformation and wave delay were also obtained. A better procedure to manage with pulse was obtained through application of vertical acceleration control as described in section 4.4.7. Applying the vertical acceleration multiplicative scheme to the pulse in the wave front provided better control avoiding wave excessive deformation, although some increment of horizontal velocity was observed.

Although initial approaches took the pulse as a problem

it was latter observed that pulse evolution, in fact, reproduced approximately another phenomenon observed in the laboratory measurements: the wave main peak oscillation. This behaviour is described in detail in Chapter 5.

An investigation on the probable causes of the pulses was carried out. A set of simulation tests using simplified entry data was performed. It explored the hypothesis of a particular relationship between h and u in the entry data as the pulse origin cause.

In the investigative simulation process, entry data comprised a range of horizontal velocity linear profiles over three fixed linear water depth profiles. Figure 4.13 illustrates the three water depth profiles and Figure 4.14 shows the horizontal velocity profiles. Values of time and of water depth peaks on the intermediate graphic of Figure 4.13 correspond, approximately, to actual data from laboratory measurements presented in detail in Chapter 5. The same approximation also applies to the velocity profile indicated with letter d) in Figure 4.14.

The simulation tests were performed using pairs of water depth variation on time (hxt) and horizontal velocity on time (uxt) as entry data on E program alternative.

Figures 4.15 to 4.20 present simulation results on five first simulated sections using entry data composed by a), b), c), d), e) and f) velocity profiles of Figure 4.14 and by the intermediate water depth profile of Figure 4.13.

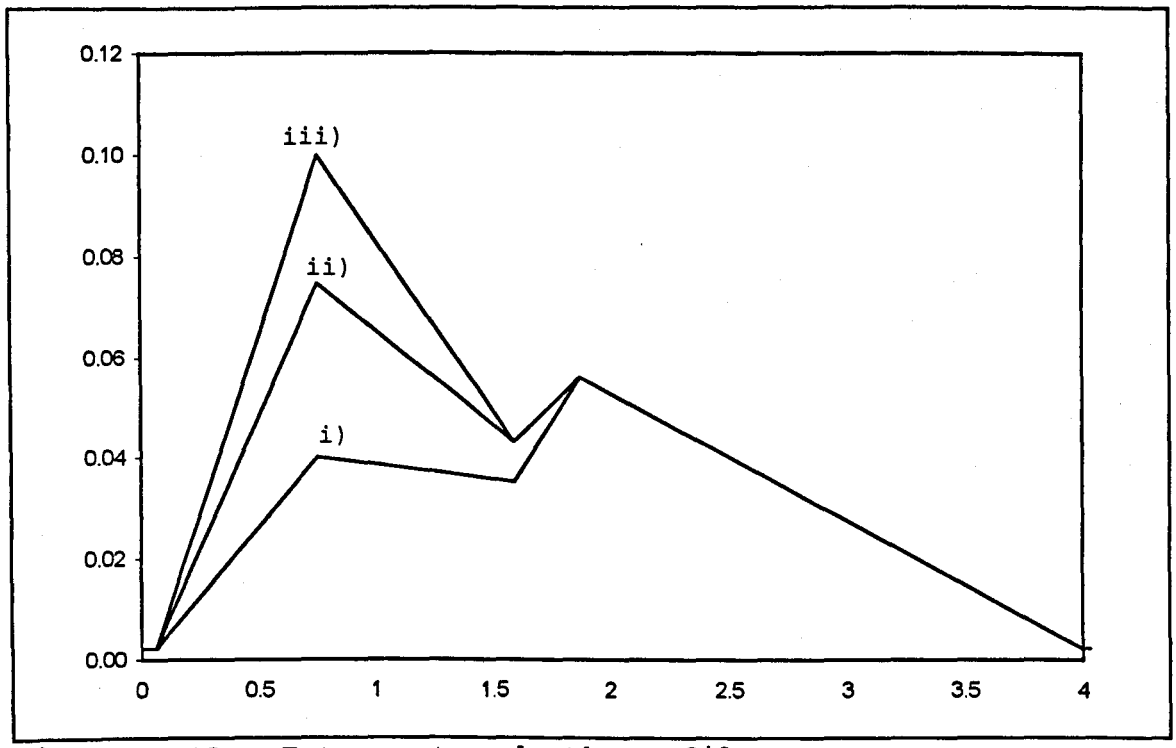

Figure 4.13 - Entry water depth profiles
Water depth (y axis, m) on time (x axis, s)

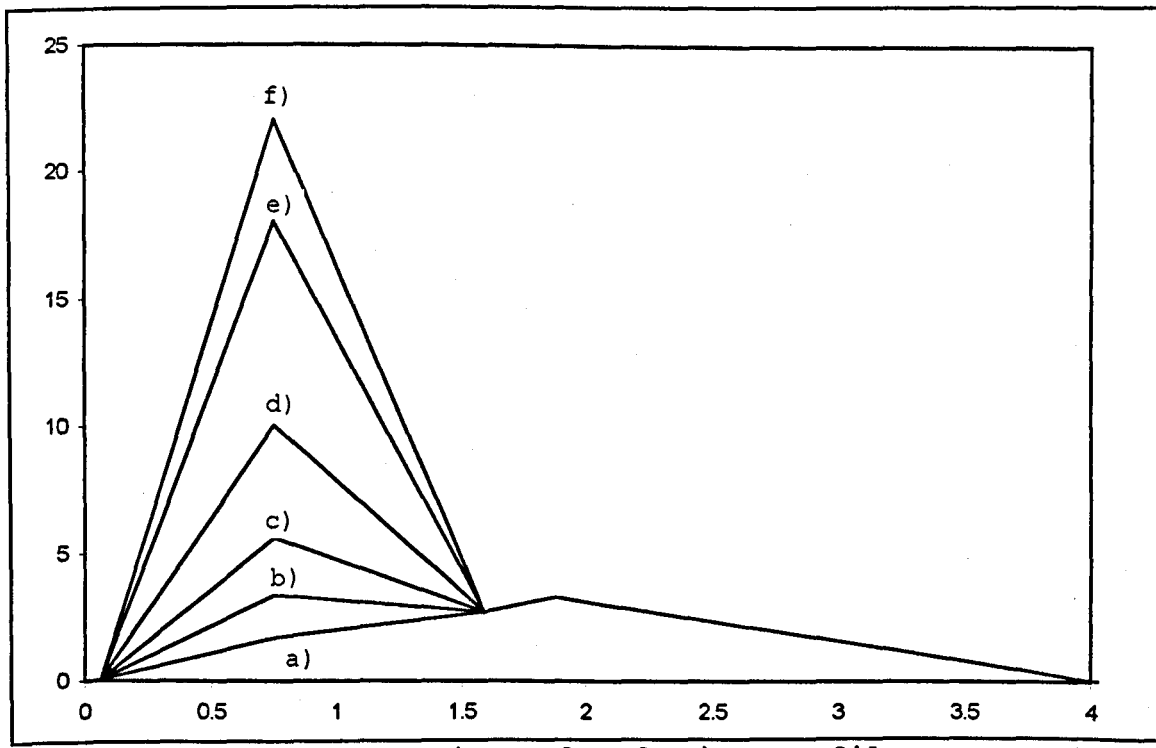

Figure 4.14 - Entry horizontal velocity profiles
Velocity (y axis, m/s) on time (x axis, s)

Exploring the hypothesis of a particular relationship between h and u in the entry data that promoted the pulse, graphics relating values of h, u, h_t and u_t were plotted. h and u values refer to the time pulse "centre", i.e., the moment corresponding to the pulse peak. This moment was taken from the disturbed water depth simulated profile in the first computed section of each pair of h and u entry data. The time "distance" between the wave front "foot" and the pulse peak position were read in these initial sections. With this time "distance", the corresponding values of h and u were read in the entry data profiles.

Dimensionless values relating h, u, h_t and u_t were created in an attempt to obtain generalized results. Each one of the three curves in Figure 4.21 refers to a fixed water depth profile indicated in Figure 4.13, combined with the horizontal velocity profiles of Figure 4.14. Each point of the curves is formed by values of h, u corresponding to the pulse "centre" as described before and to h_t and u_t, i.e., the variation of h and u on time, for each pair of entry profile.

Each curve on Figure 4.21 can be understood as the representation of a set of interrelated h, u, h_t and u_t values that for a given water depth profile produces the pulse response on the simulation. It should be observed that right extremities of curves on Figure 4.21 could be extended since high Froude numbers also produce pulses. However, the left extremities represent, approximately, the inverse limit: smaller Froude numbers do not produce the pulse response.

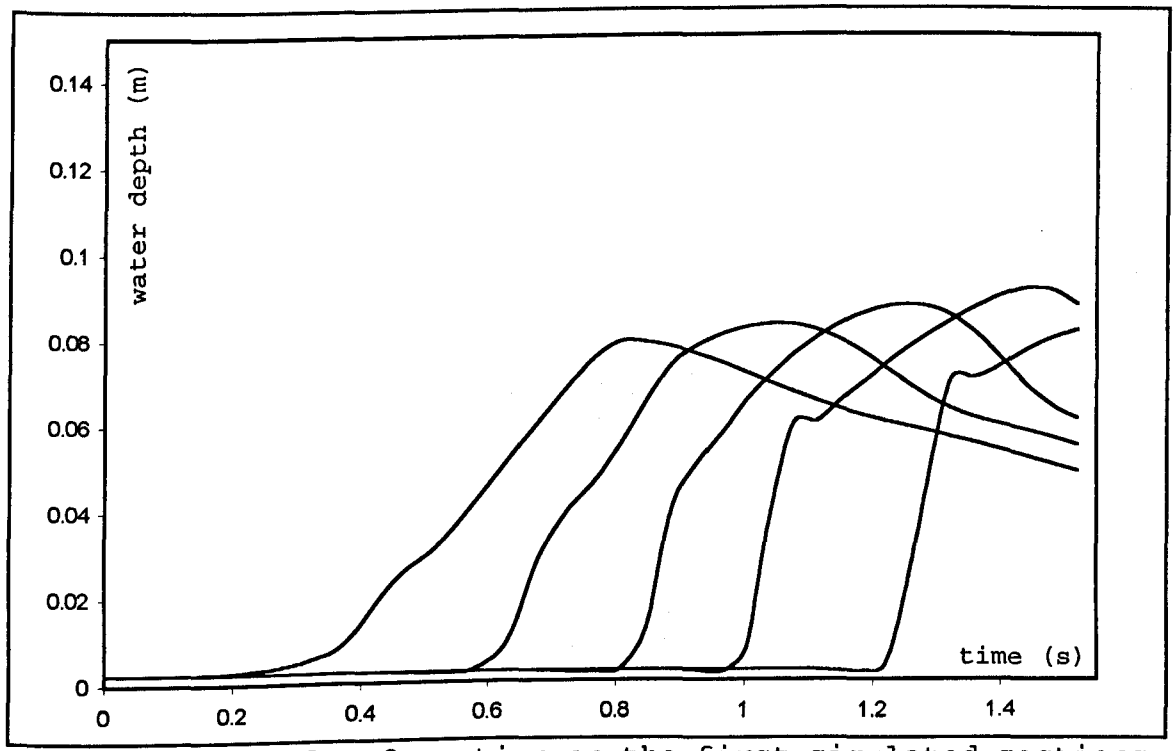

Figure 4.15 - Pulse formation on the first simulated sections Velocity entry profile a)

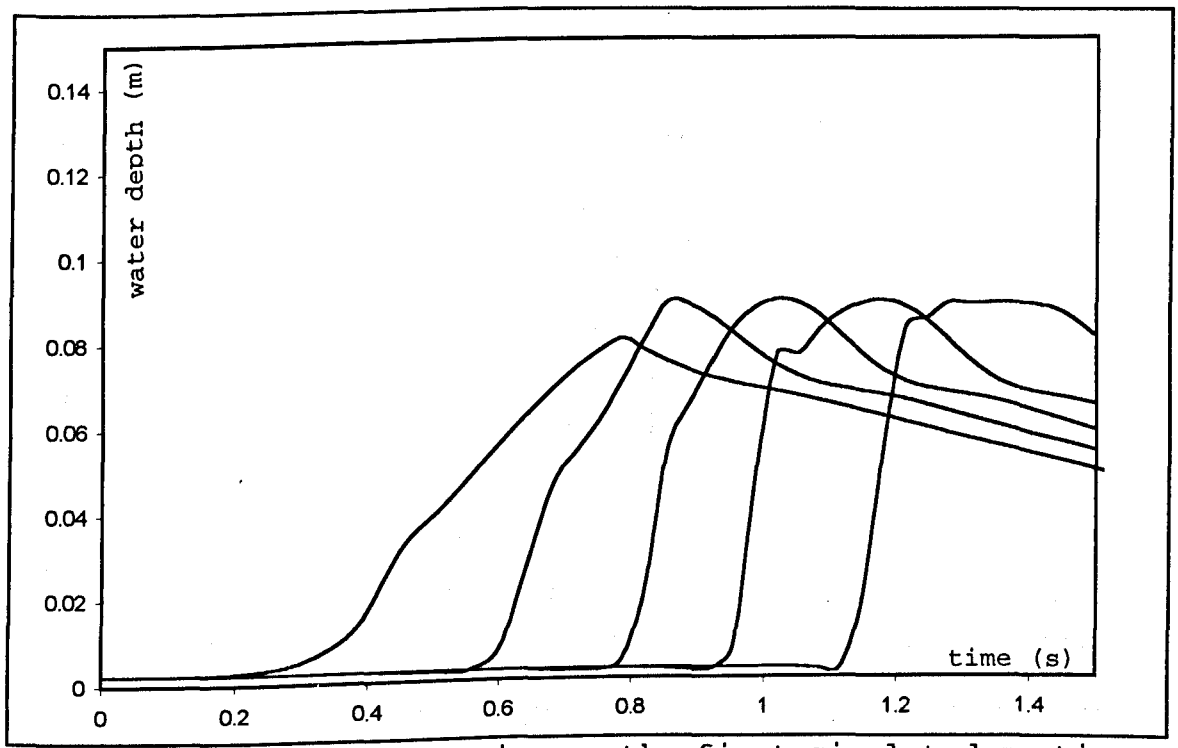

Figure 4.16 - Pulse formation on the first simulated sections Velocity entry profile b)

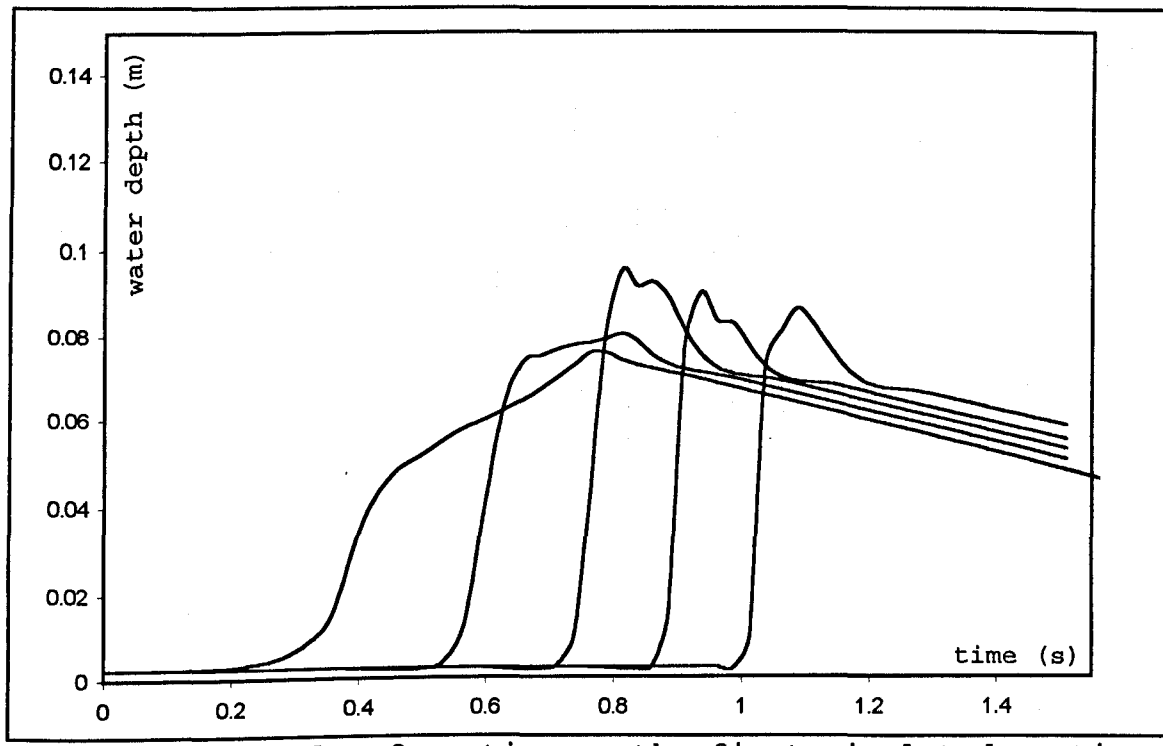

Figure 4.17 - Pulse formation on the first simulated sections Velocity entry profile c)

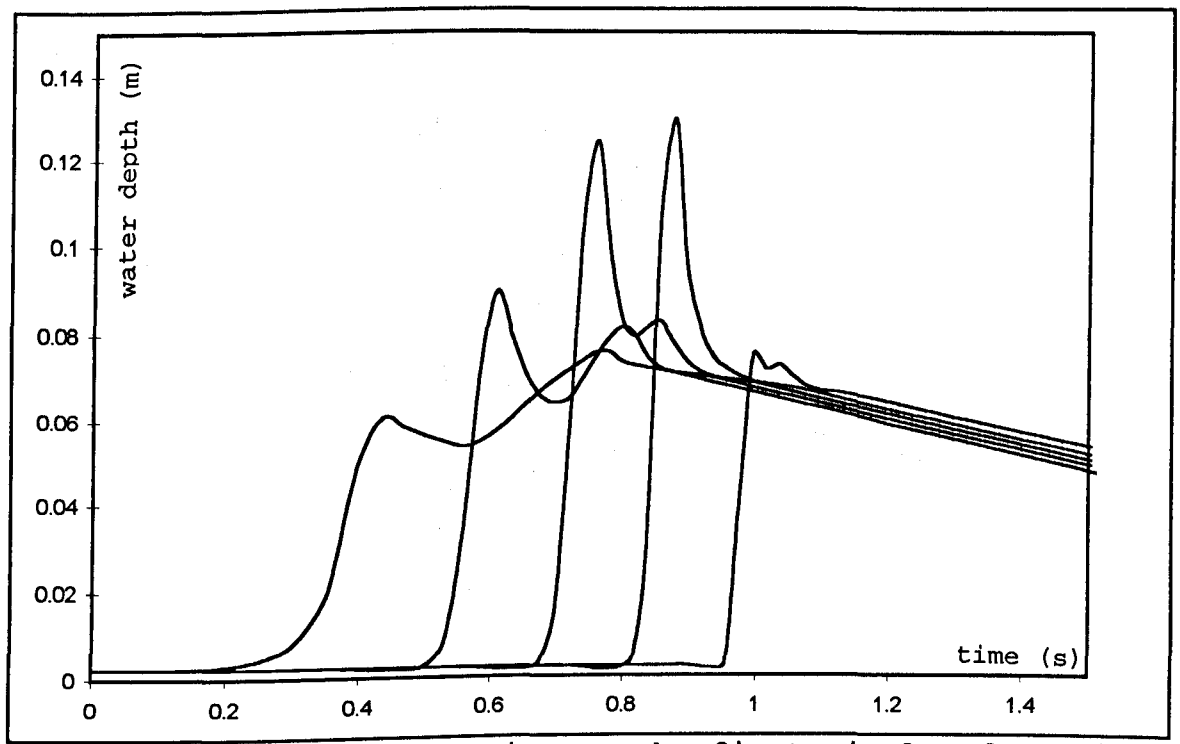

Figure 4.18 - Pulse formation on the first simulated sections Velocity entry profile d)

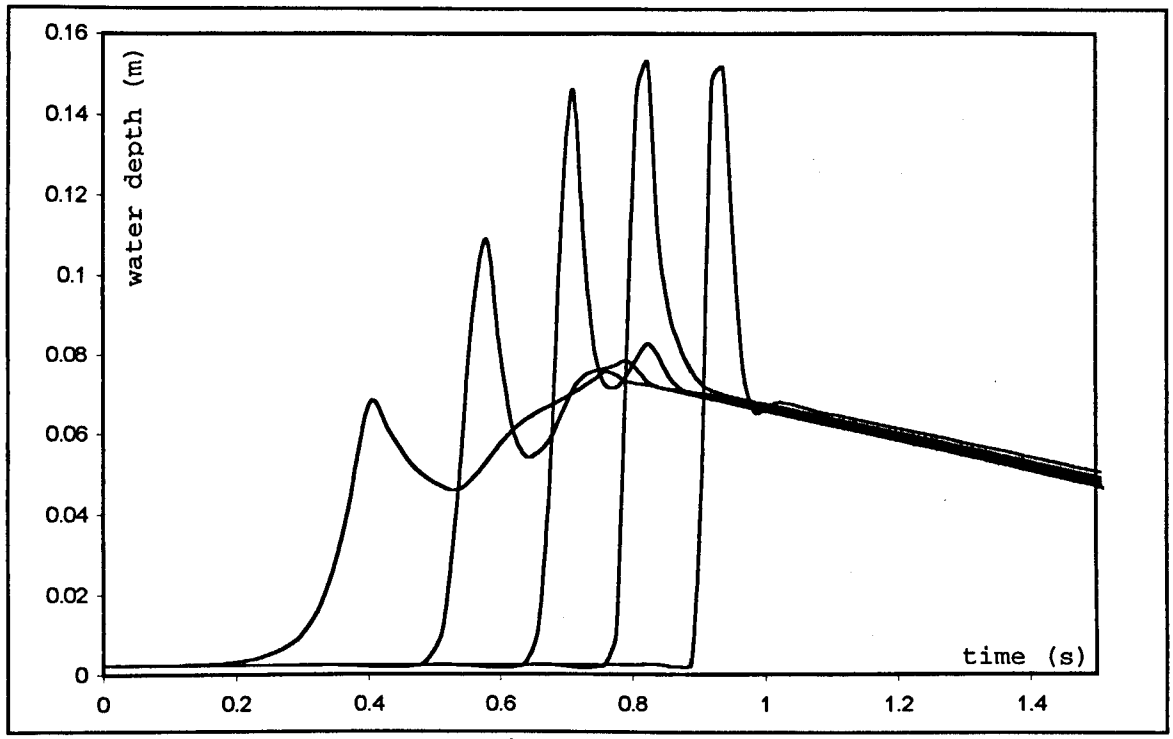

Figure 4.19 - Pulse formation on the first simulated sections Velocity entry profile e)

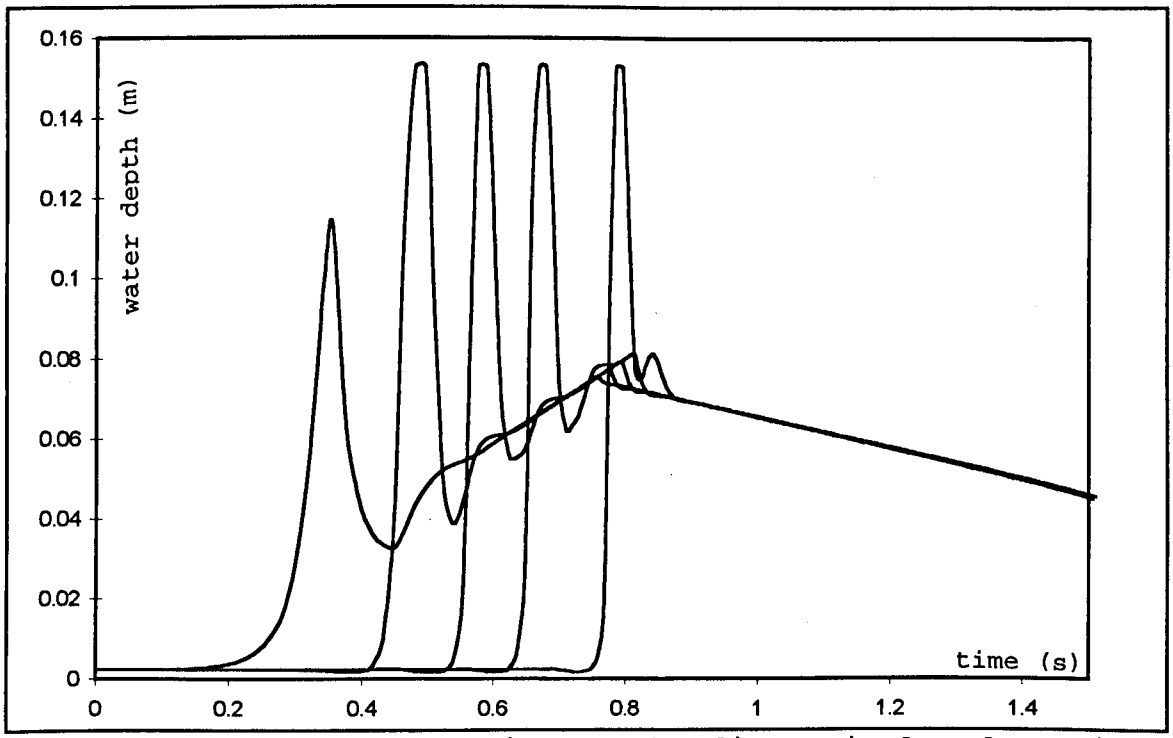

Figure 4.20 - Pulse formation on the first simulated sections Velocity entry profile f)

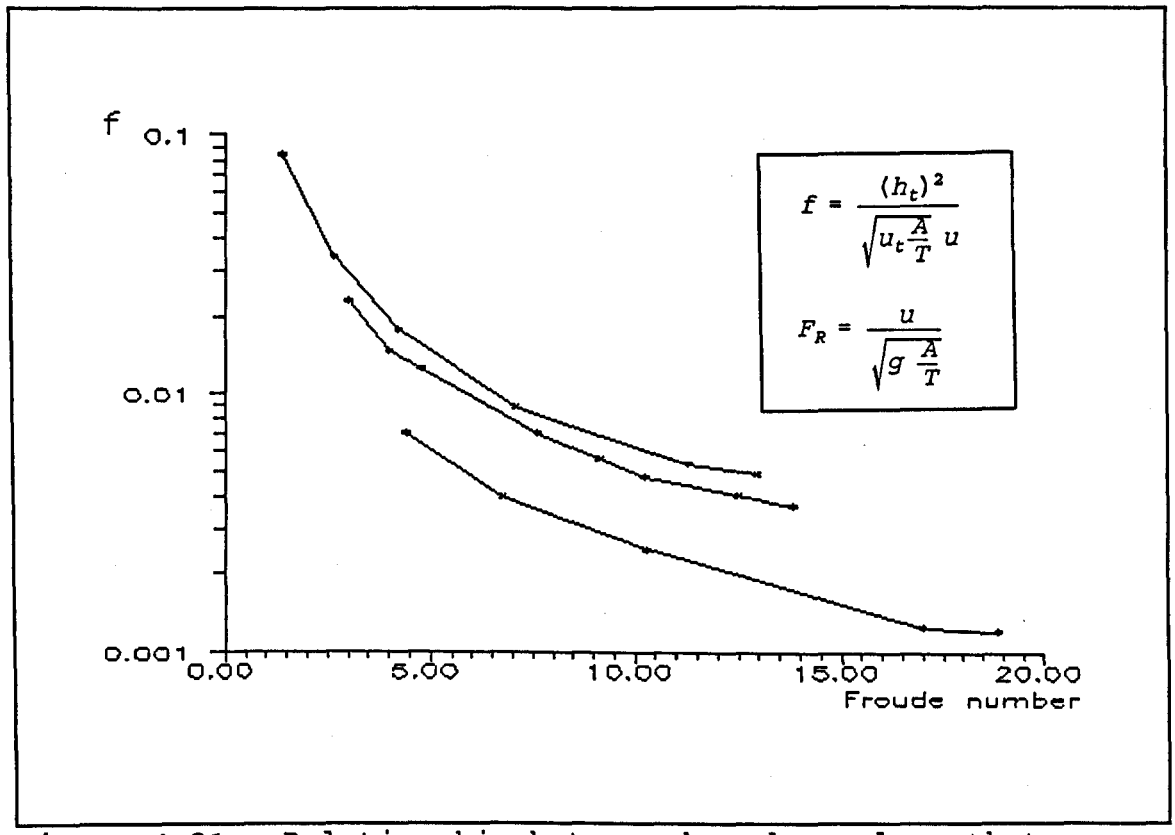

Figure 4.21 - Relationship between h and u values that produce pulse

Figure 4.21 curves do not provide any immediate evidence of a general rule for the pulse formation. No particular Froude number or relationship between h, u, h_t and u_t can be pointed. Unfortunately it was not possible to deepen the study and analysis to understand the phenomenon.

CHAPTER 5

LABORATORY APPARATUS AND EXPERIMENTAL RESULTS

5.1 Introduction

Laboratory measurements were conducted to provide data for the mathematical model validation process, which results are described in Chapter 6. In this process actual data are compared with the model generated prediction.

Also described is the procedure used to measure the tipping tank flow rate and the water depth profile at the beginning of the pipeline. These profiles constitute the entry boundary condition of the governing equations and feed the simulation program.

Other tipping tank characteristics and its performance profile in laboratory and field evaluations are provided in detail in previous works (Alves 1990, 1991).

5.2 Measurement Plan

Two groups of measurements were carried on. The first aimed to produce the entry data to feed the simulation program.

It is basically constituted by pairs of hydrographs (time X flow rate) and water depth profiles (time x water depth) according to 5 different tipping tank discharge volumes and 4 different base flow rates.

Table 5.1 portrays the whole set of measurements.

Figure 5.1 illustrates the horizontal rig used to measure the water depth in a 14 m pipeline. In this Figure section S1 indicates the initial position for the purpose of simulation. The reason for not working from the very beginning of the pipe is explained below in 5.4. The above referred entry data correspond to this section.

Table 5.1 - Measurement plan classification

BASE FLOW (L/s) / T.T. VOL. (L)	0.0	0.1	0.5	0.75
20.0	FR (A0) WD	WD (A1)	WD (A2)	WD (A3)
25.0	FR (B0) WD	WD (B1)	WD (B2)	WD (B3)
30.0	FR (C0) WD	WD (C1)	WD (C2)	WD (C3)
35.0	FR (D0) WD	WD (D1)	WD (D2)	WD (D3)
39.5	FR (E0) WD	WD (E1)	WD (E2)	WD (E3)

table code: FR = flow rate hydrograph
WD = water depth profile
( ) = classification

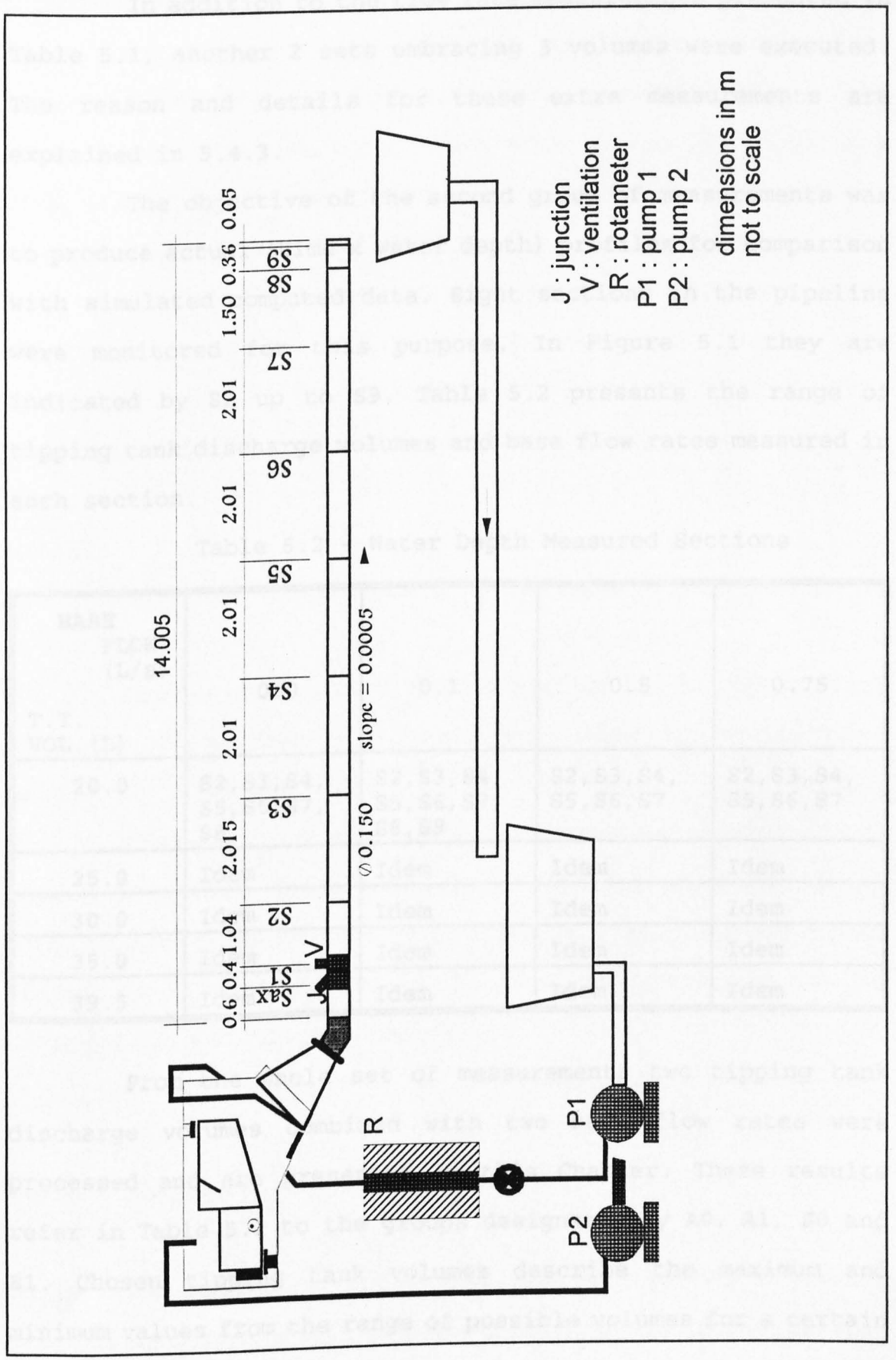

Figure 5.1 - Horizontal rig

In addition to the flow rate measurements presented in Table 5.1, another 2 sets embracing 5 volumes were executed. The reason and details for these extra measurements are explained in 5.4.3.

The objective of the second group of measurements was to produce actual (time x water depth) profiles for comparison with simulated computed data. Eight sections in the pipeline were monitored for this purpose. In Figure 5.1 they are indicated by S2 up to S9. Table 5.2 presents the range of tipping tank discharge volumes and base flow rates measured in each section.

Table 5.2 - Water Depth Measured Sections

BASE FLOW (L/s) / T.T. VOL. (L)	0.0	0.1	0.5	0.75
20.0	S2,S3,S4, S5,S6,S7, S8	S2,S3,S4, S5,S6,S7, S8,S9	S2,S3,S4, S5,S6,S7	S2,S3,S4, S5,S6,S7
25.0	Idem	Idem	Idem	Idem
30.0	Idem	Idem	Idem	Idem
35.0	Idem	Idem	Idem	Idem
39.5	Idem	Idem	Idem	Idem

From the whole set of measurements two tipping tank discharge volumes combined with two base flow rates were processed and are presented in this Chapter. These results refer in Table 5.1 to the groups designated by A0, A1, E0 and E1. Chosen tipping tank volumes describe the maximum and minimum values from the range of possible volumes for a certain

tipping tank axis position and the base flow rates try to be close to a more frequent condition verified in the head of sewers where very low flow rates are observed. This latter aspect also refers to a situation where suspended solids are more likely to settle in the pipe invert and, thus, has a special interest for further research.

The installations, instruments, hydraulic parameters, others measurement conditions and respective results are described below in two items: pipeline water depth profile (5.3) and tipping tank flow rate measurements (5.4).

5.3 Pipeline Water Depth Profile Measurements

The water surface profile generated by the tipping tank discharge was assessed in laboratory measurements as described below.

These measurements accomplish two main objectives: to obtain the water depth profiles at Section S1 to feed the simulation program together with the hydrographs and to produce actual water depth profiles in the other sections to be compared with simulated ones.

5.3.1 Horizontal Rig

The laboratory horizontal rig is depicted in Figure 5.1, namely a 14 m pipeline constituted by glass (borosilicate)

pipes, of nominal diameter 150 mm laid at 0.05% slope (0.0005 m/m or 1:2000).

The rig is part of the permanent laboratory facilities available at Department of Building Engineering and Surveying. A galvanized steel pipe frame supported the pipeline. The glass pipe segment lengths are 2 m, 1 m or 0.5 m. Each piece of glass pipe is held by two clamps where long vertical screws have one end attached. The other end pass through a steel pipe in the frame and are held by nuts that prevent movement. These nuts provide also the adjustment of the desired pipe level. The pipeline adjustment to the designed slope was performed using an optical level.

Glass pipe junctions employ rubber sleeves having two sockets that receive the pipe ends. The junction is reinforced with a metallic clamp. The glass pipe extremities joined through the rubber junction do not touch each other. A gap of about 5 mm between them is filled with rubber through a designed protuberance of the sleeve that accommodates the pipe ends.

The tipping tank is joined to the pipeline through a 45° PVC bend, 0.5 m from this bend is installed a 45° PVC junction (150 x 100 x 150 mm) together with a 0.5 m piece of PVC pipe with the same glass pipe nominal diameter. The junction is provided for future laboratory works simulating discharges of a building collector. The small segment of pipe includes a 100 mm diameter ventilation piece to relieve the air piston effect preceding the tipping tank discharge wave front. This effect is better explained in item 5.4.4.

At the pipeline downstream end there is a simple free overfall discharging into a tank from where water is returned by gravity to the main reservoir.

The simulation model initial condition is a uniform base flow. This flow can be established in the pipeline through the discharge provided by the 1 HP centrifuge pump P1 taking water from the main reservoir (see Figure 5.1). Water is conducted by a hose that enters through the conic piece that links the tipping tank to the pipeline. Water is poured from the hose at the beginning of the conic piece. For the installed configuration illustrated at Figure 5.1 the pump shows a stable performance in terms of flow rate during many hours of operation and has a maximum flow rate of 0.83 L/s.

In a short initial length the flow is not yet uniform because the water velocity in this area is higher than the normal flow velocity corresponding to steady uniform flow conditions. This occurs because the water accelerates during the flow at the inclined piece that links the tipping to the pipeline. In this area water depths are lower than the normal depth that is established downstream. This transitional segment, forming a hydraulic jump, varies in length according to the geometric configuration and the established flow rate. For 0.1 L/s the transitional length is approximately 0.6 m; for 0.5 L/s approximately 1.0 m and for 0.75 L/s, 1.3 m.

The tipping tank is fed through another pump (P2) also taking water from the main reservoir. This pump has the same specification as P1.

The tipping tank was installed and operated according

to well defined conditions providing the necessary reproducibility in the measurements.

The axis position was kept with constant coordinates of (0.245 m, 0.045 m) referred to the (x,y) axis illustrated in Figure 5.2. The axis and the absorber support position led to a maximum tipping angle α equal to 35° which corresponds to an angle Ω = 18°.

A fixed counter balance mass of 13.95 kg, installed at

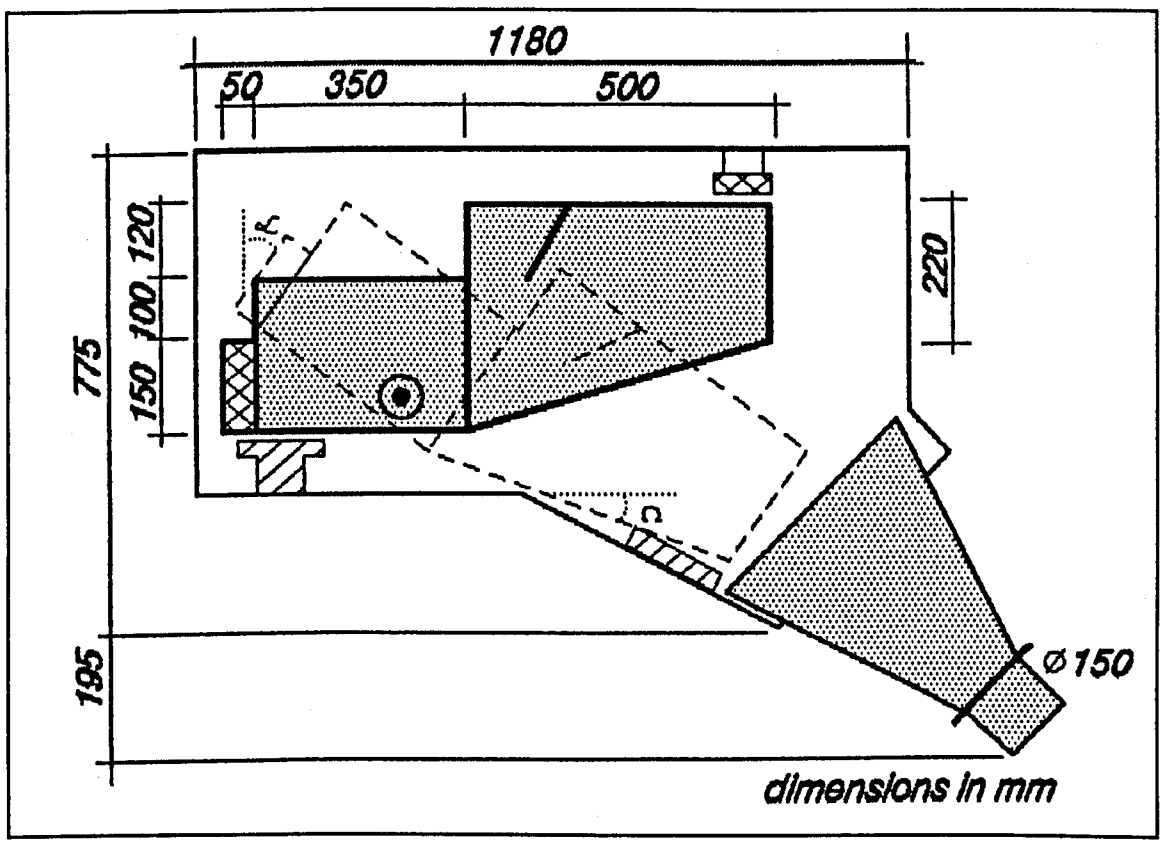

Figure 5.2 - Tipping tank installation characteristics

the proper box at the tanks rear was used for discharges of 39.5 L and 35 L. For 30 L, 25 L and 20 L it was necessary helping to start the tipping movement with an extra mass of 2.48 kg positioned on the tipping tank nose. This was considered the easiest way to avoid changing the tipping tank

pivot position that would be a very time consuming activity.

To provide identical discharge conditions the tipping tank was first filled with the suitable volume, the tipping action being avoided through a piece of wire located at the bottom under the counter balance box. After the desired volume has been reached the wire end was released and the tank tipped. The tipping tank volume was calibrated by pouring known volumes of water into it and marking the water level in its side.

5.3.2 Flow Depth Measurement

The flow depth was indirectly measured using 8 differential pressure transducers installed in the 10 instrumented positions indicated at Figure 5.1. Table 5.3 shows the associated abscissae for each section. It should be noted again that section S1 is taken as the entry section for the simulation program purposes.

Section Sax profiles were used just as a means to confirm data read at section S1.

The differential pressure transducer is an instrument that generates an electrical voltage signal linearly proportional to the water hydrostatic pressure. Figure 5.3 a) illustrates its main parts and functioning. Each branch containing water transmits hydrostatic pressure to the metallic diaphragm inside the instrument. Different water level in the branches will promote the deflection of the diaphragm leading to the electrical signal generation.

Table 5.3 - Flow depth measurement instrumented sections

SECTION	ABSCISSA X = (m)	PRESSURE TRANSDUCER NR.
Sax	(-0.400)	PT2
S1	0.000	PT1
S2	1.040	PT3
S3	3.055	PT4
S4	5.065	PT5
S5	7.075	PT6
S6	9.085	PT7
S7	11.095	PT8
S8	12.595	PT8
S9	12.955	PT8

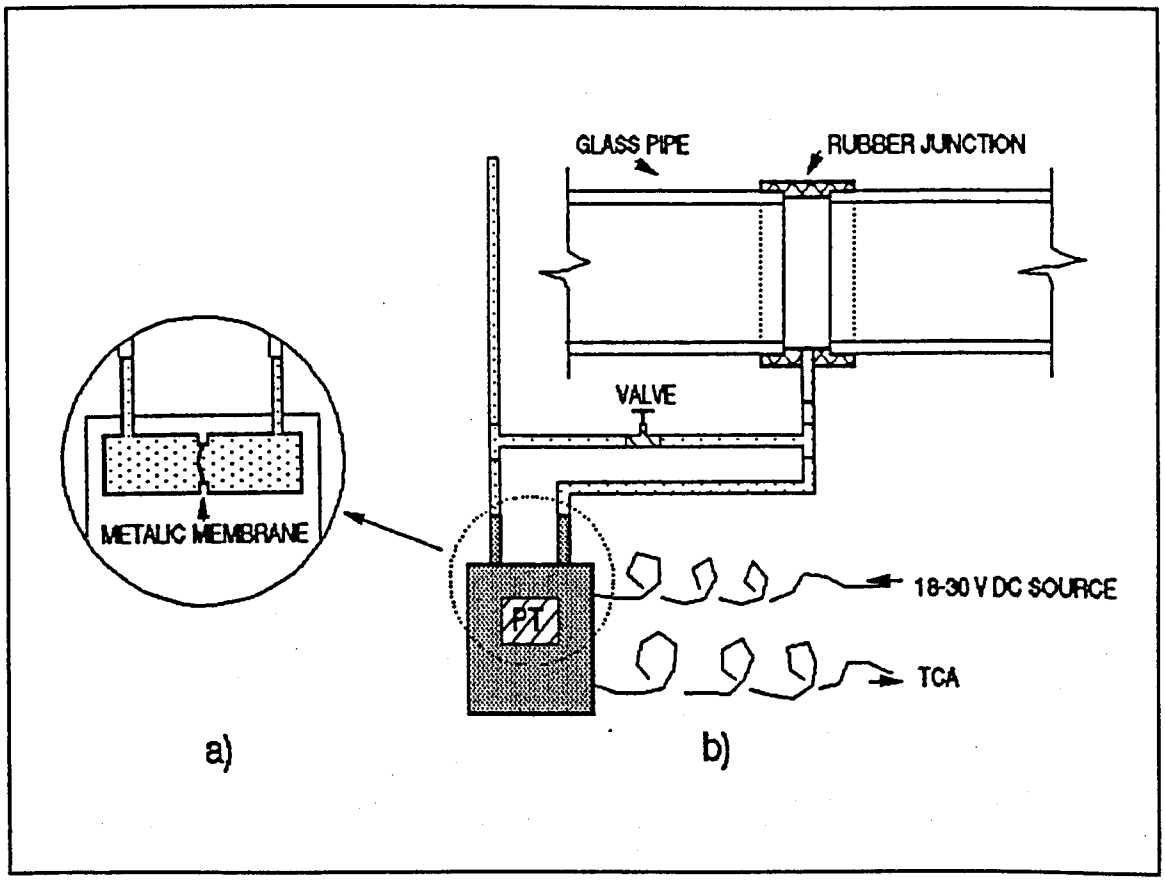

Figure 5.3 - Differential pressure transducer installation

Each side of the chamber where the diaphragm is positioned communicates with a plastic tube. One branch has a constant water level and serves as reference being kept open to the atmosphere. The other tube is connected to the pipeline through a pressure tapping at the pipe invert level as shown in Figure 5.3 b). A small tap connects the two branches and remains closed during the measurement.

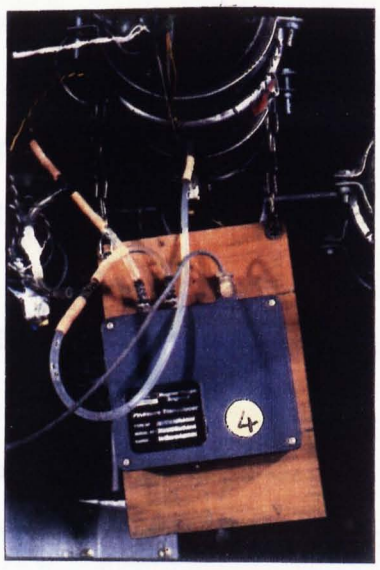

Figure 5.4 - Pressure transducer at section S3

At sections S8 and S9 there were no rubber junctions to provide the pressure tapping. In these cases it was attempted to get the water pressure installing a very fine tube entering through the open pipeline end and stuck on the pipe invert. Unfortunately this method was shown improper since the effect of the impact of horizontal streams were felt in the pressure transducer promoting overmeasurement. Thus, water depth data for sections S8 and S9 were missed.

The pressure transducers were manufactured by Sangamo-Schlumberger (type P21/V) and the measurement range was 0-34.3 kPa.

A careful pressure transducer calibration procedure was necessary since the instrument shows a quite quick variation of response with time. To deal with this characteristic the

procedure had to be performed after measurement periods no longer than 2 to 3 hours . Initially, with the tap open, the pipeline is completely drained so that the level of the reference branch equals the pipe invert. The tap is closed and a first voltage measurement is taken. Uniform flow is established in the pipeline and the voltage signal referred to the new stable water depth is read. Two pairs (voltage x water depth) are enough to provide the calibration straight line curve.

Close to the pressure transducer PT1 the flow depth is read through the water level in an extra plastic tube linked to the plastic pipe invert. The water in this tube is subject to atmospheric pressure, being the level read on a scale in the tube end. Downstream, the uniform flow depth is read indirectly. The wet perimeter is read in a paper scale positioned around the glass pipe and from this reading the water depth can be calculated.

Measurement of water depth against time in each section provides profiles for comparison with respective simulated data. Thus predicted water depth profiles can be compared with actual data.

Another flow variable in the simulation process is the water velocity. According to the exposition in Chapter 6 if the water surface profile is described by the simulation program within an acceptable degree of accuracy, it can, by extrapolation, be assumed that the water velocity profiles also were correctly predicted. However, not only the velocity profile in a certain section is important. It is also necessary

to describe the time taken by the wave to travel between subsequent sections. Chapter 6 shows that one particular suitable point to verify this parameter is the wave front.

Table 5.4 shows the whole set of section pairs monitored each time. The left column has the associated groups of tipping tank volume and base flow rate according to the classification presented in Table 5.1.

Individual section profiles yield actual data necessary for comparison purpose while simultaneous measurements give elements to verify the wave front travel time.

Table 5.4 - Simultaneously Measured Sections

TIPPING TANK VOLUME AND BASE FLOW RATE GROUPS (see Table 5.1)	SECTIONS SIMULTANEOUSLY READ
A0, B0, C0, D0, E0, A1, B1, C1, D1, E1, A2, B2, C2, D2, E2, A3, B3, C3, D3, E3	Sax and S1
Idem	S2 and S3
Idem	S4 and S5
Idem	S6 and S7
Idem	S1 and S4
Idem	S4 and S7
A0, B0, C0, D0, E0, A1, B1, C1, D1, E1	S4 and S8
A1, B1, C1, D1, E1	S4 and S9

5.3.3 Flow Rate Measurements

Flow rate measurement is necessary to control the uniform base flow and to calibrate the pressure transducers as described before. The rotameters depicted in Figure 5.5 are used to measure the flow rate.

Figure 5.5 - Rotameters

The rotameter utilized do measure the base flow rate has a reading range between 0.02 L/s - 0.86 L/s and that utilized to calibrate the pressure transducer is in the range 0.4 L/s - 3.5 L/s.

5.3.4 Data Acquisition Equipment

The pressure transducer output was acquired through signal data acquisition equipment. Generated voltage signals were read and registered in electronic data acquisition equipment where the electrical signal was transformed into a digital pattern. The equipment used was a Dual Channel Signal Analyzer (DCA,type 2032) and is manufactured by the Danish company Bruel & Kjaer. It can read a wide range of voltages in an equally wide range of frequencies. For the discharges the DCA was set to work in the time domain mode, i.e, the pressure

transducer generated voltage was read and registered in pairs (time x voltage).

Considering the short tipping tank discharge duration and the quite rapid variation of the water depth it was necessary to set the equipment for a reading time interval that accurately could describe the water surface variation with time. It was found that 0.03125 s was a proper reading time interval to provide a correct description of the flow. Using this reading time interval a 3.5 s discharge duration at section S1, for example, could be adequately represented by 112 pairs (time x voltage).

The DCA was set to that reading frequency and both its channels were utilized for simultaneous reading of two pipeline sections.

Set at that interval the DCA provides a total reading time of 64 s for each discharge. This period is enough to measure the water depth profile since before the wave front reaches the monitored section up to the moment when it attenuates to a point where the uniform base flow water depth is again reestablished.

Using the existing interface with a microcomputer each individual reading set was transferred after every discharge. Data could then be manipulated to produce the necessary profiles.

5.3.5 Data Processing

Water depth profiles were assessed from 3 discharges for each discharge volume and associated base flow rate. This number was considered enough for an average process since the profiles have shown very good repeatability.

A computer program to process data transferred from the DCA was developed. The program repeats the following procedure for each file. It reads data (pairs time x voltage), applies the calibration equation, displaces the beginning of the discharge to a common start point and fits a line to the original signals. The n water depth profiles are then added and an averaged curve is obtained.

A typical curve was adopted instead of the averaged one because the latter tended to flatten the details. The typical curve was chosen visually by comparison, taking the averaged as reference.

5.3.6 Water Depth Profile Results

From the whole set of measurements shown in Table 5.2, those corresponding to groups A0, A1, E0 and E1 of Table 5.1 will be presented.

Figures 5.6 and 5.7 refer to 39.5 L tipping tank discharges over base flow rates 0 and 0.1 L/s respectively (groups A0 and A1) while Figures 5.8 and 5.9 refer to 20 L discharges over the same flow rates (groups E0 and E1). On each

one of these diagrams the water depth is plotted against the time for a particular section.

All the profiles were arbitrarily moved to start at 1 s position to facilitate the comparison between different profiles. It is also possible to visualise the uniform base flow before the wave front reached the section. The normal water depth for the 0.1 L/s base flow is 1.6 cm. In the diagrams referring to base flow rate 0 (zero) it can be noticed a very small water depth of about 2 mm. In fact the base flow in these cases only can be considered zero nominally since that for practical reasons it was not possible to wait for the residual water in the pipeline to drain off. To dry up the pipeline would require a minimum period of about 3 hours between discharges. But, coincidentally, this situation has matched the needs of the theoretical development since the existence of a base flow, the minimum it can be, is a requisite of the simulation process.

Figures 5.6 to 5.9 show very interesting aspects of the flow generated by the tipping tank. First it can be noticed that the flow resulting from a 39.5 L discharge has two peaks during all the time in every sections. These peaks keep in a constant relative time position in all sections. However, graphs illustrating the 20 L discharge do not show this property. The existence of two peaks is a characteristic of the tipping tank according to the discharged volume. Item 5.4.7 describes this point with more detail.

Another important aspect is the steepness of the wave front. It is noticeable that the presence of a previous base

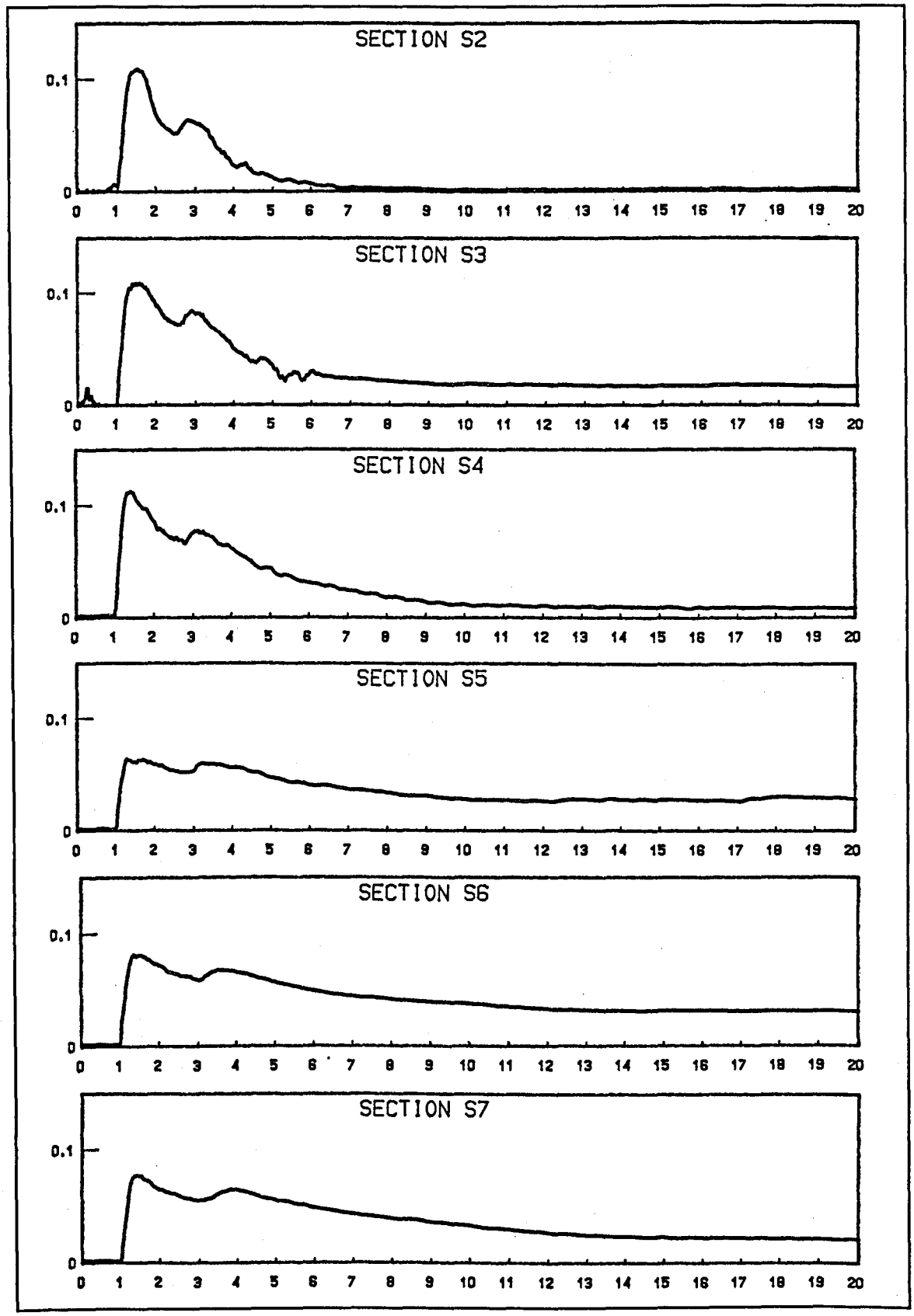

Figure 5.6 - Water depth profiles - V_t= 39.5 L ; Q_b = 0
Axis: vert. water depth in m; horiz. time in s

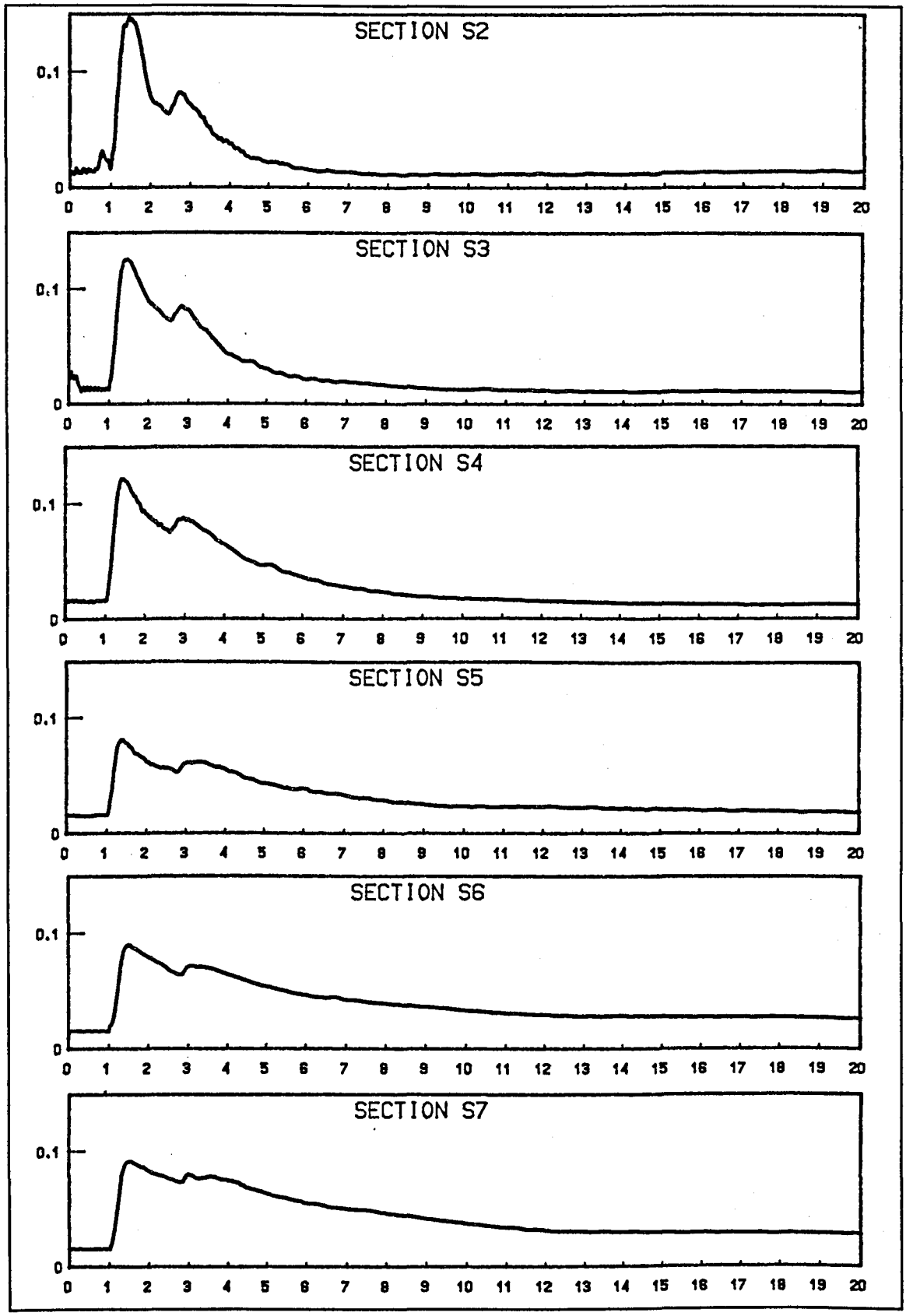

Figure 5.7 - Water depth profiles - V_t = 39.5 L; Q_b = 0.1 L/s
Axis: vert. water depth in m; horiz. time in s

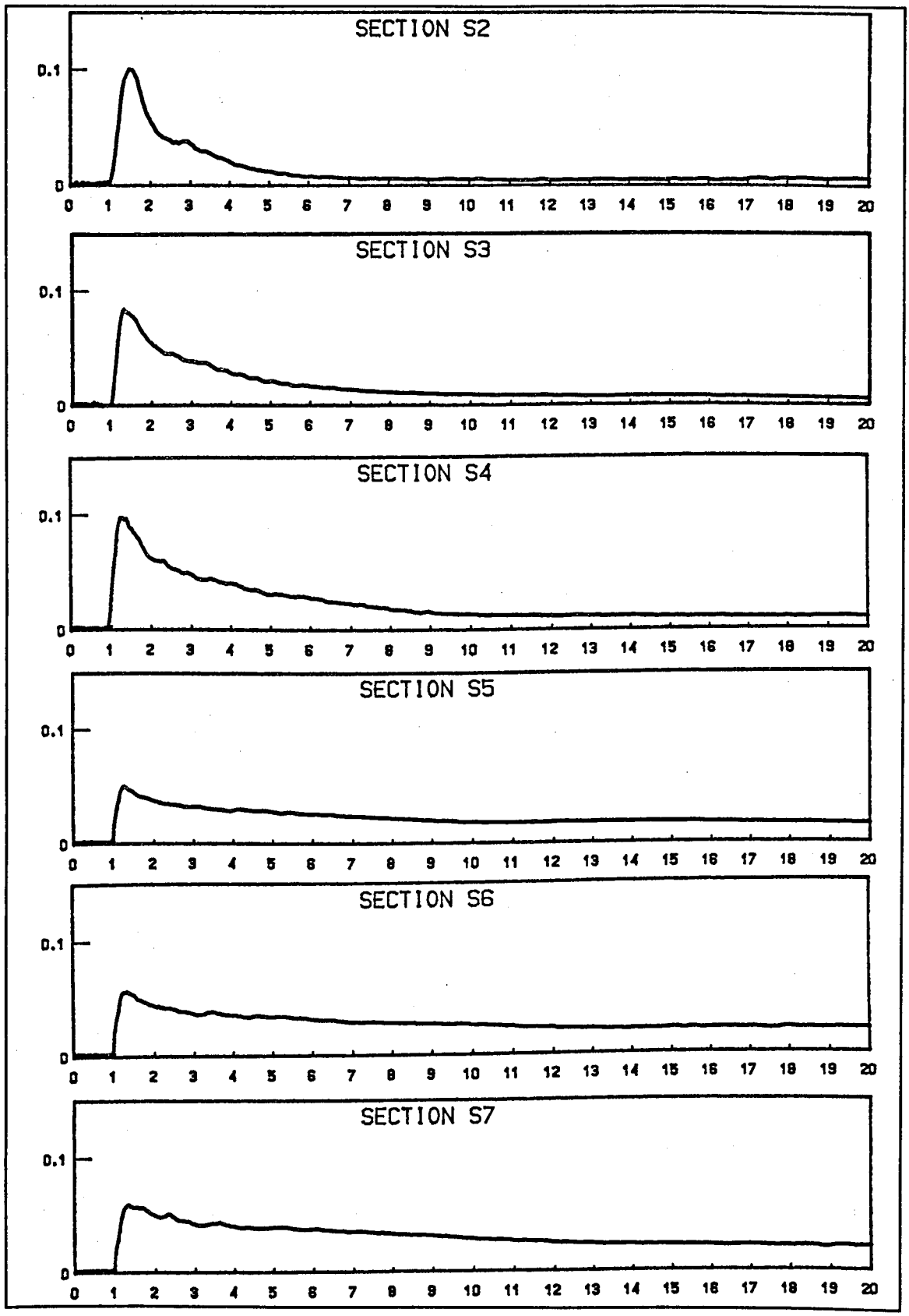

Figure 5.8 - Water depth profiles - V_t = 20 L; Q_b = 0
Axis: vert. water depth in m; horiz. time in s

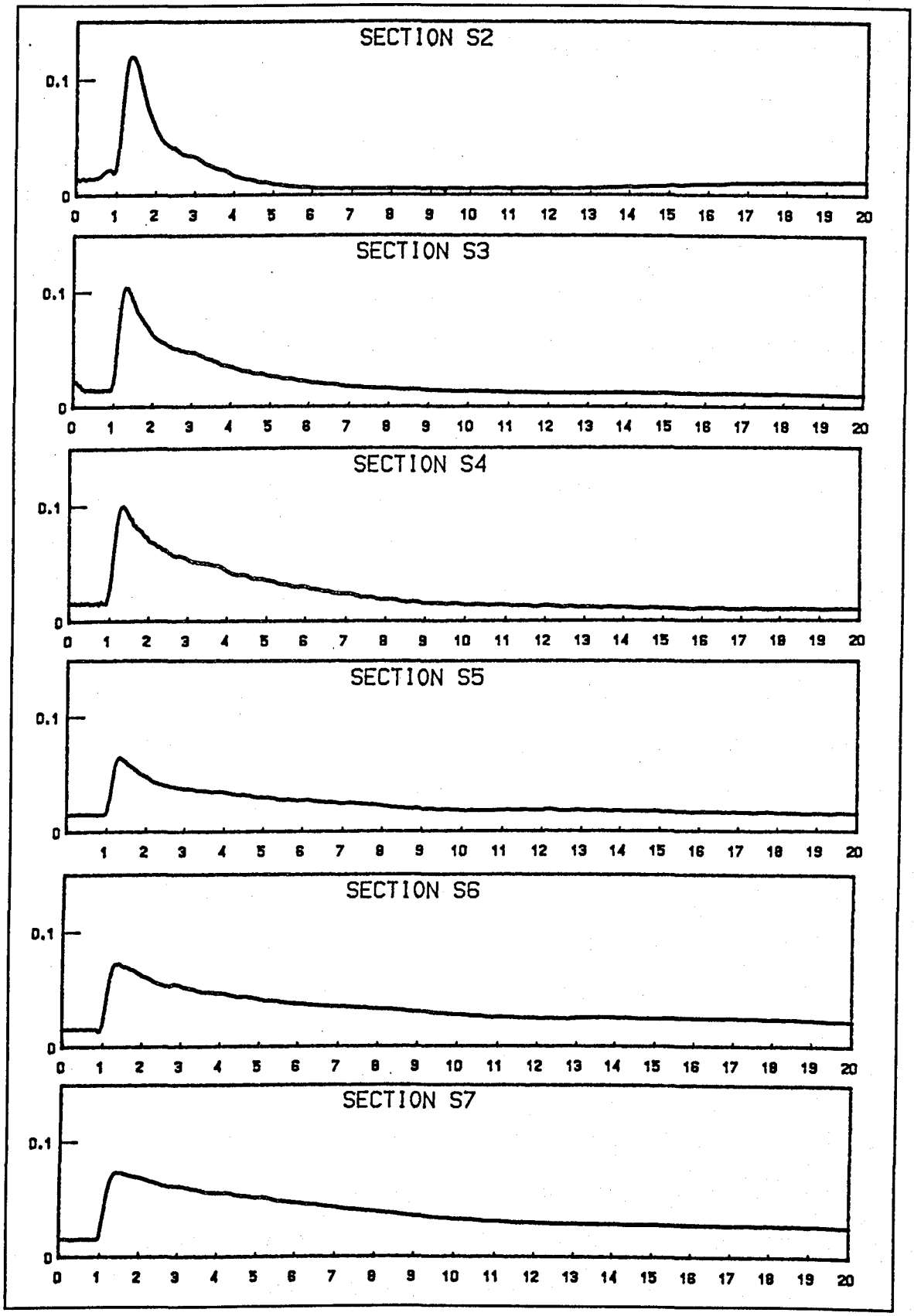

Figure 5.9 - Water depth profiles - V_t = 20 L; Q_b = 0.1 L/s
Axis: vert. water depth in m; horiz. time in s

flow results in a higher and steeper wave front. This phenomenon is also clearly observed at section S1 (see Figure 5.15).

In the first 3.5 s almost all the tipping tank volume has already passed through sections S2 and S3 in all cases. In Figures 5.7 a) and 5.9 a) it can be observed a depletion on the water surface after the main water body has passed through section S2. Although the diagrams do not show this effect, it would take about 60 s for the thorough reestablishment of the uniform base flow depth in this section. It may be observed that in this latter situation the previous base flow presents a lowered depth that gradually gains its original level.

The reasons for the water surface depletion and for the more pronounced wave front steepness in the presence of a base flow are related and can be deduced from visual observation of the experiments in the laboratory. When the tipping tank discharges into the pipeline it can be seen that its contents gain far more rapid velocities than the previous base flow established in the pipeline. Thus, the discharged tipping tank mass of water partially shocks against the slower base flow, partially passes over it and partially incorporated it onto the wave front. Even the rear or the tail of the discharged mass of water has a much higher velocity and thus, when the entire tipping tank volume has passed it leaves behind a open space that previously was occupied by the uniform flow. As part of the base flow water was incorporated by the main body of water it rests a empty space that will be gradually occupied by the base flow upstream.

Higher water depths however can only be partially justified by the presence of the base flow. The following discussion applies to the diagrams for section S2. It can be observed that the difference of peak water depth between Figures 5.7 a) and 5.6 a) is about 4 cm. Since the discharged volume (39.5 L) and others conditions are the same the difference in water depth should be explained by the presence of the base flow. Similarly, Figures 5.8 a) and 5.9 a) show a difference of 2 cm. However there is a point over which remains a doubt. Why the difference on peak water depth is not so big between the 39.5 L and the 20 L tipping tank discharge with or without base flow? In fact, based on the wave formation mechanism, it would be expected that the almost twice bigger volume would produce a much higher wave front than that due to the 20 L discharge.According to that wave formation mechanism the upper layers of the main discharge have higher celerities that would produce a piling up on the wave front. However, considering no base flow, Figures 5.6 a) and 5.8 a) show a difference of just 8 mm in the peak water depth while Figures 5.7 a) and 5.9 a) show a difference of 2 cm.

A possible explanation for the not so big difference between the peak water depths seems to be related to the role of the interaction of the more frontal parts of the wave and the bed over which the flow occurs. Observations in the laboratory suggests that the turbulence in the wave front is produced by the shock or strong friction of water particles against the bed. The presence of a base flow would reinforce this process of resistance to the flow. The upstream parts of

the discharge main body would not play an active role in this process. Thus, what would be decisive in the peak water depth is the velocity of the frontal part of the discharge regardless its total volume.

One proof of the resistance effect of the base flow is the decrease of the wave front mean velocity along the pipeline shown in 5.3.7.

The friction phenomenon is considered as a calibration factor in the adjustment process of the numerically developed model carried on at Chapter 6.

The lowering of the base flow water surface can not be observed in section S3 and in those located downstream. In these sections the wave tail has already lost velocity and the water surface raises gradually upstream to the wave front.

Finally, a very noticeable and not expected occurrence is the oscillatory trajectory of water depth peaks. For each one of the discharges both the main and the secondary peaks initially evolve according to a strong variation of their values followed by a dampening in the oscillation along the pipe length. During the validation process the simulation program has demonstrated that this phenomenon is intrinsic to the adopted model nevertheless a theoretical prediction could not be obviously deduced from the governing equations. The peak trajectories are graphically displayed in 5.3.8 and additional comments are presented in Chapter 6.

5.3.7 Wave Front Speed

Figure 5.10 presents the evolution of the wave front time duration according to the base flow rate. Time was measured with a chronometer and visual observation. It is represented in the diagram the time that the wave front takes to travel through the 14 m length pipeline. Each point results from an average of three discharges.

It is clearly demonstrated that the flow mean velocity is inversely proportional to the established base flow in the pipe. It is also shown that the flow mean velocity is inversely proportional to the discharged volume.

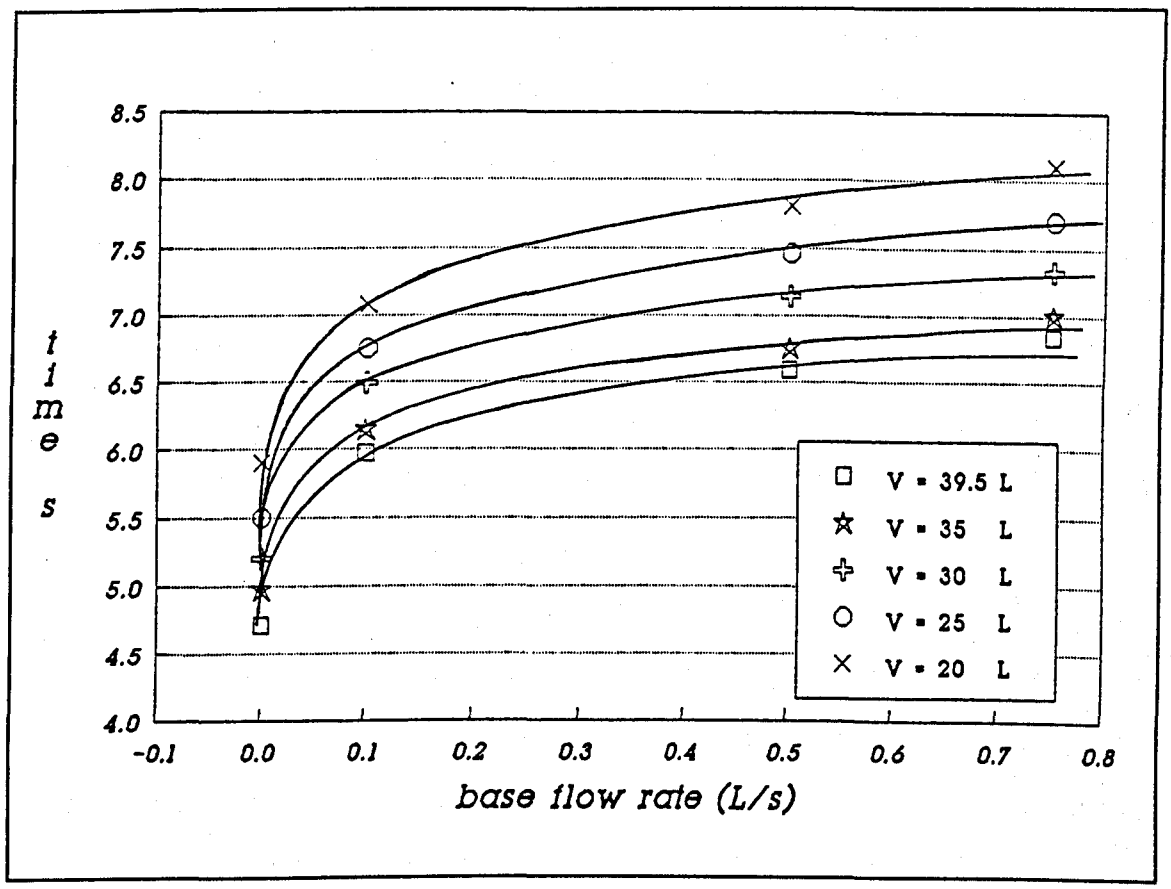

Figure 5.10 - Flow duration increase due to base flow

Figures 5.11 and 5.12 show how the wave front mean velocity decays along the pipeline. These graphs were obtained from the simultaneous water depth readings described before.

The purpose of these graphs is to give an overall view as to the velocities expected in the first few meters of the pipeline. A correct and complete description of velocity variation in all the sections during all the time only can be obtained from the simulation program.

It seems to be very difficult to extrapolate a curve of variation of velocity from the mean curves presented because probably in certain segments the wave front velocity fluctuates as occurs with the water depth. That seems to be the case at least up to section S5 (first eight meters of pipe) in spite of the general trend showed by the mean velocity.

Water depth peaks and velocity oscillation suggests that in the wave evolution a continuous transformation of energy from kinetic to potential and then again to kinetic and so on is taking place. In this hypothesis higher water depth peaks would correspond to lower velocities and the opposite would occur when the decrease in depth. However, the available laboratory data do not provide sufficient information for any conclusion at this point.

A momentum balance analysis could lead to an additional consideration. The kinetic energy can be comprised of two directions of velocity: horizontal and vertical. Thus, the transformation potential/kinetic/potential should also take into account the vertical water movement.

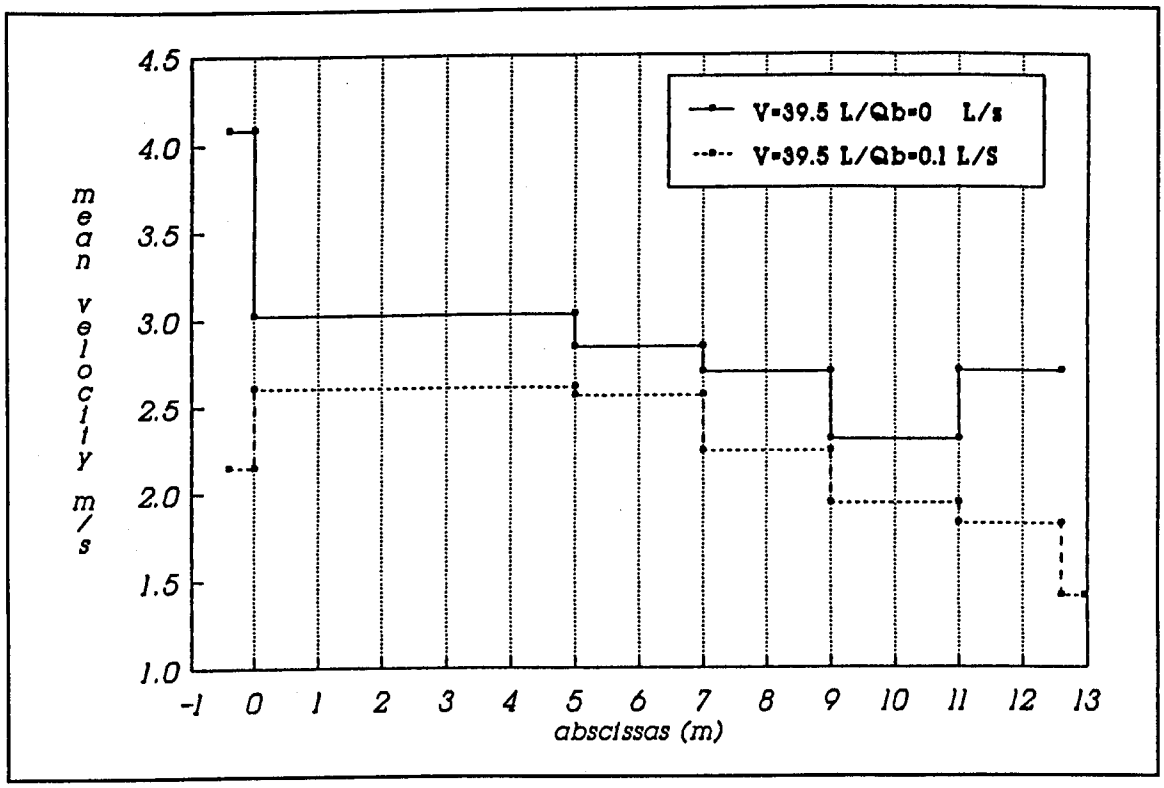

Figure 5.11 - Wave front mean velocities - V_t = 39.5 L

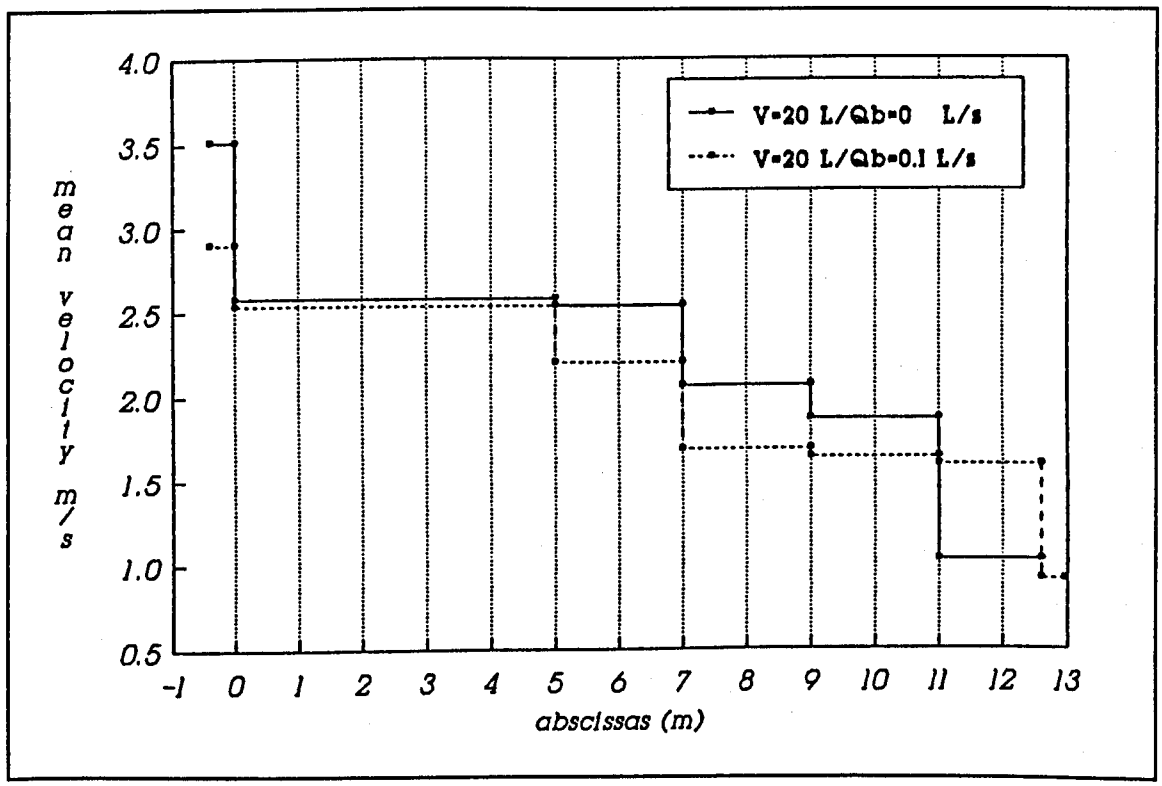

Figure 5.12 - Wave front mean velocities - V_t = 20 L

5.3.8 Peak Trajectory Profiles

Figures 5.13 an 5.14 present the main water depth peak evolution for a certain discharge flowing along the pipeline.

Plotted points correspond to water depth peaks presented in Figures 5.6 to 5.9. The line linking the points tries just to illustrate one possible tendency of the peaks trajectory. Other different adjustments would certainly also be possible. It can be observed in Figures 5.13 and 5.14 that the oscillation has a consistent pattern for all the cases. Considering the same discharged volume the amplitude is more

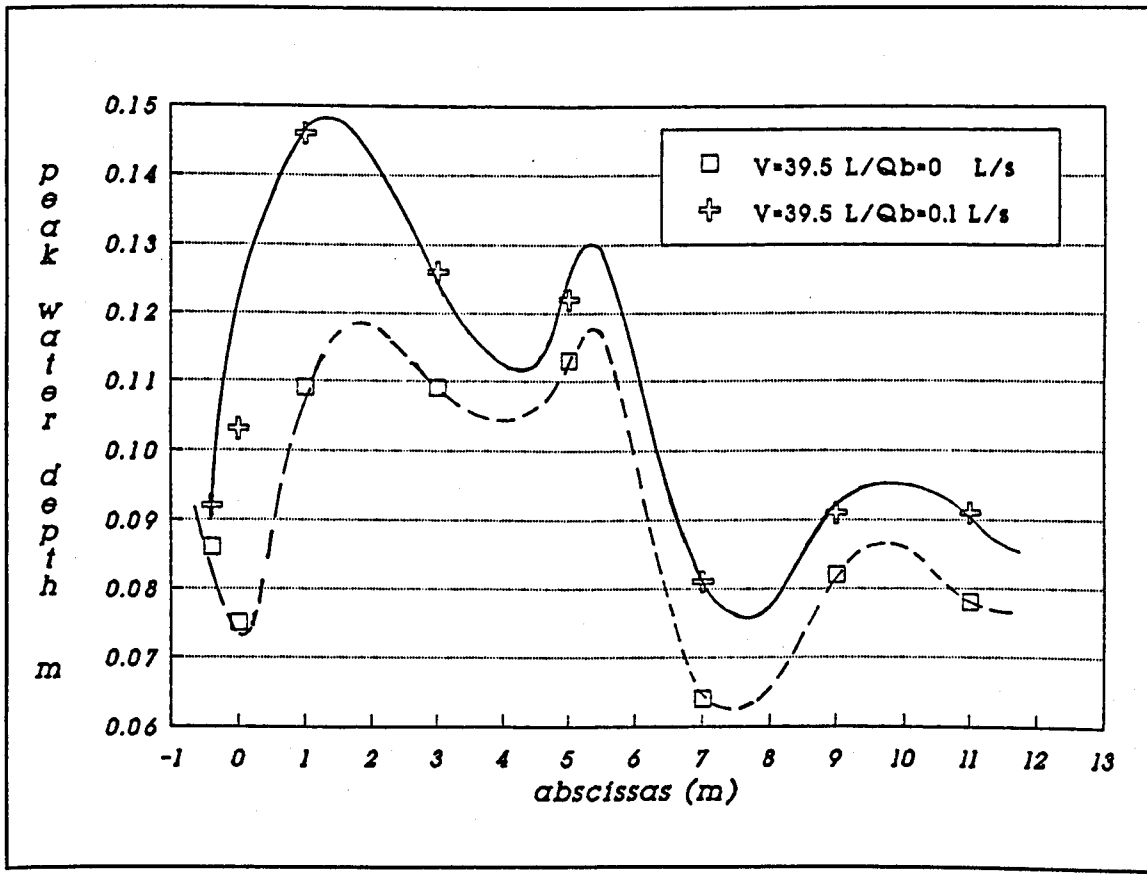

Figure 5.13 - Peak trajectory profiles - V_t = 39.5 L

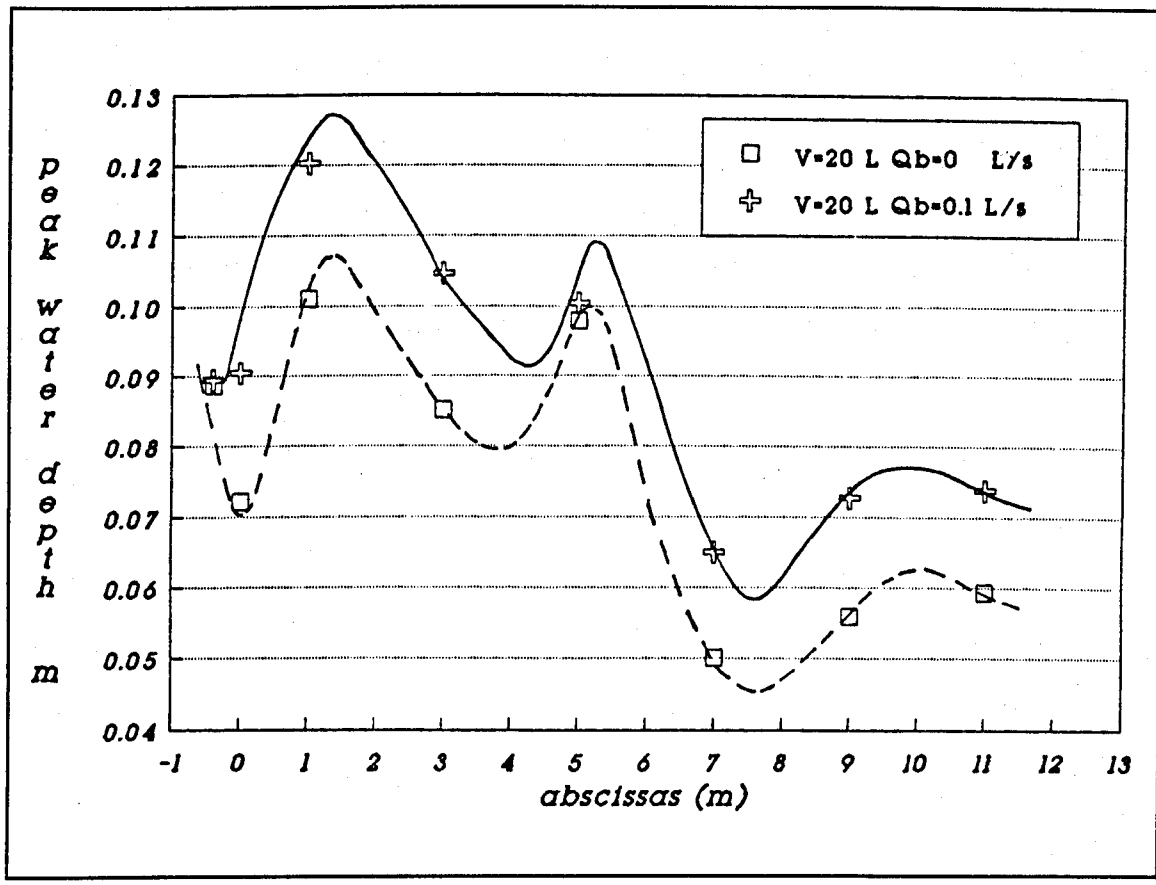

Figure 5.14 - Peak trajectory profiles - V_t = 20 L

pronounced for the higher base flow rate. For the same base flow rate the amplitude is bigger for the higher discharged volume.

5.3.9 Simulation Program Entry Profile Results

Section S1 was chosen to initialize the simulation process because this was the more suitable point where both flow rate and water depth could be obtained. It was impossible to assess the water depth profile in the very beginning of the pipeline due to the strong oscillations and turbulence of the

flow in that region as it is explained with more detail in item 5.4. Taking profiles at section S1 implied that the origin of the abscissae in the simulation program was set at this position.

Simulation program entry water depth profiles here presented refer to A0, A1, E0 and E1 groups of Table 5.1. Associated with the respective hydrographs reported in 5.4.7 they perform the boundary condition of the simulation model.

Figure 5.15 shows water depth profiles corresponding to the above mentioned groups. These diagrams demonstrate that in all the cases the generated discharge has a high speed in this region of the pipe. It can be observed that 3.5 s to 4 s are enough for the entire discharged volume to pass through section S1.

Another important aspect can be inferred comparing these diagrams with those corresponding to the next section in the downstream direction S2 (Figures 5.6 a), 5.7 a), 5.8 a) and 5.9 a). Although the general shape is maintained the peaks present higher values at S2. In this latter section profiles give the impression of having a much higher volume of water as if the discharge had grown from section S1 to S2. Obviously the volume is constant and thus the conclusion is that the enlargement of water depth profiles implies in a reduction of velocities from section S1 to section S2. In other words it can be said that the enlarged diagrams refer to discharges that have lost velocity while having gained water depth during the flow through the segment S1 to S2. This reasoning is the

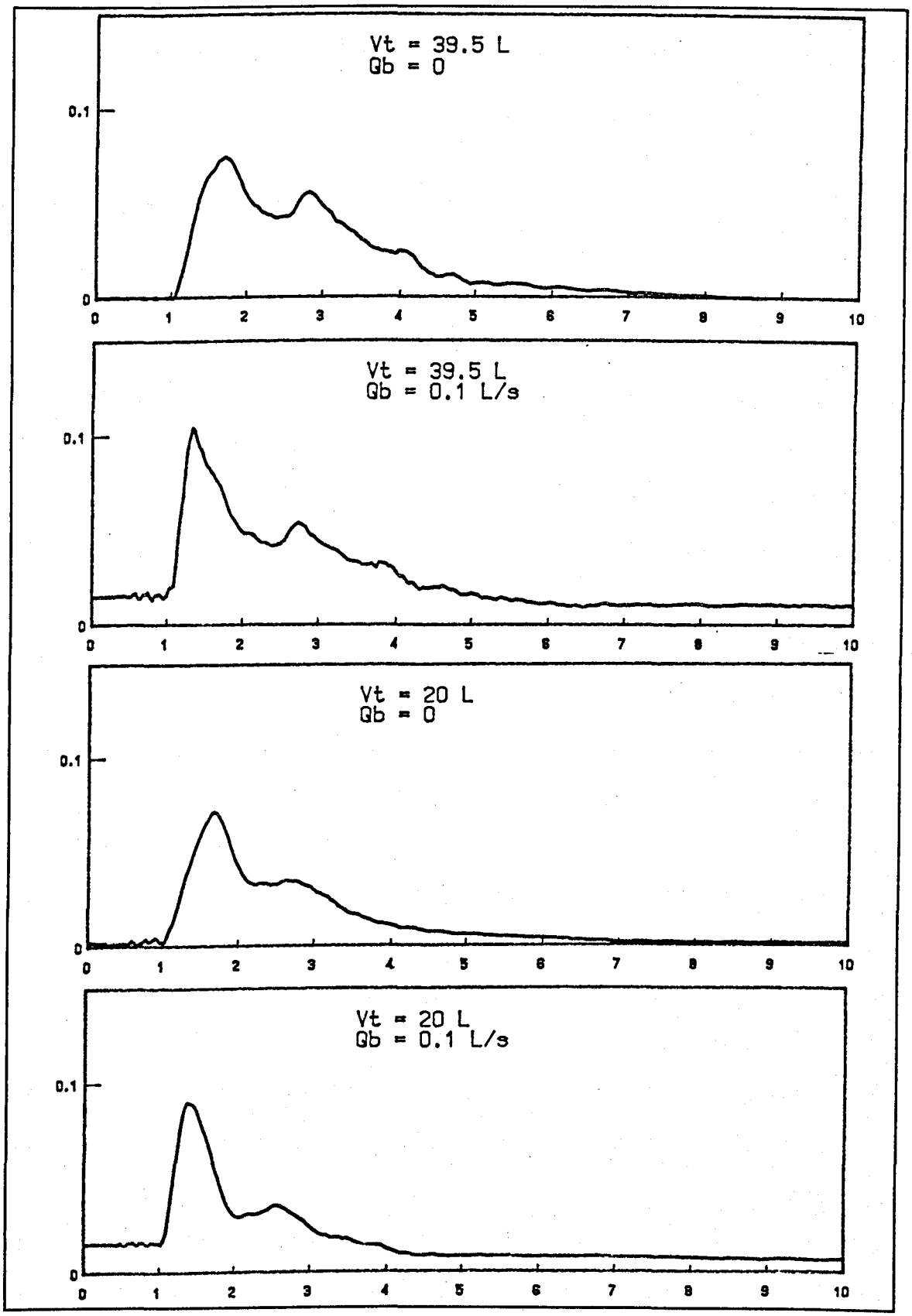

Figure 5.15 - Water depth simulation program entry profiles

base of the hypothesis present in 5.3.7 referring to the transformation of kinetic into potential energy.

5.4 Tipping Tank Flow Rate Measurements

This was a very complicated, delicate and time consuming measurement. The extremely turbulent tipping tank discharge and the very short time in which it occurs are the main reasons for the difficulties. These characteristics were also an indication not to use indirect flow rate measurements through pressure transducers as performed, for example, by Bridge (1984) and Standing (1986). These authors used water depth pressure transducer measurements to assess the flow rate of unsteady flow in pipes. In both cases a relationship between water depth and flow rate was obtained through a calibration process where several known flow rates were plotted against water depth, measured through pressure transducers in the beginning of a pipeline. This process is advantageous because it permits the simultaneous measurement of water depth profile and flow rate in a certain section of the beginning of the pipe during a certain period of discharge. Both these profiles will be necessary to feed the process of simulation for they constitute the boundary condition of the unsteady flow model.

In the case of the present research it was considered that in the beginning of the pipeline the turbulent tipping tank discharge would not have permitted the correct measurement of the pressure because the vertical components of flow

acceleration would invalidate the transducer readings and promote an enormous reading oscillation. In addition it would be very problematic to calibrate the configuration in a reasonable range of values because the high peak flow rate values of the tipping tank.

The arrangement for the tipping tank flow rate measurement is shown in Figures 5.16. In general terms the measurement can be delineated as follows. The tipping tank discharges into the large measurement tank, fitted with an electronic transducer (LVDT) that measures the water level. The transducer voltage signal is transmitted to a signal amplifier (P) and then finally it is read by the data acquisition equipment (DCA). Data is then transferred to a microcomputer where it is processed to generate the discharge hydrograph.

5.4.1 The Linear Variable Differential Transformer (LVDT)

The LVDT is an instrument that uses the property that a core has to induce a voltage in a coil. Figure 5.17 illustrates this principle. The primary coil is excited with an AC voltage that, through the displacement of the core, induces an output voltage in the secondary coils. Thus the core displacement has a direct relationship with the instrument output voltage. The relationship has a centred quasi-linear region as illustrated in Figure 5.18.

The LVDT axis was installed vertically on a ball cock float F (Figure 5.16). Previously to the tipping tank discharge

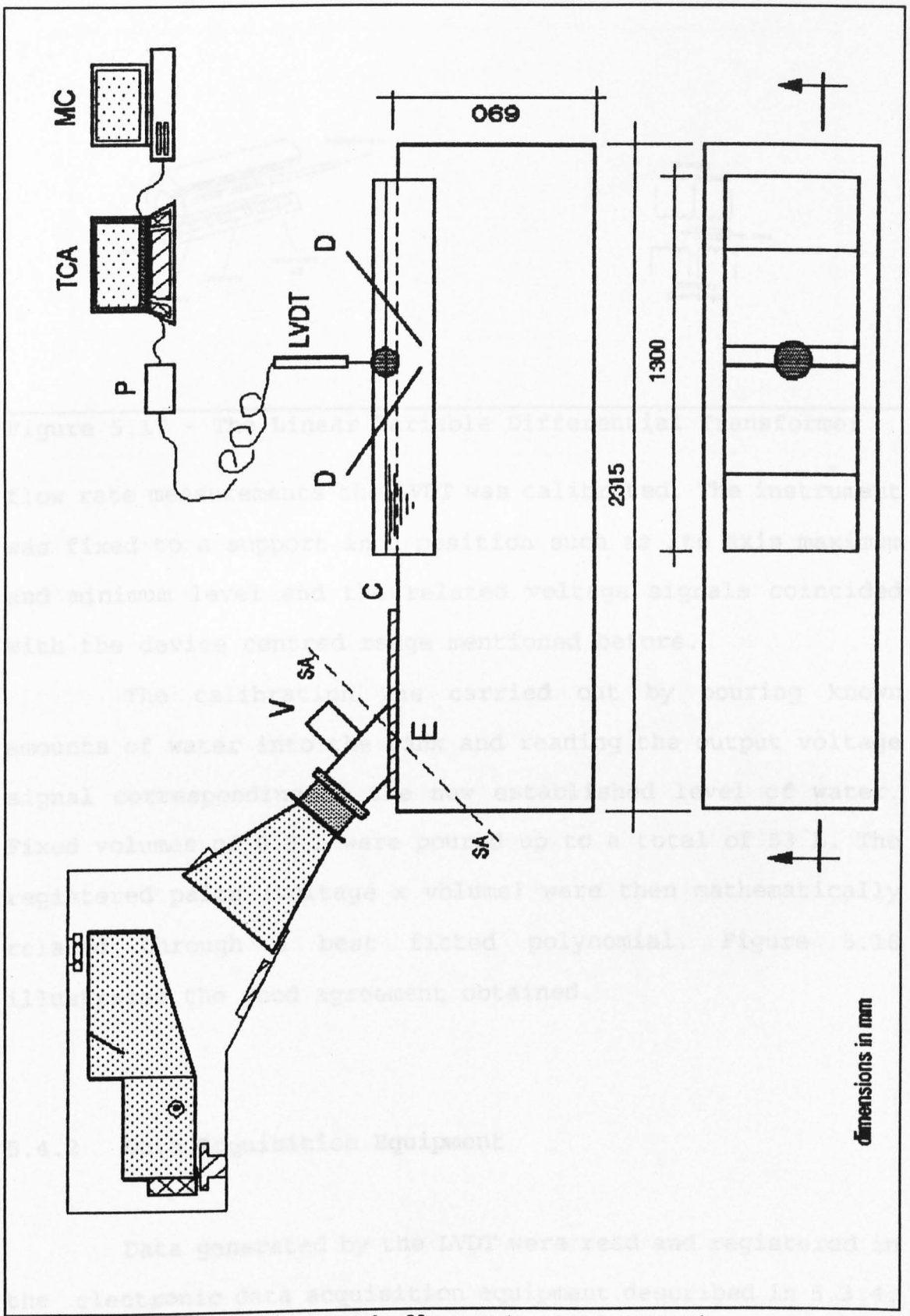

Figure 5.16 - Tipping tank flow rate measurement

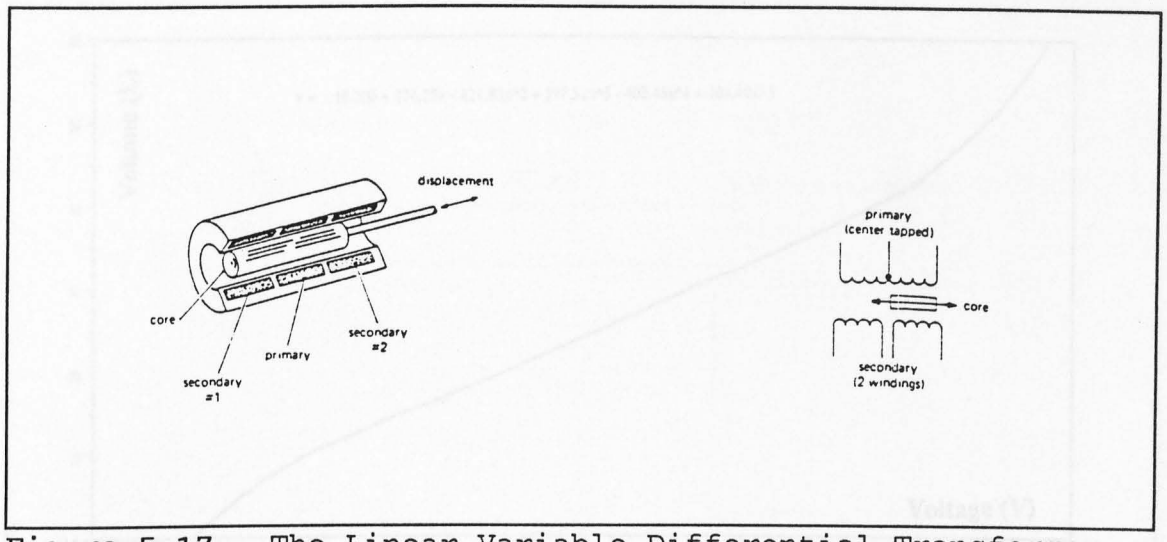

Figure 5.17 - The Linear Variable Differential Transformer

flow rate measurements the LVDT was calibrated. The instrument was fixed to a support in a position such as its axis maximum and minimum level and the related voltage signals coincided with the device centred range mentioned before.

The calibration was carried out by pouring known amounts of water into the tank and reading the output voltage signal corresponding to the new established level of water. Fixed volumes of 0.5 L were poured up to a total of 53 L. The registered pairs (voltage x volume) were then mathematically related through a best fitted polynomial. Figure 5.18 illustrates the good agreement obtained.

5.4.2 Data Acquisition Equipment

Data generated by the LVDT were read and registered in the electronic data acquisition equipment described in 5.3.4.

The tipping tank discharge duration varied from 2.6 s

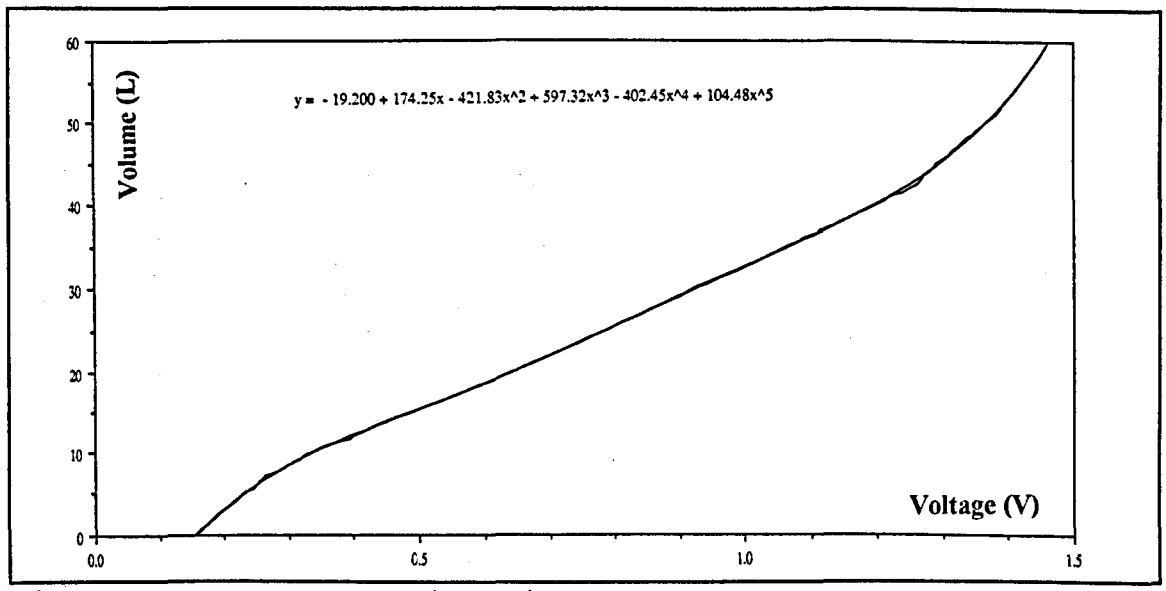

Figure 5.18 - LVDT calibration curve

to 3.5 s approximately depending on the measurement geometric configuration. The DCA was set to read in time intervals of 0.0039 s. Using this interval the discharge could be read from approximately 588 to 768 pairs (time x voltage) that were enough to characterize it.

As in the case of water depth readings the existing interface with a microcomputer permitted that each individual reading set was transferred after every discharge. Data could then be manipulated to produce the necessary hydrographs depicted in 5.4.7.

5.4.3 Geometric Configurations

The tipping tank flow rate was measured in three different sections - S1, SA and SB - as illustrated in Figures 5.16 and 5.19.

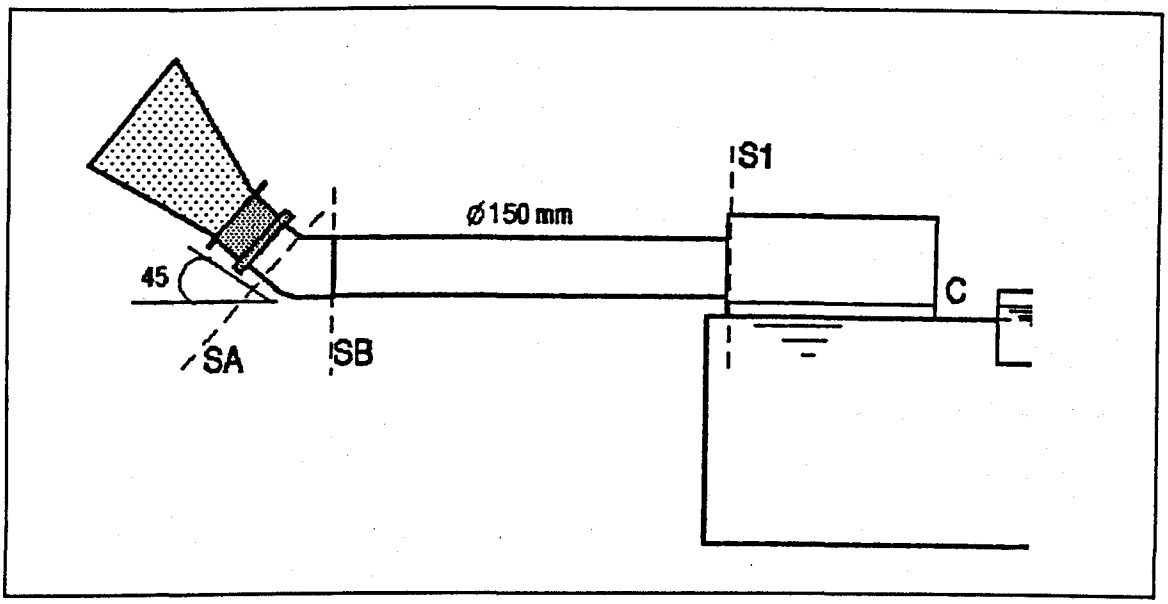

Figure 5.19 - Flow rate measurement at section S1

Flow rate taken in section SA can be considered as representative of the tipping tank itself since this position corresponds to the outlet of the conic piece designed to link the tank with the 45° junction. In sections SB and S1 the flow rate profiles are modified respectively by the junction and by the 1 m piece of pipe.

The flow rate was measured in these three positions for two main reasons. First to increase the confidence in the results since pronounced variations could not be expected from these close positions. Secondly because the simulation process requires the introduction of profiles of water depth and the associated flow rate varying with time in a certain position in the beginning of the pipe. As explained before it is impossible to assess the water depth profile just after the 45° junction in the pipeline entry. Thus it was decided to take measurements in a position 1 m downstream of the 45° junction outlet where both flow rate and water depth could be read.

5.4.4 Measurement Tank Arrangements

The measurement tank was designed to confront the adverse conditions caused by the tipping tank energetic discharge.

Direct flow rate assessment through volume and time measurement in graduated receptacles usually requires special arrangements when the discharge is very quick or turbulent and the volume is associated to the water surface level. Water surface oscillations or pressure waves can induce false results in these cases. The most common solution is to install some sort of energy dissipators inside the tank. Curtains, blinds, porous materials, etc are employed for this purpose. Normally they are interposed between the region directly hit by the discharge and the measurement region, i.e., the undisturbed area where the measurement instrument is located.

This procedure can introduce errors in the measurement mainly when the discharge is very rapid as is the case of the tipping tank. If the lag of time between the moment when the liquid hits the discharge area and the moment when it reaches the measurement area is significant it can cause flow rate undermeasurement.

To avoid these problems the tank was designed with a minimum number of pieces that could cause delay. To minimize water surface oscillations the alternative found was to use the water itself as an energy absorber. For this reason the measurement tank is lengthy and holds a considerable mass of water.

However, this provision was not enough to avoid an undue action of horizontal streams that caused the LVDT axis to grip against the body of the instrument for very short time intervals. This problem led to the formation of unreal horizontal regions in the LVDT output.

The small pool where the LVDT is installed was also subject of level oscillations at the end of discharge. The water mass displacement originated by the discharge led to the formation of wave pressures that after shocking against the tank walls reached that pool causing surface oscillations. The installation of two inclined plates beside the LVDT was enough to restrict considerably the problem of horizontal streams but some oscillations still appeared at the end of the discharge. In Figure 5.16 these curtains are indicated by the letter D.

It can be observed in Figure 5.16 that the initial free surface level is higher than the tank cover (C). This was done to force the level variation not to occur in other areas but only in the measurement pool where the LVDT is installed and in the entrance area (E) directly hit by the discharge. Thus the rest of the tank was under pressure.

During the discharge the water outflowing the tipping tank forms a piston of air that is pushed through the conic piece and then along the pipe or in the measurement tank. A proper ventilation had to be installed in the entrance pipe otherwise the air pushed into the tank would promote and undue raising of the water surface in the measurement pool. A piece of pipe 100 mm of diameter was sufficient to annul the air piston effect. Another amount of air is normally incorporated

onto the water mass being released soon after the discharge leaves the tipping tank conic piece of connection. This amount was considered negligible.

5.4.5 Tipping Tank Settings

The tipping tank operation was subject to the same conditions of installation described in 5.3.1 providing the necessary repeatability between the tipping tank flow rate measurements and the water depth profile measurements in the horizontal rig.

5.4.6 Data Processing

Flow rate hydrographs were assessed from 6 discharges for each discharge volume. Similarly to the case of the water depth measurements this number was considered enough for an average process since the profiles displayed good repeatability.

A computer program to process read data from the DCA was developed. The program repeated the following procedure for each of the files. It read its data, applied the calibration equation, displaced the beginning of the discharge to a common start point, adjusted a line to the original signal, that is very oscillating due the electric alternate current pattern, and finally calculated the accumulated volume percentage and

the flow rate. The n flow rate curves were then added and an averaged curve obtained.

5.4.7 Tipping Tank Flow Rate Results

Figure 5.20 shows 5 curves of accumulated volume percentage of 39.5 L tipping tank discharges taken at section SA together with their average curve. Figure 5.21 shows the respective flow rate curves and Figure 5.22 presents the average curve and the typical one.

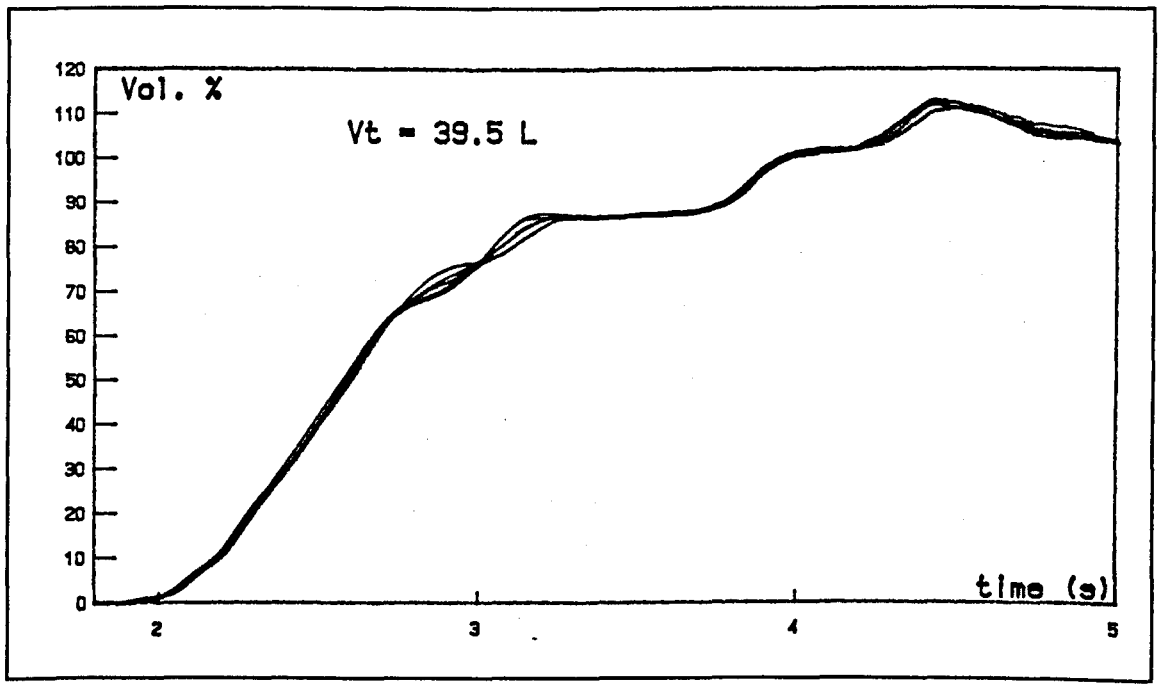

Figure 5.20 - Discharge volume percentage

Also similarly to the procedure used with the water depth data processing it was preferred to adopt a typical curve, chosen visually by comparison taking the averaged as reference.

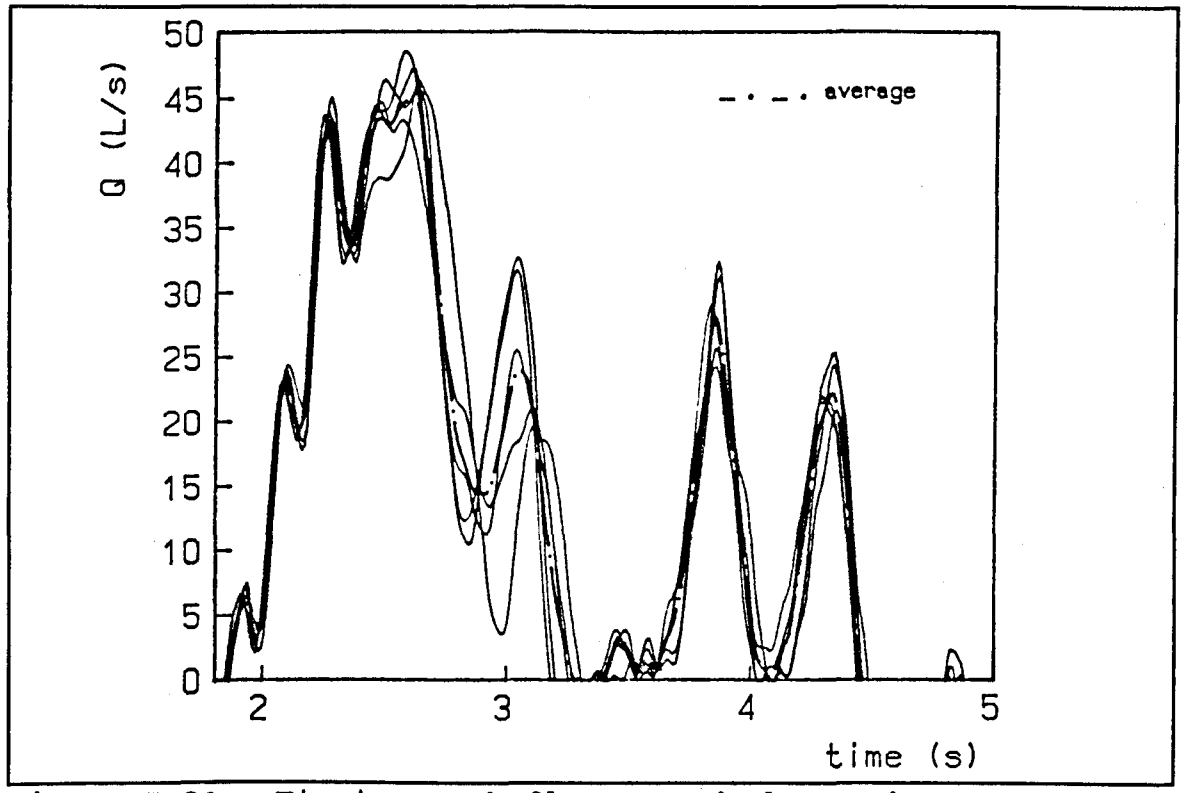

Figure 5.21 - Tipping tank flow rate hydrograph
Section SA - V_t = 39.5 L

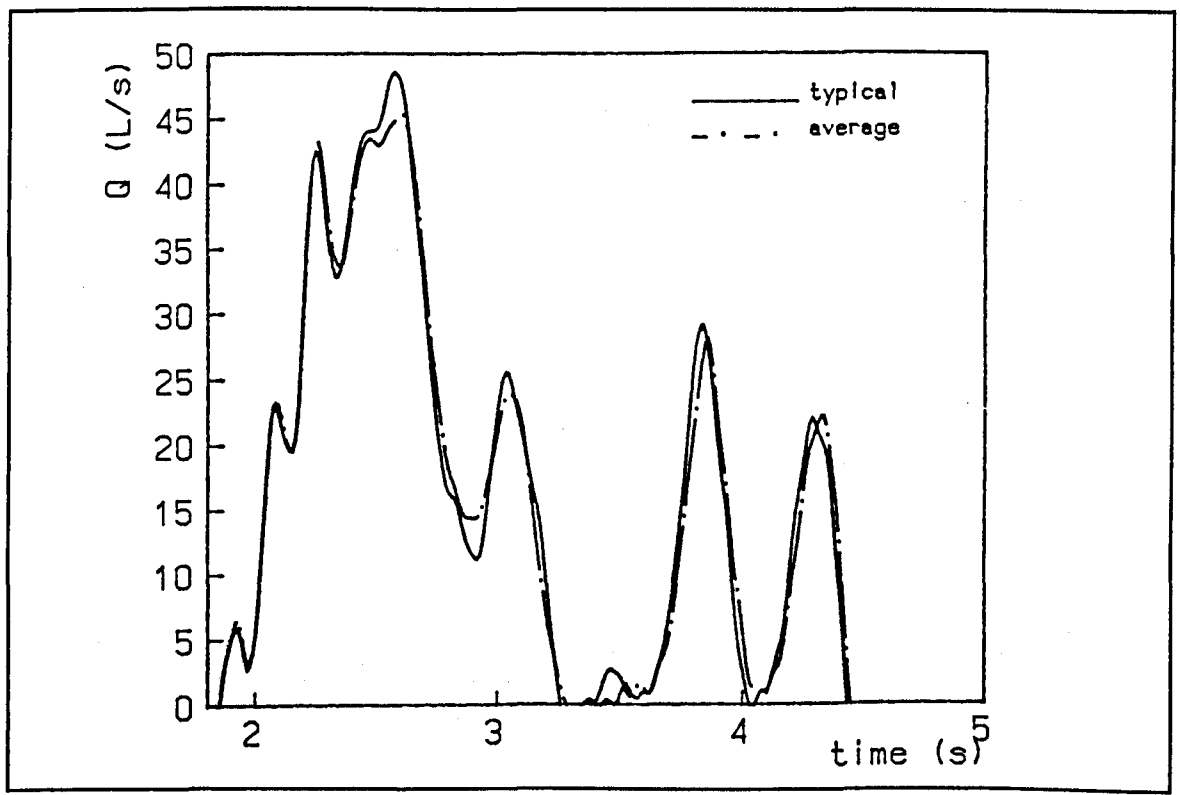

Figure 5.22 - Averaged and typical tipping tank hydrographs
Section SA - V_t = 39.5 L

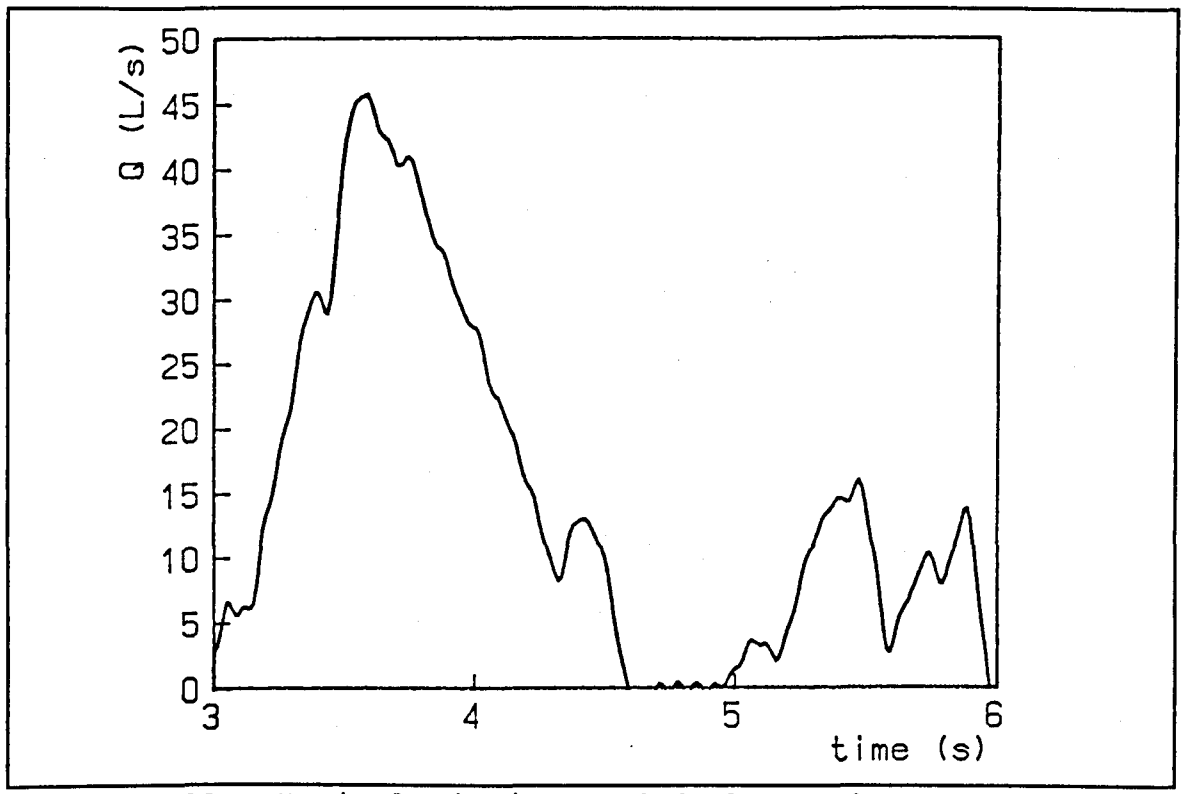

Figure 5.23 - Typical tipping tank hydrograph
Section SB - V_t = 39.5 L

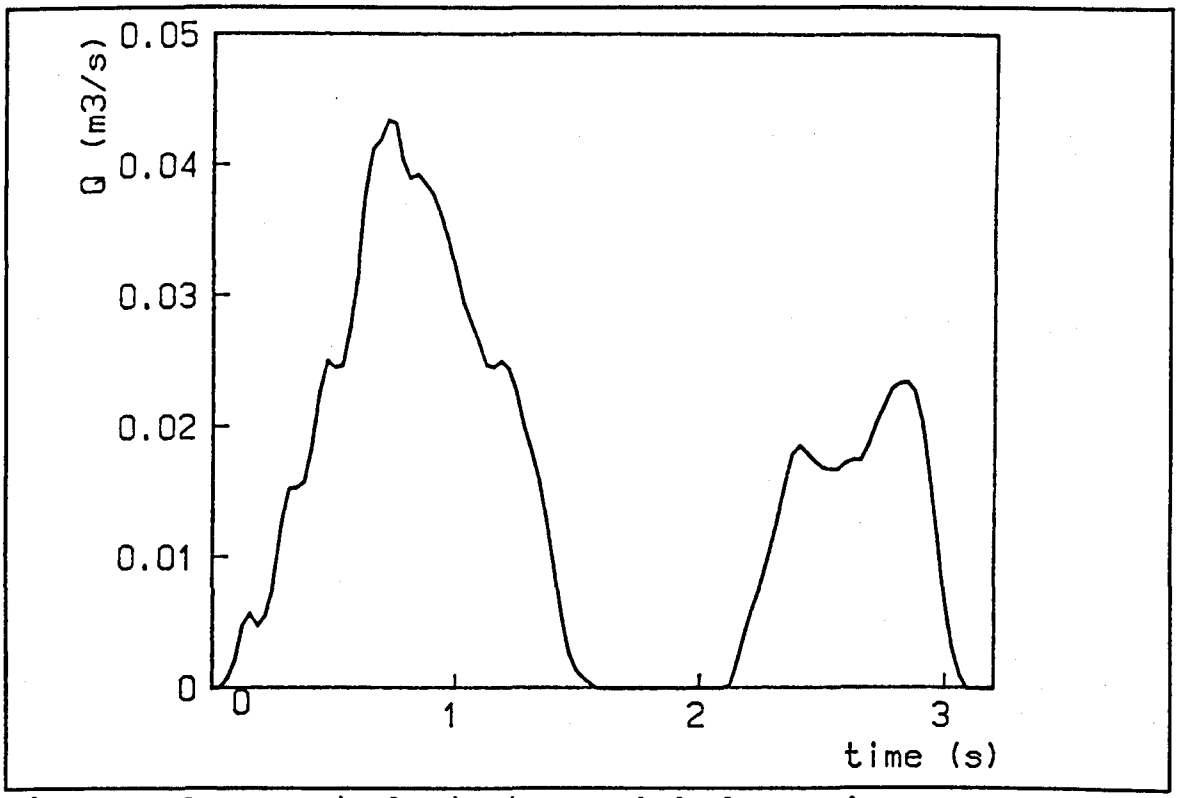

Figure 5.24 - Typical tipping tank hydrograph
Section S1 - V_t = 39.5 L

The same procedure was reproduced for discharges measured at sections SB and S1 and the results are shown in Figures 5.23 and 5.24, respectively.

As referred to previously the purpose of these measurements was to obtain the hydrograph at the entry section in the simulation process, i.e, section S1. Thus, measurements taken at SA and SB serve only to confirm the results.

Referring to the presented curves some aspects need to be commented. The duration of the very fast discharge was confirmed through direct measurements with a chronometer. For a 39.5 L discharge the entire duration is 2.3 s at section SA and no more than 3.5 s at section S1. As a consequence the profiles present very high flow rate peaks. This rapidness reflects the directive adopted during the development of the tipping tank to have a device whose discharge was very powerful in terms of its capability of promoting the pipeline self cleansing.

A second aspect to be noted is the two stage pattern of the discharges. From the beginning up to 1.5 s approximately about 85% of the tank volume is discharged. After that all the curves show different forms of oscillations including negative flow rate values. The existence of two main stages during the discharge was confirmed through video cassettes images recorded at the laboratory and reproduced through sequent frozen pictures at the television screen. Using this method it was also possible to confirm the time duration of the discharge first stage at section SA.

The presence of negative flow rate values derives from the arrangement used during the measurement. It was inevitable that some oscillation reached the water surface in the protected pool where the float ball was installed. However, the whole consideration of all factors involved permitted to assume that the profiles were accurate in the first stage.

Figures 5.22, 5.23 an 5.24 show a good consistency between the profiles in the first 1.5 s of discharge duration. The comparison between peak values, time duration and general shape shows a coherent relation. The profile at section SA (Figure 5.22) shows some local peaks in both ascending and descending branches in the hydrograph first stage while, as could be expected, the profiles measured at the downstream sections show an attenuation of these peaks.

An extrapolative conclusion from the hydrographs analysis is that there is a relative small loss of hydraulic energy between sections SA and S1 since the energy main component in this case, the kinetic part, are comparable in the three diagrams.

Hydrographs corresponding to groups A1 and E1 relative to base flow 0.1 L/s were derived from those without base flow according to a procedure based on certain properties applicable to water depth and flow rate profiles.

According to Abbott (1979) in the water propagation phenomena of the type described by the unsteady gradually varied flow equations, the velocity (or the flow rate, a dependent variable), the water depth and the energy propagate under the same characteristic curve in the (x,t) plan. This

property can be verified through the alignment of the water depth and flow rate peaks in the diagrams of water depth and flow rate against time.

To complement the hydrographs after the first stage an adjustment using the above property was carried on. The unreal flow rate secondary peak presented in Figure 5.24 had to be displaced to a position under its corresponding secondary water depth peak. In addition the total tipping tank discharge volume and the discharge time duration were controlled in parallel. The tipping tank discharge volume was computed through the numerical integral of the hydrograph that corresponds to the area under the flow rate curve. Additionally a final smooth process was carried on to obtain hydrographs with the same pattern of evolution observed in the water depth profiles. Figures 5.25 and 5.26 show the final hydrographs with their respective water depth profiles. Each pair constitute the entry data for the simulation program.

To assess the hydrographs for the case of base flow 0.1 L/s (groups A1 and E1) the same principle was used to displace the hydrograph peaks to positions aligned with the water depth profile corresponding peaks. In this case in the volume balance it was necessary to consider the base flow rate (0.1 L/s) in the total volume. Hydrographs presented in Figures 5.27 and 5.28 were obtained according to the above explained criteria.

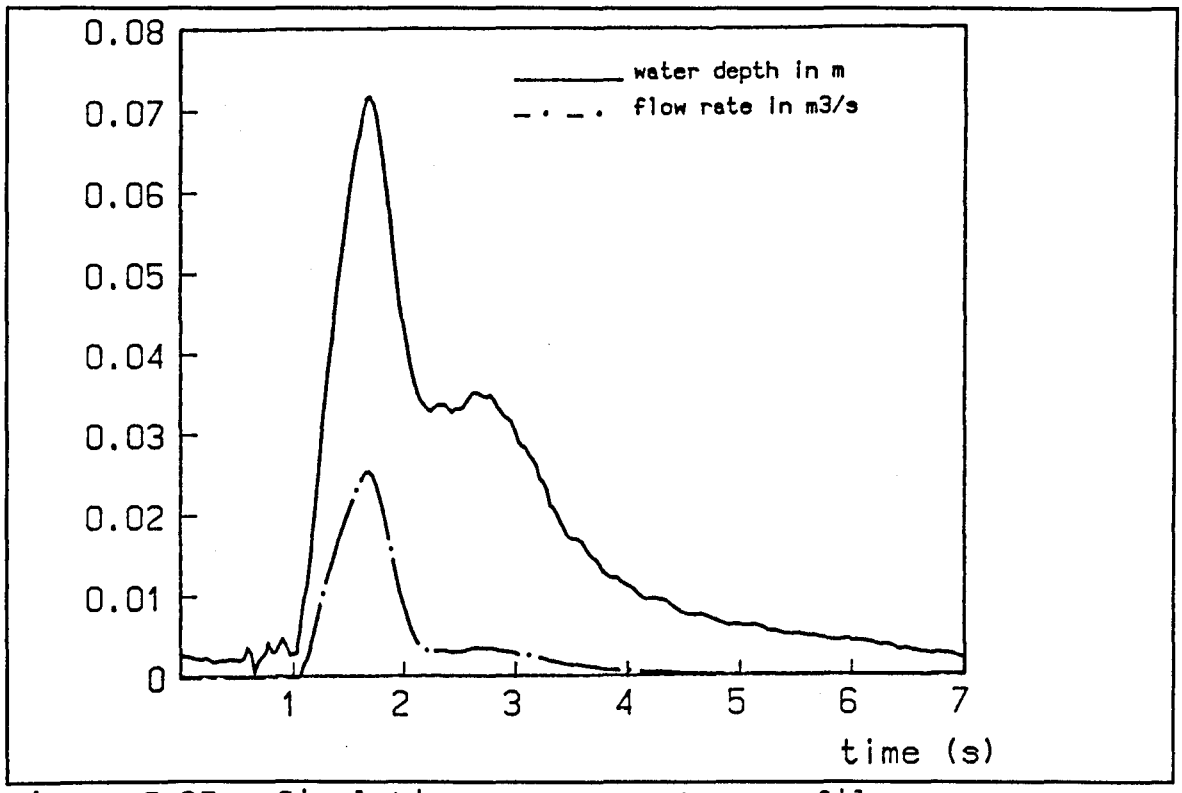

Figure 5.25 - Simulation program entry profiles
Group A0 - V_t = 20 L, Q_b = 0

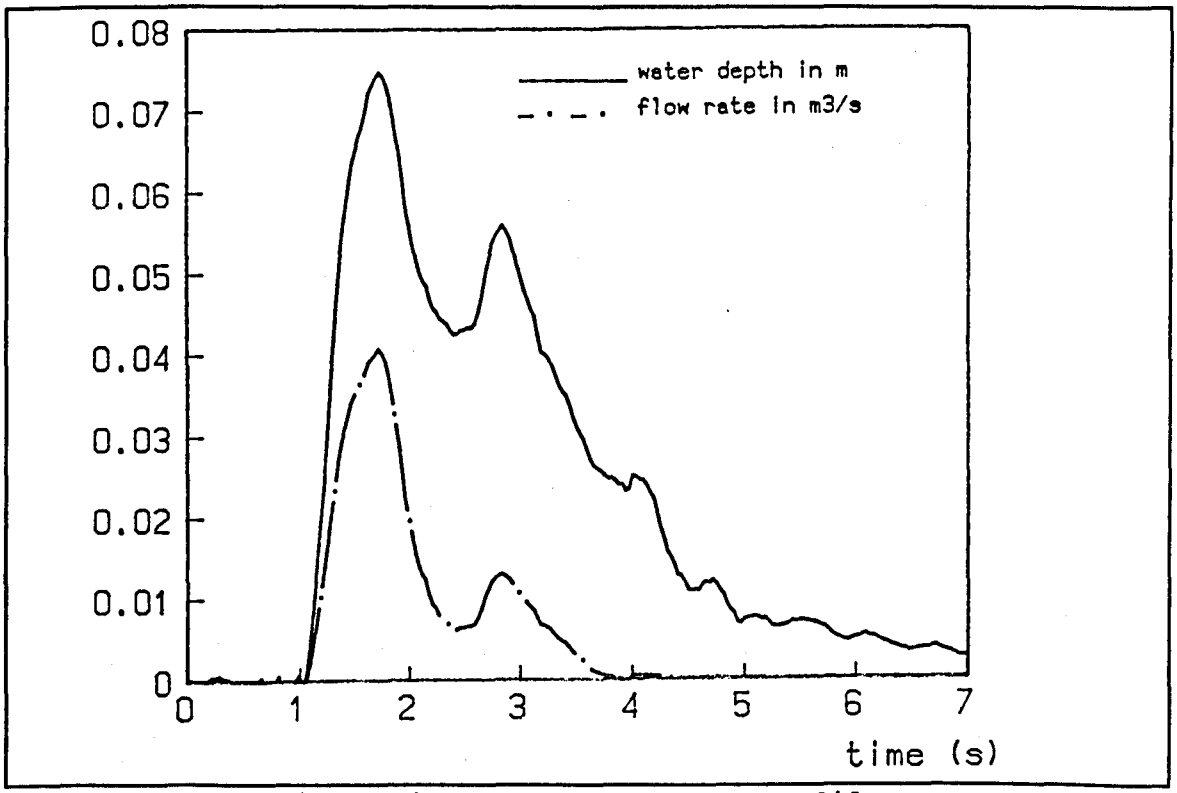

Figure 5.26 - Simulation program entry profiles
Group E0 - V_t = 39.5 L; Q_b = 0

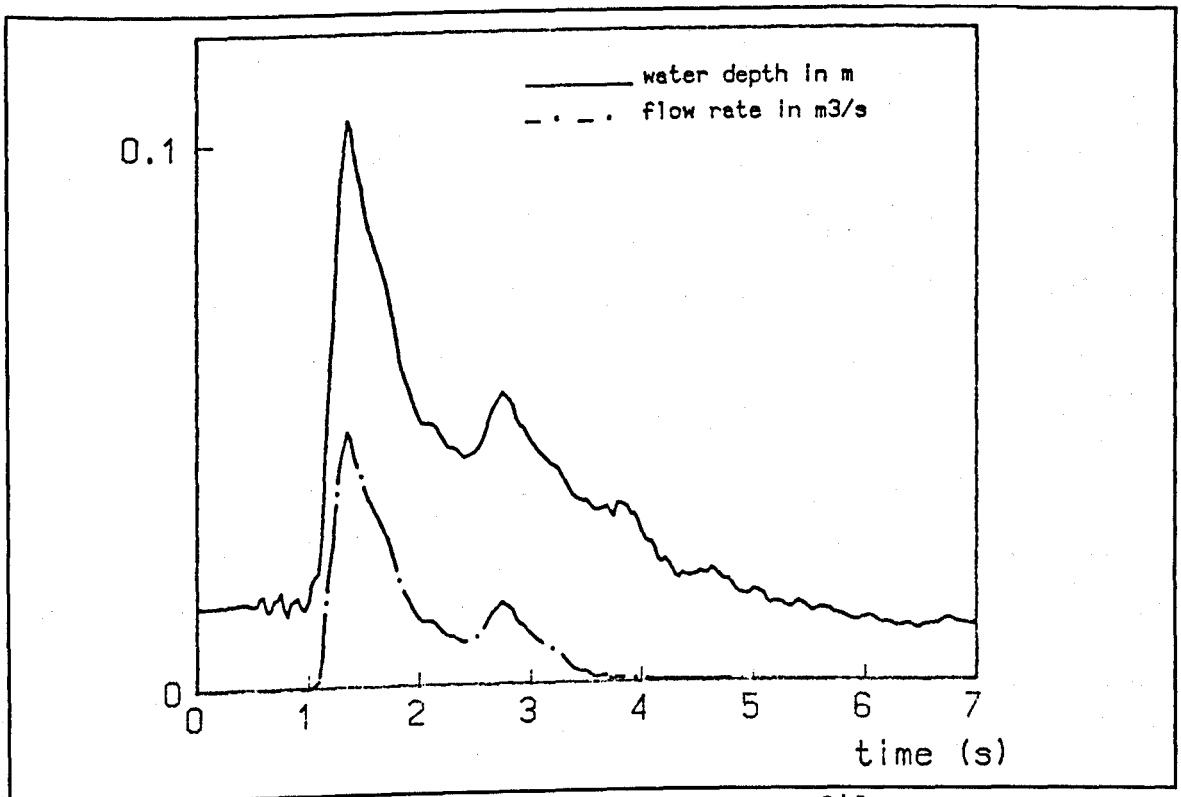

Figure 5.27 - Simulation program entry profiles
Group E1 - V_t = 39.5 L, Q_b = 0.1 L/s

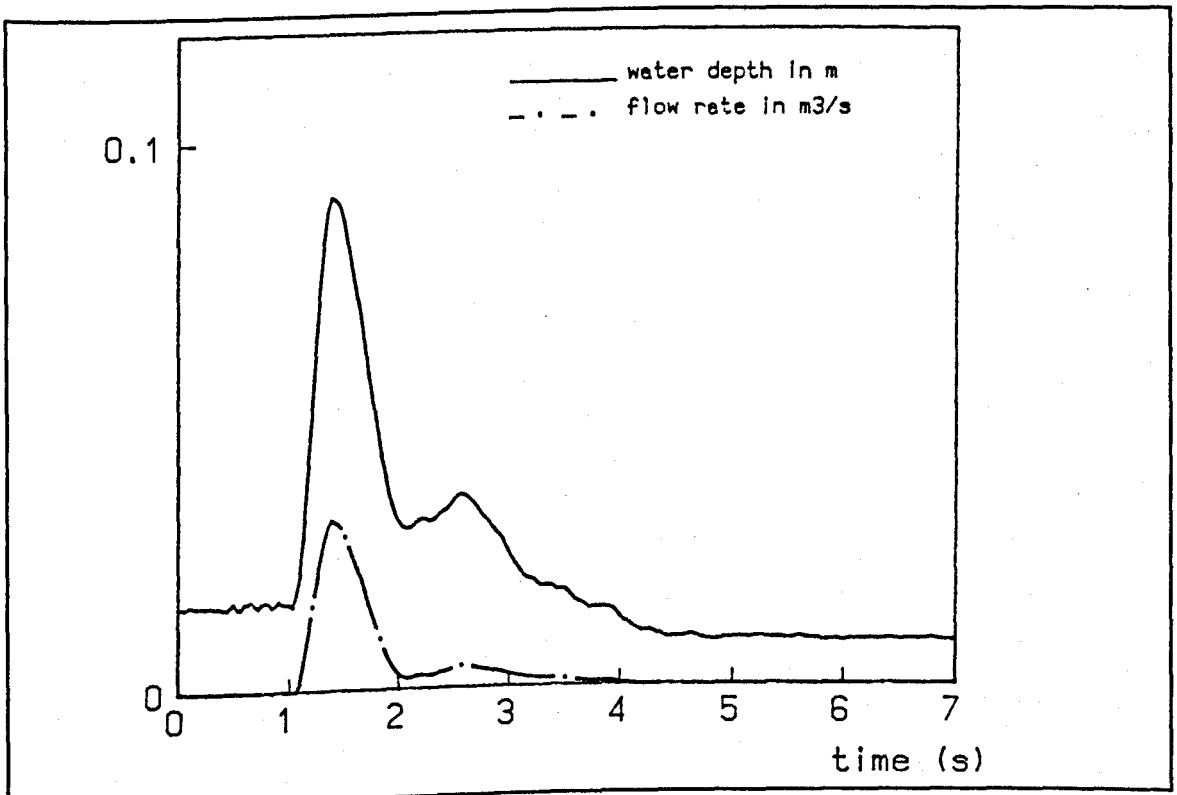

Figure 5.28 - Simulation program entry profiles
Group A1 - V_t = 20 L; Q_b = 0.1 L/s

5.5 Conclusions

Laboratory measurement provided all the necessary data for the simulation process. It was also possible to register the water depth peak oscillatory movement along the pipeline. This was an unexpected occurrence since the consulted literature does not make any mention to it. A better description of the phenomenon could be carried on through laboratory measurements embracing a wider range of discharge volumes and other pipe slopes. The water depth variation with time would require a measurement arrangement for simultaneous reading.

The difficulties involving the flow rate measurement point to the necessity of developing other forms of instrumentation. Probably combined arrangements of volumetric and mass processes would be necessary. In a volumetric process a higher number of water level measurement points would be advisable to comprise local water surface variations.

CHAPTER 6

MODEL CALIBRATION RESULTS

6.1 Introduction

This Chapter presents the results obtained with the application of the calibration process described in Chapter 4.

The three developed model alternatives B, D and E, are used for the simulation of the flow originated from two set of entry data.

Program alternatives, developed in Chapter 2, 3 and 4, are summarized in Table 6.1.

Table 6.1 - Computer program processing alternatives

math. models / num.models	Saint-Venant equations	Boussinesq equations
method of characteristics	E	-
McCormack scheme	B	-
two-four scheme	-	D

Entry data comprises one of the hydrographs presented by Standing (1986) and the group E0 of measurements, presented in Chapter 5.

Simulated water depth variation with time, (t,h), will

be used in the comparison with laboratory measured results. Simulated horizontal velocity variation with time (t,u) and water depth variation along the pipe length (x,h) also will be presented.

6.2 Laboratory and Simulated Data Comparison

6.2.1 Standing (1986) Entry Data

Standing (1986) data embraces the water depth and flow

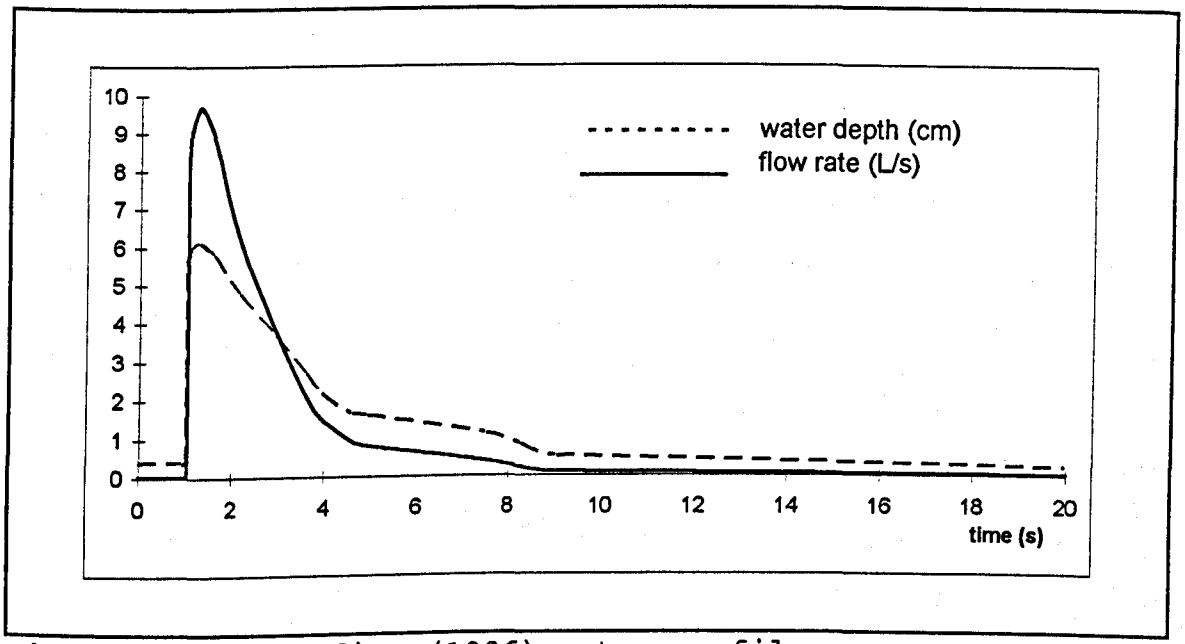

Figure 6.1 - Standing (1986) entry profiles

rate variation with time (t,h,Q) at the entry section of a pipeline. The laboratory rig used by Standing consisted of a 12 m pipeline, using glass tubes, of 0.1 m diameter. Used entry data corresponds to a slope of 0.02 m/m and to a base flow rate of 0.0000283 m^3/s. Figure 6.1 shows Standing's entry hydrograph (t,h,Q).

Standing control sections in the laboratory rig were distanced 3m, 5m, 7m, 9m and 11m from entry section. Electric pressure transducers read water depth variation with time.

Figures 6.2 to 6.4 present simulated water depth profile variation with time together with correspondent laboratory read profiles for each of program alternatives.

Simulation with Standing entry data, illustrated on Figures 6.2 to 6.4, refers to the most simple set of calibration parameters. In the friction scheme it was used a multiplicative factor K = 1, i.e., friction effect was calculated with Colebrook-White formula (2.75). No numerical filter was necessary and, in D alternative, the vertical acceleration multiplicative factor, Z, was equal to 1. A computation internode fixed distance of 0.15 m was adopted. In E alternative a Courant number (C_n) equal to 1 was adopted. In B alternative C_n was 0.8 and in D alternative C_n was 0.667.

Figure 6.2 shows simulate profiles exhibiting good shapes with well marked wave peaks. The wave "foot", however, tends to a progressive delay. The same problem was observed by Standing (1986) when the friction effect was computed through Colebrook-White formula. Standing found that a decreasing on friction force in the wave front (see 3.2.2) led to better agreement.

Figure 6.3 illustrates the simulated profiles in the program alternative B. A better adjustment of wave "feet" can be observed but, in this case, the wave peak is rounded. Several attempts to eliminate this problem were carried out. Smaller internode distances, smaller Courant numbers and

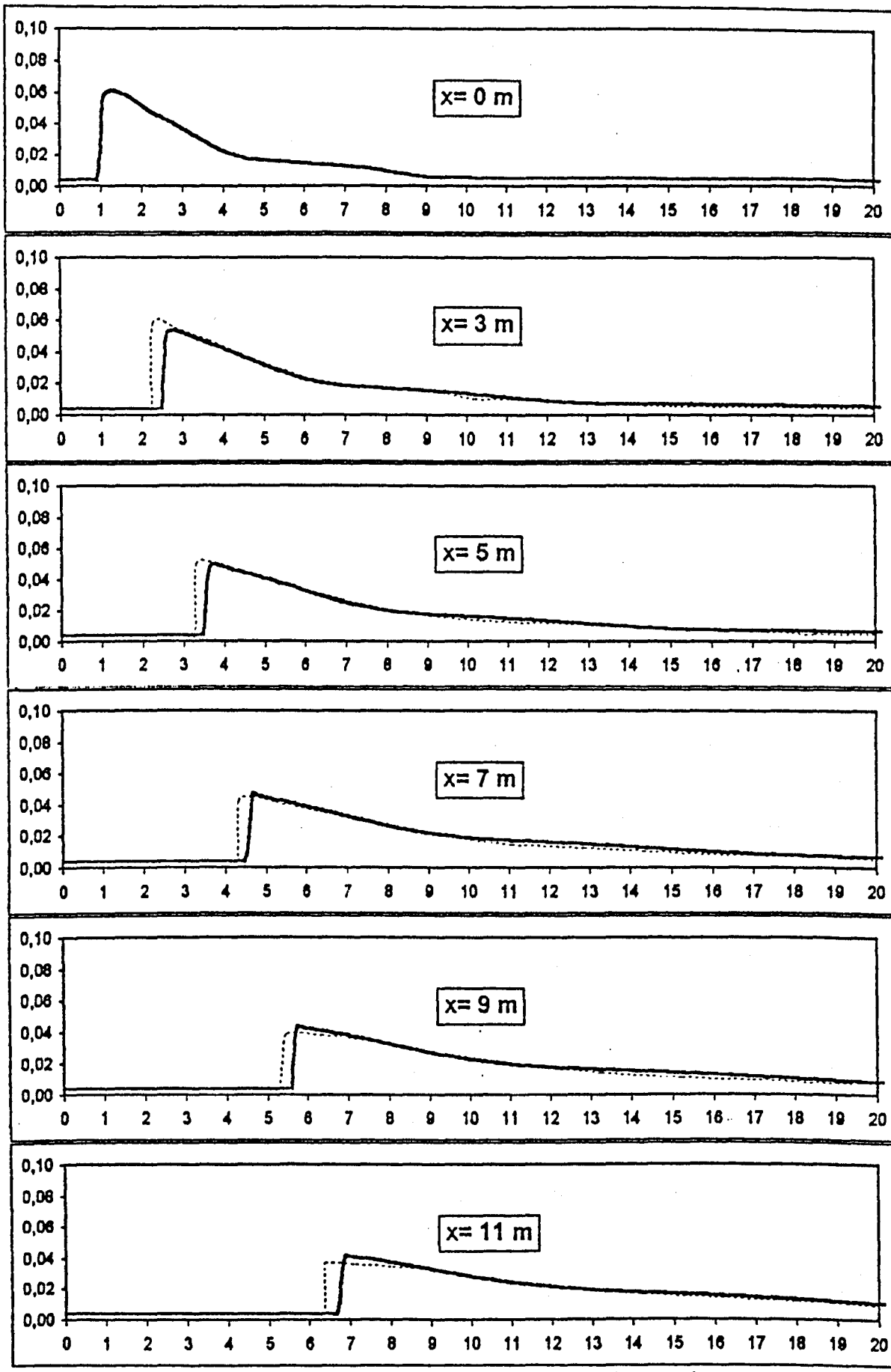

Figure 6.2 - K.M.Standing entry data - program alternative E - __lab. __sim.
Water depth profile (y axis, m) on time (x axis, s)

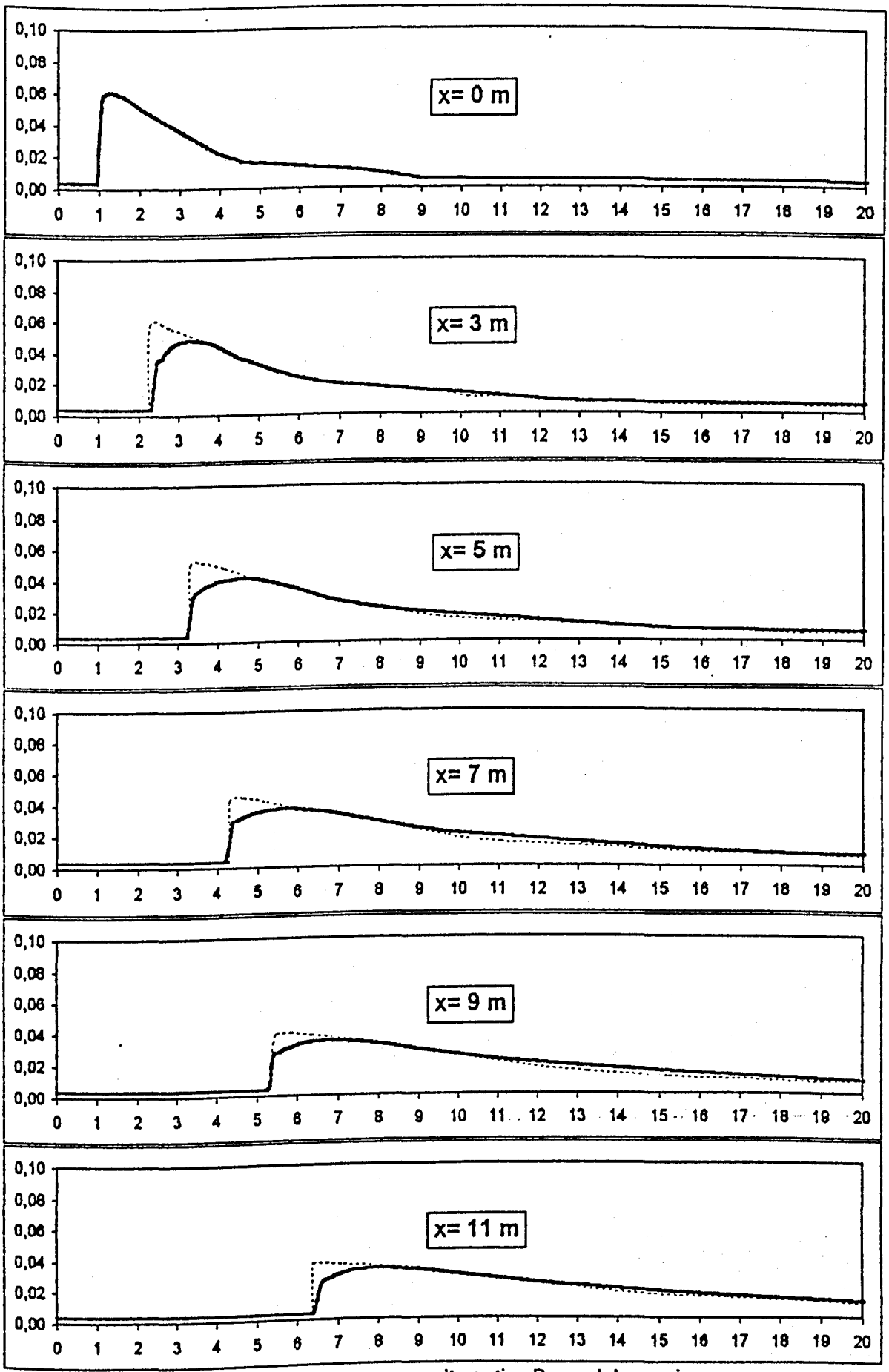

Figure 6.3 - K.M.Standing entry data - program alternative B - __lab. __sim.
Water depth profile (y axis, m) on time (x axis, s)

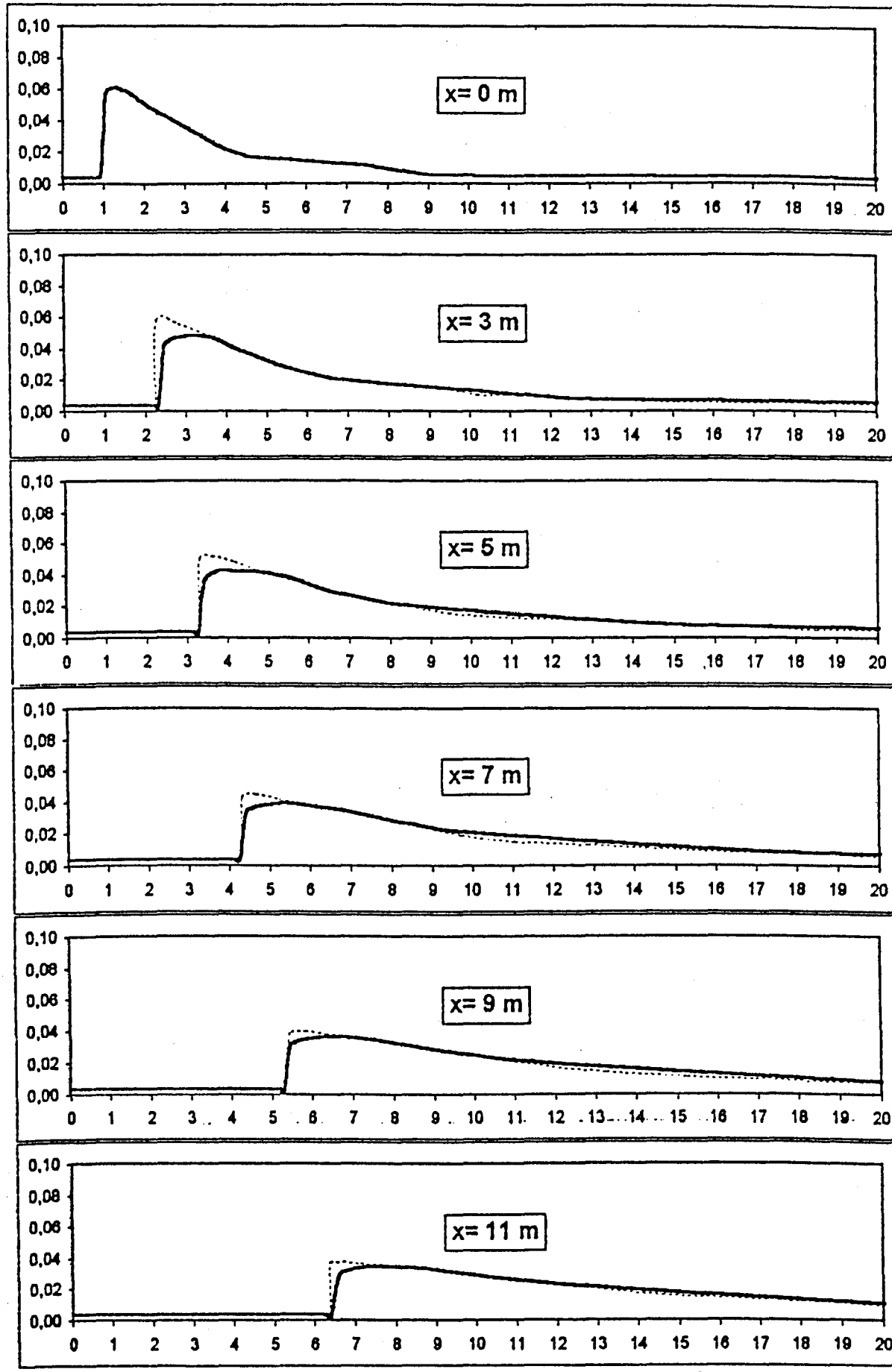

Figure 6.4 - K.M.Standing entry data - program alternative D - __lab. __sim.
Water depth profile (y axis, m) on time (x axis, s)

decreasing of friction effect at the wave front were tried. At the end it was concluded that these curved peaks, in fact, are an intrinsic response of MacCormack scheme for the water depth profile, since in all the combination of calibration parameters the same type of rounded peak profile was obtained.

Figure 6.4 shows the simulated profiles of D alternative. The wave peak is not well marked again but, rather better than in B alternative. It seems that the rounded peak tends progressively to a better adjustment in downstream sections. The simulated wave "feet" positions on time agree exactly to theirs correspondent in the laboratory measured profiles.

Figures 6.5 to 6.7 present simulated profiles of horizontal velocity variation with time, using Standing entry data, for the same program alternatives.

A distinctive characteristic of velocity profiles in alternatives B and D (Figures 6.6 and 6.7) is the well marked wave peak profile. Again, it seems to be an intrinsic behaviour of MacCormack and "2-4" schemes.

Finally, Figures 6.8 and 6.9 illustrates the profile as it would really be seen in a certain instant, i.e., the variation of water depth with distance, according to simulation alternatives E and D, respectively.

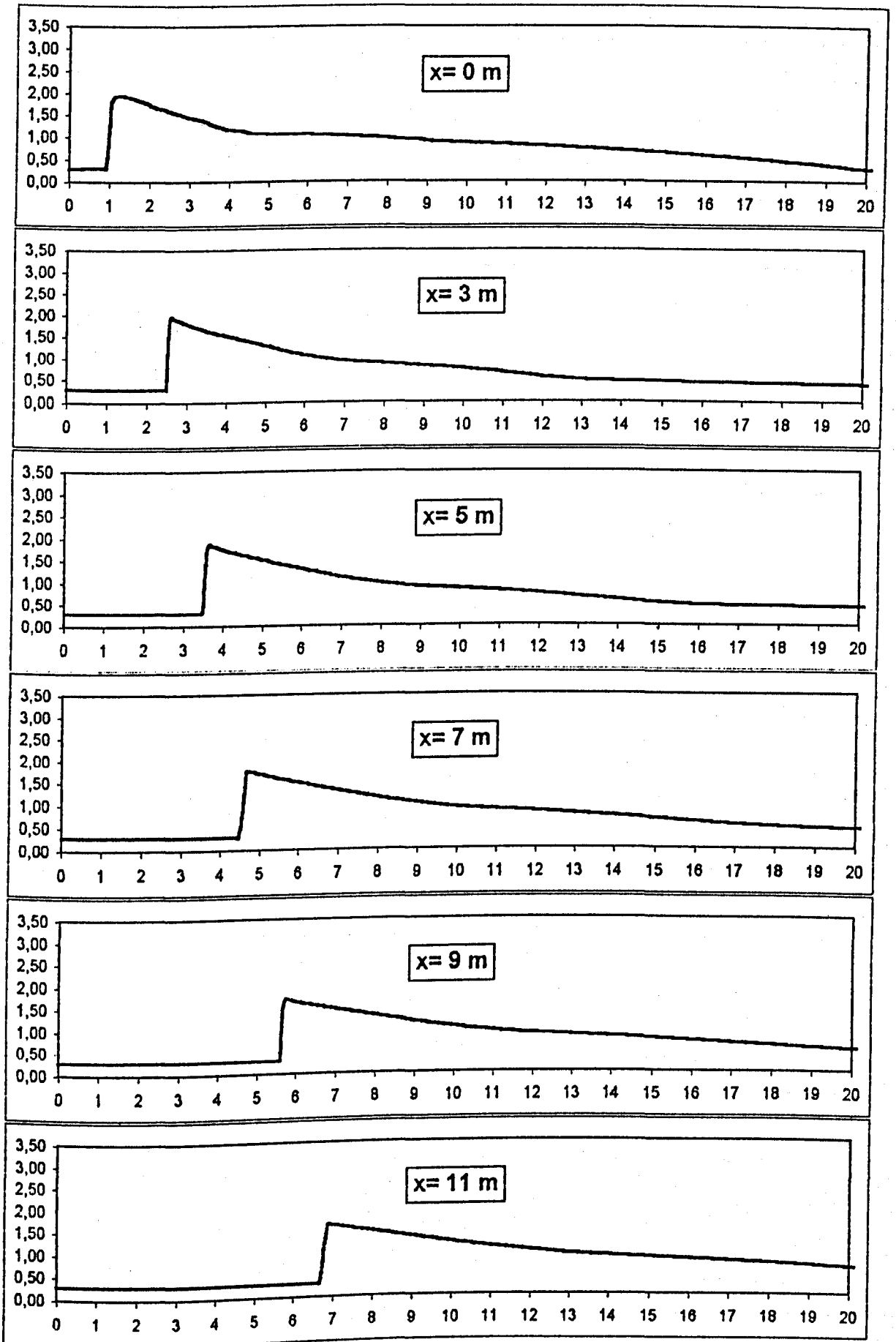

Figure 6.5 - K.M.Standing entry data - program alternative E
Horizontal velocity (y axis, m/s) on time (x axis, s)

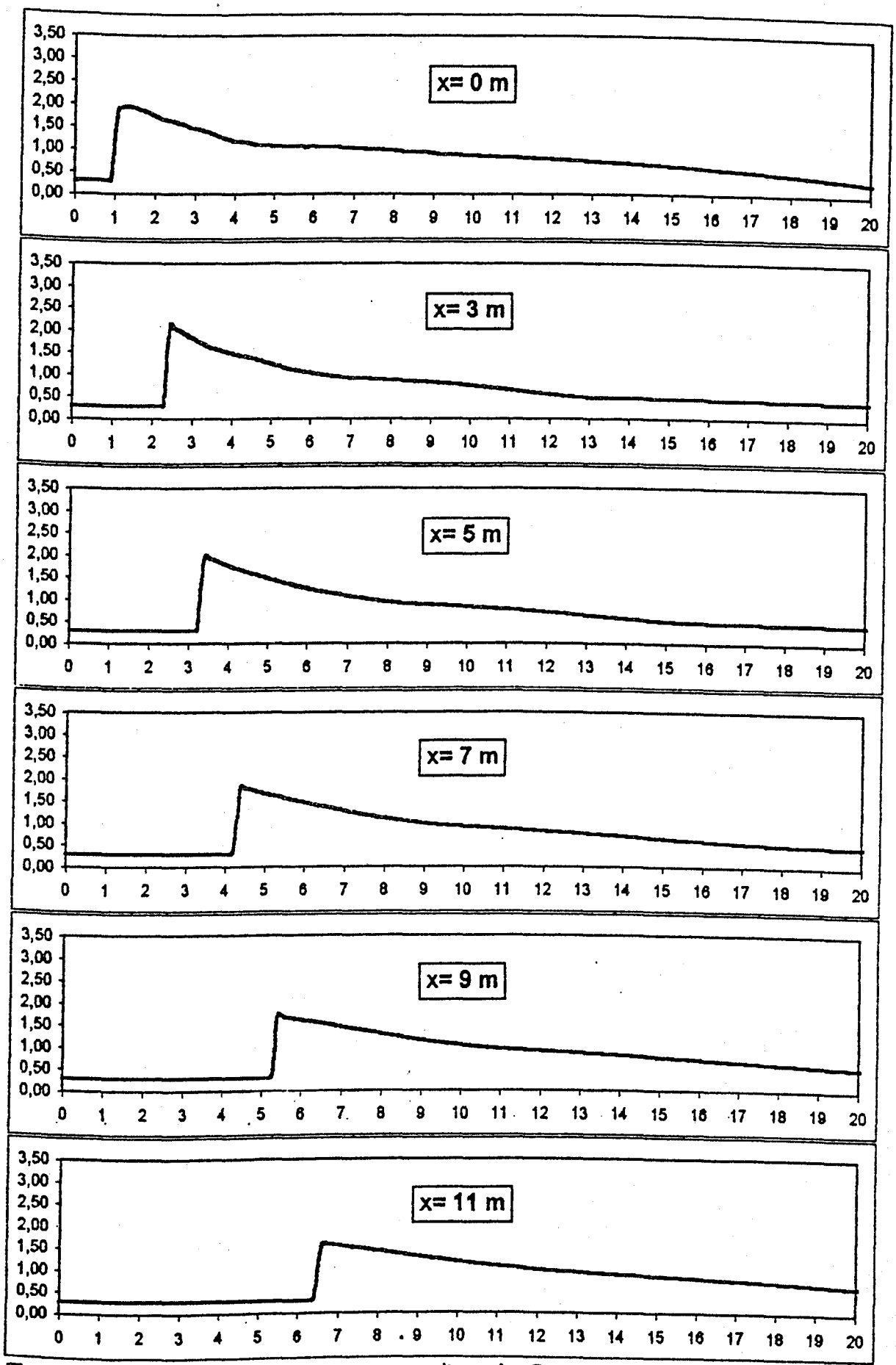

Figure 6.6 - K.M.Standing entry data - program alternative B
Horizontal velocity (y axis, m/s) on time (x axis, s)

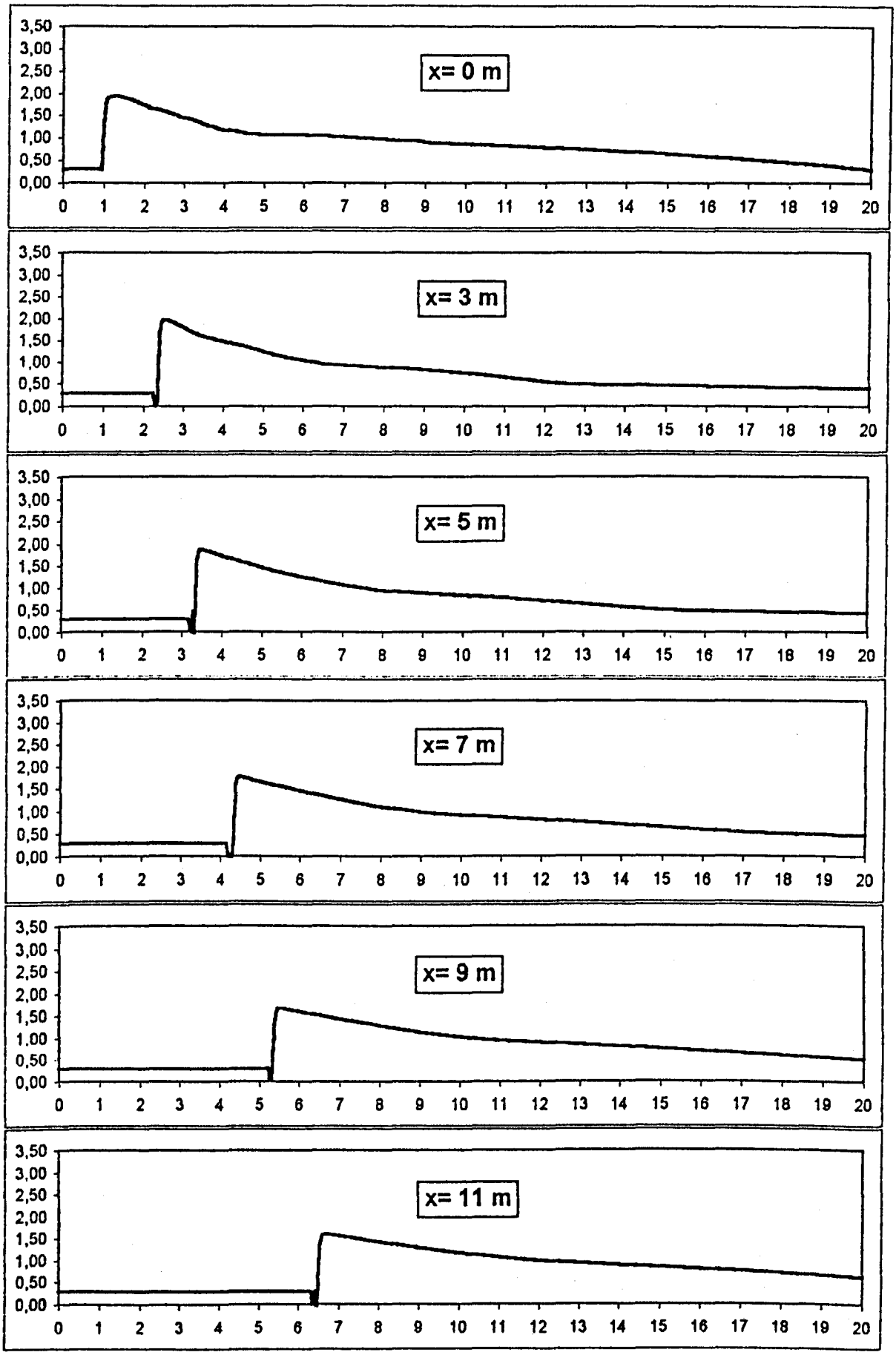

Figure 6.7 - K.M.Standing entry data - program altenative D
Horizontal velocity (y axis, m/s) on time (x axis, s)

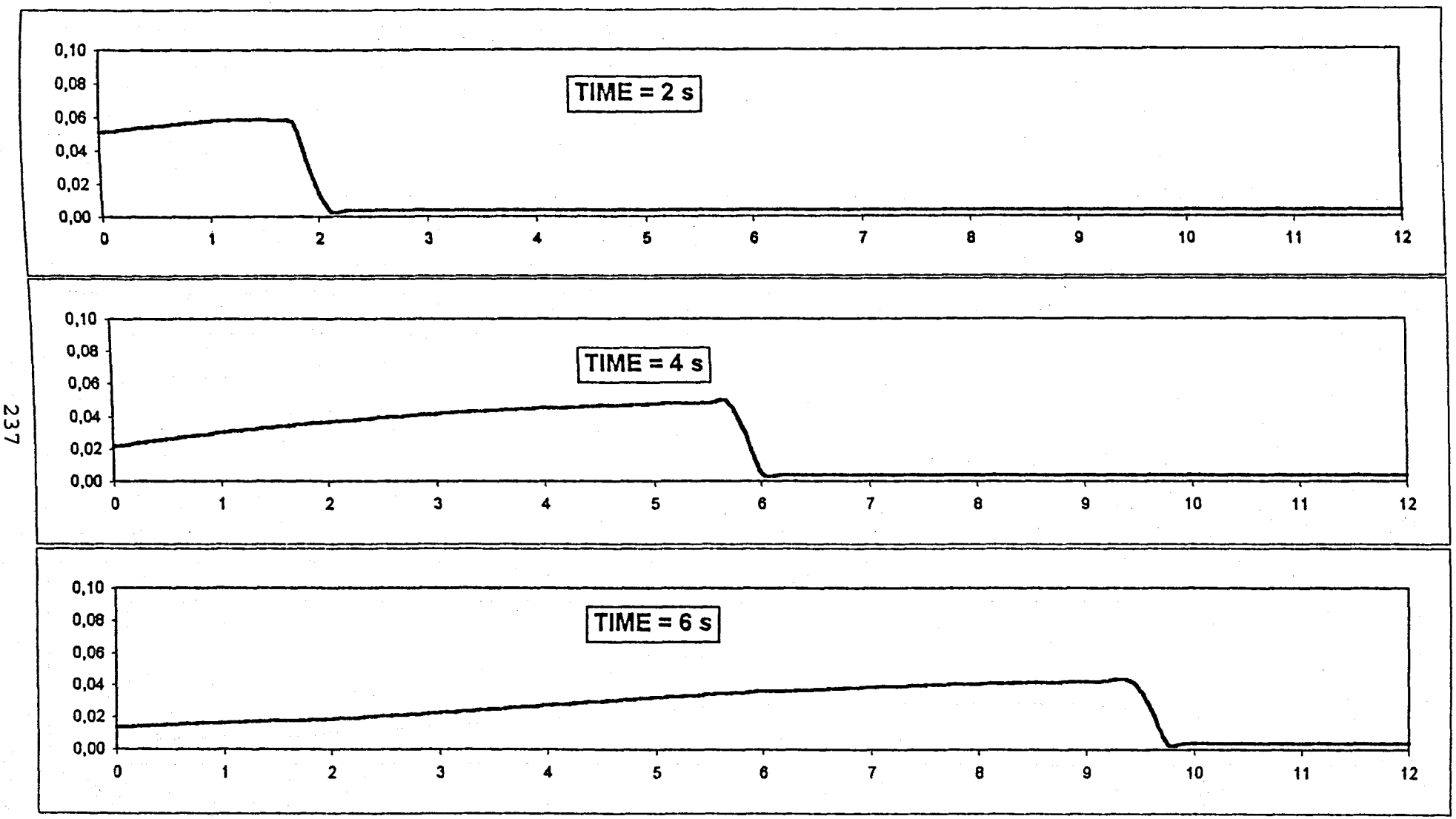

Figure 6.8 - K.M.Standing entry data - program alternative E: water depth (y axis, m) along distance (x axis, m)

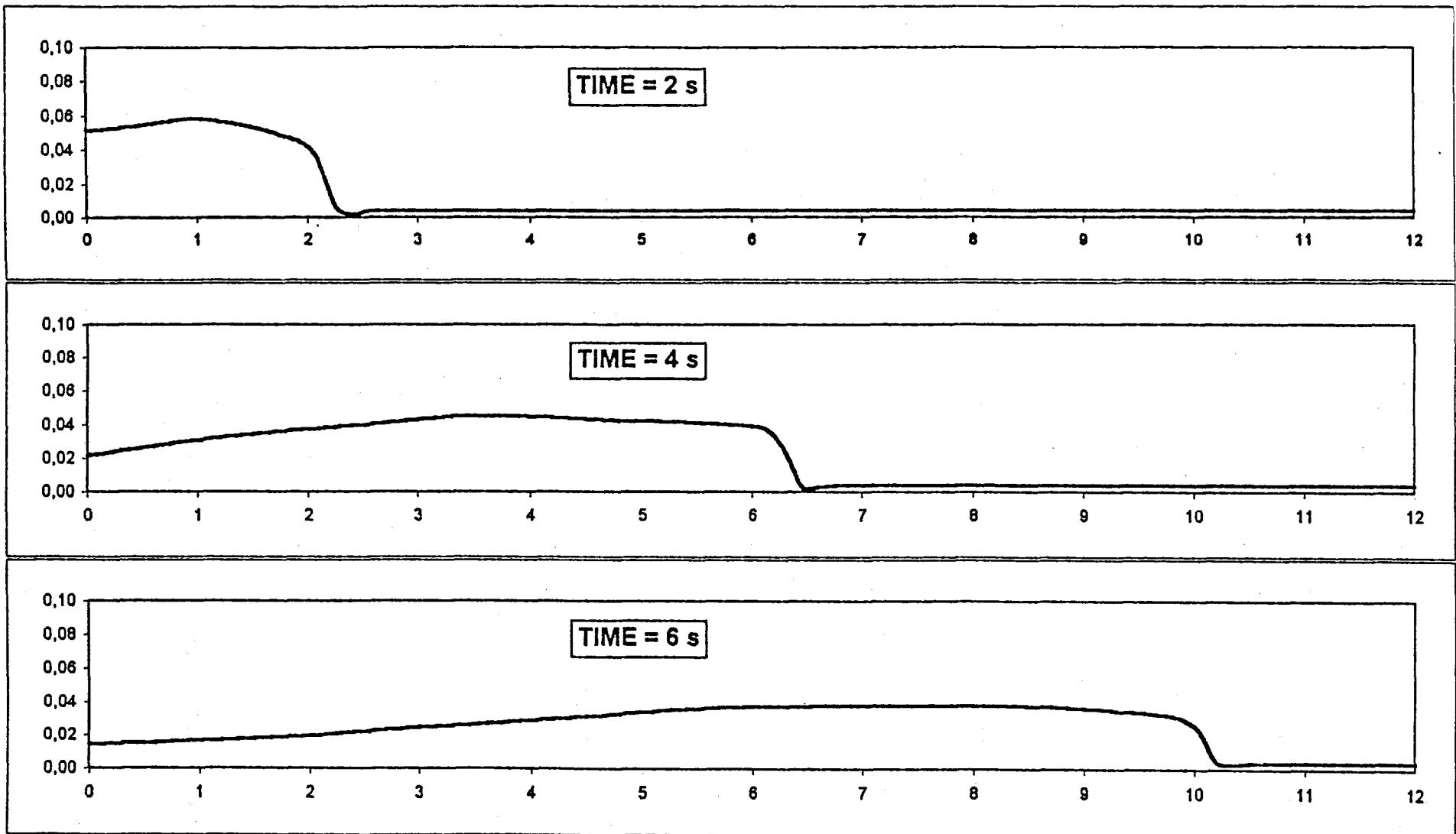

Figure 6.9 - K.M.Standing entry data - program altenative D: water depth (y axis, m) along distance (x axis, m)

6.2.1.1 Friction Adjustments

Computer program calibration possibilities can be appreciated using Standing's data. Firstly, the effect of friction effect adjustment, in isolation from other factors, will be observed. The friction multiplicative scheme presented in sections 3.2.2 and 4.4.4 is applied to the wave front in the simulation process. The evolution of the water depth peak and its "foot" position on time will be examined according to the friction increasing or decreasing.

D program alternative will be used in the following figures. Figure 6.10 shows the water depth profile variation with time, using Standing's entry data, in two conditions: full line profiles corresponds to the simulation using the friction multiplicative factor K equal to 1, i.e., the energy line slope is the same as Colebrook-White's formula. The dashed line profiles results from the friction decreasing. In this case Colebrook-White's S_f at the wave front was annulled, i.e., K multiplicative factor was equal to zero. Figure 6.11 depicts the correspondent graphics of horizontal velocity variation with time.

Friction reduction promotes an advancement of wave "foot" on time and the water depth attenuation. Another consequence is the wave front sharpening. This relationship between friction and water surface variation have almost always been observed on the calibration process. Horizontal velocity reaction is inverse: friction augmentation reduces the flow velocity while friction diminishing increases velocity.

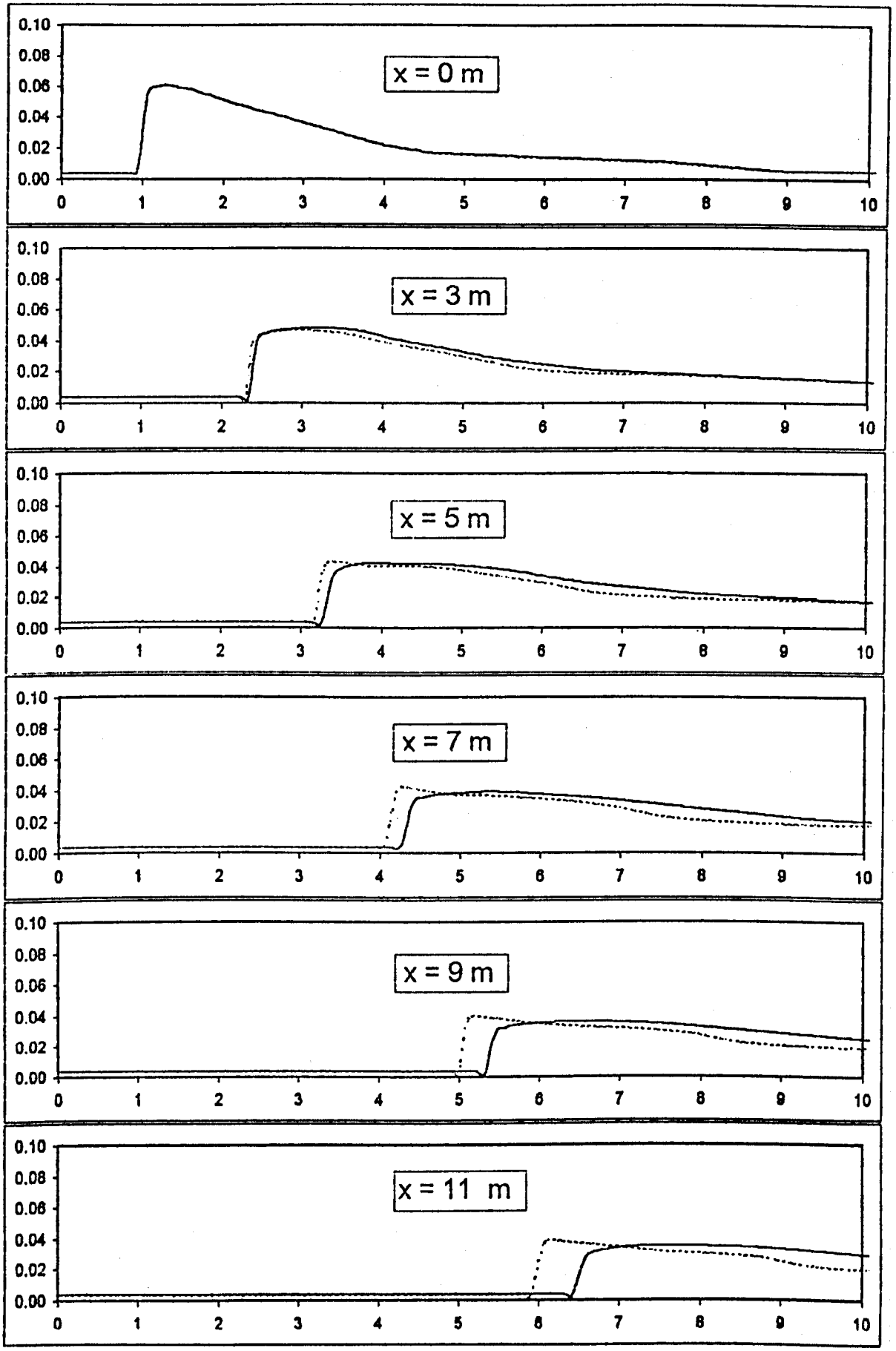

Figure 6.10 - K.M.Standing entry data - friction reduction
Water depth (y axis,m) on time (x axis,s)

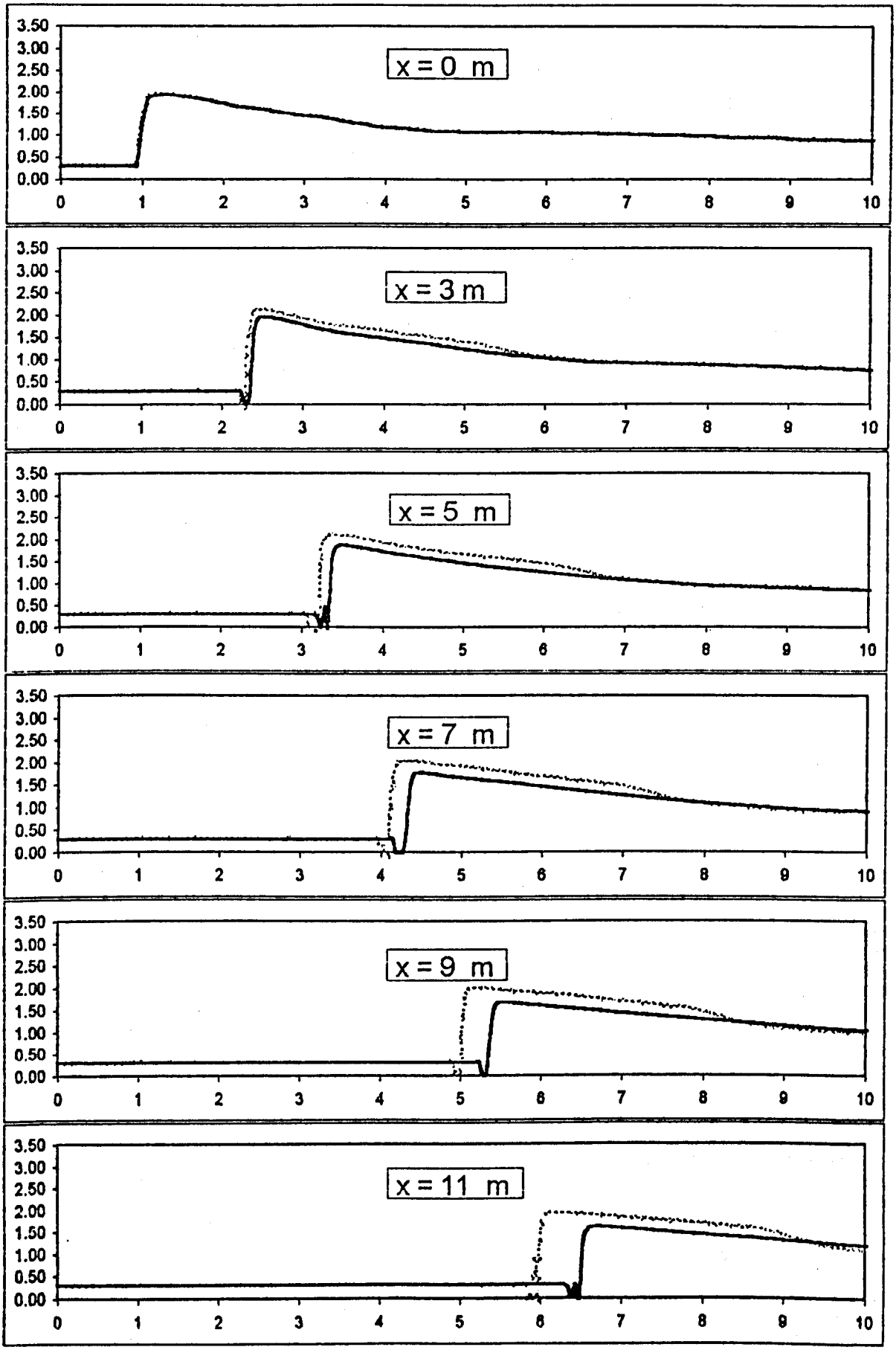

Figure 6.11 - K.M.Standing entry data - friction reduction
Horizontal velocity (y axis, m/s) on time (x axis, s)

Figure 6.12 shows the multiplicative friction factor variation with time applied to all computed sections.

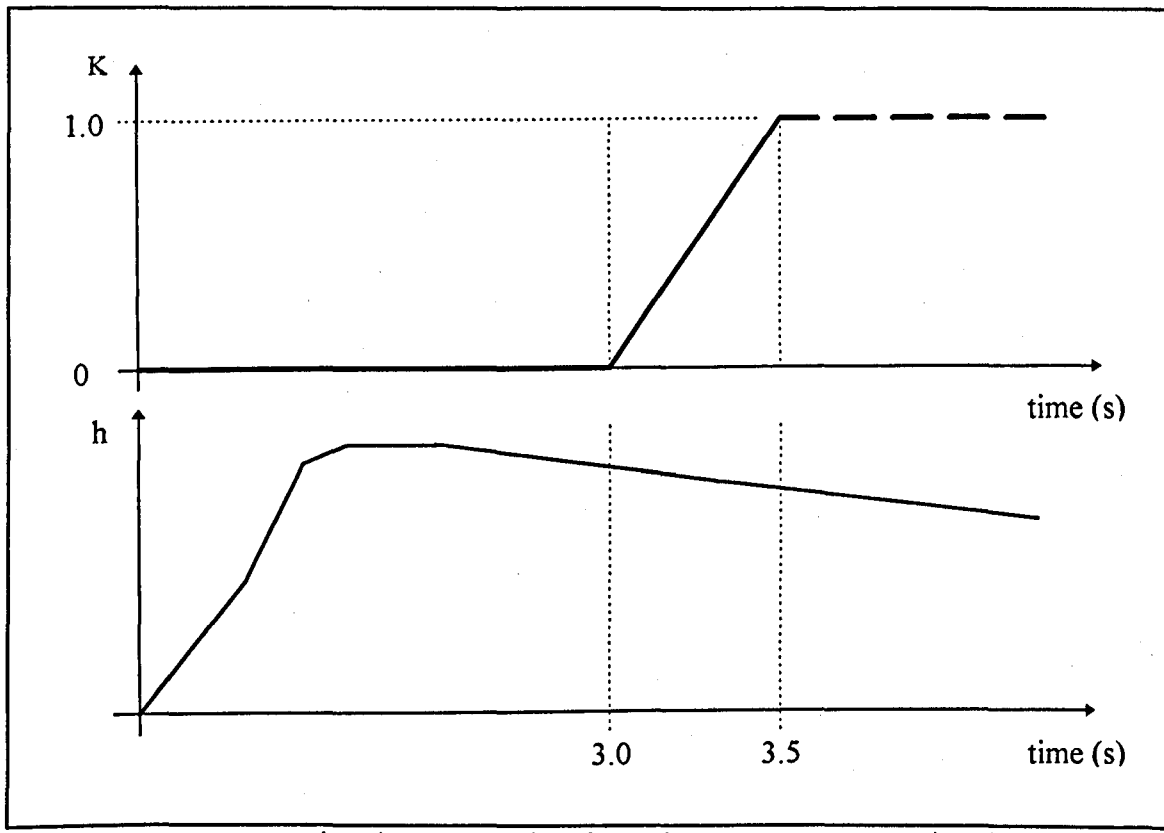

Figure 6.12 - Friction multiplicative factor variation with time

Figures 6.13 and 6.14 shows analogous results of water depth profile and horizontal velocity variation with time for a set of multiplicative factors greater than one. In this case increasing of friction causes wave "foot" delay and water depth raising at the wave front region and the correspondent inverse evolution of velocity. The set of multiplicative factors, applied to all computed sections, is shown in Figure 6.15.

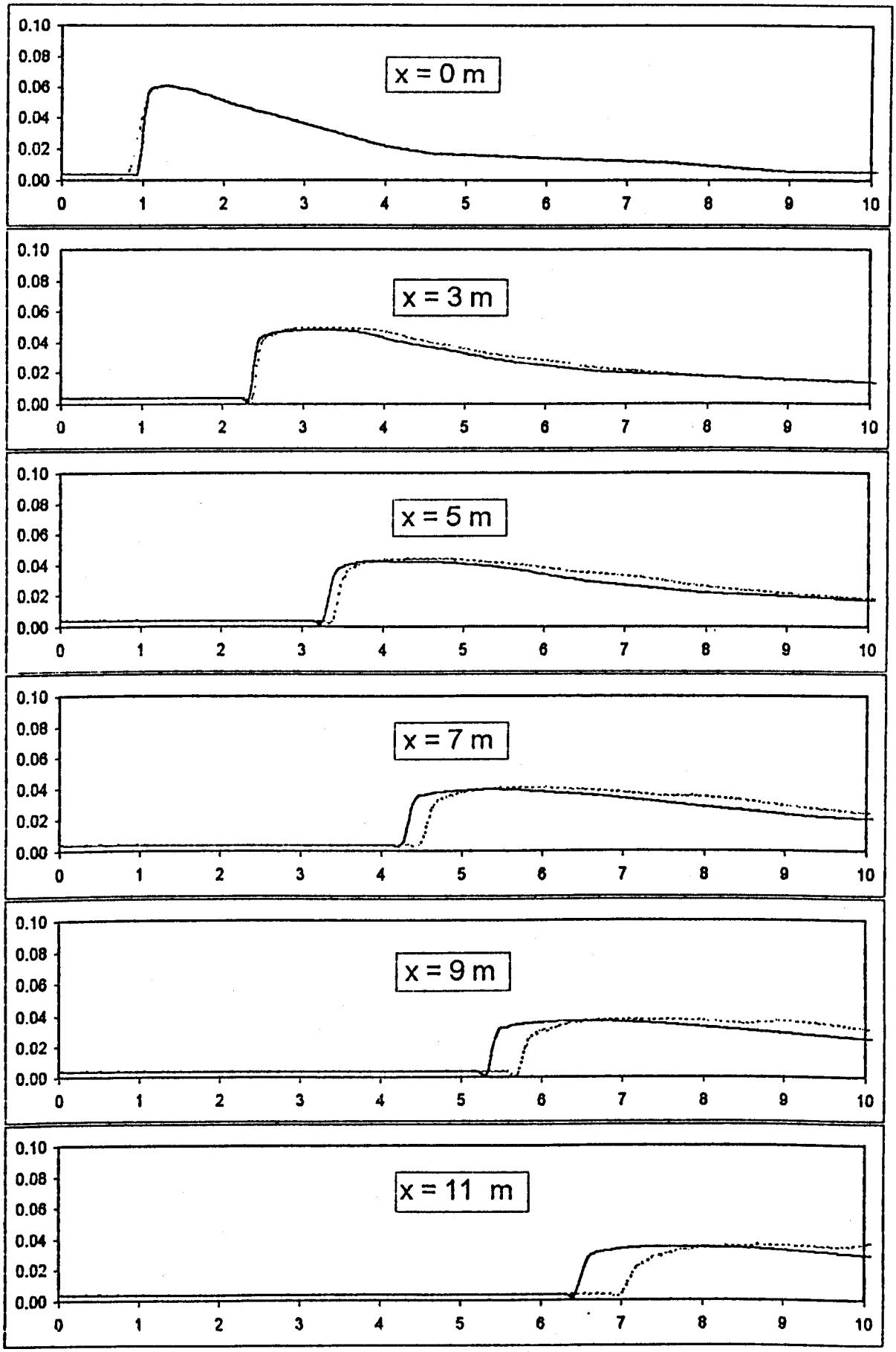

Figure 6.13 - K.M.Standing entry data - friction augmentation
Water depth (y axis,m) on time (x axis,s)

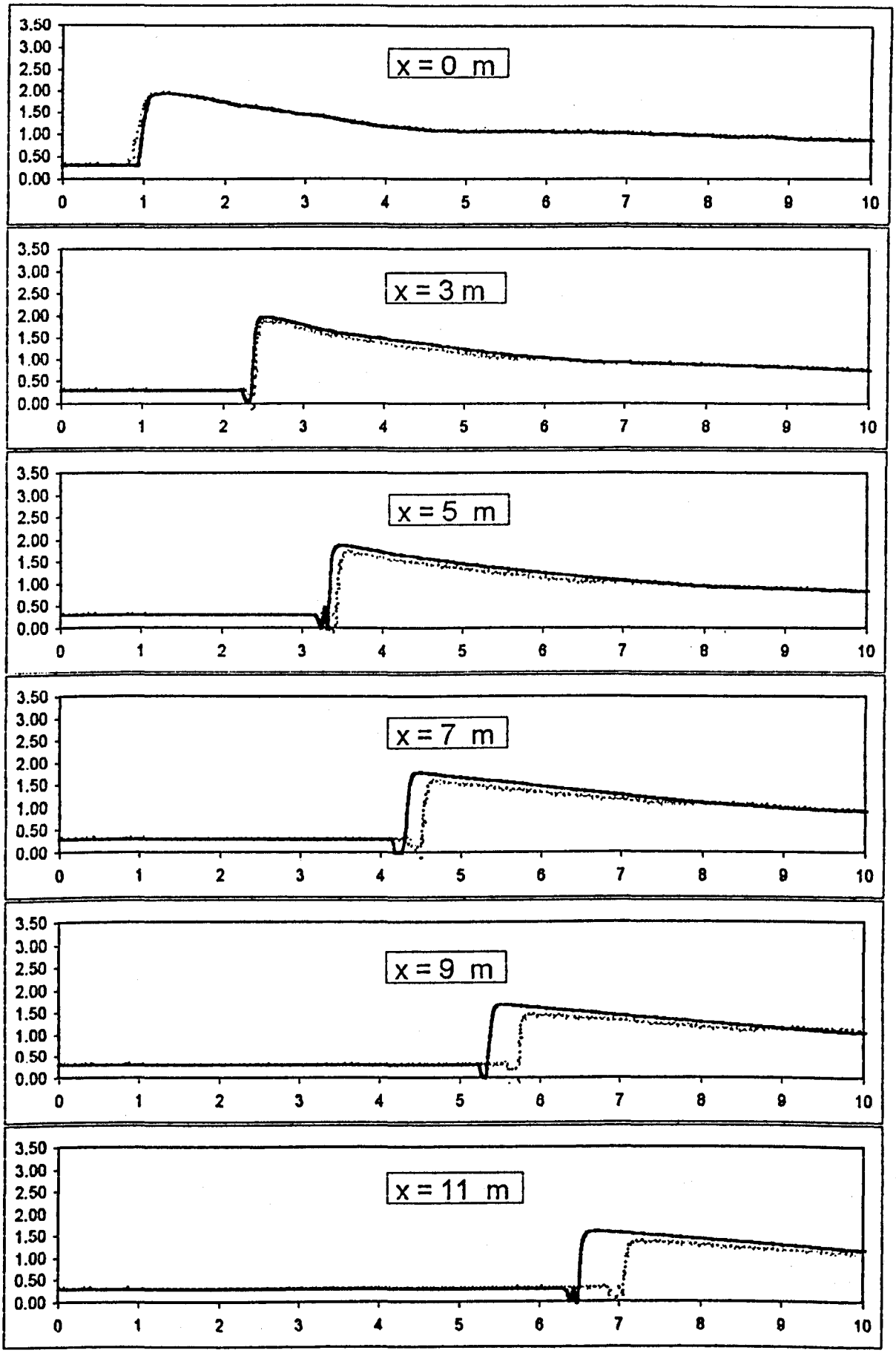

Figure 6.14 - K.M.Standing entry data - friction augmentation
Horizontal velocity (y axis, m/s) on time (x axis, s)

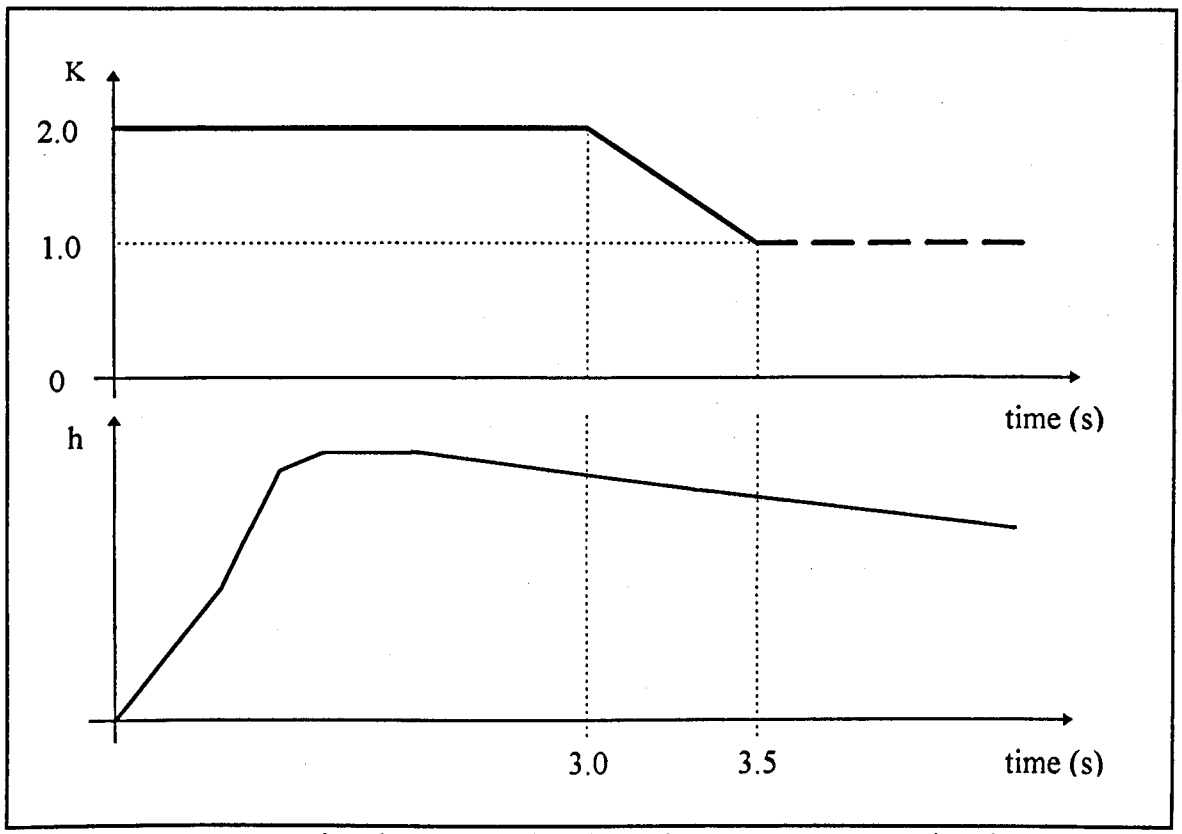

Figure 6.15 - Friction multiplicative factor variation with time

6.2.1.2 Vertical Acceleration Adjustments

Computer program calibration possibilities also provide vertical acceleration adjustments according to sections 3.4.3 and 4.4.6 explained procedure.

Analogously to friction, the isolate effect of vertical acceleration variations will be observed here. Vertical acceleration multiplicative scheme is applied to the wave front, showing the evolution of the water depth and horizontal velocity with time according to the vertical acceleration increasing or decreasing.

Figure 6.16 shows the water depth profile variation with time and Figure 6.17 the same variation of horizontal velocity, using Standing's entry data, in two conditions: dashed line corresponds to the simulation using the vertical acceleration multiplicative factor Z equal to 1, i.e., values given through the mathematical model (equation 2.90) while the full line profiles correspond to the simulation with application of Z linear variation with time given by Figure 6.18. Z values were applied to the wave front region in all computed nodes.

The physical understanding of vertical acceleration variation effect is not so immediate as friction. Figures 6.16 and 6.17 shows that applying negative multiplicative factors to the vertical acceleration promotes the water depth rising in the peak region, wave "foot" delay, and a mild horizontal velocity attenuation. If a set of positive multiplicative factors were applied a inverse response would be observed.

6.2.1.3 Friction and Vertical Acceleration Combined Adjustment

Figure 6.16 illustrates that the application of Z negative factors to the wave front provided water depth rising in the peak region, which is desirable since the original simulation (with Z = 1) had shown a flattened peak. But, water depth raising led to an undesirable wave "foot" delay. Thus, it seems reasonable to try a phase adjustment that can be

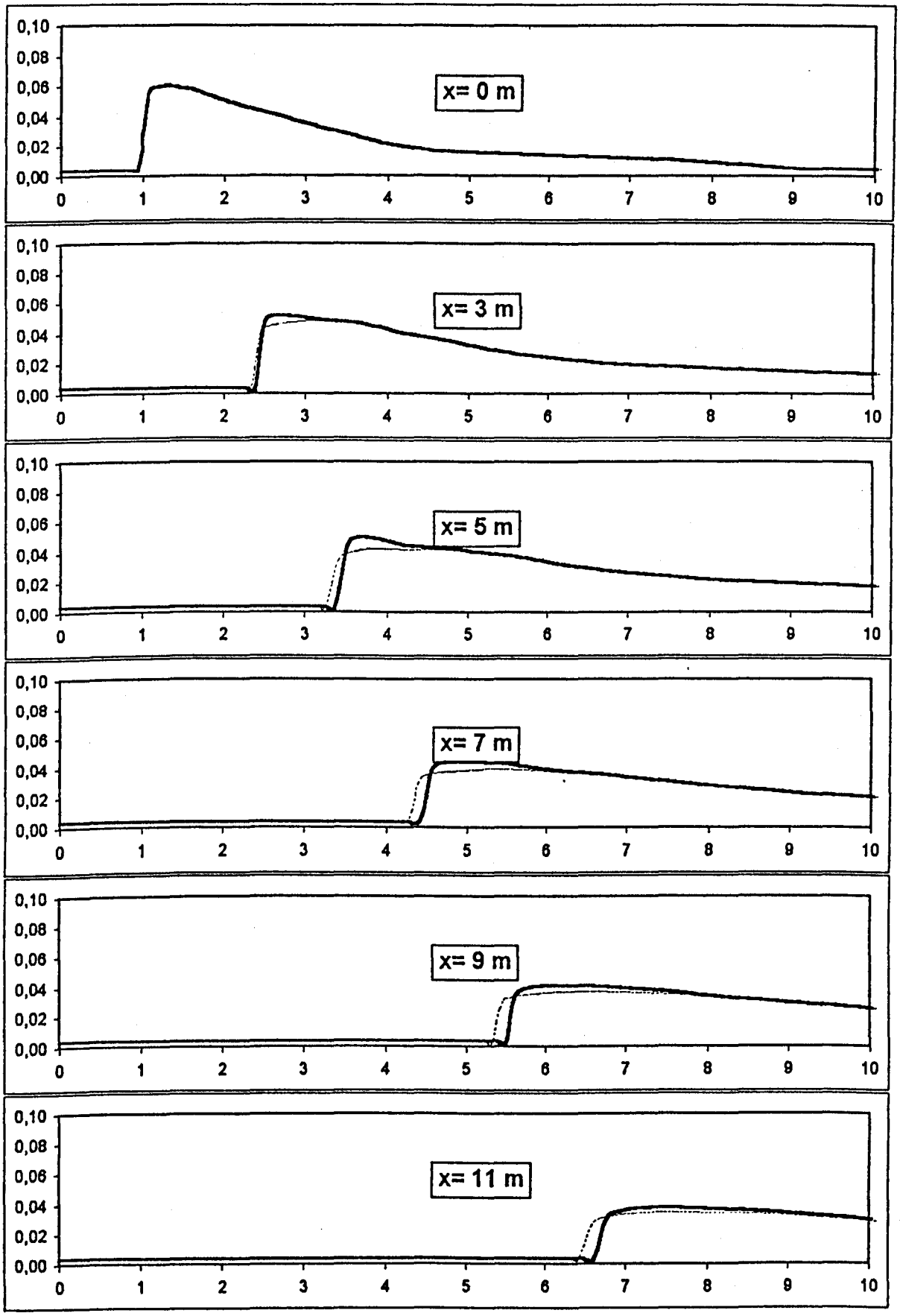

Figure 6.16 - K.M. Standing entry data - vert. acceleration variation;
Water depth (y axis, m) on time (x axis, s)

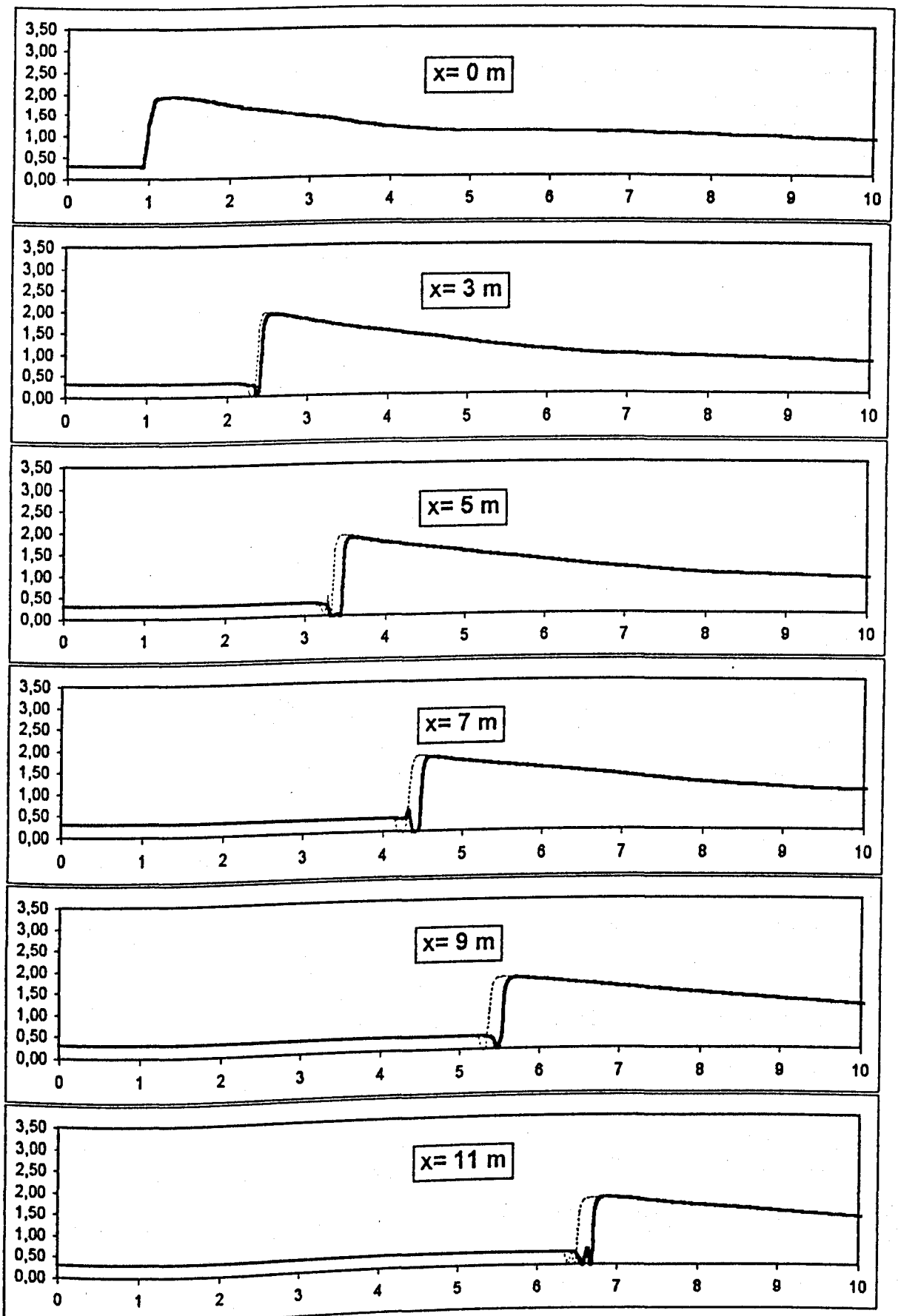

Figure 6.17 - K.M. Standing entry data - vert. acceleration variation;
Horiz. velocity (y axis,m/s) on time (x axis,s)

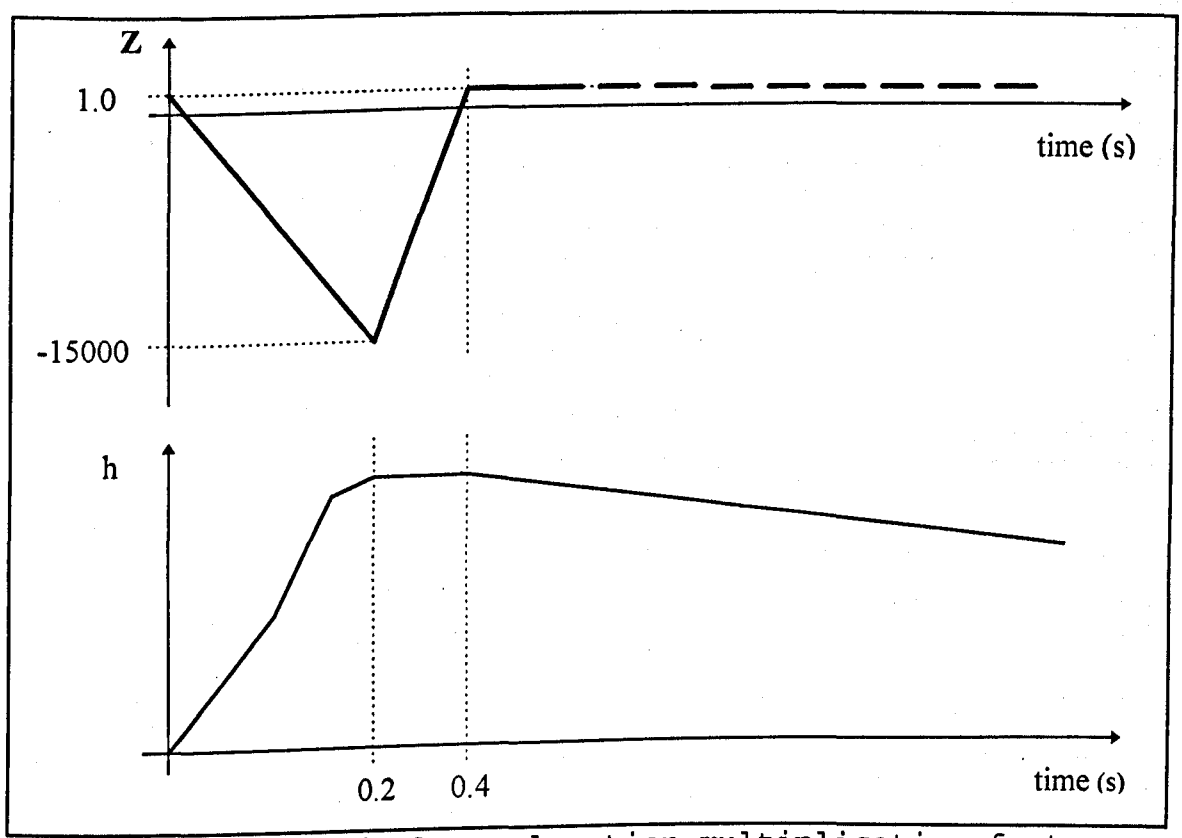

Figure 6.18 - Vertical acceleration multiplicative factor variation with time

obtained by weakening the friction effect. As seen, this can be obtained through using K factors lesser than one.

Figures 6.19 and 6.20 correspond to a simulation combining, simultaneously, a set of vertical acceleration adjustment and friction factor adjustment. For the vertical acceleration the same set of multiplicative values were used, given by Figure 6.18 and for the friction K multiplicative factors given by Figure 6.21.

Dashed lines in Figures 6.19 and 6.20 correspond to the application of Standing entry data to D program alternative without any adjustment, i.e., the reproduction of Figures 6.4 and 6.7, respectively. Full line profiles refer to the quoted set of combined multiplicative factors.

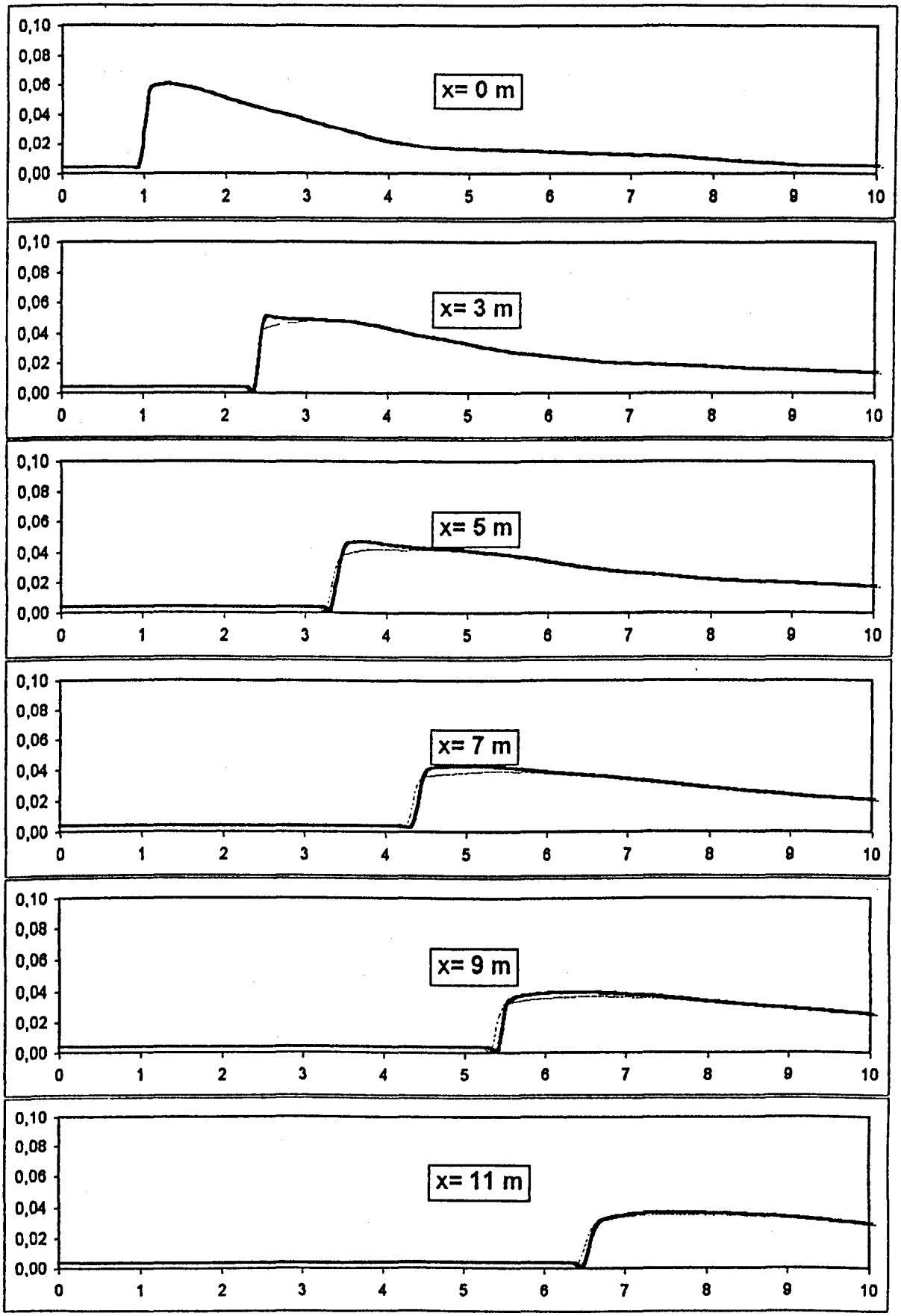

Figure 6.19 - K.M. Standing entry data - friction reduction combined with vertical acceleration variation Water depth (y axis, m) on time (x axis, s)

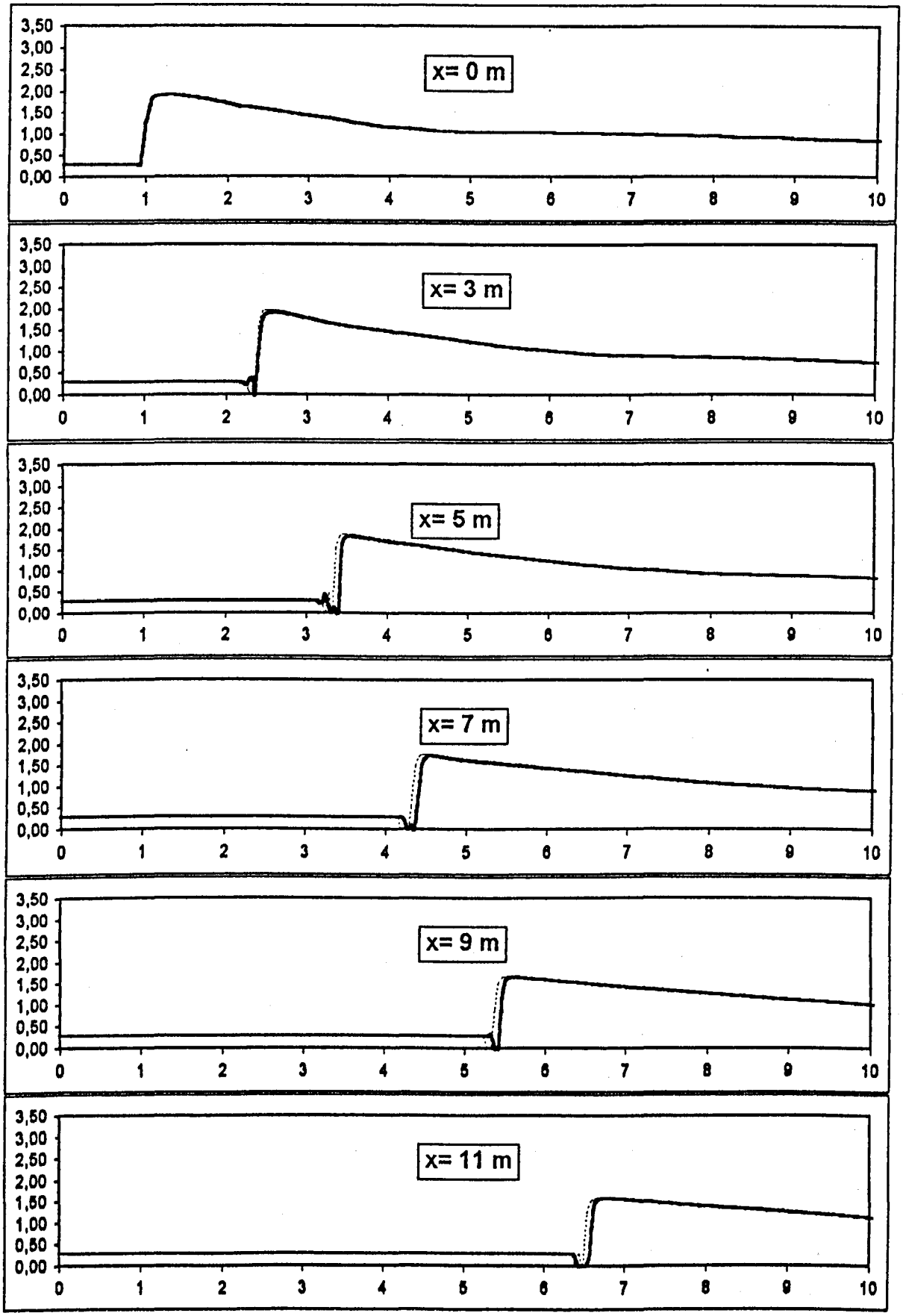

Figure 6.20 - K.M. Standing entry data - friction reduction combined with vertical acceleration variation; Horiz. velocity (y axis,m/s) on time (x axis,s)

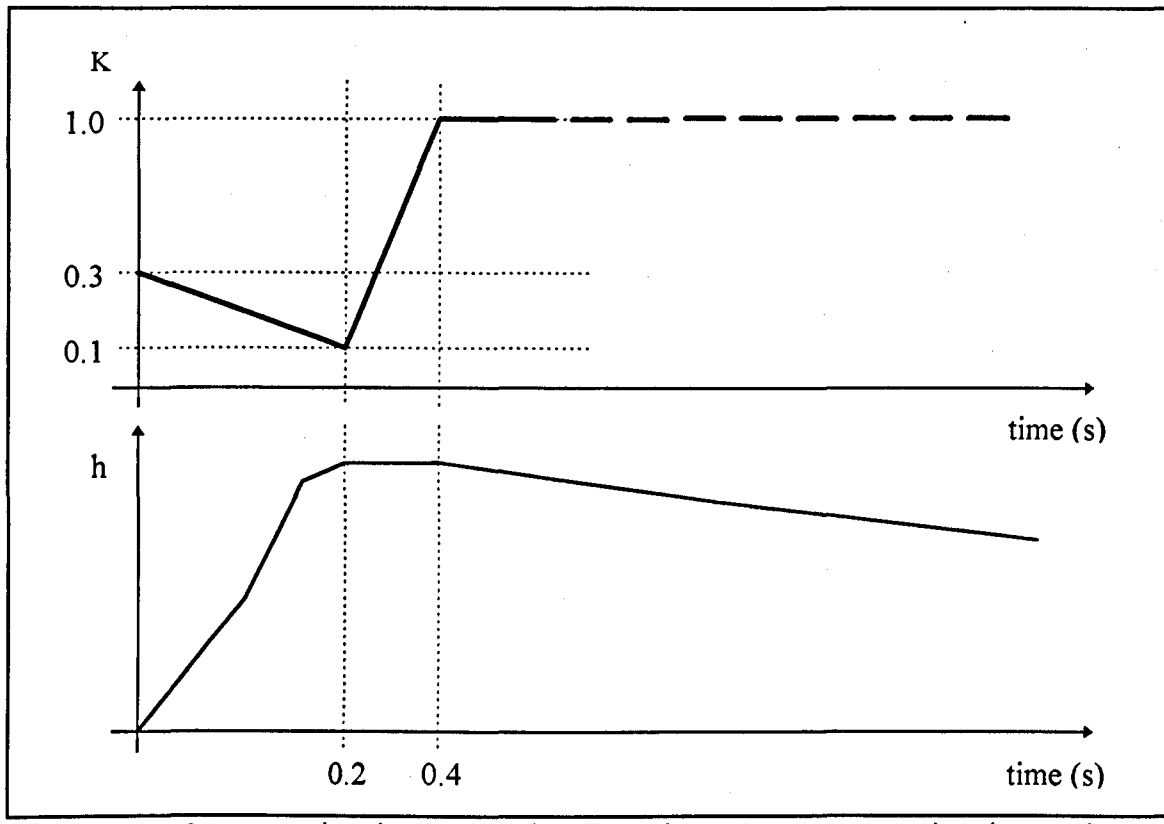

Figure 6.21 - Friction multiplicative factor variation with time

6.2.2 Group E0

According to data presented in Chapter 5, E0 group of measurements corresponds to the flow of a tipping tank discharge of 39.5 L through a glass pipeline. The pipe diameter was 0.156 m and the slope 0.0005 m/m (0.05% or 1:2000). For simulation purpose the pipeline length is 13.005 m (see Chapter 5).

The initial condition was given by a nominally zero base flow rate. In fact, a base flow rate of 0.000001 m^3/s was used in the computation, since the mathematical model numerical

development requires a non-zero initial flow rate.

Entry data comprises the water depth and flow rate variation with time (t,h,Q) at the entry section (S1) of the pipeline (see Figures 5.1 and 5.26).

Group E0 control sections in the laboratory rig were distanced 1.04 m, 3.055 m, 5.065 m, 7.075 m, 9.085 m and 11.095 m from entry section.

Figure 6.22 depicts the water depth variation with time on the six laboratory control sections. Wave front "feet" were arbitrarily moved to time position 1 s to facilitate comparison on the wave profile evolution.

Peak water depth oscillation along the pipeline length observed in the laboratory measurements was an important feature of wave evolution remarked in section 5.3.8. As will be shown in section 6.2.2.3 this phenomenon had an decisive role on the calibration process. Figure 6.23 reproduces here the wave peak trajectory of Group E0 already shown in Figure 5.13.

A computation internode fixed distance of 0.10 m was adopted. In E alternative a Courant number (C_n) equal to 1 was adopted. In B alternative C_n was 0.8 and in D alternative C_n was 0.667. In E alternative Everett and Newton-Gregory interpolation was used.

Simulation results with the three program alternatives will be shown in the following sections. It is remarkable to observe that the same set of entry data (group E0) led to quite different responses.

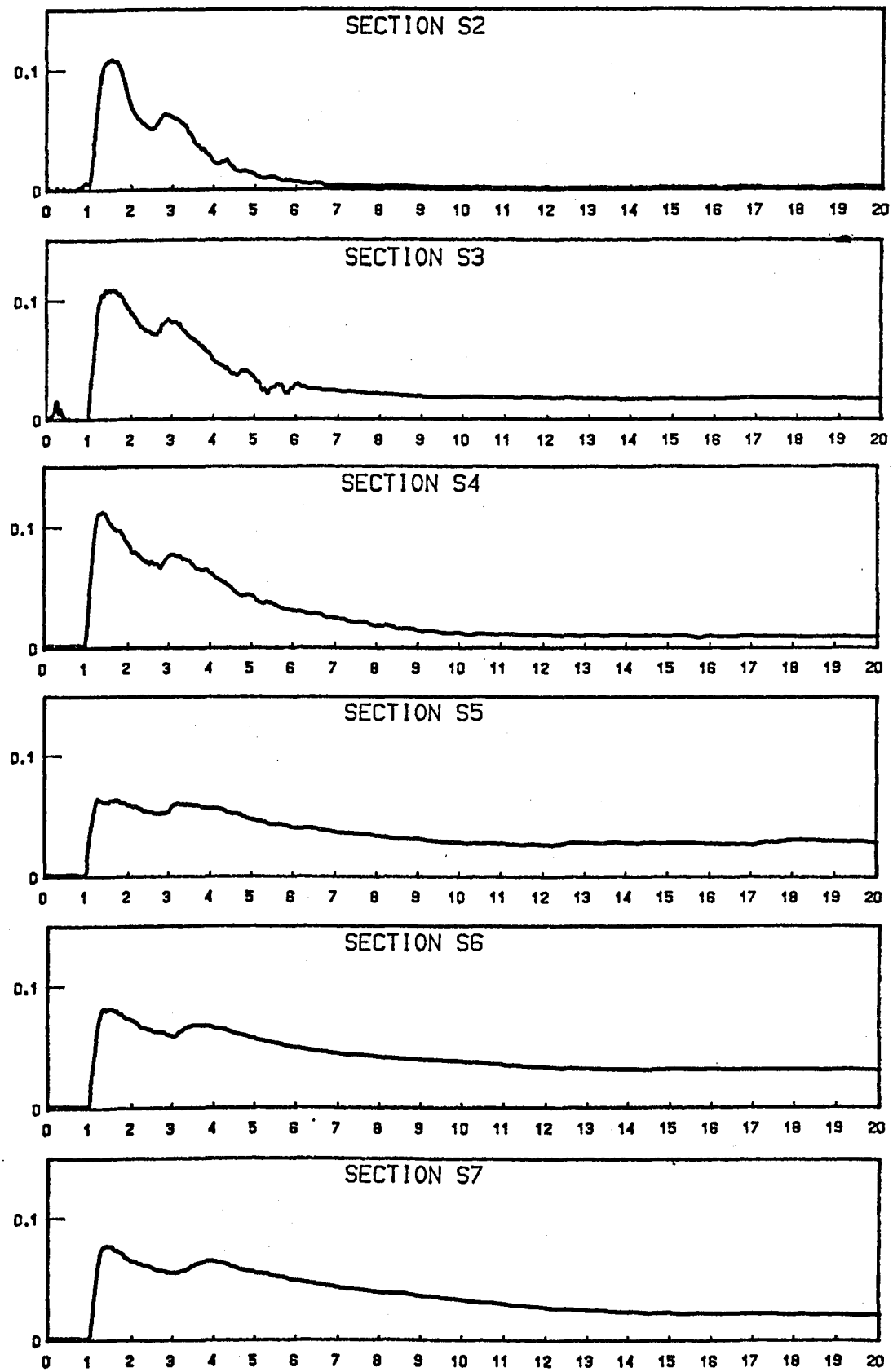

Figure 6.22 - Group E0 entry data - laboratory masurements
Water depth (y axis, m) on time (x axis,s)

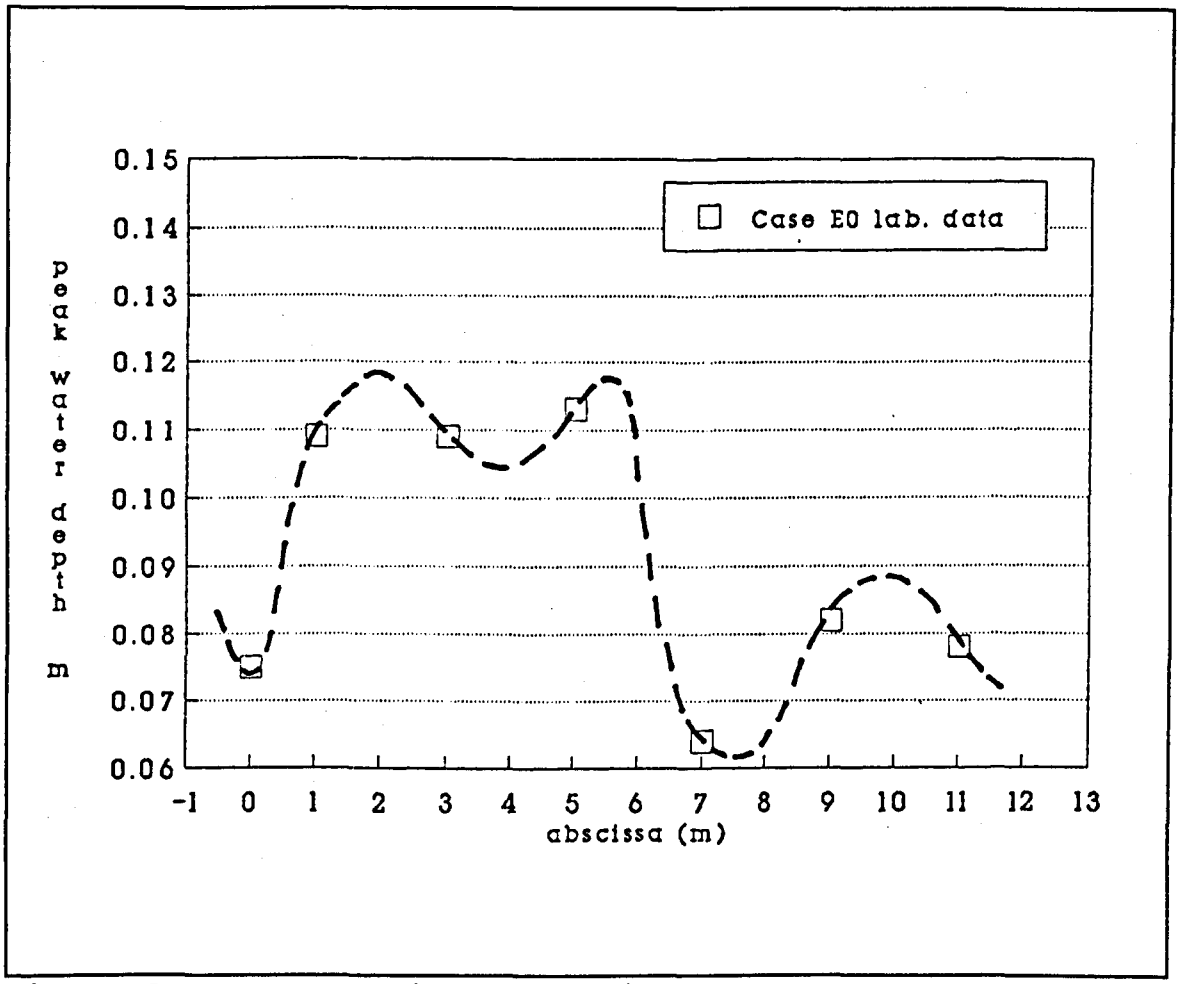

Figure 6.23 - Wave main peak trajectory

6.2.2.1 Program Alternative: E

Figure 6.24 presents the simulation of water depth profile variation with time, using E program alternative. This simulation refers to the most simple set of calibration parameters. In the friction scheme a multiplicative factor K=1 was used, i.e., friction effect was calculated with Colebrook-White formula (2.75) and no numerical filter was used. Figure 6.25 presents the respective horizontal velocity variation with time.

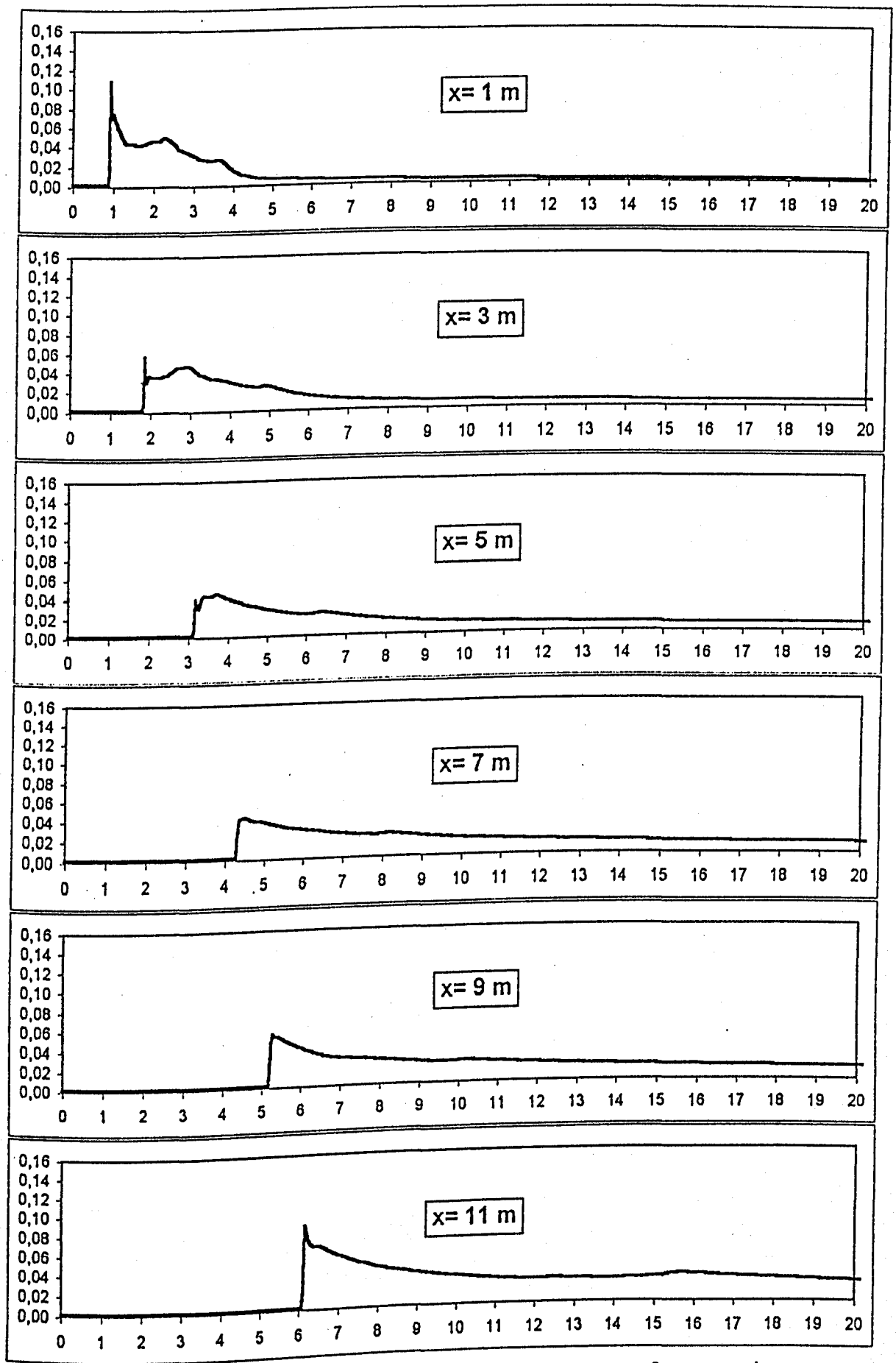

Figure 6.24 - Group E0 entry data - program alternative E
Water depth (y axis, m) on time (x axis, s)

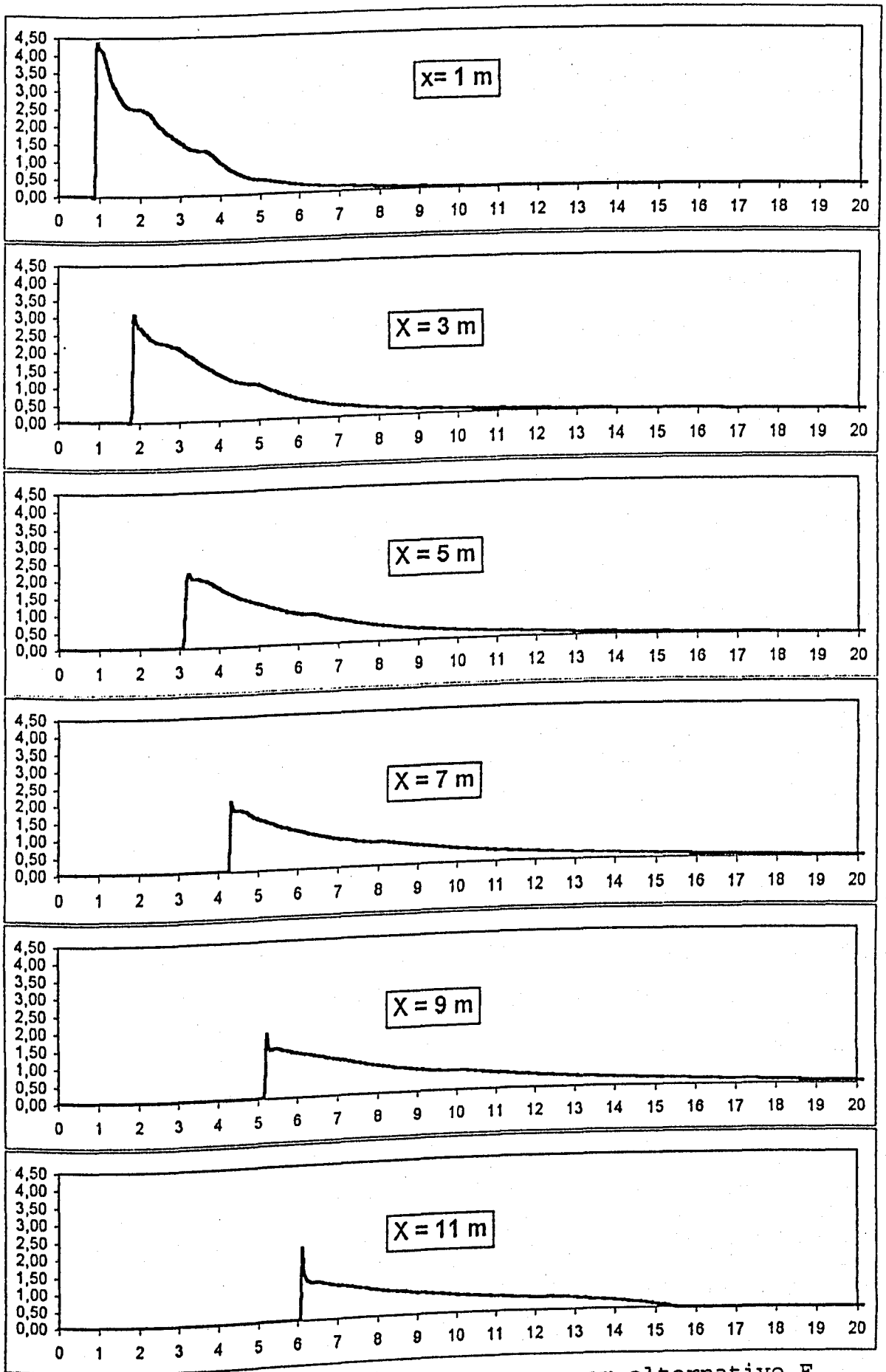

Figure 6.25 - Group E0 entry data - program alternative E
Horiz.velocity (y axis,m/s) on time (x axis,s)

Water depth profiles show that the numerical developed model response in the wave front region is problematic. The wave main peaks on sections 1.04 m and 3.055 m appear as a very fine pulse. A close observation on the time range under these pulses comparatively to the same region on horizontal velocity profiles shows that there is no corresponding pulse of velocity. As was seem in section 4.4.8 these pulses embody an intrinsic instability caused by the natural characteristics of entry data or by the numerical model.

Reduction of the computation time step, making C_n=0.5, emphasises pulses, further degenerating the process.

Some attempts to control these pulses through numerical filters have been carried on and led to unacceptable delay and excessive dampening of the wave. A counterbalance to dampening could be obtained through friction increasing but, it would promote further wave delaying.

Another important characteristic of the simulated wave profiles in Figure 6.24 is the tendency for the peak water depth to oscillate along the pipeline length. The peak trajectory shown in the six profiles of Figure 6.24 does not match that observed in the laboratory as illustrates Figure 6.23.

Another important characteristic observed in laboratory measurements was the existence of a secondary peak in the wave. As can be observed in Figure 5.6, this secondary peak is at an almost constant "time distance" from the main wave front peak along the pipeline distance. Figure 6.24 shows that in the simulation process the secondary peak tends to overcome the

main peak, incorporating it.

Figure 6.25 depicts a distinctive behaviour in the case of horizontal velocity profiles. Instability is very mild compared with water depth or, at least, it seems not to command velocity profile development. The nonexistence of strong velocities instabilities, probably, govern further evolution of the velocity wave front, leading to a mild decaying of velocity wave peaks.

6.2.2.2 Program Alternative: B

Figure 6.26 presents the simulation of water depth profile variation with time, using B program alternative. This simulation refers to the most simple set of calibration parameters. In the friction scheme a multiplicative factor K=1, was used, i.e., friction effect was calculated with Colebrook-White formula (2.75) and no numerical filter was used. Figure 6.27 presents the respective horizontal velocity variation with time.

As has occurred with the E alternative water depth profiles in the peak region seems to govern the wave evolution. The wave main peaks on sections 1.04 m, 3.055 m and 5.065 m have strong variations along the pipeline while the secondary peak and the rest of the wave gradually changes the water surface. Also in this case a close observation on the time range under these pulses comparatively to the same region on horizontal velocity profiles shows that the corresponding

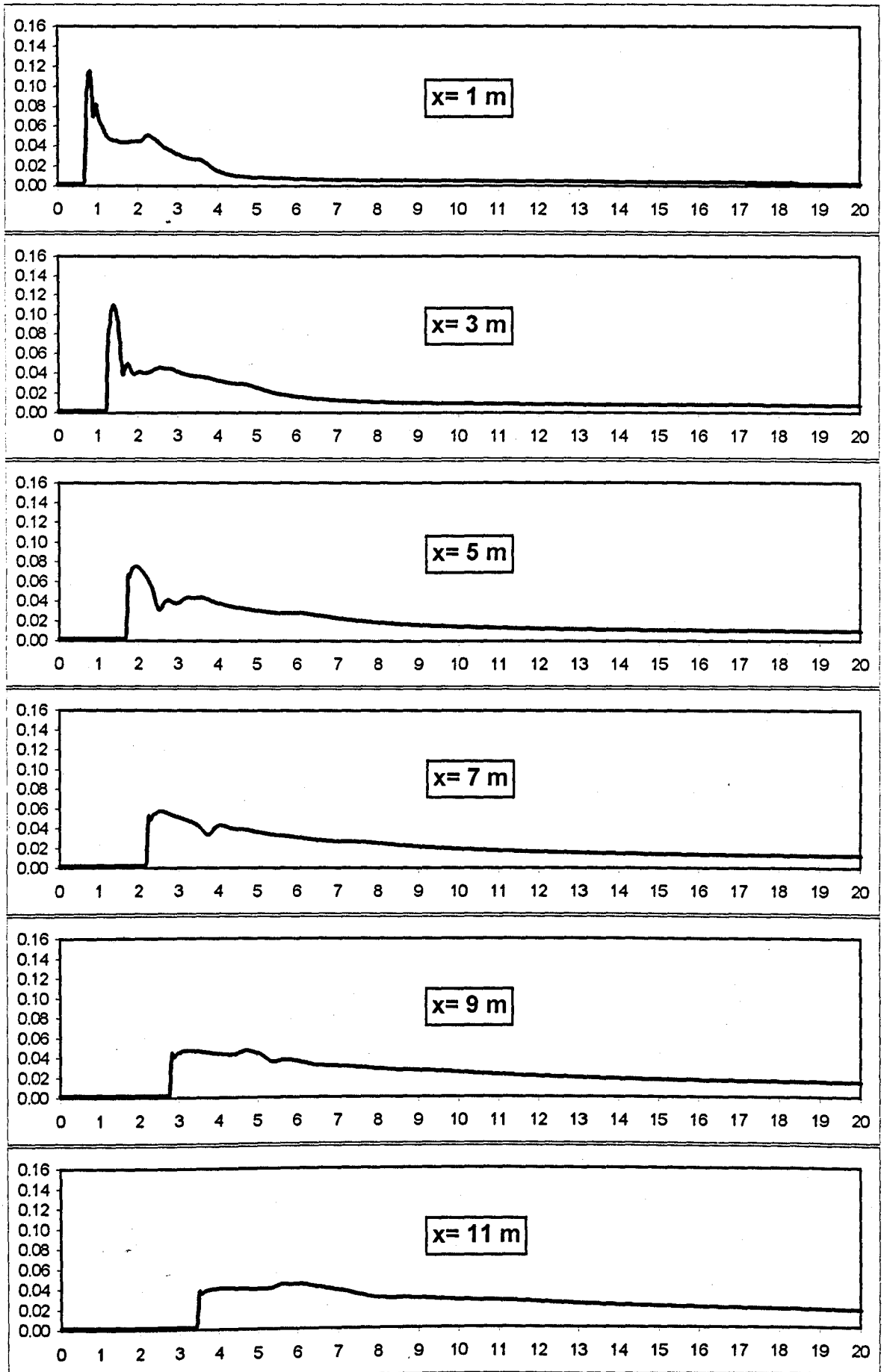

Figure 6.26 - Group E0 entry data - program alternative B
water depth (y axis, m) on time (x axis, s)

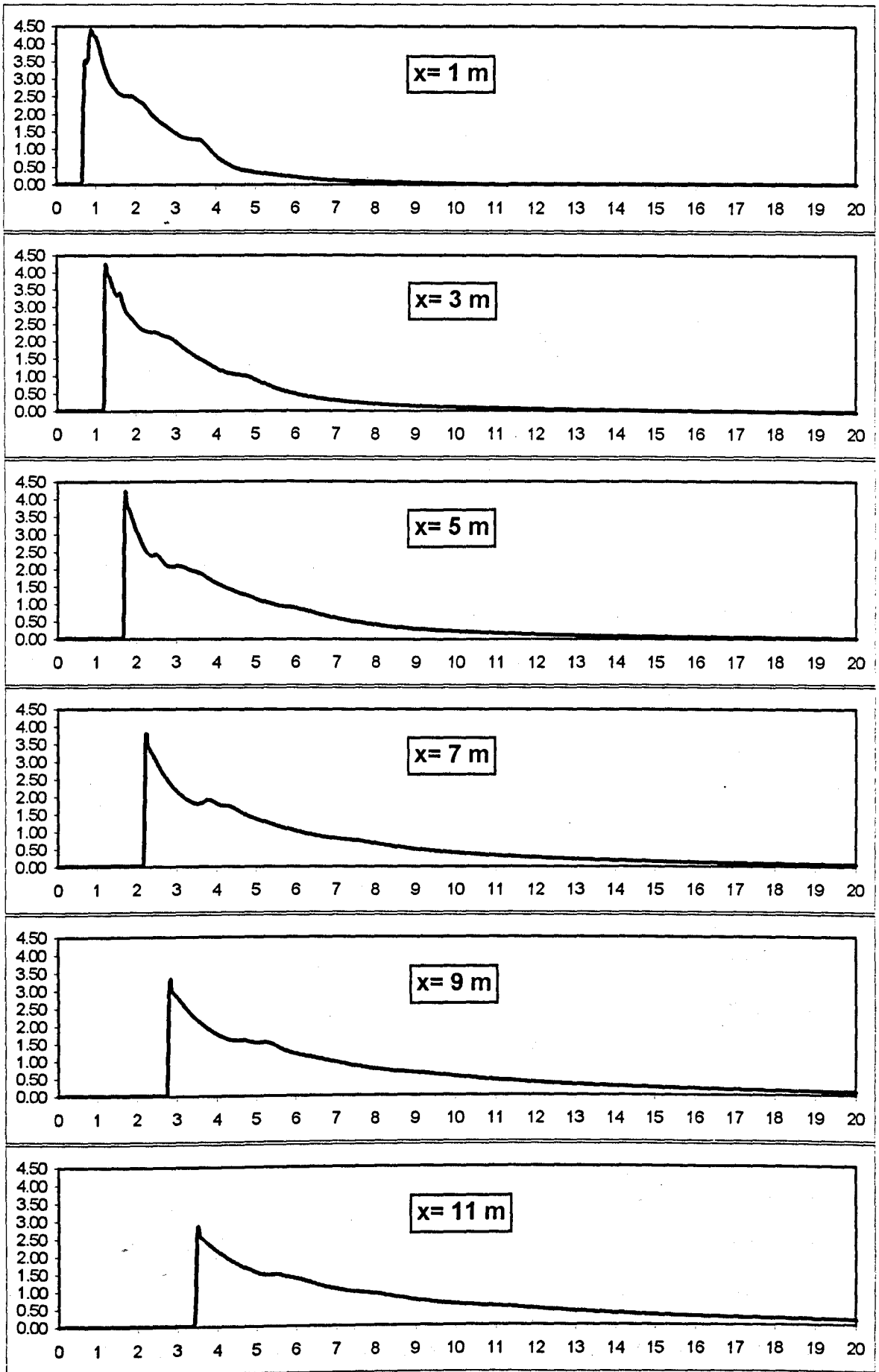

Figure 6.27 - Group E0 entry data - program alternative B
Horizontal velocity (y axis, m/s) on time (x axis, s)

velocity protuberances are much less pronounced.

Again, as in the E alternative, attempts to control these pulses through numerical filters have led to unacceptable delay and excessive dampening of the wave. Counterbalancing dampening through friction increasing promoted further wave delaying.

Contrary to the E alternative, the simulated wave profiles of Figure 6.26 do not present oscillation of the peak water depth along the pipeline length and the secondary peak evolution does not tend to overcome the main peak.

Figure 6.27 pictures a gradual decay of velocity profile peak along the pipeline length, similarly to alternative E but, of milder intensity. This fact correspond to the much faster evolution of the wave front in alternative B.

6.2.2.3 Program Alternative: D

Alternative D comprises an extra adjustment possibility given by the vertical acceleration multiplicative factor scheme originated from the Boussinesq equations, the more developed mathematical model. Thus, Group E0 calibration process was further worked out using this alternative.

Firstly, Figures 6.28 and 6.29 present water depth and horizontal velocity variation with time in a condition of non adjusted simulation, i.e., friction and vertical acceleration values are given by the original developed numerical model

without any damping application.

Although the water depth profiles also exhibit pulses of instability in the wave peak, now, they seem to be a bit more stable. In fact, in alternative D the pulse is more integrated to the wave front peak giving more consistency on the wave front evolution. This is apparent mainly in water depth profiles of the four first simulated sections.

Another favourable characteristic is the wave peak oscillation trajectory along the length tending to that inferred from laboratory measurements illustrated on Figure 6.23.

As already remarked, the analysis of peak trajectory evolution acted as a guideline in the calibration process. Peak oscillation can be associate to friction and vertical acceleration phenomena. According to the discussion in section 5.3.6, in low water depth base flow, the wave front encountered a strong resistance on its base ("foot") region. Friction with the pipe bed and shocks against the previous and slower base flow promoted steeper and higher peaks. Some turbulence was also observed mainly in the first 3 m of the pipeline. Another consequence of this phenomenon was the wave front velocity diminishing, leading to higher flow duration (see Figure 5.10).

The isolated friction effect, however, does not seem to be sufficient to explain the peak trajectory evolution. For

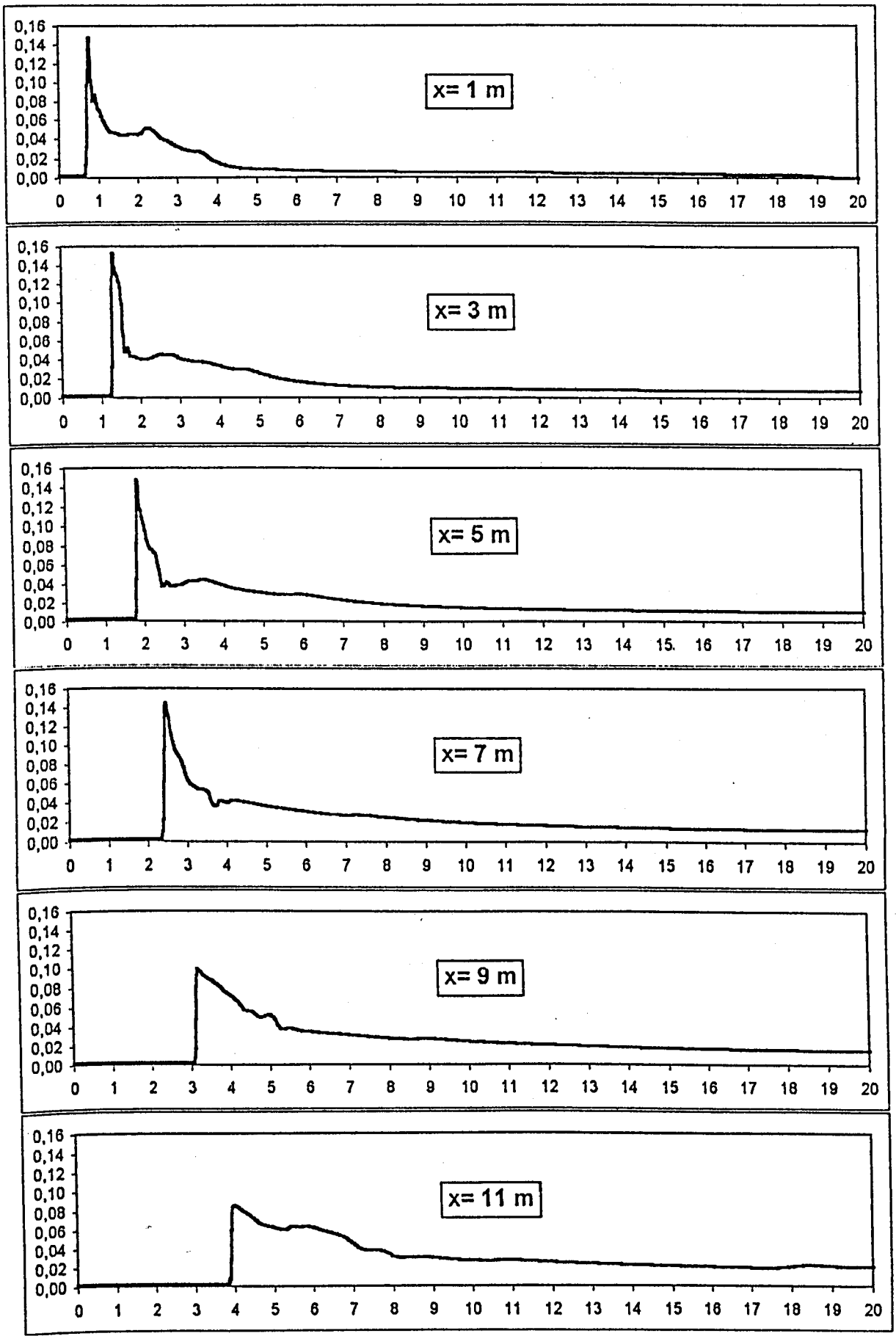

Figure 6.28 - Group E0 entry data - program alternative D
water depth (y axis, m) on time (x axis, s)

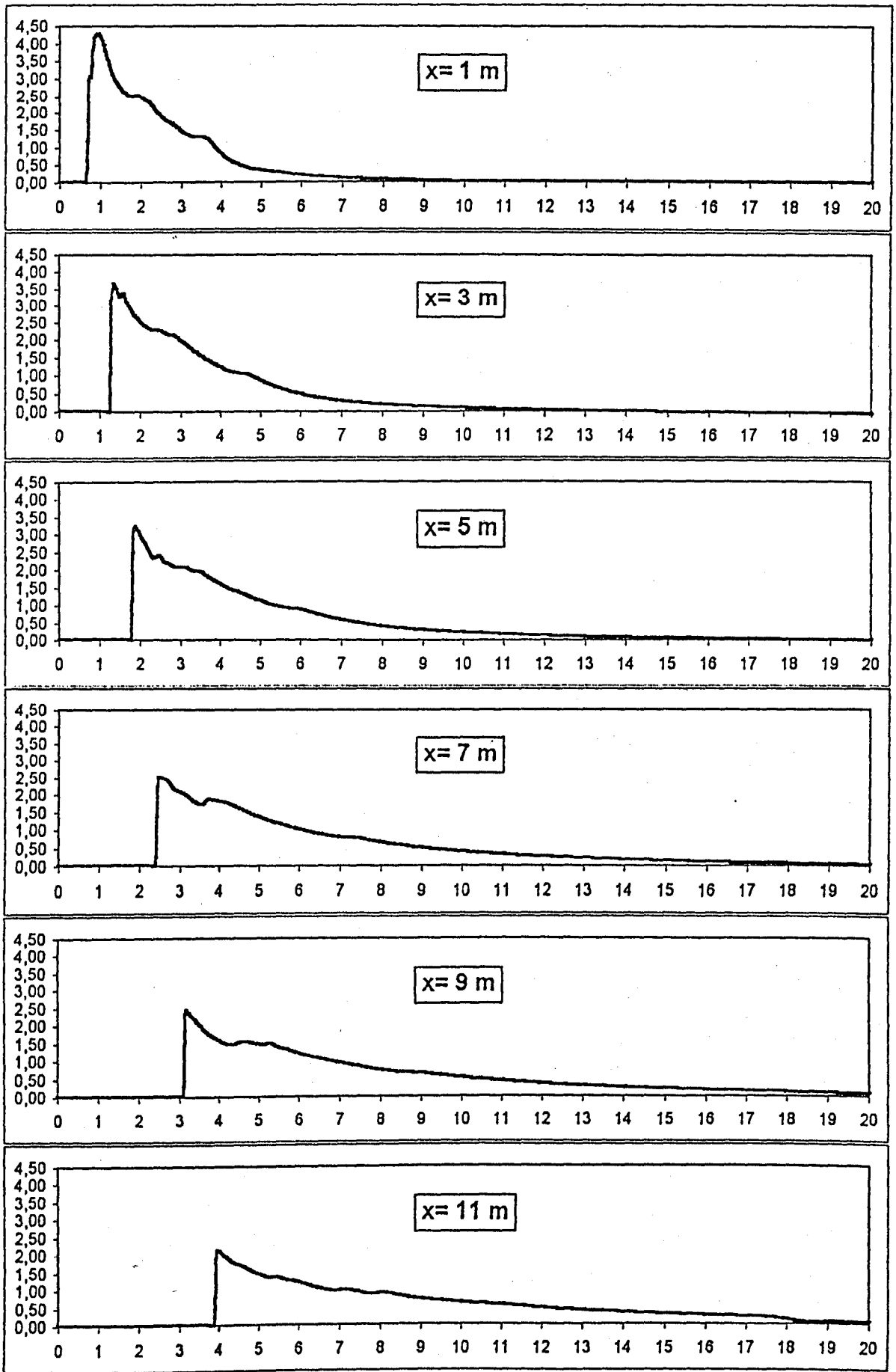

Figure 6.29 - Group E0 entry data - program alternative D
horizontal velocity (y axis, m/s) on time (x axis, s)

example, observing Figure 6.23 it would be reasonable to infer that friction was responsible for the peak rising from position $x = 0$ m to $x \approx 1.8$ m. But, what to say from the subsequent peak depletion (up to $x \approx 4$ m)? A reasoning relating velocity decreasing and friction force in this segment would be possible. Velocity decaying would imply less friction force since friction is a function of the square of velocity. Less friction force would conduce to smaller peaks. But, how to explain velocity retaken from $x \approx 4$ m to $x \approx 5.5$ m? Thus, it seems reasonable to suppose that another sort of phenomenon is occurring concurrently. The peak up and down movement is also associated to the water mass momentum in the vertical direction. According to Boussinesq's hypothesis it was possible to incorporate this momentum to the horizontal momentum equation through the pressure variation on depth as was derived in Chapter 2.

Momentum in the vertical direction can be infered from water surface and horizontal velocity behaviour in the simulated profiles. While the wave front water depth oscillates in a up-and-down movement along pipeline length (Figure 6.28) the correspondent horizontal velocity decays continually (Figure 6.29). Therefore, it seems that the vertical movement of the peak would be afforded by momentum on the vertical direction. This inference can not be definitive because the friction and the turbulence behaviour are not well known. In other words, the momentum balance would require a better knowledge of the dissipative role.

Another important characteristic of adjustments with

vertical acceleration and friction is the theoretical difference in the nature of these phenomena. Friction corresponds to a spending of momentum since it is concerned with a phenomenon of shocks between water and the flow bed leading to the transformation of movement energy in to heat. On the other side, vertical acceleration simply refers to a different direction of movement, conserving momentum. Although developed equations refer to momentum only in the horizontal direction, the possibility of significant momentum in the vertical direction should not to be forgotten.

Contrary to the procedure used with the Standing data, it was unfortunately not possible to obtain conclusive results working with isolated factors. For example, in the segment from section x = 0 m to section x ≈ 1.8 m, laboratory measurements show a clear ascension of wave peak. This could result either from friction or vertical acceleration action. However, Figure 6.28 shows that the program response in this segment, although exhibiting a rising peak, has an associated pulse that had to be controlled through vertical acceleration and numeric filter adjustments. Thus, after several initial attempts, the necessary conclusion was the impossibility of carrying on calibration with isolated factors. An embraced analysis of the role of calibration factors, orientated by the peak trajectory and by measured laboratory profiles, led to the development of combined sets of calibration multiplicative factors applied mainly to the water depth and horizontal velocity variation with time at the wave front region considering the wave position on the pipeline.

Combined sets of friction, vertical acceleration and damp factors were applied in successive simulation processes, gradually adjusting simulated profiles from the initial sections to downstream sections. This was an extremely time consuming and exhausting work. From the mathematical point of view, this was a trial-and-error optimization process.

Figure 6.30 presents the best set of simulated profiles resulting from the calibration process where a complex combination of factors were applied. Figure 6.31 shows the correspondent horizontal velocity profiles. Dashed lines correspond to laboratory measurements and full lines refer to simulated profiles.

Multiplicative and damping factors were introduced in the beginning of computer program processing through digital files. In total, four calibration files involving friction multiplicative and damp factors and ten vertical acceleration calibration files were applied.

The calibration files with the multiplicative and damping factors used on the simulation are presented in the Appendix. "t" values refer to Figure 4.7 points of the wave water depth variation with time. J values refer to computed sections, being J_i the initial section and J_f the final section.

Figure 6.32 depicts the probable wave main peak trajectory of laboratory measurements and simulated results.

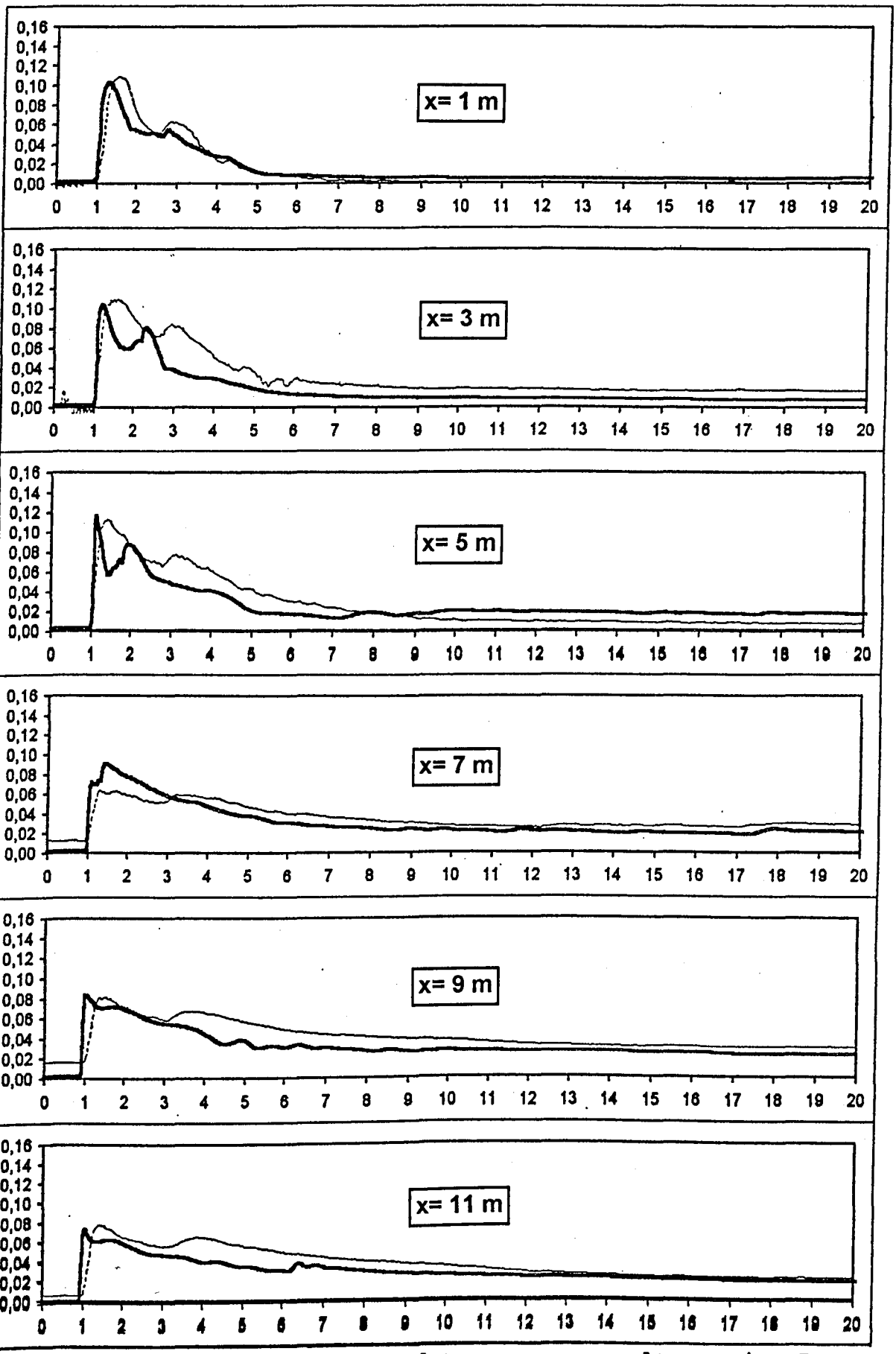

Figure 6.30 - Group E0 entry data - program alternative D
best calibrated simulation
Water depth (y axis, m) on time (x axis, s)

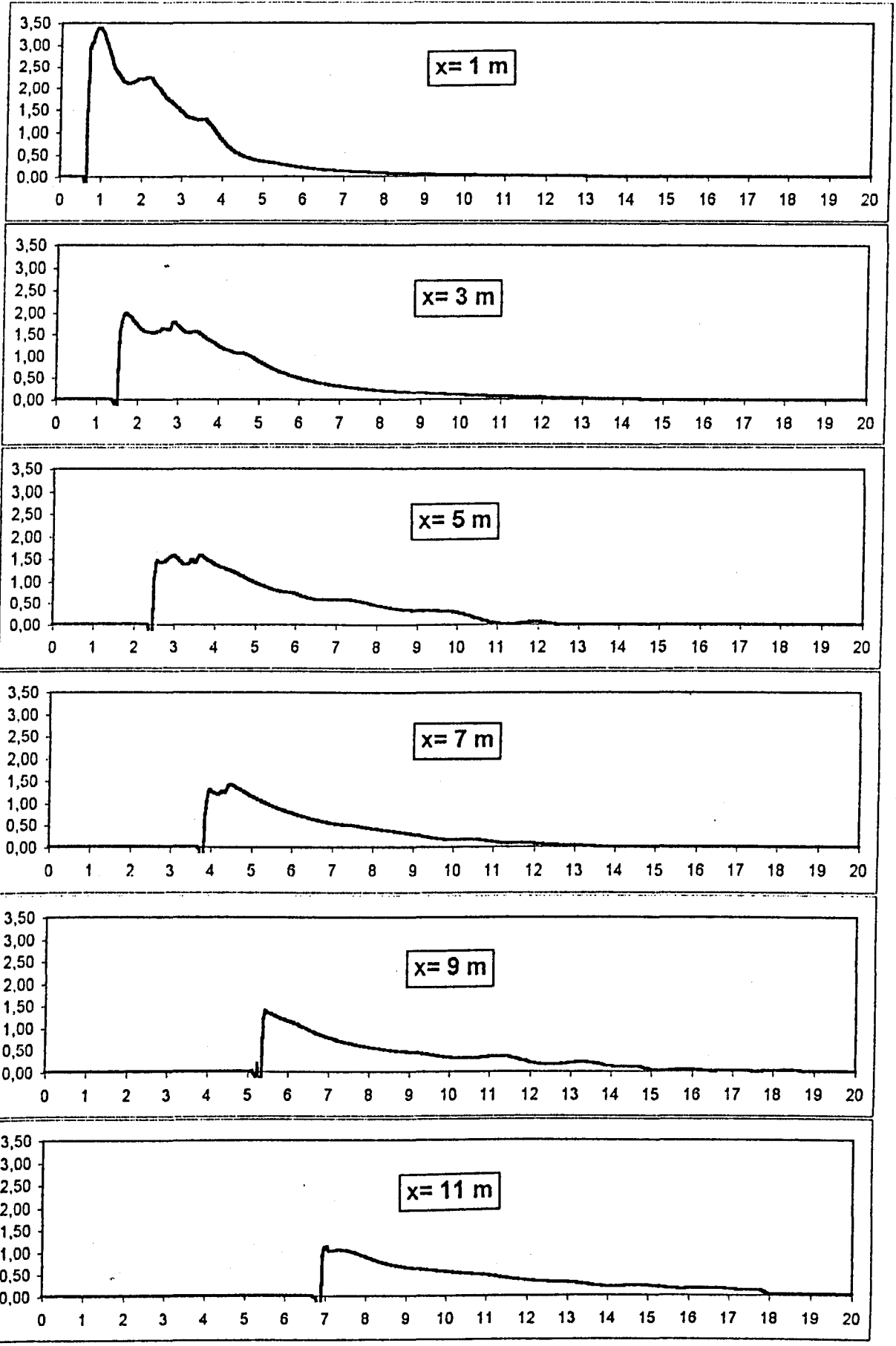

Figure 6.31 - Group E0 entry data - program alternative D
best calibrated simulation
Horiz.velocity (y axis,m/s) on time (x axis,s)

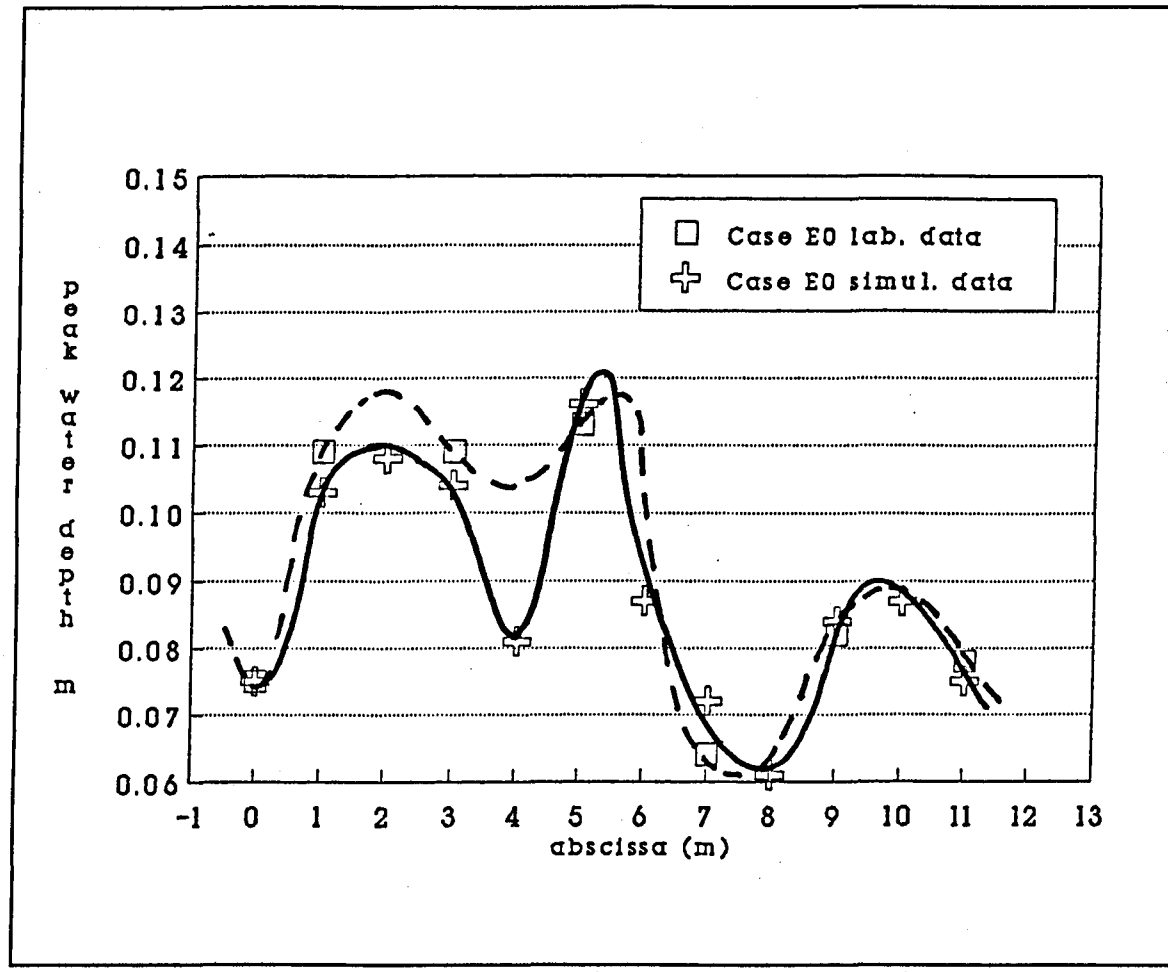

Figure 6.32 - Laboratory and simulated wave main peak trajectory

6.3 Result analysis

The comparison between simulation results obtained with Standing (1986) data and group E0 data provides evidence that seems to have major importance: data from Standing did not lead to wave front pulse formation, described in section 4.4.8. Pulse, in its turn, could degenerate almost completely the simulation process. But, pulse, also, seems to be responsible for the wave front peak oscillation along the pipeline length,

a phenomenon observed in laboratory. Contrarily, the simulation of Standing data showed a mild constant decaying of peak water depth.

Referring to the pulse evolution when running with group E0 entry data, each computer program alternative presented a different response. Figure 6.24 (alternative E) shows pulse evolving from initial sections, incorporating wave main peak in section x = 1 m and then flattening up to section x = 7 m, after which, the wave main peak retakes an ascendent movement. On B alternative (Figure 6.26) the pulse trajectory is more lengthened. Only after section x = 9 m the pulse, incorporating the wave peak, is not more present. Figure 6.28, showing the D alternative results, depicts the more consistent evolution of pulse integrated into the wave peak. Although this integration manifests through a quite thin peak, it is capable to hold an evolution in which the peak trajectory is similar to that measured in laboratory and presented in Figure 6.23, at least up to section x = 5 m. In section x = 7 m, the simulated profile should have a sudden drop to be in accordance with laboratory results. Instead, simulated results on Figure 6.28, shows that the peak starts a progressive decaying from section x = 7 m downwards.

Another distinctive aspect of the group E0 simulated profiles according to each program alternative is the velocity of wave propagation. On the E alternative (Figure 6.24) the wave front reached position x = 11 m in 6 s, approximately. On B alternative the same position is reached in 3.5 s while on D alternative this position is reached in 3.9 s

approximately. Figure 5.10 shows that, for group E0, the wave "foot" reached the final laboratory pipeline section (x = 13.005 m) in 4.75 s, approximately.

A verification of the program alternative response in terms of the total time for the wave front to move from computed initial section to the last computed section was accomplished. The simulated profile showed that the wave "foot" reached the final section in 4.7 s when using the same conditions for the simulation process through which profiles of Figure 6.28 were obtained, i.e., program alternative D, without any adjustment. Using E alternative the wave was late on reaching the same section while in B alternative the wave reached the final section prematurely.

Another verification referred to the wave front predicted position in time can be performed using simultaneously read sections in the laboratory, presented in Table 5.4. The wave "feet" time distance between simultaneously registered sections, respectively from the laboratory measurement and the correspondent simulated profiles, were read on the computer screen. The same conditions in which profiles of Figure 6.28 were obtained were used in the simulation. Table 6.2 presents the results for comparison.

Table 6.2 results shows a good degree of agreement and, perhaps, most importantly, non-formation of progressive divergence between simulated and laboratory results. It should be remarked that readings on the wave front position on time had a normal inaccuracy due to wave profile oscillations both on laboratory and on simulation.

Table 6.2 - Comparison between laboratory and simulated wave position on time

		Laboratory	Simulation	
Section	Abscissa x = (m)	wave "feet" "time distance" (s)	wave "feet" "time distance" (s)	difference (s)
S1	0.0	-	-	-
S2	1.040	-	-	-
S3	3.055	S2->S3 0.69	S2->S3 0.59	0.1
S4	5.065	S1->S4 1.67	S1->S4 1.68	-0.01
S5	7.075	S4->S5 0.71	S4->S5 0.62	0.09
S6	9.085	-	-	-
S7	11.095	S4->S7 2.31 S6->S7 0.87	S4->S7 2.14 S6->S7 0.85	0.17 0.02
S8	12.595	S4->S8 2.87	S4->S8 2.80	0.07

Still referring to group E0 simulations, it should be observed that the horizontal velocity profiles exhibit a much more favourable development. Figures 6.25, 6.27 and 6.29 show that horizontal velocity profiles have a more tranquil pattern of evolution in time in all sections.

The velocity of simulated wave propagation also had different results using the Standing (1986) data. Comparing Figures 6.2, 6.3 and 6.4 it can be observed that alternative E presents a consistent delay on the wave front while B and D alternatives show a good concordance. It should be remembered, however, that these concordances or disagreements can not be immediately related to the particular mathematical model used.

In fact, E and B alternatives refer to the same mathematical model (Saint Venant equations), although using distinct numerical models. This comment reinforce an important aspect on wave modelling: the consequences of numerical model use on a particular mathematical model are not well known. Different results on the wave propagation velocity using the same mathematical model (Figures 6.2 and 6.3) and coincident results on the same parameter observed with different mathematical models (Figures 6.3 and 6.4), seems to be a proof.

Better results from D program alternative in terms of wave front velocity propagation raise a question: would the vertical acceleration be playing a more important role in comparison with friction effect? Or, is that just a consequence of the numerical method accuracy. This question could be explored if the numerical model's response had better known characteristics. Unfortunately, as was commented before, different numerical models (E and B) using the same mathematical model produced different response for the same entry date, it being very difficult to assess the reasons for these dissimilarities. It could be argued that the B alternative uses the McCormack second-order accurate scheme while the E alternative uses the method of characteristics with first-order finite differences. This is certainly an important difference but, to be considered a definitive and embracing judgment, it should include the other side effects observed on the B alternative predictions, for example, bounded wave front peaks. In other words, a general appraisal of numerical method response remains to be undertaken.

A simpler way to compare friction and vertical acceleration effects would be to use the same numerical scheme for each of the developed mathematical models (Saint-Venant and Boussinesq equations). This would be possible using, for example, the "2-4" numerical schemes. A supplementary computer simulation process was performed using group E0 entry data on D computer program alternative. To simulate with the Saint-Venant mathematical model it was necessary to annul vertical acceleration. A special calibration file using vertical acceleration multiplicative factor Z = 0 applied to all sections was used. There is no need to present simulated results because they are identical to those presented on Figure 6.28. Thus, both the Saint-Venant and the Boussinesq equations have the same response when processed through "2-4" numerical scheme. One possible explanation is that vertical acceleration magnitude is too small and could not alter significatively the results.

Continuing with this supplementary exploration, two other computer simulation processes were carried out. The Saint-Venant and Boussinesq equations were again tested using the "2-4" numerical scheme, but now zeroing the friction through a multiplicative factor K = 0 applied to all sections. Friction effect reduction showed to be significant. Both the Saint-Venant and the Boussinesq equation response resulted in the same profiles. Compared with Figure 6.28, however they exhibits a progressive advancement on the wave front "foot" position in time together with an attenuated decaying effect on the wave peak.

Referring particularly to the iterative and interpolation processes, a comparison was carried out using the Standing entry data. Simulation using linear interpolation and no iterative process produced better results, depicted in Figures 6.2 and 6.3. Simulation using Everett and Newton-Gregory interpolation without iteration produced very damped and late profiles while processing with these interpolations and Lister iteration yields very high and acute wave peaks.

Referring to the adjustment process it should be remarked that the necessity to develop special schemes to calibrate the models yielded an important set of instruments for model analysis. Friction and vertical acceleration multiplicative factor schemes combined with other computer program possibilities provided the necessary capability for the flow study.

The friction effect on a steepened wave front, a recurrent theme in the literature, for example, could be studied varying friction through the friction multiplicative scheme. The friction zeroing exercise developed with Standing entry data and illustrated in Figure 6.10 shows the progressive advancement and flattening of the wave. This disagreement could be eliminated since the friction multiplicative scheme provides a means for the systematic friction adjustment up to an optimum simulated response in comparison with real data.

Standing (1986) showed that a small decrease in friction based on the "slipping" (see section 3.2.2) of the wave front over the base flow had optimized the simulated result. Considering, however the distinct behaviour of the

discharges generated by the experimental tipping tank, as described in Chapter 5, it is natural to conclude that Standing's rule could not be generically applied. This assertion can be deducted from the laboratory observations described in Chapter 5. It was shown that the previously established base flow constituted a barrier for the flow generated by the tipping tank, i.e., exactly the opposite effect to Standing's proposed friction scheme. A proof of this is given by Figure 5.10 where it is clear that the resistance to flow increases with the base flow value.

It seems reasonable to explain these different behaviours by reference to the interaction between wave and base flow, i.e., the phenomena of the region of shock between wave and base flow. Two phenomena can be identified: resistance and turbulence. Laboratory observation showed that the discharge of the tipping tank had a natural turbulence. Discharges over a base flow of very small water depth seemed to increase turbulence at the wave front. Higher base flow water depths, however, had the tendency to destroy or absorb the wave front natural turbulence. In any case the resistance effect originating from base flow obstruction promoted wave detainment. On the other hand, the flow studied by Standing appears in fact to slip over the previously established base flow. Less turbulence and a higher base flow water depth in relation to wave front, seemed to provide other sort of conditions for wave propagation. It should also be remarked that the Standing data used on the simulations here performed, refer to a pipe slope of 2%. The base flow in this slope is in

the supercritical regime. In this condition the velocity of the steady uniform base flow relatively to the wave front is much higher than the analogous of case E0.

These observations formed the basis for the friction adjustment process using the friction multiplicative scheme. In the simulation with group E0 entry data multiplicative factors higher than one were used. But, as already mentioned in 6.2.2.3, it was impossible to study the phenomenon in isolation. Thus, a combined adjustment procedure of friction and vertical acceleration had to be carried out.

Because the lack of knowledge involved and complexity of the interacting factors, the calibration process using friction and vertical acceleration, as described in 6.2.2.3, had an artistic nature. Thus, although, simulated water depth profiles approximated to laboratory measured profiles (Figure 6.30), this was associated with a collateral unacceptable consequence. As Figure 6.31 depicts, the wave front velocity was deeply modified. While in the simulation with no multiplicative factors (Figures 6.28 and 6.29) the wave front reached section x = 11 m in 3.9 s approximately, the best water depth profile adjustment promoted a strong wave front delay. Figure 6.28 shows that in this case the wave front reached section x = 11 m in 6.9 s approximately.

K (friction factor), Z (vertical acceleration factor) and α (numerical filter coefficient) values, presented in the Appendix, represent a synthesis of the artistic process mentioned. Combined consideration on the use of K , Z and σ previously described in sections 4.4.5, 4.4.6 and 4.4.7, were

the basis for this adjustment process. Obviously, the ignorance of the relationship between the involved phenomena has led to a very particular result in this case. This strict result, however, has the merit of bringing up the possibility of an adjustment process that could be a useful tool in further work in a condition in which better knowledge of involved phenomena has been accomplished.

6.4 Conclusions

In the model calibration process two types of entry data have been worked out. Standing's (1986) entry data presented water depth simulated profiles without pulse formation in the wave front. Contrarily, group E0 entry data produced strong pulse on the simulated wave front.

Program alternative E has been shown to be suitable for predicting water depth profiles exhibiting a well shaped contour of wave front when running entry data free of pulses. In this case, however, the wave front suffers from a systematic delay on its propagation velocity. A small reduction of friction force at the wave region can correct the phase problem. Standing's friction reduction scheme, described in section 3.2.2, produced good results when applied to the data presented by the same author. Program alternative D running with Standing's entry data predicts wave propagation at correct velocity. The wave front, however, presented rounded peaks, contrary to laboratory measured profiles. Combined friction and

vertical acceleration adjustments can diminish the curved peak problem. With the same entry data program alternative B also predicts profiles at correct velocity and bounded peaks. In this case, however, there is no possibility of adjustment.

Program alternative D yielded better predictions for group E0 entry data. When processing with no adjustment factors applied, D alternative produced well phased wave fronts, despite exhibiting water depth profiles in disagreement with laboratory measurements. An adjustment process combining a particular set of friction and vertical acceleration factors, together with an instability numerical filter, produced closer water depth profiles, but the wave front propagation velocity escaped from control.

Additional computer simulation processes showed clearly that numerical models played a decisive role on the results. Both the Saint-Venant and the Boussinesq equations presented the same response for E0 group entry data when running in the "2-4" numerical scheme demonstrating that vertical acceleration is irrelevant in that case or that the numerical method is not accurate enough to estimate vertical acceleration values. Concerning friction, the same mathematical equations with the same numerical scheme presented, both, progressively advanced profiles and mildly attenuated wave peaks when friction was reduced to zero.

The role of vertical acceleration remains unclear, as appears in the Boussinesq equation, on the wave peak oscillation as commented on section 6.2.2.3. The conclusion on this point can not be definitive because simulation with group

E0 entry data exhibits pulses on the wave front, making an overall appraisal practically impossible since the pulse formation mechanism remains unknown.

Additional exploratory simulations could also lead to the conclusion that the better wave front position response of program alternative D, running with Standing (1986) entry data, are related to a better performance of the "2-4" numerical scheme. Thus, using friction reduction in program alternative E to obtain better results would be just a mean to compensate numerical scheme inaccuracy.

Referring to pulse formation, it seems that its evolution on the wave front seemed to have a certain compatibility with wave peak trajectory observed in the laboratory.

Strong pulses can ruin simulation processing. In these cases the simulated wave front and pulse evolution can be better controlled using vertical acceleration multiplicative scheme available at D alternative.

In the adjustment and controlling process, the friction and vertical acceleration multiplicative schemes, together with numerical filters, are very useful tools. Expanded schemes providing more points than that set available on the computer program would be desirable. Thus, a more fine adjustment to the particular behaviour of the wave front would be obtained. Also the type of variation of these factors could be improved from linear to other types of functions.

The artistic character of adjustment used on the simulation process can also be developed, transforming the

process in a refined mathematical method. Available computer mathematical optimization packages are planned to be used in the research sequence. Not well known phenomena, such as friction and vertical acceleration variation at the wave front, could be studied through this optimization process. In a computer mathematical optimization process, quoted expanded multiplicative schemes would be used. Viscosity effect terms from the Navier-Stokes equations could also be incorporated in the process.

A particular important aspect on the relationship between the laboratory measurements and simulation emerged during the computer processing. In Chapter 5 it was shown that the flow rate measurements were a very delicate and time consuming work mainly because of the very quick discharge of the tipping tank. Thus, the precision of these measurements could be questioned. This consideration introduces a quite complicated problem in the simulation process because entry data precision is of paramount importance for the subsequent computation. For practical purpose an relatively easy solution can be applied. Transferring entry data laboratory measurements to a position where less turbulence is observed, for example, from 9 m to 10 m from the pipeline entrance, would provide better certainty on entry data values. This procedure corresponds to saying that the flow could remain unknown on the initial length of the pipeline, what seems to be acceptable in actual applications.

From the theoretical point of view an important assessment is the evaluation of equation term magnitudes.

Comparison of magnitudes can be performed using the developed computer program with some suitable arrangements on the output alternatives.

CHAPTER SEVEN

CONCLUSIONS AND FURTHER WORKS

7.1 The Sanitation Field Needs and the Global Approach

World Health Organization data show that in 1990 about 28% of urban population in developing countries was not provided with a sanitation service. Considering the tendency for strong urban population growth and the level of available investments, it is more probable that the unprovided urban population is being augmented. For Brazil, in particular, estimates show that about 65% of its urban population is not covered by sewer networks.

The global approach in the sector through the International Drinking Water Supply and Sanitation Decade (1981-1990) has brought important acquirements in terms of covered population increasing and in terms of conceptual and technical development. In historical terms the thrust on concepts and techniques started during the Decade represents a differential step compared with the incremental development of the sector on the last 150 years.

Referring to sewer network concepts, design criteria and construction, the Brazilian contribution through several innovative appropriate technologies should be noted.

Concluding, the present deficit of population coverage points to the necessity to continue and improve the Decade achievements. Within this objective, the four guiding principles of the "New Delhi Statement" shall be used to direct further development. Particularly, the use of intermittent discharge devices is a innovative form of providing drastic reduction on pipe slope laying, that can lead to sewer network construction economy.

7.2 The Wave Mathematical Model

A model directed to simulate the flow generated in sewers through intermittent discharge devices was presented. To obtain a good level of generality and considering the steep wave front generated by the discharge device, mathematical simulation of the rapidly varied unsteady flow case was chosen.

The literature review showed that the Boussinesq type equations have been consistently developed in the field of general theory of unsteady open channel flow and water waves. The Boussinesq equations can be regarded as the second order approximation equations of the shallow water theory derived by Stoker (1957) arising from the basic Euler's formulation.

A positive facet of all derived forms of Boussinesq equations is the general convergence on the reduction to the simpler Saint-Venant equations case.

The derived mathematical model are equations of the Boussinesq type, developed to be applied to unsteady pipe flow

and constituted by the mass conservation equation (2.57) and by the momentum conservation equation (2.90).

The literature review and the theoretical development permit to conclude that unsteady pipe flow analysis can be applied to sewer network systems aiming to obtain more rational and, probably, more economic design criteria.

7.3 Numerical Model Development

Numerical integration, using finite-differences approximation, was used to solve the mathematical system. Three numerical models were applied: first-order accurate finite-difference applied to the method of characteristics; the second-order accurate McCormack explicit scheme and the two-four scheme (Gottlieb et Turkel, 1976). The two-four scheme is fourth-order accurate in space and second-order accurate in time.

On the method of characteristics two interpolation formula were used: linear interpolation and Everett central difference formula and Newton-Gregory formula. Two iterative methods were applied: the simplified Lister's based Standing (1986) iterative process and the Lister (1960) process itself.

The stability of the three numerical method were controlled through the Courant number. For the method of characteristics $C_n = 1$ was used. With the McCormack method $C_n=0.8$ and in the two-four method, $C_n=0.67$. Oscillation problems were controlled through two schemes: the Lax-Wendroff two-step

method and Jameson's method.

Friction and vertical acceleration adjustments have been provided through special multiplicative factor schemes. Together with other adjustment factors, the computer program affords the necessary environment for the model manual optimization process.

In the method of characteristics, a special flow regime identification on the node under computation was developed based on the method theory. Special routines were inserted in the computer program to perform this function. Specific computer processing has shown the effectiveness of the developed flow regime identification method.

The three numerical methods were combined with the mathematical model resulting in three model alternatives: the Saint-Venant equations using the method of characteristics (alternative E); the Saint-Venant equations using the McCormack method (alternative B) and the Boussinesq equations using the two-four method (alternative D).

A major problem observed on the model response for certain type of entry data was the pulse formation at the wave front. This was an extremely troublesome problem that could not be controlled. The same kind of problem, found by Swaffield et Standing (1986), could be eliminated through a more refined interpolation method. In the present case these interpolation methods together with Lister(1960) complete iteration were not able to deal with the pulse. Some attempts to study the origin of the wave front pulse problem were initiated but could not be completed. The analysis of this question remains open. **Thus,**

it is a basic necessity to establish definitely, in further studies, if pulse formation is a phenomenon related to a hydrodynamic relationship or if it results from numerical treatment.

7.4 Laboratory Measurements

An extensive range of tests involving the device discharge volume generated flow combined with several base flow rate were measured in the horizontal rig. Also the device hydrographs for several discharged volumes were determined. These results have been used in the validation process when simulated data were compared with laboratory measured data.

The tipping tank flow rate measurement was very problematic due to the very rapid discharge of the device (about 2.5 s). In the model validation process the accuracy of the flow rate, as part of entry data, was of paramount importance. **Thus, it is advisable to improve flow rate measurements using more sophisticated equipment. Gravimetric methods using large tanks or volumetric methods with the measurement of water free surface displacement with a proper number of instruments, could be attempted.**

7.5 Conclusions on the Model Performance

Simulation using Standing's (1986) entry data with

program alternative D and B showed better results in terms of the wave front position despite presenting rounded wave front peaks. Alternative E showed well marked peaks but an increasing delay on the wave front position.

Simulation with E0 entry data suffered from pulse formation problems on the wave front. Better simulated results were obtained with D alternative. Although the water depth profiles did not match with the measurements in the laboratory, the wave front position has shown very good agreement.

The friction and vertical acceleration multiplicative factor schemes have been shown to be a very useful tool in the adjustment process. Applied to simulation with E0 entry data these resources permitted the prediction of water depth profiles closer to those measured in the laboratory. However, the process promoted an unacceptable delay on the wave velocity.

Comparison of simulation processing using the same mathematical model but, different numerical models, provided results of foremost importance. E and B alternatives refer to the same mathematical model (Saint Venant equations), although using the method of characteristics and the McCormack numerical models. The response of each of those alternatives for the same entry data was quite different. This fact reinforce an important aspect on wave modelling: the consequences of numerical model use on a particular mathematical model are not well known. Different results on the wave propagation velocity using the same mathematical model (Figures 6.2 and 6.3) and coincident results on the same parameter observed with

different mathematical models (Figures 6.3 and 6.4), seems to provide a proof. The analysis becomes more complicated because these facts are not only referred to accuracy levels, other kinds of unknown phenomena interact together.

Computer simulation processes showed clearly that numerical models played a decisive role in the results. Both the Saint-Venant and the Boussinesq equations presented the same response for E0 group entry data when running in the "2-4" numerical scheme. **This result leads to two possible conclusions: a demonstration that vertical acceleration is irrelevant in that case or a proof that the numerical method is not accurate enough to appraise vertical acceleration values.** On the other hand, the same mathematical equations with the same numerical scheme both presented progressively advanced profiles and mildly attenuated wave peaks when friction was reduced to zero. When using the method of characteristics the significance of the interpolation and iterative method seems to be relative to entry data. For example, Standing entry data had better simulated profiles using linear interpolation without iteration. **Thus, it can be concluded that the use of more accurate interpolation and iterative processes are not always necessarily advantageous. For certain entry data types and flow conditions these procedures can be ignored.**

Referring to the friction role it has been verified that the type of wave front and its interaction with the base flow and with the flow bed have importance. Standing's friction reduction scheme (see section 3.2.2) has shown good results for waves that appears in fact to slip over the previously

established base flow. Contrarily, waves with high turbulence on its fronts and flowing over small water depth base flows tends to generated strong impacts. In these cases, therefore, the resistance to flow is higher than that calculated through steady uniform flow formula. The dissipation of energy, probably, will be relevant in this case, requiring additional formulations.

It is possible that the pipe slope had a relationship with the friction behaviour. High pipe slopes tend to have base flows in the supercritical regime, with velocities that will pose less resistance to wave movement.

These types of interactions of discharge and base flow and the existence of turbulence in the wave front are important aspects when related to sediment transport. Laboratory exploratory work has shown that turbulence plays a major role in sediment movement.

Numerical methods have also shown an important role related to friction effects. Better wave front position response of program alternative D, running with Standing (1986) entry data, are related to a better performance of the two-four numerical scheme. Thus, using friction reduction in program alternative E to obtain better results would be just a means to compensate numerical scheme inaccuracy.

The vertical oscillation of the wave peaks along the pipeline suggested speculation as to its origin and nature. The oscillation seems to have two basic dynamic components: firstly, the inertial movement due to the form in which the mass of liquid originated from the tipping tank discharge

enters into the pipeline. Secondly, the effect on water particles of the shock between the wave front and the existent base flow with a much lower velocity and depth. These considerations would convey the hypothesis that the Boussinesq assumption would not be complete enough for the kind of flow studied here. It seems that the momentum equation on the vertical direction should also be considered to provide a better description of wave peak oscillation. Thus, it would be necessary to consider the flow equations in two dimensions, i.e., two dimension flow. **The phenomenon of the wave peak water depth oscillation along the pipeline shall be further analyzed. Its is probable that this phenomenon has importance also in other fields of hydraulics like in suddenly water release from reservoirs, for example.**

Results obtained points directly to the crucial role of numerical models. The development of higher order partial derivative equations requires correspondent development of numerical models with suitable degree of approximation. Particularly referring to the Boussinesq equations a stable third order approximation scheme shall be developed.

7.6 Further Work

Further developments are planned in the research continuing. Two lines of work derive from the research hitherto. Firstly, the application of knowledge on unsteady flow to sewer design and operation can be implemented. Building

sewage discharges on pipe collectors have to be better described. Data on actual sewage hydrographs are now more easily obtained with modern instruments that can be installed on pipe collectors. Analysis of these elements can provide new parameters for sewers dimensioning. Even without the knowledge of the effect of unsteady flows on sediment transport, assessments can be done using present dimensioning parameters, for example, those on the Brazilian standard of sewer network design.

The second line of work refers to model development. The necessary studies can be grouped in two areas: the sewage contribution modelling and the unsteady flow modelling development, including the study of sediment hydraulic transport under unsteady flow conditions and the influence of network singularities on the flow.

Referring to the role of vertical acceleration and friction effects a magnitude analysis should be performed. This analysis could be carried out using the developed computer program and suitable entry data, avoiding the pulse problems.

Concerning the numerical methods, for the computation of Boussinesq type equations a stable third order method shall be developed as Basco (1983) recommends, quoting Abbott.

The artistic character of adjustment used on the simulation process should be transformed in a refined optimization mathematical process using available computation packages.

REFERENCES

ABBOTT M.B., *Computational Hydraulics: Elements of Theory of Free Surface Flows.* Pitman Publishing Limited, London, 1979.

ABBOTT, M.B. "Computational Hydraulics and Modelling: Some Social Aspects". *XXII IAHR-Congress*, Lausanne, 1987. École Polytechnique Fédérale, Lausanne, 1987.

ABBOTT M.B. et BASCO, D.R. *Computational Fluid Dynamics. An Introduction for Engineers.* Longman Scientific & Tech., Essex, 1989.

ABBOTT M.B. et RODENHUIS, G.S. "A Numerical Simulation of the Undular Hydraulic Jump". *Journal of Hydraulic Research*, 10 (1972), nr. 3. (Discussion by D.H. Peregrine, Jour.Hydr.Res., 12 (1974), nr. 1).

ABBOTT, M.B. et al. "On the Numerical Modelling of Short Waves in Shallow Water". *Journal of Hydraulic Research*, 16, nr.3, pp. 173-204, 1978.

ABES/OPS - ASSOCIAÇÃO BRASILEIRA DE ENGENHARIA SANITÁRIA E AMBIENTAL/ORGANIZAÇÃO PANAMERICANA DA SAÚDE. Avaliação Nacional da Década Internacional do Abastecimento de Água e do Esgotamento Sanitário *("International Drinking Water Supply and Sanitation Decade National Evaluation")*. *Revista BIO*, Rio de Janeiro, edição especial, 1991.

ABNT - ASSOCIAÇÃO BRASILEIRA DE NORMAS TÉCNICAS (*"technical standard Brazilian association"*). *NBR 9649 - Projeto de redes coletoras de esgoto sanitário* (*"sewage collection networks design"*). ABNT, Rio de Janeiro, 1986.

ACCIOLI, A.A.N. et FERNANDEZ, M.F. "Tanques fluxíveis, tecnologia de baixo custo" (*"flush tanks, low cost technology"*). Proceedings of the 11° Congresso Brasileiro de Engenharia Sanitária e Ambiental, Fortaleza, 1981. ABES - Associação Brasileira de Engenharia Sanitária e Ambiental, Rio de Janeiro, 1981.

ALVES, W. "Modelagem hidrodinâmica do escoamento em redes coletoras de esgoto" (*"hydrodynamics sewer network modelling"*). *Proceedings of the 18° Congresso Brasileiro de Engenharia Sanitária e Ambiental.* Salvador, 1995. ABES - Associação Brasileira de Engenharia Sanitária e Ambiental, Rio de Janeiro, 1995.

ALVES, W. "Desenvolvimento de dispositivo gerador de descargas intermitentes aplicado a redes coletoras de esgoto" (*"development of intermittent discharge devices for application in sewer networks"*). *Proceedings of the 17° Congresso Brasileiro de Engenharia Sanitária e Ambiental.* Natal, 1993. ABES - Associação Brasileira de Engenharia Sanitária e Ambiental, Rio de Janeiro, 1993.

ALVES, W. "Development of Intermittent Discharge Devices for Application at the Head of Sewers. A Research in Course." *Proceedings of CIB W62 Seminar*, Brussels, 1991. Belgian Building Research Institute, Brussels, 1991.

ALVES, W. *Development of Intermittent Discharge Devices for Application in Sewer Networks.* Unpublished MPhil thesis presented to Heriot-Watt University, Department of Building Engineering and Surveying, Edinburgh, 1990.

ANDERSON, D.A. et al. *Computational Fluid Mechanics and Heat Transfer.* McGraw-Hill, Inc., New York, 1984.

ANDERSON, D.A. in *Computational Fluid Dynamics: An Introduction.* (several authors, edited by Wendt,J.F.) Springer-Verlag, Berlin, 1992.

AZEVEDO NETTO, J.M. "Cronologia dos serviços de esgotos, com especial menção ao Brasil" (*"sanitation chronology, with special reference to Brazil"*). *Revista do Departamento de Águas e Esgotos. São Paulo.*

BASCO, D.R. *Computation of Rapidly Varied Unsteady, Free-Surface Flow*, U.S. Geological Survey, Water-Resources Investigations Report 83-4284, Reston, Virginia, 1983.

BASCO, D.R. "Limitations of de Saint-Venant Equations in Dam-Break Analysis". *Journal of Hydraulic Engineering*, (115), nr. 7, pp. 950-965, ASCE, July, 1989.

BHALLAMUDI, S.M. et CHAUDHRY, M.H. "Numerical Modelling of Aggradation and Degradation in Alluvial Channels". *Journa of Hydraulic Engineering*, (117), nr. 9, pp. 1145-1164, ASCE, September, 1991.

BOUSSINESQ, J. "Théorie des ondes et des remous qui se propagent le long d'un canal rectangulaire horizontal, en communiquant au liquide contenu dans ce canal des vitesses sensiblement pareilles de la surface au fond". *Journal de Mathématiques Pures et Appliquées*, 2ème Ser., 17, pp. 55-108, 1872.

BRIDGE, S. *A Study of Unsteady Flow Wave Attenuation in Partially Filled Pipe Networks.* Unpublished PhD thesis presented to Brunel University, Department of Mechanical Engineering, London, 1984.

BRITO, R.S. *Obras completas de Saturnino de Brito - Engenharia Sanitária.("The Saturnino de Brito complete work - sanitary engeneering")*. Instituto Nacional do Livro, Rio de Janeiro, 1943. (Qriginally published between the last decade of nineteenth century and first decades this century).

CARMO, J.S.A. *Efeitos hidrodinâmicos resultantes de deslizamentos de encostas em albufeiras. Modelação a duas dimensões horizontais. ("hydrodinamics effects resulting from reservoir bank slipping. Two horizontal dimensions modelling")*. Unpublished thesis (Master in Hydraulics) presented to Departamento de Engenharia Civil do Instituto Superior Técnico da Universidade Técnica de Lisboa, 1990.

CEPAM - FUNDAÇÃO PREFEITO FARIA LIMA. *"Sistemas não convencionais de infra-estrutura urbana" ("non-conventional systems of urban infrastructure")*. Fundação Prefeito Faria Lima - CEPAM and Caixa Econômica Federal, São Paulo, 1988.

CHOW, V.T. *Open-Channel Hydraulics*. McGraw-Hill Book Co., New York, 1959.

CHRISTMAS J. et ROOY C. "The Decade and Beyond: at a Glance". *Water International*, (16), nr. 3, September 1991.

CYNAMON, S.E. "*Sistema não convencional de esgoto sanitário a custo reduzido, para pequenas coletividades e áreas periféricas" ("low-cost nonconventional sewer system for small communities and peripheric areas")*. Fundação Oswaldo Cruz/Escola Nacional de Saúde Pública, 1986, 2nd.ed.

CUNGE, J.A. "Numerical Hydraulics Modelling: Late '80s context and cross-roads". *XXII IAHR-Congress*, Lausanne, 1987. École Polytechnique Fédérale, Lausanne, 1987.

FENNEMA, R.J. et CHAUDHRY, M.H. "Explicit Numerical Schemes for Unsteady Free-Surface Flows with Shocks". *Water Resources Research*, (22), nr. 13, pp. 1923-1930, December 1986.

FRENCH, R.H. *Open-Channel Hydraulics*. McGraw-Hill Book Co., New York, 1985.

GARCIA, R. et KAHAWITA, R.A. "Numerical Solution of the Saint-Venant Equations with the McCormack Finite-Difference Scheme". *International Journal for Numerical Methods in Fluids*, (6), pp. 259-274, 1986.

GHARANGIK, A. et CHAUDHRY, M.H. "Numerical Simulation of Hydraulic Jump". *Journal of Hydraulic Engineering*, (117), nr. 9, ASCE, September 1991.

GOTTLIEB, D. et TURKEL, E. "Dissipative Two-Four Methods for Time-Dependent Problems". *Mathematics of Computation*, (30), nr. 136, pp. 703-723, October 1976.

GUIMARÃES, A.S.P. "Sistemas simplificados de redes des esgotos sanitários" (*"simplified sewer network systems"*). *Proceedings of the Seminário Latino-Americano de Alternativas Tecnológicas para Habitação e Saneamento*, Olinda, 1987. Ministério da Habitação Urbanismo e Meio Ambiente, Brasilia, 1988.

HAUGUEL, A. "A Numerical Model of Storm Waves in Shallow Water". *Proceedings of the 17th Int. Conf. on Coastal Engineering*, Sydney, 1980.

HENDERSON, F.M. *Open Channel Flow*. The Macmillan Co., New York, 1966.

IMPARATO, I. et ABIKO, A.K. "Urbanização, abastecimento de água e saneamento" ("urbanization, water supply and sanitation"). *Proceedings of the II Seminário Internacional: Recuperação de áreas urbanas degradadas*, Salvador, 1993, pp. 99-111, PNUD-MBES, Brasilia, 1994.

INSTITUTO BRASILEIRO DE GEOGRAFIA E ESTATÍSTICA - IBGE. *Pesquisa Nacional por Amostra de Domicílio - PNAD ("national survey through house sampling")*. IBGE, Rio de Janeiro, 1996.

INSTITUTO BRASILEIRO DE GEOGRAFIA E ESTATÍSTICA - IBGE. *Pesquisa Nacional de Saneamento Básico - PNSB - 1989 ("national survey on water supply and sanitation")* . IBGE, Rio de Janeiro, 1992.

JAMESON, A., SCHMIDT, W. et TURKEL, E. "Numerical Solutions of the Euler Equations by Finite Volume Methods Using Runge-Kutta Time-Stepping Schemes". *AIAA 14th Fluid and Plasma Dynamics Conference.: AIAA 81-1259*. American Institute of Aeronautics and Astronautics, Palo Alto, California, 1981.

KALBERMATTEN, J.M. "Water and Sanitation for All, Will it Become Reality or Remain a Dream?". *Water International*, (16), nr. 3, September 1991.

LEME, F.P. *Planejamento e projeto dos sistemas urbanos de esgotos sanitários*. CETESB, São Paulo, 1977.

LISTER, M. "The Numerical Solutions of Hyperbolic Partial Differential Equations by the Method of Characteristics". *Mathematical Methods for Digital Computers*. Ralston and Wilf, Eds., John Wiley and Sons, 1960.

LONG, R.R. "The Initial-Value Problem for Long Waves of Finite Amplitude". *Journal of Fluid Mechanics*, (20), part 1, pp. 161-170, 1964.

McCOWAN, A.D. "Equation Systems for Modelling Dispersive Flow in Shallow Water". *Proceedings of the 21st IAHR-Congress*, Melbourne, 1985.

McCOWAN, A.D. "The Range of Application of Boussinesq Type Numerical Short Wave Models". *Proceedings of the AIRH-Congress*, Lausanne, 1987.

MACEDO, E.S. Cálculo do escoamento na rede de esgotos sanitários do sistema separador absoluto ("sewer flow computation in separated systems"). *Presented in the VIII Congresso Inteamericano de Engenhária Sanitária*, Washington, D.C., June 1962. Departamento de Esgotos Sanitários, SURSAN, Rio de Janeiro, 1962.

MACIEL, G.F. "Aplicação das equações da "classe Boussinesq" no estudo de ondas de gravidade geradas por impacto localizado" ("application of "Boussinesq class" equations to the study of gravity waves generated by limited impact"). *Proceedings of the XIV Congressso Ibero-Latino-Americano de Métodos Computacionais em Engenharia*, São Paulo, pp. 656-664, Instituto de Pesquisas Tecnológicas do Estado de São Paulo -IPT, December 1993.

MARA, D.D. "*The Design of Ventilated Improved Pit Latrines*". TAG Technical Note nr. 13, United Nations Development Programme. The World Bank, Washington, 1984.

MARA, D.D. "*The Design of Pour-Flush Latrines*". TAG Technical Note nr. 15, United Nations Development Programme. The World Bank, Washington, 1985.

MELO, J.C. "Sistemas condominiais de esgoto" ("*condominium sewer systems*"). *Proceedings of the Seminário Latino-Americano de Alternativas Tecnológicas para Habitação e Saneamento*, Olinda, 1987. Ministério da Habitação Urbanismo e Meio Ambiente, Brasilia, 1988.

MONTENEGRO, M.H.F. et ALVES, W. "Alternativas de baixo custo em saneamento (1a. parte)" ("sanitation low cost alternatives - 1st part") in Tecnologia das Edificações. Instituto de Pesquisas Tecnológicas do Estado de São Paulo - IPT/Editora PINI, São Paulo, 1988.

MOORE, E.C.S. *Sanitary Engineering*. B.T. Batsford, London, 1898.

MURRAY, A.C.F. *Appraisal of Intermittent Wave Generation Aplicable to Water Conserving Drainage Systems*. "Final Year Project Report" for Brunel University, Building Technology, unpublished, 1982.

OTIS, R.J. et MARA, D.D. "*The Design of Small Bore Sewer Systems*". TAG Technical Note nr. 14, United Nations Development Programme. The World Bank, Washington, 1985.

PEREGRINE, D.H. "Calculations of the Development of an Undular Bore". *Journal of Fluid Mechanics*, (25), part 2, pp. 321-330, 1966.

PEREGRINE, D.H. "Long Waves on a Beach". *Journal of Fluid Mechanics*, (27), part 4, pp. 815-827, 1967.

PEREGRINE, D.H. "Long Waves in a Uniform Channel of Arbitrary Cross-Section". *Journal of Fluid Mechanics*, (32), part 2, pp. 353-365, 1968.

PONCE, V.M. et SIMONS, D.B. "Shallow Wave Propagation in Open Channel Flow". *Journal of Hydraulics Division, Proceedings of the of ASCE*, (103), nr. HY12, December 1977.

PRIESSMANN, A. *Use of Mathematical Models - Critical Remarks, the Future Outlook.* Proceedings of the International Symposium on Unsteady Flow in Open Channels, Newcastle-upon-Tyne, 1976. BHRA Fluid Engineering, Newcastle-upon-Tyne, 1976.

RANGA RAJU, K.G. *Flow Through Open Channels.* Tata McGraw-Hill Pub. Co., New Delhi, 1981.

SANCHEZ, M.G. *Aplicações do método das características. ("method of characteristics applications").* Unpublished Master of Engineering thesis present to Escola Politécnica da Universidade de São Paulo, São Paulo, 1978.

SEABRA SANTOS, F.J. "Ondas de gravidade em água pouco profunda" ("gravity waves in not too deep water"). *Proceedings of the II Simpósio Luso-Brasileiro sobre Hidráulica e Recursos Hídricos*, Lisboa, 1986.

SERRE, F. *Contribution à l'étude des écoulements permanents et variables dans les canaux*. La Houille Blanche, 374-388, 1953.

SILVA, R.C. (published interview). *Água Viva*. Santo André, November 1990.

SOUZA, P.A. (several personal communications mainly referring to particle hydraulic movement, mathematical model derivation, terms significance, etc), 1993 and 1994.

STANDING, K.M. *Surge Generation as an Aid to Water Conserving Building Drainage Design*. Unpublished PhD thesis presented to Brunel University, Department of Mechanical Engineering, London, 1986.

STOKER, J.J. *Water Waves. The mathematical Theory with Applications*. John Wiley & Sons, New York, 1957.

SWAFFIELD, J.A. "Application of the Method of Characteristics to Predict Attenuation in Unsteady Partially Filled Pipe Flow". NBS Report, October, 1980.

SWAFFIELD, J.A. "Transient Full Bore Flow in Building Drainage Networks". 2nd Quarterly Progress Report under NBS CBT grant 60NANB5DO581, Heriot-Watt University, April 1986.

SWAFFIELD, J.A. et BRIDGE, S. "Applicability of the Colebrook-White Formula to Represent Frictional Losses in Partially Filled Unsteady Pipeflow". *Journal of Research of the National Bureau od Standards*, (88), nr. 6, November-December 1983.

SWAFFIELD, J.A. et GALOWIN, L.S. "Multistorey Building Drainage Network Design - An Application of Computer Based Unsteady Partially Filled Pipeflow Analysis". *Building and Environment*, (24), nr. 1, pp 99-110, 1989.

SWAFFIELD, J.A. et STANDING, K.M. "Improvements in the Application Of the Numerical Method of Characteristics To Predict Attenuation in Unsteady Partially Filled Pipe Flow". *Journal of Research of the National Bureau of Standards*, (91) nr. 3, May-June, 1986.

TERZIDIS, G. et STRELKOFF, T. "Computation of Open-Channel Surges and Shocks". *Journal of the Hydraulics Division. Proceedings of the ASCE,* (96), nr. HY12, December, 1970.

TSUTIYA, M.T. et MACHADO NETO, J.G.O. Tensão trativa: um critério econômico para o dimensionamento das tubulações de esgoto (*"tractive stress: an economic criteria for sewage pipeline dimensioning"*). *Revista DAE*, nr. 134, pp. 23-28, September, 1983.

UNITED NATIONS. "Earth Summit - Agenda 21, The United Nations Programme of Action from Rio". Rio de Janeiro, 1992.

UNITED NATIONS. Habitat II Bulletin; "Global Report on Human Settlements reveals: 500 million homeless or poorly housed in cities worldwide". United Nations Conference on Human Settlements, Istanbul, Turkey, 3-14 June,1996.

URSELL, F. "The Long-Wave Paradox in the Theory of Gravity Waves". *Proceedings of the Cambridge Phil. Soc.*, (49), pp. 685-694, 1953.

WAKELIN, R. et alii. "Appraisal of Intermittent Wave Generation Applicable to Water Connserving Drainage Systems.". *Proceedings of the Water Supply and Drainage for Buildings, CIB W62 Seminar*, Lostorf, 1982.

WARING Jr.,G.E. *Sewerage and Land Drainage*. D. Vann Nostrand Company, New York, 1889.

WARNER D.B. et LAUGERI L. "Health for All: the Legacy of the Water Decade". *Water International*, (16), nr. 3, September 1991.

WATER AUTHORITIES ASSOCIATION. *Sewers for Adoption*. Water Research Centre, Medmenham, 1989 (3rd. edition).

WRIGHT, L. *Clean an Decent - the History od the Bathroom and the WC*. Routledge & Kegan Paul. London, 1980.

APPENDIX

Calibration Files

Table B.1 - Friction factor

	$J_i = 1$	$J_f = 3$
$T_A = 0.00$	10	11
$T_B = 0.17$	7	8
$T_C = 0.45$	7	8
$T_T = 1.60$	1	5

Table B.2 - Damp factor

	$J_i = 1$	$J_f = 3$
$T_A = 0.00$	0	0
$T_B = 0.20$	0	0
$T_C = 0.20$	0	0.2
$T_T = 1.00$	0.5	0.5

Table B.3 - Friction factor

	$J_i = 4$	$J_f = 11$
$T_A = 0.00$	12	20
$T_B = 0.14$	9	15
$T_C = 0.80$	9	15
$T_T = 1.60$	1	5

Table B.4 - Damp factor

	$J_i = 4$	$J_f = 11$
$T_A = 0.00$	0	0
$T_B = 0.14$	0	0
$T_C = 0.80$	0	0.2
$T_T = 1.60$	0	0.5

Table B.5 - Friction factor

	$J_i = 12$	$J_f = 21$
$T_A = 0.00$	20	15
$T_B = 0.14$	15	9
$T_C = 0.80$	15	9
$T_T = 1.60$	5	5

Table B.6 - Damp factor

	$J_i = 12$	$J_f = 21$
$T_A = 0.00$	0	0
$T_B = 0.20$	0	0
$T_C = 0.20$	0.2	0.2
$T_T = 0.70$	0.5	0.5

Table B.7 - Friction factor

	$J_i = 22$	$J_f = 31$
$T_A = 0.00$	1	1
$T_B = 0.14$	1	1
$T_C = 0.80$	1	1
$T_T = 1.60$	1	1

Table B.8 - Damp factor

	$J_i = 22$	$J_f = 31$
$T_A = 0.00$	0	0
$T_B = 0.20$	0	0
$T_C = 0.20$	0.2	0.2
$T_T = 0.70$	0.5	0.5

Table B.9 - Vert.Accel. Factor

	$J_i = 1$	$J_f = 3$
$T_A = 0.00$	-7000	-7000
$T_B = 0.09$	12000	15000
$T_C = 0.15$	-12000	-12000
$T_T = 0.55$	-20000	-20000

Table B.10- Vert.Accel. Factor

	$J_i = 4$	$J_f = 11$
$T_A = 0.00$	-6000	-6000
$T_B = 0.10$	18000	18000
$T_C = 0.20$	-15000	-15000
$T_T = 0.60$	-25000	-25000

Table B.11 - Vert.Accel. Factor

	$J_i = 12$	$J_f = 21$
$T_A = 0.00$	-8000	-8000
$T_B = 0.08$	21000	24000
$T_C = 0.12$	-17000	0
$T_T = 0.35$	-20000	0

Table B.12 - Vert.Accel. Factor

	$J_i = 22$	$J_f = 31$
$T_A = 0.00$	-5000	-4000
$T_B = 0.08$	10000	8000
$T_C = 0.12$	-2000	-2000
$T_T = 0.40$	-1000	-1000

Table B.13 - Vert.Accel. Factor

	$J_i = 42$	$J_f = 55$
$T_A = 0.00$	-1000	-2000
$T_B = 0.08$	3000	6000
$T_C = 0.12$	-1000	-3950
$T_T = 0.40$	-1000	-1050

Table B.14 - Vert.Accel. Factor

	$J_i = 56$	$J_f = 76$
$T_A = 0.00$	-2000	-1000
$T_B = 0.08$	6000	3000
$T_C = 0.12$	-3100	-2500
$T_T = 0.40$	-900	-900

Table B.15 - Vert.Accel. Factor

	$J_i = 77$	$J_f = 91$
$T_A = 0.00$	-1000	-1000
$T_B = 0.08$	3000	3000
$T_C = 0.12$	-2500	-3500
$T_T = 0.35$	-900	-1500

Table B.16 - Vert.Accel. Factor

	$J_i = 92$	$J_f = 99$
$T_A = 0.00$	-1000	-1000
$T_B = 0.08$	3000	3000
$T_C = 0.12$	-3550	-4500
$T_T = 0.35$	-1550	-1800

Table B.17 - Vert.Accel. Factor

	J_i= 100	J_f= 112
T_A = 0.00	-1000	-1000
T_B = 0.08	3000	3000
T_C = 0.12	-4200	-5000
T_T = 0.35	-1200	-2000

Table B.18 - Vert.Accel. Factor

	J_i= 113	J_f= 131
T_A = 0.00	-1000	-1000
T_B = 0.08	3000	3000
T_C = 0.12	-4000	-500
T_T = 0.35	-1500	-100